DOCTOR OF PHILOSOPHY

Air-Multiple PCMs for the Free Cooling and Ventilation of Buildings

Iten, Muriel

Award date:
2015

Awarding institution:
Coventry University

Air-Multiple PCMs for the Free Cooling and Ventilation of Buildings

By

Muriel de Carvalho Iten

August, 2015

Air-Multiple PCMs for the Free Cooling and Ventilation of Buildings

By

Muriel de Carvalho Iten

August, 2015

A thesis submitted in partial fulfilment of the University's requirements for the Degree of Doctor of Philosophy

DECLARATION

I declare that the work in this research project entitled “Air-Multiple PCMs for the Free Cooling and Ventilation of Buildings” has been performed by me in the Faculty of Computing and Engineering under the supervision of Prof. Shuli Liu, Dr. Ashish Shukla and Prof. Mark Gaterell. The information derived from the literature has been duly acknowledged in the text and list of references provided.

DATE: _ _ _ _ _ _ _ _ _ _ _ _ _

_ _ _ _ _ _ _ _ _ _ _ _ _ _ _ _ _ _

Muriel de Carvalho Iten

Abstract

Thermal energy storage (TES) including phase change materials (PCMs), is an important technology to provide free cooling and ventilation in buildings. They have potential advantages over mechanical ventilation systems in terms of energy requirements, economic and environmental benefits.

The main aim of this research is to study an air-multiple PCMs unit for the free cooling and ventilation applications relying on the daytime and night-time temperature difference during the summer. The research work carried out and reported in this thesis includes an extensive literature review on TES, incorporating PCMs, experimental investigation of the parameters influencing the charging and discharging time and the air outlet temperature of an air-PCM unit. It has been observed that the heating/cooling rate of PCM is important factor in studying charging/discharging behaviour of a PCM. For this, the determination of the thermophysical properties of the selected PCMs by Differential Scanning Calorimetry (DSC) is carried out. Similar heating rate, as per experimental testing, established better validation results when used in CFD model. The CFD model aims to predict the outlet air temperatures and the PCM temperatures for validation of the experimental data. Further on, parametric study will use the verified CFD model of an air-multiple PCM unit to identify significant parameters affecting the air outlet temperature, the cooling time and the PCM charging time. Finally, this thesis will investigate the potential of an air-multiple PCM unit for free cooling and ventilation of an office building under Portuguese climatic conditions through a CFD model.

The experimental study has shown that the air inlet temperature and velocity play a major role on the PCM charging/discharging time and on the air outlet temperature. The numerical and experimental studies show that the developed CFD model has the ability to give good agreement for the prediction of the PCM charging and discharging times and the air outlet temperature with experimental results. Based on the experimental work and numerical analysis, an air-multiple PCM unit is proposed with a cooling load of 1.02 kW for office building. This allowed the reduction of the initial capital cost, the maintenance cost and the environmental benefits when compared to a traditional air conditioning unit.

Acknowledgement

I would like to express my sincere gratitude to Prof. Shuli Liu and Dr. Ashish Shukla for their supervision and valuable advice during the work.

My special thanks to the staff in the John Lang Building at Coventry University namely Mr. Tim Davis, Dr. John Karadelis and Dr. Abdulalahi Ahmed for providing supports and thoughtful advices to my research work.

My special thanks to the technicians of the John Lang Building at Coventry University Mr. Ian Breakwell, Mr. Terry Teeling, Mr. Kieran Teeling, and Mr. Steve Hutton. I owe sincere and earnest thankful to Mr. Ian Breakwell who helped me substantially with my experimental work. My project would not have been successful without his assistance.

Also a special thanks to Prof. Keith Burnham from CTAC, Dr. Vannessa Goodship from the University of Warwick and Dr. Pedro Silva from the Universidade da Beira Interior for allowing me the use of their lab facilities to carry on my experimental work.

These acknowledgments would not be complete without thanking my family, my partner and friends for their constant support and care. I could not have accomplished my goal without their unfaltering support, encouragement, and inspiration. During the past years, they stubbornly refused to allow my mind's stressed and exhausted state to distort reality. They also selflessly accepted my lack of attention and time.

A special thanks to my friend Yvonne Cullen for her precious assistance with the English writing. At least but not last, I would also like to thank Father Jimmy for his spiritual guidance and comfort during these years living abroad.

CONTENTS

Abbreviations

AC	Air conditioning
Anal	Analytical
ASHRAE	American Society of Heating, Refrigeration and Air-conditioning Engineers
CFD	Computational Fluid Dynamics
DNS	Direct Numerical Simulation
DSC	Differential Scanning Calorimetry
DTA	Differential Thermal Analysis
EU	European Union
Exp	Experimental
FLUENT	CFD Software
HTF	Heat transfer fluid
HVAC	Heating, ventilation and air conditioning
IAQ	Indoor Air Quality
LES	Large-Eddy Simulation
LH	Latent heat
LHS	Latent Heat Storage
LHTES	Latent Heat Thermal Energy Storage
LNEC	National Laboratory for Civil Engineering in Portugal
Num	Numerical
PCM	Phase change material
RANS	Reynolds-Average Navier-Stokes
RCCTE	Characteristics of Thermal Performance of Buildings Regulation in Portugal
RSECE	Energy Systems and Air Conditioning of Buildings Regulation in Portugal
RNG	Re-Normalisation Group Theory
SCE	National Energy Certification (Portugal)
SH	Sensible heat
SHS	Sensible Heat Storage
TES	Thermal energy storage
UDF	User defined function

Nomenclature

A	Area (m^2)
A_0	Constant based on the standard sample (DSC)
C_p	Specific heat (J/kg °C)
Ceff	Effective heat capacity (J/kg °C)
D	Diameter of tube (m)
D_h	Hydraulic diameter (m)
erf	Error function solution
erfc	Error function solution
f_l	Liquid fraction of the PCM
g	Gravitational acceleration (m^2/s)
H	Enthalpy (J/kg)
$H_{channel}$	Air gap height (m)
H_{panel}	Height of the PCM panel (m)
H_{TOTAL}	Total internal height of air-PCM unit
h	Sensible enthalpy (J/kg)
h_c	Convective heat-transfer coefficient (W/m^2 °C)
I_T	Turbulent intensity (%)
$\vec{J}$	Diffusive mass flux vector ($kg/m^2.s$)
k	Thermal conductivity of the PCM (W/m °C)
L	Latent heat of fusion (enthalpy) (J/kg)
$L_{channel}$	Lenght of the air channel (m)
L_{panel}	Lenght of the PCM panel (m)
L_T	Turbulent length scale (m)
ℓ	Length of the storage system (m)
m	Mass (kg) or mass flow rate (kg/s)
N	Number of time steps
M	Molecular mass (kmol)
P	Static pressure (Pa)
P_{AC}	Power of the air conditioner (kW)

Q	Load (W)
s	Distance from moving boundary to interface with heat source element
ΔT	Change in temperature (°C)
S	Source term
Ste	Stefan number
T	Temperature (°C)
t	Time (s or h)
V^{DSC}	DSC signal
W_{AC}	Energy consumption of the air conditioner (kWh)
$W_{channel}$	Width of the air channel (m)
W_{fan}	Energy consumption of the fan (kWh)
W_{panel}	Width of the PCM panels (m)
v	Velocity (m/s)
$\vec{v}$	Velocity vector (m/s)
v'	Root-Mean-Square of the turbulent velocity
X	Interface location
x	Length coordinate
x_i	PCM mass fraction
y	Length coordinate.
y^+	Dimensionless wall thickness
λ	Numerical constant, dimensionless
ρ	Density (kg/m^3)
ε	Effectiveness over the phase change process
μ	Dynamic viscosity (kg/m s)
$\bar{\bar{\tau}}$	Stress tensor (Pa)
ΔH	Change in enthalpy (J/kg)
ΔQ	Change in stored heat (J)
∇	Vector differential

Subscripts

air	Air
air duct	Air duct of air-PCM unit
amb	Ambient air
avg	Average
c	Cooling
channel	Air channel
cruc	Crucible
end	Endset
Exp	Experimental
h	Heating
i	Initial condition
j	Mass fraction of species
in	Inlet
f	Final condition
l	Liquid
m	Melting
Num	Numerical
on	Onset
out	Outlet
panel	PCM panel
peak	Peak
ref	Reference sample
s	Solid
sp	Standard sample
w	Container wall
1	Step 1
2	Step 2

List of Figures

List of Tables

CHAPTER 1 -INTRODUCTION

1.1 Overview

Research findings have indicated that buildings account for 40% of the world's energy consumption. This constitutes 30% of the annual greenhouse gas emissions (Building and Climate Change, 2009). The reduction of the energy consumption in buildings has been one of the priorities of the recent EU directives. The Energy Performance of Buildings Directive (EPBD) in 2002 requires all Member States of the EU to introduce a general framework and to set building energy codes based on the global building approach (Laustsen, 2008; Annunziata et al., 2013). This is followed by several other directives. The most energy consumption in buildings is associated to ventilation, heating and cooling systems (Lombard et al., 2008). The necessity of improving the energy efficiency of the built environment resulted in the development of various techniques of better usage and conservation of energy for heating and cooling (Diaconu, 2011). The use of solar energy for heating and night-time ambient air for cooling has been known for a long time in passive systems (Arkar et al., 2007).

Thermal Energy Storage (TES) is useful technology for improving energy efficiency and energy saving (Jeon et al., 2010). TES in buildings can be implemented by sensible heat (increasing and decreasing the temperature of the building envelopes, for example), or by latent heat (with the inclusion of phase change materials – PCMs – to increase thermal inertia) (Cabeza et al., 2011). PCMs are compounds that melt and solidify at a certain range of temperatures and in doing so are capable of storing and releasing large amounts of energy. A large number of PCM (organic, inorganic and eutectic) are available in several temperature ranges (Farid et al., 2004). Latent heat storage (LHS) including PCMs is one of the most efficient ways of storing thermal energy (Sharma et al., 2009), since they provide a higher storage density requiring a smaller temperature difference between storing and realising heat.

The application of latent heat storage system (LHTES) presents limitations including phase segregation, low thermal conductivity, subcooling, non-long-term stability, non-mechanical stability and corrosion with the encapsulation (Farid et al., 2004).

Intensive research has been carried out on improving the heat transfer of these materials. The heat transfer enhancement methods can be categorized mainly in three methods: i) embedding PCM into metallic structures/matrixes, ii) addressing compounds directly to the PCM storage and iii) use of multiple PCMs. The first two methods enhance the heat transfer through the use of materials with high conductive properties such as aluminium, graphite and carbon. The use of multiple PCM has been explored recently as an enhancement technique. This allows a higher temperature difference between the heat transfer fluid (HTF) and the PCM (Mosaffa et al., 2013). Therefore when different PCMs are used, a temperature difference will remain between the PCM and HTF along the flow direction promoting the heat transfer.

LHTES has been extensively studied in buildings through passive and active systems for free cooling of buildings. Free cooling is achieved by storing the night coldness and realising it during day time to achieve comfort indoor temperatures. Passive systems are described as systems that do not include electrical devices. They are related with the encapsulation of PCMs into building materials or structures such as walls (Chen et al., 2008 and Lee et al., 2015), floor (Xu et al., 2005), roof (Alawadhi and Alqallaf, 2011) and glass (Inglas, 2002). In passive methods HTF exchanges heat by natural means. In warmer climates passive ways may not operate as effectively and active systems are instead proposed. In active systems the HTF is actively moved (forced convection) exchanging heat with the PCM. Different designs of active systems namely ventilation systems with LHTES for free cooling can be found in the literature (Turpenny et al, 2000, Yanbing et al, 2003; Nagano et al, 2005; Arkar and Medved, 2007; Butala and Smith, 2009; Wakas and Kumar, 2011 and Evola et al. 2014). Research on heating has been mostly studied using auxiliary sources such as air conditioning (Vakilaltojjar, 2000) and solar collectors (Halawa, 2005).

The studies of LHTES included experimental testing and/or mathematical study. Most of the experimental studies on LHTES for free cooling applications investigated both the melting and solidification time and the air outlet temperature for different air inlet temperatures and velocities as in Zalba et al. (2004) and Osterman et al. (2015). Numerical or analytical methods of LHTES have also been reported in the literature. The enthalpy and effective heat capacity methods are presented as the most common numerical methods for the phase change of PCMS. Both methods have been

extensively used for the thermal performance analysis of LHTES units e.g. Raj and Velraj (2011) and Wang et al. (2015).

1.2 Statement of the Problem

Extensive research has been carried out on the performances of LHTES for free cooling applications. However, only a few comprehensive experimental or computational studies have been undertaken for LHTES integrating multiple PCMS (Liam et al., 1992; Farid and Khalaf 1994; Brousseau and Lacroix, 1996; Gong and Mujumbar, 1996; Aceves et al., 1998; Fang and Chen, 2007; Adine and Quarine, 2009; Rady, 2009; Huang, 2011; Mosaffa et al., 2014 and Wang et al. 2005). These studies combine the use of multiple PCM with heat recovery, solar energy, power plants and desiccant cooling applications. Mosaffa et al. (2014) investigated the potential of multiple PCMs for free cooling application relying on the daytime and night-time temperature difference. However, the study considered constant air inlet temperature and was therefore unrepresentative of the real climatic conditions. Hence, present research will address this shortfall in data and will provide a significant contribution to knowledge in the area of incorporating multiple PCMs for free cooling in buildings. This new data will provide a designing methodology for air-multi PCMs units. In addition, this research will establish facts such as, which parameters are important to use as data input in the numerical methods.

1.3 Aim and objectives

The project aims to develop an air- multi PCMs unit which will provide free cooling and ventilation for buildings, relying on the night and day air temperature difference during the summer time. In order to utilize efficiently the daytime and night-time temperature difference, the melting (i.e. discharging) time, solidification (i.e. charging) time and the air outlet temperature are the essential parameters in the thermal performance of the unit. Most precisely, the system must be designed in such way that within a certain time, both the completed charging and discharging of the PCMs and a desirable air outlet temperature should be achieved. Consequently the

system achieves its maximum efficiency. Hence, the aim of the current research will be accomplished by successfully completing the following objectives:

1) Conduct an exhaustive literature review on TES incorporating PCMs, especially on air- PCM units employed in the thermal conditioning of buildings, including experimental and numerical formulations to evaluate their thermal performance;

2) To investigate the influence of the air inlet temperature and velocity on the charging/discharging time, the air outlet temperature of an air-PCM unit, heating/cooling load and the effectiveness over the phase change;

3) To determine the thermophysical characteristics of the selected PCMs including phase change temperatures, specific heat and enthalpy values;

4) To stablish the most suitable numerical method between the enthalpy and effective heat capacity;

5) To undertake a parametric study of an air –multiple PCM unit to achieve the best solution (PCMs selection, encapsulation dimensions and air mass flow rates) for free cooling application under real climatic conditions and

6) To evaluate the potential of multiple PCMs for the free cooling and ventilation of buildings for a case study that will include an economic and environmental analysis of the proposed unit.

1.4 Research methodology

In order to accomplish the objectives, the proposed research strategies are listed below and summarised in Figure 1-1:

1) Design and construct an experimental facility to investigate the influence of air inlet temperature and velocity on the thermal performance of air-PCM unit;

2) Thermal characterisation of selected PCM by Differential Scanning Calorimetry (DSC);

3) 2D CFD model to calculate the PCM charging/discharging time and air outlet temperature obtained experimentally in 2) for the different air inlet conditions;

4) Extend the CFD model in 3) for multiple PCMs unit and conduct a parametric study based on the PCMs selection, geometry of the containers and air mass flow rate under real climatic data registered in Portugal and

5) Adapt the CFD model in 4) for a case study of free cooling and ventilation of an office building in Portugal.

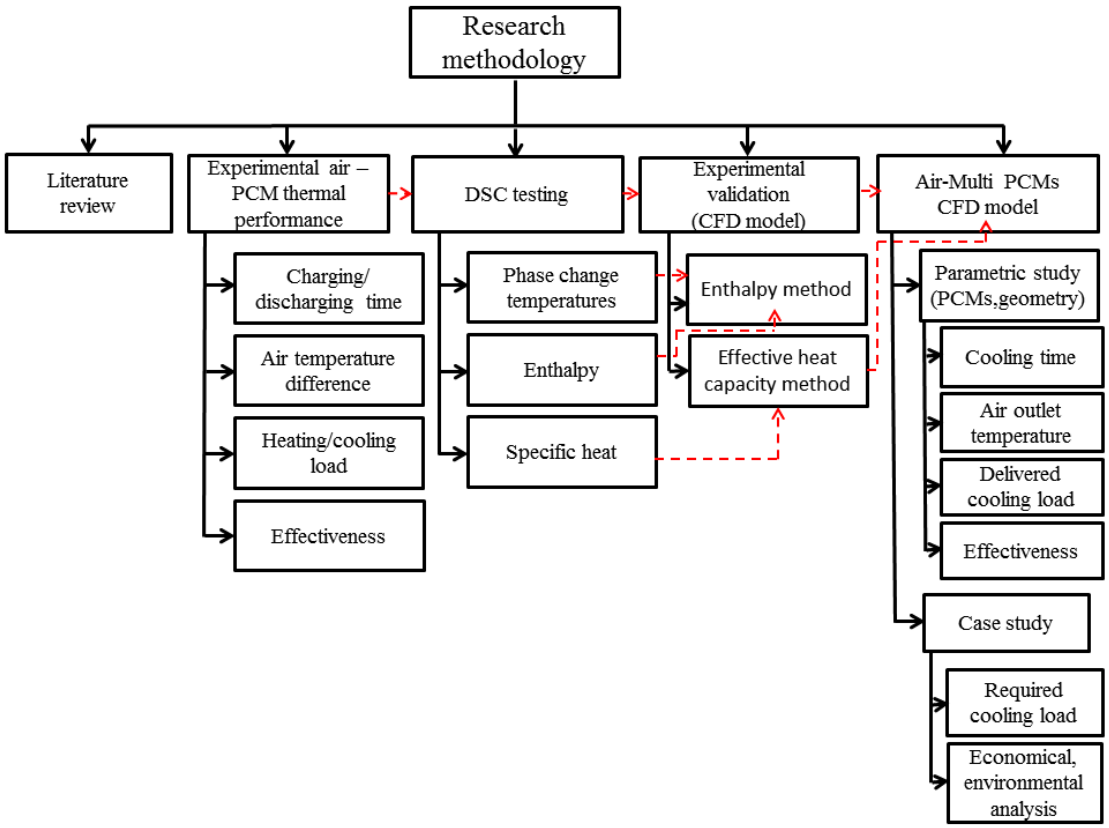

Figure 1-1 Research methodology

1.5 Thesis Outline

This thesis consists of seven chapters. The first chapter includes the introduction of the research scope, the aim and objectives, the research methodology and the outline of the thesis. Chapter Two presents an extensive literature review of general TES, specifically TES systems using PCMs and related application. In this chapter the PCMs are classified any problems associated to their use are identified. This chapter establishes the facts for identifying the most suitable PCMs and appropriate design for the intended application. Major applications of TES in buildings are identified as active air-PCM systems including a review on mathematical and experimental models used for this type of systems. This chapter identifies the knowledge gap and consequently informs the scope of the present work.

Chapter Three deals with the experimental testing of a lab-scale air-PCM storage rig. An experimental analysis is carried out for an air -PCM prototype and it is organized as follows. Firstly, the design of the air- PCM heat transfer unit based on selection of the materials is described. Then the geometry of the encapsulation and the dimensions of the PCM panels and air channels are established. This chapter also describes each component of the experimental rig, the measuring instruments and the experimental uncertainty. At the end, the experimental procedure is defined and results are discussed. This chapter intends to investigate the influence of the air inlet temperature and velocity on the charging/discharging time, inlet and outlet air temperature difference, cooling load and effectiveness over the phase change.

Chapter Four presents the Differential Scanning Calorimetry (DSC) testing carried out to determine the phase change temperatures, specific heat and enthalpy for the selected PCMs.

Chapter Five describes the development of a CFD model in order to validate the experimental results, namely the PCM and air outlet temperatures. The procedure includes the description of the geometry, mesh generation, materials properties, boundary and initial conditions, governing equations and model assumptions in order to calculate and evaluate the experimental transient temperatures of the air-PCM unit. Two models are suggested, the enthalpy method and the effective heat capacity

method. Both methods require the input of thermophysical properties of the selected PCMs and determined in Chapter Four.

The application of multi-PCM unit for free cooling and ventilation is evaluated in Chapter Six by using the verified CFD model for multi-PCMs. Firstly a parametric study is carried out in order to find the most suitable case for the required cooling time (i.e discharging time), the air outlet temperature and the charging time based on climate data for Portugal during Summertime. For that purpose, the PCMs selection, length and height of the PCM panels, and the air mass flow rates are investigated. The best performing solution is then further investigated to achieve the free cooling and ventilation of an office building located in Castelo Branco, Portugal. In addition an economic and environmental study is conducted to establish the benefits of the proposed unit to a convectional air conditioning unit.

Finally, Chapter Seven concludes the research work by describing the main outcomes of the research and provides recommendations for future work in this field.

In addition, Appendixes are attached at the conclusion of the thesis to provide more details and explanations for different sections.

CHAPTER 2 - LITERATURE REVIEW ON THERMAL ENERGY STORAGE

2.1 Introduction

The global contribution of commercial and residential buildings towards overall energy consumption has steadily increased. The building sector is known as a large contribution to CO_2 emissions, resulting in the significant environmental impacts of global warming and climate change. In 2010, building consumption (residential and services) in the EU was 59.12 % of overall final energy consumption, higher than industry (36.47%) and transportation (2.38%) (JRC, 2012). However there are significant changes in the energy consumption in the individual Member States, overall the residential energy consumption per capita in the EU in the years 2005 and 2010 in the EU-27 remained almost constant (JRC, 2012). Therefore, the reduction of energy consumed by buildings has been one of the priorities of the recent EU directives.

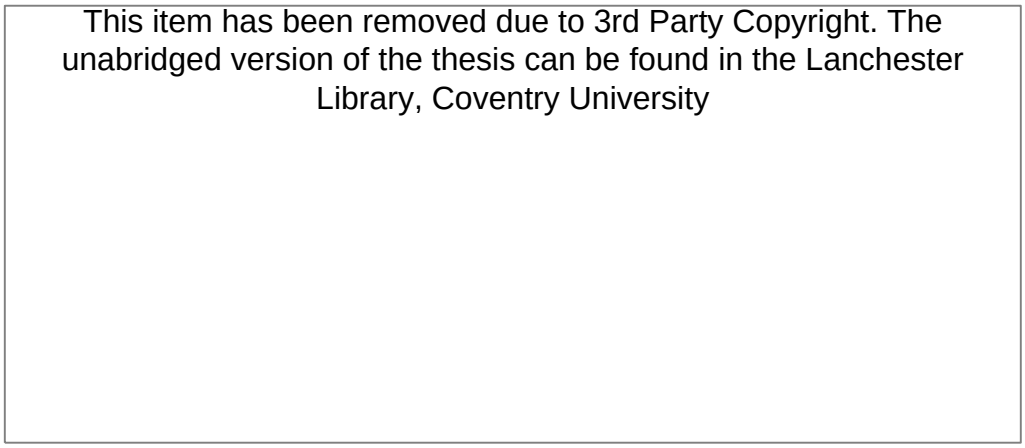

Figure 2-1 Final residential energy consumption per capita in the EU-27, 2005 & 2010. Source: Eurostat and JRC

The most energy consumption in residential buildings is associated with space conditioning and ventilation, domestic hot water and lightning, as it can be seen in Table 2-1. Heating, ventilation and air conditioning (HVAC) systems are the highest consumer of energy in building services. This represents approximately half the final energy use in the building sector, and between one tenth and one fifth of the energy

consumption in developed countries (Pérez-Lombard et al, 2011). In southern countries this accounts for more than 50% of the European market, creating serious supply difficulties during peak load periods (Pérez-Lombard et al, 2008).

Figure 2-2 Consumption by end use for different building types. Source: EIA (Pérez-Lombard et al., 2008)

Table 2-1 Energy consumption by end uses in the residential sector, 2009. Source: EIA

Actually, many developed countries are seeking solutions via renewable sources, but this figure is still well below the government's target of 15% of all energy to be generated in this way. Therefore, to achieve this goal it is necessary to enlarge the share of renewable and natural energy sources for the heating, ventilation and cooling of buildings by utilizing advanced buildings services systems (Arkar and Medved, 2007). The necessity of improving the energy efficiency of the built environment has resulted in the development of various techniques of better usage and conservation of energy for heating and cooling (Zalba et al., 2003). For the heating and cooling of buildings, heat recovery is significantly applied to reduce the energy consumption and CO_2 emissions. Also, traditional systems have accomplished a thermal store, which

plays an important role in the conservation of available energy resources and on the improvement of their use. The most common way to store solar energy is through large water tanks (sensible energy storage). However, recently an alternative method has been developed. These are LHS systems, in which thermal energy is stored as latent heat in substances undergoing a phase transition, e.g., the heat of fusion in the solid–liquid transition (Hamdan and Elwerr, 1996). These concepts lead to the categorization of TES mainly in two systems. One is the traditional sensible energy storage and another is using PCMs to achieve the LHS. LHS has been qualified as the most efficient way to store thermal energy with higher storage density and smaller temperature changes when storing and releasing heat (Farid et al., 2004 and Zalba et al., 2004). Solar energy and thermal storage has long been known for its passive design specifically using solar energy for heating and cold night-time ambient energy for cooling (Arkar and Medved, 2007). Recently, PCM has been popular in buildings through the combining of HVAC systems, supplied individually, then joined with construction materials in the construction wall, roof and ground. PCMs attract an abundance of research owing to three characters: the relative steady melting/freezing temperature in a certain range, the wide range of categories of PCMs such as organic, inorganic and eutectic with various of melting/freezing temperature and the high thermal density. There are different designs of ventilation systems with LHTES for free cooling found in literatures (Arkar et al., 2007). Free cooling is known as the process of storing the coolness of the night air to cool down the warm air during day time, presenting a better performance in places where the diurnal temperature range is greater than 15 °C. The different systems can be distinguished through their location within the building. Some studies propose them mounted in the ceiling (Turnpenny et al., 2000; Yanbing et al., 2003; Hed and Bellander, 2005 and Butala and Stritih, 2009) others in the floor (Takeda et al., 2004 and Nagano et al., 2005) and also near to the walls (Arkar et al., 2007 and Arkar and Medved, 2007). For heating applications a few systems are known. However they are combined it with auxiliary sources, such as air-conditioning (Vakilotjjar, 2000), solar collector (Halawa, 2005) or other heat sources such as electrical heaters (Farid et al., 1989).

2.2 Thermal Energy Storage (TES)

Among the various forms of energy, thermal energy is widely encountered in nature through solar energy, geothermal energy and thermally stratified layers in oceans (Fan and Khodadadi, 2011). Solar energy is a great source of energy since it's free, clean and potentially inexhaustible, but only available during the day. Therefore it is necessary to store this energy and reuse it when it is unavailable during night-time. Hence, it is necessary and important to develop efficient and inexpensive energy storage devices. There are two optimal reversible methods to storage heat and cold: physical processes and chemical processes (Butala and Stritih, 2009). Physical processes involve both sensible heat (SH) and latent heat (LH) and will discussed in this section.

2.2.1 Sensible Heat Storage (SHS)

SHS is the most usual way to store thermal energy, through increasing material temperature and then releasing the energy by decreasing the temperature. Therefore this process is not isothermal, as heat losses are increased due to the high temperature storage. SHS capability mainly depends on the specific heat capacity, mass and quantity of the material and also the change of the materials' temperature. The working substance of SHS can be liquids (water or oil) or solids (rocks, pebbles and refractorys). As indicated in the Equation 2-1 a multiple large number of energy storage requires a large amount of material that translate into significant requirements for space, insulation and economic costs.

The ratio of stored heat (ΔQ) to the mass (m) and temperature rise, (ΔT) is the specific heat (c_p) of the storage medium (Mehling and Cabeza, 2008).

$$\Delta Q = m.\, c_p.\, \Delta T \tag{2-1}$$

2.2.2 Latent Heat Storage (LHS)

LHS is based on the heat absorption or release when storage materials undergo a phase change (Sharma et al., 2009). This melting/ freezing processes occurs isothermally, as is shown for the heating and cooling cycle for phase change material

in the Figure 2-3. The procedure of thermal storage is to accumulate latent heat when hot/cold source is available and higher/lower than the melting/freezing temperature and then melting/freezing mode occurs due to the potential energy-difference. Melting and freezing processes can be incorporated together to realize the heating and cooling potential through night and day times. During the day time the thermal solar energy is charged and stored, which will be discharged for the purpose of space heating. The reverse process is applied to store coolness during the night-time, supplying cooling energy to the space in the day time. These storage systems are denominated as short-time storage, presenting some benefits such as less space requirement, less insulations and are more economical compared to large storage systems.

Figure 2-3 Phase change diagram for the phase change materials (source: http://www.chemicalonline.com)

Figure 2-3 shows the typical curves for the phase change materials for the heating and cooling cycles. For the heating cycle, the material undergoes through three phases: solid (sensible heat), melting (latent heat: solid-liquid) and liquid (sensible heat). And vice versa is observed for the cooling cycle. Each phase change uses vast amounts of energy that can be stored/ released. For instance, the heat of fusion for melting/freezing of a commercial paraffin (RT25) requires 148, 000 J/ kg and that can translate to a high storage density with latent heat. Table 2-2 list the different methods of heat storage (sensible and latent) through different materials. Through Table 2-2 it

can be seen that storage materials such as rock and water have a lower energy storage density compared with PCMs, hence they require more mass to store the same quantity of energy. PCMs also have an advantage in that thermal energy is stored and released at an almost constant temperature. Those can be significant advantages in many applications such as the domestic space heating and cooling.

Table 2-2 Comparison between the different methods of heat storage (Farid et al., 2004)

PCMs may undergo various physical and chemical transformations, accompanied either by the absorption or the release of heat:

i) Solid ↔ gas phase change;
ii) Liquid ↔ gas phase change;
iii) Solid ↔ solid transition;
iv) Solid ↔ liquid phase change;
v) Crystalline solid ↔ liquid solution transformation

Although the solid ↔ gas and liquid ↔ gas transformation experience the greatest heats in transition, this is accompanied by very large volume changes. These will complicate the containers' design and significantly impact upon the practicable of these processes. Solid ↔ liquid melting processes involve less volume changes, providing substantial energy storage capacity during the melting and solidification processes, thus presenting themselves as the most popular application in energy storage especially in the building sector. PCM can be incorporated in buildings either passively or actively as it will be shown further in section 2.7.

2.2.3 Storage Capacity of LHS

The storage capacity of latent heat is based not on temperature change, but in the phase change of the storage medium at a constant temperature (Beckaman and Gilli, 1984). The heat supplied upon melting is called latent heat and the process as LHS. There are small requirement of volume change involved and the stored heat is equal to the enthalpy difference

$$\Delta Q = m\,\Delta H \tag{2-2}$$

As the latent heat corresponds to the heat stored during the phase change process, it is calculated from the enthalpy difference ΔH between the solid and the liquid phase, known as phase change enthalpy, melting enthalpy or heat of fusion. If the melting is completed, further transfer of heat results again in the form of sensible heat storage

Solid-liquid PCMs

As previously discussed, latent heat is usually associated with the heat changing of the solid ↔ solid, solid ↔ liquid and liquid ↔ vapour phase changes.
The phase change from the liquid to the gaseous phase involves the largest latent heat. However, the volumetric storage capacity of the vapour phase is rather low, also the temperature of phase change depends on the boundary conditions being unsuitable for the storage of heat just through itself. Therefore, this type of latent heat storage has neither been used nor suggested (Beckaman and Gilli, 1984) and the terms "latent heat storage" and "phase change material" are commonly only used for the first two kinds of phase changes transformations and not for liquid-vapour phase transformation (Butala and Stritih, 2009). Solid ↔ liquid PCMs are practicable because they store a relatively large quantity of thermal heat over a narrow temperature range, without a corresponding large volume change.

The storage capacity of overall LHS is detailed in Beckaman and Gilli (1984). LHS is a constant pressure and mass system; the enthalpy increase of a solid/liquid system for $T_1<T_m$ to $T_2>T_m$ is

$$\Delta h = c_{p,m}\,(\mathrm{T_m} - \mathrm{T_1}) + \Delta H + c_{p,m}(\mathrm{T_2} - \mathrm{T_m}) \qquad (2\text{-}3)$$

with,

$c_{p,m}$specific heat capacity, melting phase (p=constant), J/kg. °C

Δh enthalpy of phase change (melting at T_m =constant), J/kg

The first term of the equation is the sensible part of the solid phase, while the second is related to the latent heat and the third, again to the sensible part of the liquid phase. Δh has different analogies for pure substances:

- For organic substances:

$$\Delta h = 0.7\ \mathrm{T_m} \qquad (2\text{-}4)$$

$$\rho\ \Delta h = \rho\ 0.7\ T_m \qquad (2\text{-}5)$$

where Δh is in kJ/kg, T_m in°C, ρ in kg/m^3 and ρ Δh in kJ/m^3.

- For inorganic substances:

$$\Delta h = \left(\frac{24}{M}\right) T_m \qquad (2\text{-}6)$$

$$\rho\ \Delta h = \left(\frac{24\rho}{M}\right) T_m \qquad (2\text{-}7)$$

where M is the molecular mass in kmol and ρ is in kg/m^3. For most substances ρ/M is of the order of 40.

2.2.4 Designing TES

For TES, independent of their type, several stages need to be followed in order to create a suitable system. Figure 2-4 displays a clear procedure to design a TES unit. The procedure can be divided into two sections. The left column is related to a full characterization of the material to be used as thermal storage, the right column the heat exchanger and their configurations. In practice a PCM storage system can be described as a heat exchanger, in which the heat transfer fluid exchanges heat with the PCM at the phase change temperature (Belusko and Bruno, 2008). The following section presents a review on PCMs, their classifications, their associated problems

and the requirements for choosing them. This will define and enable the left hand column steps. For the development of the heat exchanger development, sections 2.3.5 and 2.3.6 will be necessary.

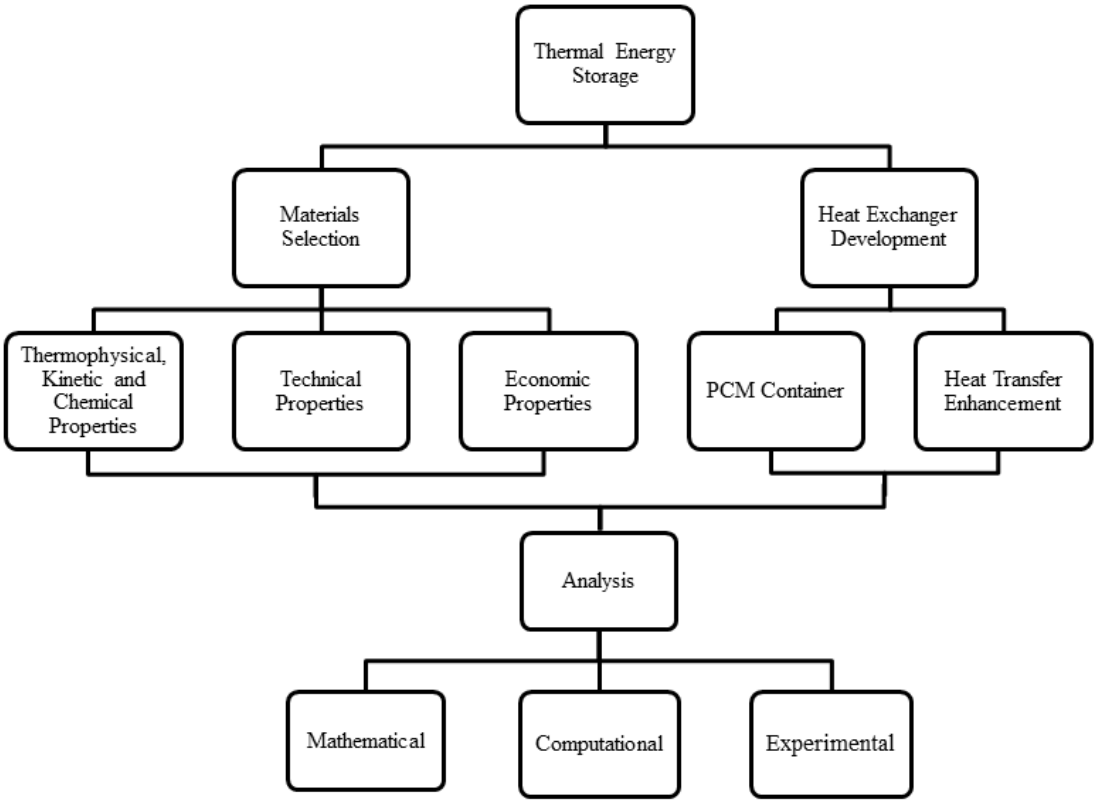

Figure 2-4 Designing Thermal Energy Storage

After defining the TES system, early stage experimental and mathematical models will be required to simulate the behaviour of the system. This will ensure that the correct technology is developed. For that purpose sections 2.4 and 2.6 reviews the experimental and numerical methodologies used for TES systems and in particular PCM-air based systems.

2.3 Phase Change Materials (PCMs)

2.3.1 Classification and properties of PCMs

PCMs are compounds which melt and solidify at certain temperatures and in doing so are capable of storing or releasing large amounts of energy. The commonly studied PCMs during the last 40 years have been salt hydrates, paraffin waxes, fatty acids and eutectics of organic and non-organic compounds (Farid et al., 2004). One of the first reviews on this subject was from Hasnain (1998). Solid ↔ liquid phase change materials are commonly used due their practical and suitable application and they may be divided into three groups: inorganic compounds, organic compounds and eutectics of inorganic and/or organic compounds. Figure 2-5 displays a clear structure to classify various PCMs used for different purposes in the industry. Organic PCMs can be subdivided into paraffin or fatty acids, the first one are the most common for buildings applications and are usually referred as "paraffin waxes". Paraffin waxes have a consistent characteristic in that the phase change temperature increases with the number of alkene chains in its composition (Sharma et al., 2009). They are very expensive and commonly a mixture of different hydrocarbon are used - technical grade paraffin (Hasnain, 1998). The different hydrocarbons will allow a larger temperature range of the phase change process compared with the pure paraffin wax. In building applications, salts hydrates are the most common inorganic compounds. These are alloys of inorganic salt and water, their phase change process essentially being the process of hydration and anhydration. Sometimes a third category is added (eutectics), which is a mixture of multiple solids in such proportions that the melting points is as low as possible. However, limited data is available on their thermal and physical properties (Baetens et al., 2010). There are several techniques to study the thermophysical properties of PCM, such as calorimetry, differential scanning calorimetry (DSC) and differential thermal analysis (DTA). Through these techniques it is possible to arrive at a deeper understanding of the different compounds and begin to know which are more suitable for the intended application. Figure 2-5 presents the most common organic compounds: paraffins as commercial grade or analytical grade, fatty acids and the hydrate salts as the most common inorganic compounds.

Figure 2-5 Classification of PCM (Ravikumar and Srinivasan, 2008)

All PCMs to be used in any application need to fulfil different thermophysical, kinetic and chemical properties as listed in Table 2-3. For the thermophysical properties (depending on the practical applications), melting temperatures is the prior consideration to select the suitable PCMs. Materials that melt below 15 °C are mostly used for storing coldness in air conditioning applications, while materials that melt above 90 °C are used for absorption refrigeration. All others materials that melt between these two temperatures may be applied in solar heating and for heat load levelling applications (Farid et al., 2004). The range of 0~65 °C is the most suitable choice for domestic heating/cooling (Agyenim et al., 2010). The same approach need to be considered for the other thermophysical properties such as the latent heat of fusion, specific heat, thermal conductivity and density. Independently of the type of application, the chosen PCM need to present desirable kinetic and chemical properties such as high nucleating rate, complete reversible cycles, no degradation and no corrosiveness with the container material. These aspects will be discussed in section 2.3.4.

Table 2-3 Thermophysical, Kinetic and Chemical requirements of PCMs (Tyagi V, Buddhi, 2007)

PCMs are also divided according to their melting characteristics. Figure 2-6 summarised the melting characteristics of the most commonly used materials. This can be used as the first scale plate for the melting/solidification temperature and for the melting enthalpy. In the Figure 2-6 (a), the salts and their eutectics mixtures are suitable for the storage of high temperature energy above 150 °C with the highest melting enthalpy. Salt-water eutectics are applicable for low temperature energy below 0 °C. Sugar-alcohols are used for the temperature of 100~200 °C. Salt hydrates and their mixtures i.e. gas hydrates, water and paraffins are proper for the temperature from 0°C to 100°C (ZAE Bayern, 2012). Previous researches and applications projects have indicated that inorganic compounds such as $KF.4H_20$, Mn $(NO_3)_2.6H_2O$, CaCl2.6H20 and $Na_2SO_4.10H_2O$. Similarly, organic compounds such as Capric acids, paraffin C16-C18, Dimethly sabacate and commercial compounds such as PCMs RT20, RT26, RT27, ClimSel C 23, ClimSel C 24, ClimSel C 32, S27, E17, E19, E21,

E30 are also frequently used for building energy purposes (Zalba et al., 2003). In some cases, the mixtures of different kind of PCMs may be utilized for specific applications requirements. The mass/volume specific melting enthalpies vary as the melting temperature increases. Figure 2-6 (b) shows the melting temperature for the most common organic and inorganic compounds. Paraffins have the widest melting temperature range followed by fatty acids and salt hydrates. All of them might be applied for building applications that normally require comfort temperatures around 20~25 °C. Figure 2-6 (c) displays the enthalpy per unit mass of commercial PCM in the range of 50,000~30,000 J/kg when the melting temperature increased from -40 °C to 120 °C (ZAE Bayern, 2012). However, the enthalpy per unit volume varies in a bigger range with the melting temperature increases. Therefore, the optimal selection of the category of PCMs for specific practical application should be based on these varying characteristics.

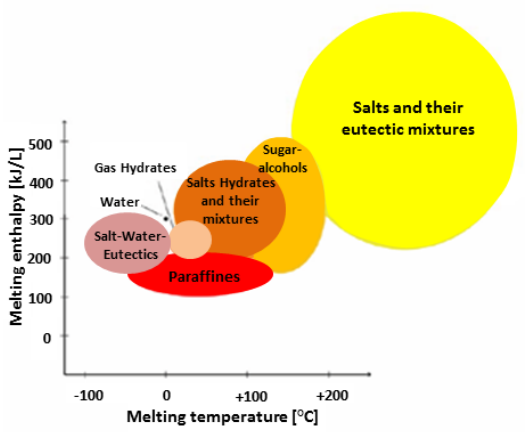

a) Melting temperature and enthalpy ranges (source: ZAE Bayern)

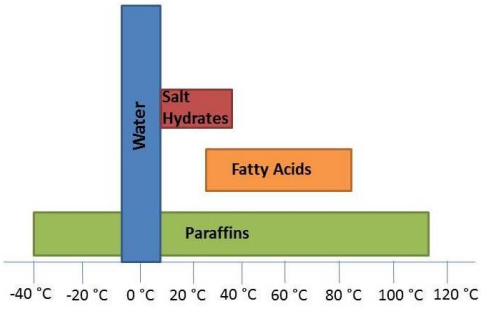

b) Principal PCM melting temperatures

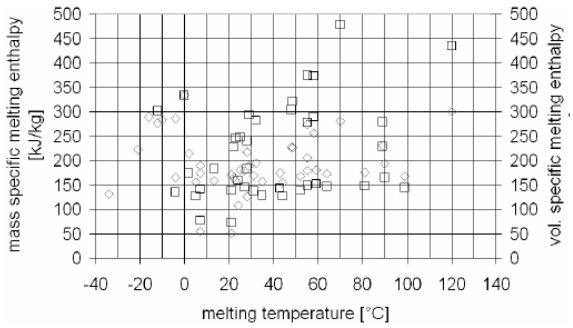

c) Phase change temperature and enthalpy per volume (□) and mass (◊) of commercial PCM (source: ZAE Bayern)

Figure 2-6 Classes of materials to be used as PCM with regard to their melting characteristics.

Table 2-4 is a useful tool to compare organic and inorganic materials for heat storage, allowing a simpler choice of the best materials depending on the proposed application. Zalba et al. (2003) concluded that the strongest strength of inorganic PCM is the greater phase change enthalpy, but to widely use this kind of PCM the barriers such as undercooling, corrosion, phase separation and segregation, and lack of thermal stability need to be overcome. Although, the organic PCMs present lower phase change enthalpy in addition to lower thermal conductivity and inflammability, their lack of corrosion, lower/non undercooling and chemical and thermal stability increases their practicable application.

Table 2-4 Comparison of organic and inorganic materials for heat storage (Zalba et al., 2003).

2.3.2 Commercial PCMs and suppliers

Many compounds have been named as potential PCMs, but not all of them are commercialised. The most commercial PCMs are based on materials from these classes: salt hydrates, paraffins and eutectic water-salt solution (Mehling and Cabeza, 2008). The main supply companies in the market of phase change heat and cold storage materials include Cristopia (France), TEAP Energy (Australia), Rubitherm GmbH (Germany), EPS Ltd. (UK), PCM Thermal Solutions (USA), Climator (Sweden), Mitsubishi Chemical (Japan), Doerken (Germany) and Merck (USA).

Appendix A lists the commercial PCMs within the range of – 10°C to 32 °C corresponding to an acceptable range of environmental temperatures in most of European countries and their potential for heating/cooling buildings. The majority of listed PCMs have a low price ranging from £6 to £9, even though the melting temperature and enthalpy vary in a relatively large range. Figure 2-7 presents different types of packages for PCMs from different commercial companies. Currently, the most common shapes for PCMs include plastic/metallic capsules and flat plates.

Figure 2-7 Commercially manufactured phase change heat storage products (Kensiarin and Mahkamov, 2007).

As described, the paraffins are subdivided into commercial grade and analytical (technical) grade. Commercial paraffin waxes consist of a mixture of mostly straight chain nalkanes CH_3–(CH_2)–CH_3 and the crystallization of the (CH_3)-chain releases a large amount of latent heat (Sharma et al., 2009). They are inexpensive with moderate thermal storage densities (~ 200,000 J/kg or 150 MJ/m^3) and a wide range of melting temperatures. In addition, they undergo negligible subcooling and are chemically inert and stable with no phase segregation. However, they present low thermal conductivity (~ 0.2 W/m °C), which limits their applications (Farid et al, 2004). Pure paraffin waxes are very expensive therefore only analytical grade paraffin may be used in TES (Farid et al, 2004). Salts hydrate are attractive materials for use in TES due to their high volumetric storage density (~ 350 MJ/m^3), their relatively high thermal conductivity (~ 0.5 W/m °C) and moderate cost compared to paraffin waxes, with few exceptions (Farid et al, 2004). However even with larger energy storage density and

higher thermal conductivity, they experience supercooling and phase segregation – requiring the use of some nucleating and thickening agent. In solving this kind of problems the thickened mixture reduces storage capacity of the PCM. This will be discussed in section 2.3.3. For a more extensive reading regarding PCMs, several review articles can be found such as Abhat (1983), Kürklü (1998), Zalba et al. (2003), Ravikumar and Srinivasan (2008), Tyagi and Buddhi (2007), Kenisarion and Mahkamov (2007), Hasnain (2008), Mehling and Cabeza (2008), Sharma et al. (2009), Agyenim et al. (2010), Raj and Velraj (2010), Tyagi et al. (2011), Cabeza et al. (2011), Zhou et al. (2012) among others, including the thermophysical data such as its melting point, heat of fusion, density and in some case its thermal conductivity.

2.3.3 Problems associated with PCMs

During the PCM selection procedure, potential issues should be evaluated after a comparison against a range of benchmarks including thermophysical aspects, kinetic and chemical properties and in addition to economic factors. Farid et al. (2004) identified that all PCMs involve undesirable thermophysical, kinetic and chemical properties listed in Table 2-5. They include low thermal conductivity (more often in paraffins), density change, stability of properties under extended cycling and sometimes phase segregation and sub cooling that is more often found in inorganic compounds.

Table 2-5 Problems associated to PCMs

Problems associated to PCMS	**Property**
Phase separation (or segregation)	Thermophysical
Low thermal conductivity	Thermophysical
Supercooling or subcooling (particularly for salt hydrates)	Kinetic
Long term stability	Chemical
Mechanically stability	Chemical
Corrosion of the materials and compatibility of the PCM with the container	Chemical

i) Phase separation (or segregation)

Phase separation occurs when two-component systems separate into two different phases after the melting and solidification. This problem is usually associated with inorganic PCMs, affecting the thermal behaviour of the material. Phase segregation of Glauber's salt was noticed in one of the first studies of the use of PCM for space heating - Telkes (1978). The author found that in the third winter the PCM had suffered from thermal degradation and proposed the use of thickening agents to address the problem of segregation in Glauber's salt. This technique was not shared by Abhat (1983) who argued that the heat storage of salt hydrates might still be unsuitable even with the use of additives. The other solution proposed by Telkes (1978) was to discuss thickening with clay, also being adressed by Farid et al. (2004). They claimed that the use of some thickening agents for example bentonite clay with the Glauber Salt, reduced the rates of crystallization and heat transfer to the salt due to the lower thermal conductivity. Furthermore, other methods were proposed, as introducing a certain amount of water to the PCM. According the research carried by El-Sebaii et al. (2009), although the extra amount of water had been added to the PCM during its thermal cycling, it did not prevent the phase separation problem that usually happens during melting process of most salt hydrates. This solution also reduced the storage density of the PCM system and required a large temperature swing in order to operate this system (Farid et al, 2004). Due to these divergences among the suggested solutions, the choice of the best solution should be carefully tested under several cycles. In recent years, the most common methods to solve phase separation problem include mixing, gelling or thickening the PCM (Mehling and Cabeza, 2008). Also, according to the same authors in order to prevent phase separation and to achieve a good cycling process, a new concept emerged, that of the eutectic mixture. These are mixtures of two or more constituents which solidify simultaneously from the liquid at a minimum freezing point (also called eutectic point).

ii) Low thermal conductivity

Latent heat storage systems, especially those employing organic materials have been reported to have a rather slow thermal response (Mettawee and Assassa, 2007). The

organic PCM typically has a thermal conductivity of 0.24 W/m °C or less compared to the inorganic PCM is 1.0 W/m °C. In the liquid phase, convection can significantly enhance heat transfer; however this is often insufficient (Mehling and Cabeza, 2008). In the solid phase, there is only conduction and therefore some studies were carried out to enhance thermal conductivity. This will be further discussed in section 2.3.6. Also, the inclusion of additives to the PCM will reduce or eliminate the convection in the liquid phase and therefore it is necessary to determine the best option for this issue (Mehling and Cabeza, 2008). Hence, the heat exchanger or the design of the PCMs containers is very important in order to fulfil free cooling requirements due to the low thermal conductivity of general PCMs (Lázaro *et al*., 2009).

iii) Subcooling

Subcooling or supercooling is the process by which a saturated liquid is cooled below the saturation temperature to ensure the completed phase transformation. This is another of the major problems of inorganic compounds. During the heat extraction process, the latent heat is not released until the melting temperature is reached due to the subcooling phenomenon (Mehling and Cabeza, 2008). If nucleation does occur, the latent heat will never be released and the only sensible heat is stored. The common approach to overcome the subcooling of the PCM is to add special additives, also called nucleator, to the PCM to induce heterogeneous nucleating. Although these nucleating agents can be added to PCMs to reduce this problem, they are frequently discovered by trial and error (Lane, 1981).

iv) Long term stability

El-Sebaii et al. (2011) describes that the used PCM must be stable, with repeated melting/solidification cycles and must show good compatibility with the container. Zalba et al. (2003) found that poor stability can be induced by two factors: thermal cycling and corrosion between the PCM and the container. Thermal cycling defines the life time of a system by analysing how thermophysical properties will change over repeated cycles. This assures that no-degradation should occur to the PCM material and especially its container over time. Thus, the thermal cycling must be directed towards the demonstration of physical and thermal stability, as the PCM will process

repetitive cycles of heating and cooling (Farid et al. 2004). Several thermal cycling tests were done in recent years to confirm the suitability of different thermal storages systems. One of the first studies was from Porisini (1988), where 5650 thermal cycles were carried out involving the repeated melting and freezing of a few salt hydrates. Only the two commercial $CaCl_2 \cdot 6\ H_2O$ showed good thermal stability after massively repeated thermal cycling. Tyagi and Buddhi (2008) also confirmed $CaCl_2$ $6H_2O$ as a promising PCM after conducting a thousand accelerated thermal cycle, showing small variations in the latent heat of fusion during the thermal cycling process. Shukla et al. (2008) found that the selected inorganic PCMs (NaOH, $NaB_4O_7.H_20$, $Fe(NO_3)_3$. $6H_20$ and Ba (OH). $8H_20$) were not found to be suitable after some cycles while thermal cycling, while organic PCMs that had undertaken up to 1000 thermal cycles had shown a gradual change in melting temperature and latent heat of fusion. Gibbs and Hasnain (1995) confirmed that the paraffins have excellent thermal stability as neither the cycles nor their contact with metals degrades their thermal behaviour (Farid et al, 2004). Also Sharma et al. (2002) indicated that paraffin wax and acetamide have shown reasonably good thermal stability for their melting temperature and for variations in the latent heat of fusion during the cycling process. From the several studies on thermal cycles, organic compounds in general and specially paraffin were considered suitable for TES unlike inorganic compounds such as salts hydrates.

v) Mechanically stability

Composites of a PCM and another material as a mechanically stable structure are often called shape-stabilized PCM (ss-PCM). An example is shape-stabilized paraffin, which can be produced by incorporating paraffin on a microscopic level into a supporting structure, such as high-density polyethylene (HDPE) (Mehling and Cabeza, 2008). Guobing et al. (2007) numerically studied the thermal performance of two PCM composites: mixed type PCM-gypsum and shape-stabilized PCM plates in a passive solar building in Beijing. The main conclusions were that the shape-stabilized PCM (ss-PCM) plates responded more quickly than the mixed type PCM gypsum and were more thermally effective in terms of utilizing the latent heat.

vi) Corrosion of the materials and compatibility with the container

Another disadvantage of PCMs as TES media is corrosion when in directly contact with metal piping, plates or housings (Farrel *et al*., 2006). The use of salt hydrates as PCM has this as one major inconvenience. The corrosion of the contact material has been studied by different authors including Lacroix and Voller (1990), Abhat et al. (1981), Hasnain (1998), Ismail and Batista de Jesus (1999), Khudhair and Farid (2004). Farrel et al. (2006) calculated the corrosion rate between two salt hydrates (E17 and C18) and a heat pipe constructed from copper onto aluminium fins. The main results were as follows. Pitting was not observed but oxidation was observed in the surfaces of the copper samples. Pitting corrosion was observed in the aluminium alloy samples in different levels, the least amount being observed in the E17 PCM samples. Porisini (1988) concluded that stainless steel was the most corrosion resistant of metals that includes carbon steel, aluminium alloys, and Cu, for use with salt hydrates, though copper was shown to have a corrosion zone that did not increase after long periods of time Farrel et al. (2006). The same was concluded by Oró et al. (2013). The most suitable metal to act as a cold storage container to encapsulate a PCM containing salts solution is stainless steel when compared with copper and carbon steel. This is due to their high corrosions rate and also because of the presence of precipitates and pH changes. Also, García-Romero et al. (2009) tested the corrosion behaviour of four aluminium alloys: EN AW 2024, 3003, 6063, and 1050 in contact with a commercial Glauber ´s salt ($Na_2SO_4 \cdot 10\ H_2O$). Results indicate that the Al 2024 alloy is not compatible with this material due to the extended formation of $NaAlCO_3 \cdot (OH)_2$ in contact with air. The aluminium alloys 3003, 6063 and 1050 showed to be fully compatible with the material of $NaAlCO_3.(OH)_2$. However, not only inorganic compounds (salt hydrates) show corrosion, organic PCMs can also have a negative impact, such as changes to the plastic properties (Mehling and Cabeza, 2008). Werner et al. (1987) found that polyethylene could not be used with paraffin wax and that fatty acids softened polypropylene. Thus later, Castellón et al. (2011) studied the compatibility of high density polyethylene (HDPE) and low density polyethylene (LDPE, RIBLENE, FM34) with some commercial organic PCMs. Results showed that polyethylene immersed in organic PCM exhibited a PCM

absorption by the plastic, but that immersion in inorganic PCMs did not affect the thermal behaviour.

2.3.4 Summary: Requirements for choosing PCM

As described in section 2.2.4, the first step should be the selection of the PCM based on the desired melting temperature. Usually materials with a melting temperature below 15 °C are used to store coolness in air conditioning applications; while those with a melting temperature above 90 °C are used for absorption refrigeration. Other melting temperatures between these two can be applied in solar heating and for heat and load levelling applications (Farid et al., 2004). Next, the selected PCM needs to present desirable thermophysical, chemical and kinetic properties as listed in Table 2-3. The materials to be used as TES must present large latent heat and high thermal conductivity. They must possess a melting temperature lying in the practical range of operation also they should melt congruently with minimum supercooling and be chemically stable. Be low in cost, non-toxic and non-corrosive (Farid et al., 2004). The most appropriate technical and economic requirements as listed in Tables 2-6, 2-7 and 2-8 must then be defined. The technical requirements involve pressure, chemical stability, compatibility with other materials and safety constrains. Finally the economic requirements which are in respect of price and recyclability.

Table 2-6 Physical requirements for PCM selection

Requirements	**In order to**
Suitable phase change temperature	Assure storage and release of heat in an application with given temperatures for heat source and heat sink
Large phase change enthalpy	Achieve high storage density compared to sensible heat storage
Cycling stability (reproducible phase change)	PCM storage and the release of the heat as many times as required by an application. If there is phase segregation, phases with different composition are separated from each other microscopically, translating a lower capacity to store heat
Little subcooling	Assure that melting and solidification can proceed in a narrow temperature range
Good thermal conductivity	Be able to store or release the latent heat in a given volume of the storage material in a short time. It strongly impacts the application and the design of the storage
High density	Storage effectiveness per unit volume

Table 2-7 Technical requirements for PCM selection

Requirements	In order to
Low vapour pressure	Reduce requirements of mechanical stability and tightness on a vessel containing PCM
Small volume change	Reduce requirements of mechanical stability on a vessel containing the PCM
Chemical stability of the PCM	Ensure long lifetime of the PCM if it is exposed to higher temperatures, radiation, gases, etc.
Compatibility of the PCM with other materials	Assure long lifetime of the vessel that contains the PCM, and the other surrounding materials in the case of leakage of the PCM
Safety constraints	The construction of a storage can be restricted by laws that require the use of non-toxic, non-flammable materials

Table 2-8 Economics requirements for PCM selection

Requirements	In order to
Low price	Be competitive with other options for heat and cold storage, and to be competitive with the heat and cold methods
Good recyclability	For environmental and economic reasons

2.3.5 PCM containers

As presented in Figure 2-4, once the most suitable PCM is selected due to its thermophysical, technical and economic properties, the next step is to define the PCM container. The selection of the container is related to the practical application such as the boundary conditions, the contact heating/cooling fluid, the available space and also the potential geometry. In the process of the material selection, the corrosion of the material discussed in section 2.3.3 needs to be taken into account. Contrary to inorganic compounds, organic compounds present low corrosion and therefore a large range of materials are suitable for use. Only polyethylene was found in the literature to present corrosion with this organic PCM. On the other hand, as the organic compounds, usually present lower thermal conductivity compared to inorganic compounds, metallic containers are used to enhance the heat transfer. It has been published that steel shows the highest energy storage, although aluminium presents a

much higher thermal conductivity than rock within the first 6.5 hours (Aly and El-Sharkawy, 1990). Subsequently it appears that the higher energy storage presented by the rock material in comparison to aluminium might be happening due to the degradation of the aluminium material. Aluminium is not recommended because of the appearance of pitting and bubbles on its surface when in contact with certain PCMs. This could cause changes in material properties such as holes in the container (Oró et al., 2013). Regarding the geometry, PCMs are typically placed either in cylindrical, rectangular and packed bed macro-containers or in spheres micro-container as presented in Table 2-9. Rectangular containers are being widely used not only due to their easy manufacturing process but mostly because of the high storage density of PCM which can be up to 90% of the total volume (Belusko and Bruno, 2008). In a spherical PCM heat exchanger the PCM volume per total system volume can be as low as 50% (Bédécarratas et al., 1996). The literature also presents another type of container, the packed bed. Packed bed is characterised as a volume of porous media obtained by packing particles of selected material into a container (Singh et al., 2010). Table 2-9 lists the property of some solid materials that can be used in the packed bed storage. The geometry selection should not only concern in how the PCM itself will be stored but most importantly in how to the heat transfer can be enhanced due the low thermal conductivity of most of the PCMs. These characteristics are one of the key elements in thermal storage systems. They define the thermal performance of this kind of system such as the charge/discharge time of the PCM. This will be discussed in more detail in 2.3.6.

Table 2-9 Typical PCM containers

Container	Shapes	85 Published researches	Percentage	
			Individual	Total
Macro-container	Cylindrical	Shamsundar and Srinivasan, 1978; Solomon, 1979; Abhat, 1983; Lecomte and Mayer, 1985; Prakash et al.,1985; Hirata and Nishida, 1989; Farid and Kanzawa, 1989; Choi and Kim, 1992; Bansal and Buddhi, 1992; Lacroix, 1993; Hasan, 1994; Esen, 1994; Hamdan and Elwerr, 1996; Chow et al.,1996; Gong and Mujumdar, 1997; El-Dessouky and Al- Juwayhel,1997; Velraj et al., 1999; Horbaniuc et al.,1999; Ismail,2000; Zivkovic and Fujii,2001; Ismail et al.,2001; Sari and Kaygusuz, 2002; Ismail and Silva,2003; Hamada et al.,2003; Fukai et al.,2003; Jones et al.,2006); Jian-you, 2008; Sharma et al., 2009; Agyenim et al.,2010	33.7%	
	Rectangular containers	Shamsundar and Sparrow,1975; Morrison and Abdel-Khalik,1978; Patankar,1980; Zhang and Bejan,1989; Costa et al.,1991; Costa et al.,1998; Laouadi and Lacroix,1999; Vakilaltojjar,2000; Vakilaltojjar and Saman, 2001; Silva et al.,2002; Bruno and Saman, 2002; Stritih,2004; Halawa,2005; Halawa et al.,2005; Saman et al.,2005; Marín et al.,2005; Zivkovic and Fujii, 2001; Ye et al.,2001; Zalba et al.,2004; Zukowsky,2007; Vynnycky and Kimura,2007; Belusko and Bruno,2008; Lázaro et al.,2009; Amin et al.,2009; Butala and Stritih,2009; Halawa et al.,2010; Dolado,2011; Dolado et al.,2011; Waqas and Kumar,2011; Halawa and Saman,2011	38.4%	87.2%
	Packed bed	Garg et al.,1985; Naumann and Emons,1989; Jotshi et al.,1992; Dumas et al.,1994; Bédécarrats et al.,1995; Zhang et al.,2001; Kousksou et al.,2005; Benmansour et al.,2006; Cheraltathan et al.,2007; Kousksou et al.,2008; Bédécarrats et al.,2009	15.1%	
Micro-container	Spheres	Farid and Kanzawa,1989; Kürklü et al.,1996; Esen and Ayhan,1996; Gong and Mujumdar, 1997; Arkar and Medved,2007; Dubovsky et al.,2011); Raj and Velraj, 2011; Liu and Wang,2006; Ettouney et al.,2006; Regin et al.,2006; Arkar et al.,2007		12.8%

2.3.6 Heat transfer enhancement methods

Most phase change materials have low thermal conductivities, requiring heat transfer enhancement techniques to improve their rates of charging and discharging energy (Agyenim et al, 2010). One of the first reviews on heat transfer enhancement in latent heat storage system was from Velraj (1998), who divides the enhancement technique into fins configurations and other configurations.

Metallic structures and graphite appears in the literature as the most commonly used materials for the heat transfer enhancement techniques. There are different ways to associate them with thermal energy storage. One is the embedding of the PCM into metallic matrixes. Others are the embedding of high conductive structures into the storage medium and use of multiple PCMs. Therefore in the present study the heat transfer enhancement techniques are divided into three main groups: embedding the PCM into metallic structures/matrixes, addressing compounds directly to the PCM storage and using multiple PCMs.

The most common materials used as heat transfer enhancements are aluminium, copper, nickel, stainless and carbon fibres due to their high thermal conductivity (Aly and El-Sharkawy, 1990). These materials might be applied as various forms: containers, matrixes, fins, honeycombs, brushes, etc. A summary of the different techniques are presented in Table 2-10.

i) High conductivity structures/ matrixes

Generally, the containers are filled with a PCM allowing it to transfer heat to a moving fluid medium that passes through the container. There are different geometries: rectangular, cylindrical and packed bed as mentioned in 2.3.5.

Metallic and Graphite Matrixes

Embedding of the PCM in the metal matrix is a common technique that enhances the heat transfer. The major studies related to the use of metallic matrixes involve aluminium and graphite as the applied material. For the first case, an example in Jong and Hoogendoorn (1980) shows how an aluminium matrix structure was used and in turn, induced a reduction of the solidification time. Also, Tong et al. (1996) used an

aluminium metal matrix resulting in a remarkable enhancement with small volume fractions. However it was found that the increase of the volume fraction did not enhance linearly the heat transfer. Bugaje (1997) applied the same technique and obtained enhancement effects on freezing times. For this technique, Zalba et al. (2003) references a few advantages such as higher heat conductivity in the PCM without much reduction in energy storage and a lower subcooling of salt hydrates and also smaller volume change in paraffins. PCM-graphite composites are mentioned as one of the most suitable ways to increase the thermal conductivity. It can be trough PCM-graphite matrix or PCM-graphite compounds (Mehling and Cabeza, 2008).
Marín et al. (2005) used a porous matrix of graphite where the PCM was embedded. This option allowed that the plates could be 70% thicker and the power consumption of the fans was decreased by 50%. Py et al. (2001) presented new supported paraffin impregnated by a capillary forced in a compressed natural graphite matrix (CNEG). Composite PCM/CENG was found to be equivalent to those of the sole graphite matrix (4~70 W/m°C) instead of the 0.2 W/m°C of the pure paraffin, reducing the solidification time. Several other research studies were completed employing graphite matrixes to strengthen the heat transfer efficiency of TES systems such as Tayeb (1996), Satzger and Eska (1997), Mehling et al. (1999), Satzger and Eska (2000), Mehling etc. (2000). However an intrinsic problem of a graphite matrix is its anisotropy, in that the thermal conductivity depends on the direction (Zhao et al., 2010).

Finned Tubes

The applications of finned tubes have been proposed by various researches as an efficient mean to improve the thermal performance of TES systems. Different studies investigating the influence of finned tubes in the melting and solidification of PCMs can be found in the literature listed in Table 2-10. Stritih (2004) concluded that heat storage (melting) is not a problem for the thermal storage applications, however the extraction of heat (solidification) can be effectively enhanced by fins. Jong and Hoogendoorn (1980) used finned cooper tubes to improve the heat transfer of a pure eicosane ($C_{20}H_{42}$). The proposed enhancement technique allowed a significant decrease in the solidification time. Costa et al. (1997) developed a theoretical model to calculate thermal performance and natural convection during the melting and

solidification of 7 aluminium rectangular PCM containers that were heated by an electrical heater. The magnitude of the melt fraction with fins was found to be considerable, dominating the melt fraction when no fin was used. The uses of finned tubes show a significant improvement in heat transfer rate, although the high cost of the finned tubes may make their application uneconomical. This is because such arrangements may improve heat transfer significantly only when a liquid is used as a HTF, because in an air based system the heat transfer coefficient of both the air and the PCM side is low (Farid et al., 2004). Also several authors such as Stritih (2004) verified that the natural convection, which is dominant during melting, was reduced because of the fins. However, the heat transfer during solidification is greater if fins are included in this case a 40% reduction in the solidification time was calculated.

Honeycomb Filler

Abhat (1976) designed and investigated a PCMs-based with honeycomb filler. Aluminium was the chosen material for both the containers and the honeycomb filler material. The aluminium acted as heat path between the two surfaces (heated and insulated) allowing the melting to initiate on both sides. The same enhancement technique was applied by Jong and Hoogendoorn (1980) including aluminium honeycombs (10% volume fraction) and aluminium thin-strip matrices (0.1; 0.8; 1.6% volume fraction). Again, this technique reduced the solidification time. The thermal conductivity of the enhanced PCM apparently also increased. Recently, several studies discussed the use of heat pipes to increase the heat transfer rates to or from the PCM as listed in Table 2-10.

Heat Pipes

Turnpenny et al. (2000) constructed a LHS unit incorporating heat pipes embedded in a PCM. Besides, which only a limited study tested this technique experimentally as Robak et al. (2011). In this study, the inclusion of heat pipes increased the PCM melting rates by approximately 60% while the fins were not as effective. Also, during the solidification, the heat pipes doubled the energy between the heat transfer fluid (HTF) and the PCM relatively to the fins.

Carbon Fibres

Fukai et al. used carbon fibres to enhance paraffin wax thermal conductivity in (2000), (2002), and (2003), respectively. For the first study in 2000 (Fukai et al., 2000), the application of the carbon was randomly included. Later fibre brushes were employed as reported in Fukai et al. (2002 and 2003). The fibre brushes presented higher effective thermal conductivity because the heat flows along the fibre brush direction. Nakaso et al. (2008) explored the application of carbon fibre cloths with copper tubes of a shell-and-tube type heat exchanger to enlarge the heat exchange area and enhance the thermal conductivity of a LHS unit. However, as the fibres lay parallel to the copper tubes it did not affect the heat transfer. The same author also investigated experimentally the use of carbon fibre cloths in the heat transfer tubes of TES tanks. The results show that by using only 0.4% volume of fibre cloths, the heat exchange rate has improved significantly in the tanks.

ii) High conductivity particles

Recent studies suggested enhancement could be achieved by adding certain compounds or particles into the PCM. The major advantage of adding high conductive particles is the increase of heat conductivity within the PCM without any significant reduction in energy storage. By reviewing the present studies, this technique is categorized by the use of aluminium powder, metallic pieces and a composite of PCMs with graphite, as listed in Table 2-11. The addition of the metal Ni of 5% volume fraction within the PCM was investigated and the mixture was encapsulated in a cylindrical capsule. This technique was able to enhance the thermal conductivity of the original PCM (Chow et al.,1996). From the research carried out by Zhong et al. (2010), it is found that the thermal diffusivity of the paraffin-graphite foam can be enhanced by 190, 270, 500 and 570 times compared with pure paraffin. Siegel (1977) used salt dispersed with high conductivity particles. However in improving the heat transfer rate there is a compensating effect due to the reduction in volume fraction occupied. Another proposed technique was the embedding of aluminium powder in the PCM (Mettawee and Assassa, 2007). It was found that the useful heat gained increased when adding aluminium powder in the wax as compared to the case of pure paraffin wax.

Table 2-10 Different techniques to enhance heat transfer in PCMs

Techniques trough geometry	Authors'	Images
Metallic (aluminium) matrix structure	Jong and Hoogendoorn,1980; Kamimoto et al., 1985; Kamimoto et al., 1986; Khan and Rohatgi, 1994; Tong et al., 1996; Bauer and Wirtz, 2000; Tyagi and Buddhi, 2007	
Graphite matrix structure	Tayeb, 1996; Satzger and Eska, 1997; Py et al., 2001; Mehling et al., 1999; Satzger and Eska, 2000; Mehling et al., 2000	
Honeycomb structure	Bentilla et al., 1966; Hoover et al., 1971; Abhat, 1976; Pal and Joshi, 1998	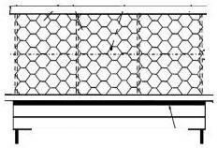
Finned tubes	Shamsundar and Srinivasan, 1978; Jong and Hoogendoorn, 1980; Abhat et al., 1981; Henze and Humphrey, 1981; Sparrow et al., 1981; Smith and Koch, 1982; Eftekhar et al., 1984; Padmanabhan and Murthy, 1986; Morcos, 1990; Sadasuke and Naokatsu, 1991; Lacroix, 1993; Chow et al., 1996; Zhang and Faghri, 1996; Velraj et al., 1997; Costa et al., 1998 Velraj et al., 1999; Turnpenny et al., 2000; Ismail et al., 2001; Sreeniraj and Velraj, 2002; Butala and Stritih, 2009	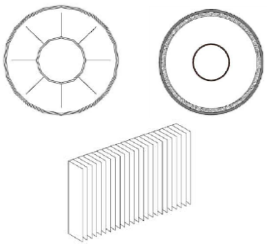
Heat pipes	Turnpenny et al., 2000; Liu and Wang, 2006; Shabgard et al., 2010; Robak et al., 2011	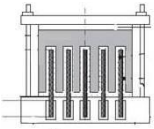
Carbon fibre	Fukai et al., 2000; Fukai et al., 2002; Fukai et al., 2003; Nakaso et al., 2008	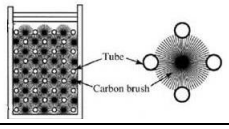

Table 2-11 Techniques trough PCM composition

Embedding high conductive particles	Authors'
Aluminium powder	Hoover et al., 1971; Mettawee and Assassa, 2007
Metallic pieces	Siegel, 1977; Chow et al., 1996; Velraj et al., 1999; Hafner and Schwarezer, 1999; Ettouney et al., 2006
Composite of PCM with graphite	Vakilaltojjar, 2000 Xiao et al., 2001; Zhong et al.,2010

iii) Multiple phase change materials

Recently another technique has been suggested in the literature that should enhance the heat transfer performance of TES systems: the use of multiple PCMs. For PCM containers in contact with a fluid medium it is known that the heat transfer rate in the TES systems depends strongly on the temperature difference between the heat transfer fluid (HTF) and the PCM. If a single PCM is used the temperature difference between the PCM and HTF will decrease along the flow direction. However if multiple PCMs are arranged, a temperature difference will remain between the PCM and the HTF along the flow direction promoting the heat transfer rate (Mosaffa et al., 2013). Figure 2-8 displays the temperature profile for single and multiple PCMs. Moreover the increase of heat transfer rate can lead to decrease in the volume and mass of the TES, and consequently the economic investment (Cui et al., 2003).

Multiple PCMs have been reported in the literature as a means to enhance TES systems, showing the following advantages:

- Increase in the heat transfer rate during charging/discharging process especially when change of phase is occurring (Seeniraj and Narasimhan, 2008)
- Maintain a higher driving temperature difference for the heat transfer process in charging and discharging processes (Chiu and Martin, 2012);

- Faster charging and discharging process (Wang et al., 2001)
- Maintain nearly constant heat flux from the PCM to the HTF (Mostaffa et al., 2013) and
- Higher storage capacity and higher melt fraction can be achieved (Fang and Cheng, 2007).

However, not much work has been done yet in multiple PCMs. A few studies have been carried numerically (Chiu and Martin, 2013; Mosaffa et al., 2014 and Wang et al., 2015), experimentally (Peiró et al., 2015) and experimental and numerically (Rady, 2009) as further detailed in sections 2.4 and 2.6

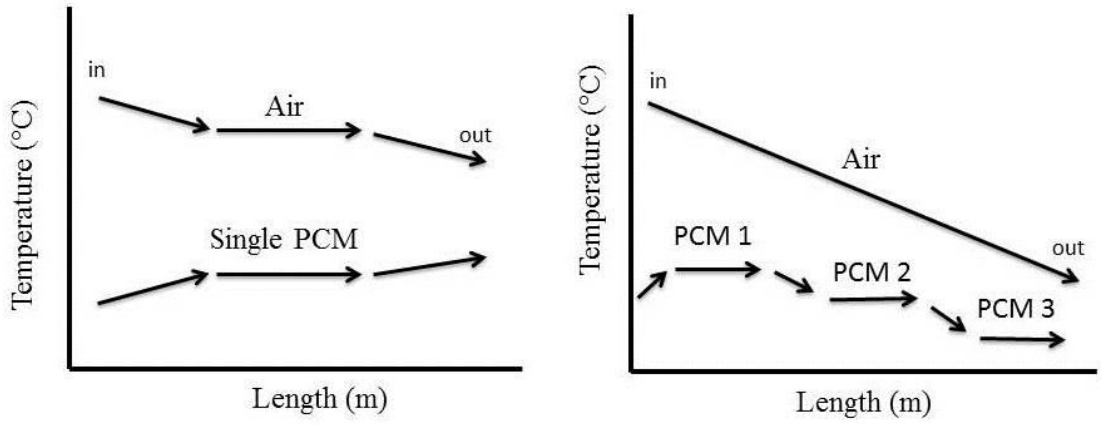

Figure 2-8 Single PCM (left) and multiple PCMs (right) temperature profile for the discharging process

TES using PCMs require careful design owing to the low thermal conductivity of PCMs. It must be ensure that the encapsulated PCMs completely melt in a desired time by choosing suitable physical geometry and dimensions. Therefore, after defining the most suitable PCM and the proper heat exchanger with a potential enhancement technique, the first prototype will be developed. The following stage is to either numerically and/or experimentally analyse and evaluate the prototype. A review follows on the mathematical, computational and experimental studies on PCMs encapsulated in a rectangular container with air fluid as the heat or coolness source.

2.4 Mathematical formulation on air- PCM TES systems

Mathematical models are widely used to obtain appropriate solutions for the thermal behaviour and maximization of the performance through optimal designing the TES systems. For TES applications, mathematical methods are a useful tool to solve the following:

- Heat transfer during melting and solidification of the PCM, evaluation of the temperature distribution inside the PCM, interface transient location, and the effect of natural convection in the molten zone (Agyenim et al., 2010);
- Moving boundary problems (Vakilaltojjar,2000; Halawa, 2005);
- The overall thermal performance, system heat capacity, charging and discharging rates and storage temperature (Agyenim et al., 2010);
- Optimization of the system, controlling the parameters such as diameter/thickness, length and spacing of the PCM tubes/layers which could be costly and time-consuming to be determined by experiments (Kürklü et al., 1996; Laouadi and Lacroix, 1999; Vakilaltojjar, 2000; Vakilaltojjar and Saman, 2001; Halawa, 2005).

The design of the heat exchanger containing the PCMs requires quantitative analysis regarding the phase change process within the PCM and also the heat transfer rate absorbing from or releasing to the heat sources. Hence, through mathematical models it is possible to obtain heat transfer rates, boundary temperatures, solidified/melted fraction, and interface position all as function of time. Designing TES requires quantitative analysis regarding the phase change process within the PCM and also the heat transfer rate to the heat transfer fluid. The problem of the phase change of PCMs falls into the category of moving boundary problems (Zukvovic and Fujii, 2001). In the phase change process a boundary is noticed separating the material in its liquid and solid phase. This boundary changes with time, depending on the speed at which the latent heat is absorbed or released at the boundary. The moving boundary problem is difficult due to its inherent non-linear nature at moving interfaces for which displacement rate is controlled by the latent heat lost or is absorbed at the boundary (Dutil et al., 2011). This problem was noticed when studying the thickness

of ice and therefore the problem of freezing is commonly denominated as the "Stefan problem". In such problem the main issue is to understand the evolution of the boundary in movement, X(t). The energy equation at the soli-liquid interface given by Stefan is

$$L\rho\left(\frac{dX(t)}{dt}\right) = k_s\left(\frac{\delta T_s}{\delta t}\right) - k_l\left(\frac{\delta T_l}{\delta t}\right) \quad (2\text{-}8)$$

where L is the latent heat of fusion of the substance, k_s and k_l the thermal conductivity of the material in the solid and liquid phase respectively, T_s the temperature when the material is in solid phase ($T_s < 0$ °C) and T_l the temperature when the material is the liquid phase ($T_l > 0$°C). The heat conducting material occupies the domain $-\infty < x < \infty$ where the liquid phase fills the domain $0 < x < \infty$ and solid $-\infty < x < 0$. At $x = 0$ the material is maintained at a constant temperature $T < 0$ °C and the solidification occurs isothermally at $T_m = 0$ °C (melting temperature). This approach is related to pure conduction in a semi-infinite medium, but it was followed by other studies where natural convection was also considered (Regin et al., 2006). The solution of the Stefan problem may be achieved through analytical or numerical formulation as presented in Figure 2-9. For the analytical formulation the most common method is called the Neumann method and for the numerical formulation the enthalpy method and effective heat capacity methods are used. These methods will be described through the next section.

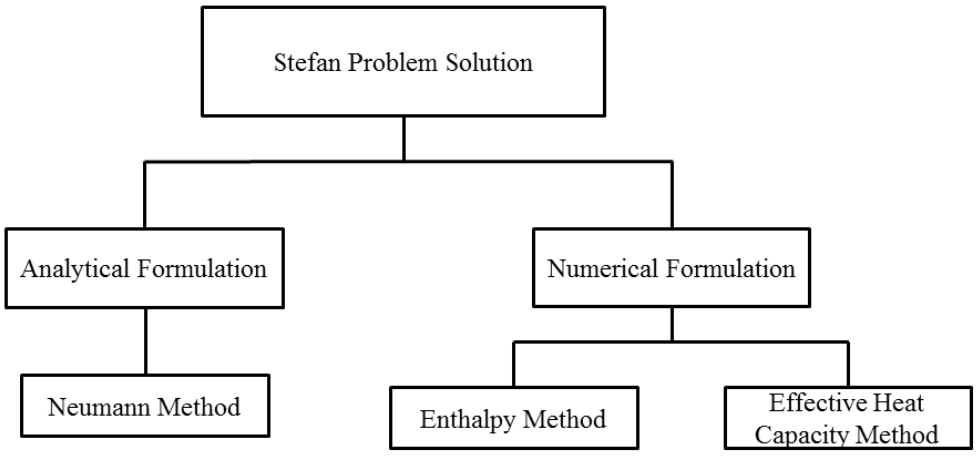

Figure 2-9 Stefan Problem solutions

2.4.1 Analytical formulation

The most common solution to solve the Stefan problem is the solution from Neumann for the semi-infinite region. This method is presented in Carslaw and Jaeger (1959) and will be transcribed here. The outcomes of this method are the interface location (X), solid phase temperature (T_s) and the liquid phase temperature (T_l). For a semi-infinite region x>0 initially at a constant temperature T_i which is grater that the melting-point, and with the surface x=0 subsequently maintained at zero temperature. An approximation which is frequently made consists of neglecting the heat capacity of the material between x = 0 and the surface separation, that is, of assuming that the flow through this region is of a steady type. Contrary, there are no available exact solutions for other regions such as the slab –a< x <a with its surface maintained at zero, or for the region –a< x < a initially liquid and $|x|$ > initially solid.

The solution to the Stefan Problem is the temperature distribution T(x,t) and the interface location X(t) that depends on the derivation of the Neuman Solution. The general Neuman's Solution of melting and solidification in one-dimension presents two boundary conditions and the differential equation of the heat transfer.

The first boundary condition to satisfy the surface separation between solid and liquid phase at X(t) is

$$T_s=T_l=T_m \qquad \text{when } x= X(t) \tag{2-9}$$

The second boundary condition is related to the absorption and liberation of latent heat at this surface.

$$L\rho \frac{dX}{dT} = k_s \frac{\partial T_s}{\partial x} - k_l \frac{\partial T_l}{\partial x} \tag{2-10}$$

It can be seen through these two boundary conditions that if at any distance, x located before the interface location (x< X) the state is liquid at T_l(x, t) and if located after the interface (x > X) the state is solid at T_s (x, t). Considering curves of constant temperature T_s(x, t) = T_m = T_l (x, t) in the xt-plane, Equation 2-9 becomes

$$\frac{\partial T_s}{\partial x} dx + \frac{\partial T_s}{\partial t} \partial t = 0 = \frac{\partial T_l}{\partial x} dx + \frac{\partial T_l}{\partial t} dt \tag{2-11}$$

and Equation 2-10 can be written thus:

$$k_s \frac{\partial T_s}{\partial x} - k_l \frac{\partial T_l}{\partial x} = -L\rho \frac{\partial \mathrm{T_s}/\partial \mathrm{t}}{\partial \mathrm{T_s}/\partial \mathrm{x}} = -\mathrm{L}\rho \frac{\partial \mathrm{T_l}/\partial \mathrm{t}}{\partial \mathrm{T_l}/\partial \mathrm{x}} \quad (2\text{-}12)$$

In these form the non-linearity of the problem is apparent. For a linear flow the temperatures T_s and T_l in the solid and liquid regions have to satisfy the following.

$$\frac{\partial^2 T_s}{\partial x^2} - \frac{1}{k_s}\frac{\partial T_s}{\partial t} = 0 \quad (2\text{-}13)$$

$$\frac{\partial^2 T_l}{\partial x^2} - \frac{1}{k_l}\frac{\partial T_s}{\partial t} = 0 \quad (2\text{-}14)$$

These equations are valid for other cases with the addition of other fixed boundaries within the region as:

- For region x>0, initially liquid at constant temperature T_i with the surface x=0 maintained at zero for t>0
- Melting in the region x>0
- The region x>0 initially liquid and the region x<0 solid
- Melting in the region x>0 caused by hot solid in x<0
- Melting range

Moreover Carslaw and Jaeger (1959) presented the solid and liquid interface (X) for the first case: region x>0, initially liquid at constant temperature T_i with the surface x=0 maintained at zero for t>0 as

$$X = 2\lambda(k_s t)^{\frac{1}{2}} \quad (2\text{-}15)$$

Hence, a numerical constant, λ need to be determined from the remaining Equation (2-10). The detailed procedure can be found in the Carlslaw and Jaeger (1959). When λ has been found, T_s and T_l can be determined bellow:

$$T_s = \frac{T_m}{\text{erf}\,\lambda}\,\text{erf}\frac{x}{2(k_s t)^{1/2}} \tag{2-16}$$

$$T_l = T_i - \frac{(T_i - T_m)}{erfc\ \lambda\ (k_s/k_l)}\,erfc\ \frac{x}{2(k_l t)^{1/2}} \tag{2-17}$$

where, erf and erfc correspond to error function solutions. A simple scheme of Neuman's solution procedure to determine the temperature distributions T_s and T_l and the interface location X is presented below (Figure 2-10).

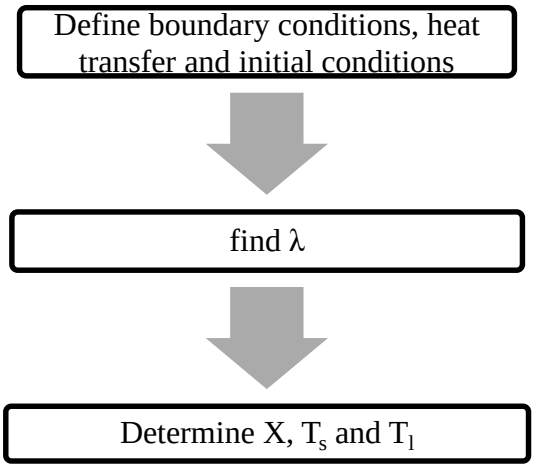

Figure 2-10 Procedure scheme of Neuman's solution

However, analytical formulations are generally applied for one dimension and only in a limited number of scenarios. Numerical models are currently used to evaluate phase change in two or three dimensional geometries, failing to explicitly track the phase change boundary in some cases.

2.4.2 Numerical formulation

Apart from the few analytical solutions most problems are necessarily tackled by numerical methods. Numerical methods have this advantage in that they take into account the variations in the thermal properties of temperatures usually involved in melting and solidification problems. Hence, these methods mathematically link the heat storage capacity described by specific heat (c_p), enthalpy (H) and the temperature (T). The most common numerical methods are the enthalpy method and the effective

heat capacity method. For the first method, the presence of the moving interface in the mathematical model is eliminated and the problem is made equivalent to one f nonlinear heat conduction without phase change (Shamsundar and Sparrow, 1975). A description of both methods can be seen in this section.

- Enthalpy formulation

Several researches have proposed numerical models to deal with the Stefan problem. The enthalpy method developed by Voller (1990) is one of the most commonly applied methods due to its advantage of the implicit treatment of the conditions on the phase change boundary. This means that a numerical treatment can be carried out on a fixed grid facilitates the arrangement with complex geometries (Agyenim et al., 2010). This method is used in a particular way so that the only unknown variable is the enthalpy-temperature dependency of the phase change material H (T), and the solidification occurs at a uniform temperature (Sharma et al. 2009). Therefore the calculation of the temperature distribution and the rate of melting and solidification is indispensable. Voller (1990) proposed a simple one-dimensional solidification problem using an implicit scheme. The implicit scheme is generally selected due its ability to accommodate a wide range of the Stefan number (Ste) – ratio of sensible heat to latent heat.

The first step is a definition of the enthalpy formulation for a conduction controlled phase change. Energy equations in terms of enthalpy can be expresses as follows:

$$\frac{\partial H}{\partial t} = \nabla . (k \nabla T) \tag{2-18}$$

The solution of this equation requires knowledge of the enthalpy-temperature functional dependency – H (T). H (T) is related to the sum of the sensible enthalpy and the temperature in terms of the local liquid fraction, f_l and the latent heat L as

$$H(T) = \int_{T_m}^{T} \rho \ c_p \ dT + \ \rho \ f_l \ L \ dT \tag{2-19}$$

The liquid fraction formed during melting process of the material is given as

$$f_l = \frac{T - T_s}{T_l - T_s} \tag{2-20}$$

and the liquid fraction- temperature relationship is given by

$$f_l = \begin{cases} 0 & if\ T < T_s\ (solid) \\ \frac{T - T_s}{T_s - T_s} & if\ T_s < T < T_m (mushy) \\ 1 & if\ T > T_l (liquid) \end{cases} \tag{2-21}$$

The H (T) for an impure substance is as shown in Figure 2-11 (Zalba et al., 2003). Such a representation is valid only for materials that change phase over a range of temperatures (Shamsundar and Sparrow, 1975) and that correspond to most of the commercial PCMs available.

There are 3 regions, the solid phase, mushy phase and liquid phase obtained by replacing the liquid fraction defined in Equation 2-21 into Equation 2-19, the enthalpy of PCM and are written as:

$$H = \int_T^{T_s} \rho\, c_{p,s}\, dT \qquad T < T_s (solid) \tag{2-22a}$$

$$H = \rho\, \frac{T - T_s}{T_l - T_s}\, L \qquad T_s < T < T_l\ (mushy) \tag{2-22b}$$

$$H = \int_{T_l}^{T} \rho\, c_{p,l}\ dT + \rho \frac{T - T_s}{T_l - T_s} L \qquad T > T_l (liquid) \tag{2-22c}$$

Equation 2-22a represents the sensible enthalpy that characterizes the first step when a substance is heated. Equation 2-22b represents the liquid fraction formation in the beginning of the phase change process and Equation 2-22c describes the complete phase change process where sensible heat and liquid fraction prevail at the same time.

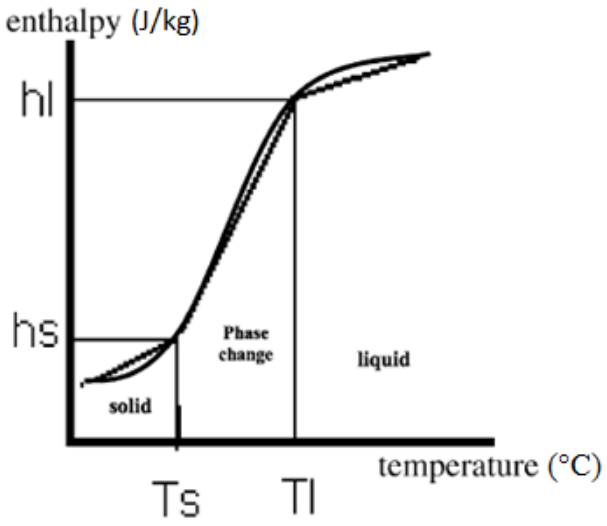

Figure 2-11 Enthalpy variation with temperature (Zalba et al., 2003).

- Effective Heat-Capacity Method

The energy equation in terms of effective heat capacity is achieved by replacing $\frac{\partial \mathrm{H}}{\partial \mathrm{t}}$ by $\mathrm{c}_{\mathrm{eff}}\frac{\partial \mathrm{T}}{\partial \mathrm{t}}$ into the energy conservation equation Equation (2-18)

$$\mathrm{c}_{\mathrm{eff}}\frac{\partial \mathrm{T}}{\partial \mathrm{t}} = \nabla(\mathrm{k}\nabla^2\mathrm{T}) \tag{2-23}$$

As for the enthalpy method, it is necessary to declare local values of the material specific heat for the characteristics points of the curve obtained from the measurements. The C_p (T) curves can be obtained using Differential Scanning Calorimetry (DSC) analysis. The C_p (T) relation is

$$c_p = \begin{cases} c_{p,s}, & T < T_l \\ c_{eff}, & T_l \leq T \leq T_s \\ c_{p,l}, & T > T_s \end{cases} \tag{2-24}$$

The effective heat capacity of the material (c_{eff}) during the phase change is directly proportional to the stored and released energy and also to the specific heat capacity (Lamberg, 2004) and it is described in the following equation

$$c_{eff} = \frac{L}{(T_l - T_s)} + \frac{c_{p,s} + c_{p,l}}{2} \quad (2\text{-}25)$$

A review of mathematical models of rectangular PCM- air heat exchangers that employ different methods are listed in Table 2-12. For most of the studies, the thermophysical properties of the selected PCMs were considered to be independent of temperature but different for solid and liquid states within majority of the studies. Some studies did not taken into account the sensible heat that is predominant in the beginning of the process of melting/solidification and others ignored the natural convection within the melted PCM. Reported results from the numerical methods appear to show that they offer a good approach to solving the phase change problems, although most of the available solutions to phase change problems apply to one or two-dimensional systems, due to the complexity of the equations involved in the phase change (Agyenim et al., 2010).

There are several mathematical models regarding the thermal performance of PCM-air based systems. These models study various thermal storage geometries such as spheres and flat slabs. They may be placed vertically or horizontally. For the first case mathematical models are presented in the literature for further reading: Farid and Kanzawa (1989), Kürklü et al. (1996), Esen and Ayhan (1996), Gong and Mujumdar (1997), Arkar and Medved (2007), Raj and Velraj (2011), Dubovsky et al. (2011). However, in this review the numerical models for flat panels will also be discussed as this will be applied to this research. As mentioned in section 2.3.5, flat panels present up to 90% high storage density of PCMs compared with 50% for the spherical type. Rectangular geometry requires nearly half the melting time as a cylindrical container of the same volume and heat transfer area (Zivkovic and Fujii, 2001). Also for this configuration the heat transfer in the PCM can be controlled through the choice of thickness (Bardon, et al., 1979). The processes of phase change are symmetric in relation to both sides and provoke less pressure drop in the air (Zalba et al., 2004). Intensive research on mathematical formulation for rectangular PCM-air heat

exchangers are reported in literature such as in Morrison and Abdel-Khalik (1978), Shamsundar and Sparrow (1978), Hadmand and Elwerr (1996), Küklü et al. (1996), Laouadi and Lacroix (1998), Costa et al. (1991, 1998), Zivkovic and Fujii (2001), Vakilaltojjar and Saman (2001) and Dolado et al. (2006). This approach was also used for heat transfer enhancement of TES units by Costa et al. (1998), Zukowski (2007) and Silva et al. (2002). Despite the existence of several published papers analysing heat transfer and change of phase, the modelling of TES systems by latent heat continues to be a challenge (Zalba et al., 2003).

Table 2-12 Review on PCM-air heat exchanger mathematical models

Method	Dimensional	Aims	Assumptions of the model	Validation	Ref.
Neumann Solution	2D	Investigate the effect of the design parameters on the thermal storage performance	PCM supercooling effects are neglected; axial conduction of the PCM and the fluid is negligible; The heat capacity of the fluid is ignored; heat capacity and axial conduction of the container walls are negligible; natural convection in the liquid portion of PCM is ignored	Exp.	Vakilaltojjar, 2000
	2D	Predict the temperature profile during solidification	The thermophysical properties PCM are independent of temperature; The value of density for the PCM is chosen as the mean of the values of the solid and liquid materials; The solidification process is isothermal	-	Halawa, 2005
Effective Heat Capacity Method	1D	Solve the liquid fraction and temperature of the nodes of the PCM	The physical properties of the liquid and solid phases can be different but the properties within a phase are constant. Axial conduction is negligible, temperature variations normal to the flow direction are negligible, the heat losses to the surroundings are negligible, and heat capacity of the heat transfer fluid is negligible	Exp.	Halawa et al., 2010
	3D	Analyse the heat and mass transfer in a ventilation duct filled with encapsulated PCM	PCM is homogenous and isotropic; Heat flux is isotropic on the whole PCM capsule area Thermal conductivity and density of the PCM are different for the solid and liquid phase; Thermal capacity of unit's casing is neglected	Exp.	Zukowsky, 2007
	-	How the PCM heat exchanger unit can be modelled to fit into indoor climate and energy simulation software	Thermophysical properties of the PCM are constant; specific heat varies with temperature.	Exp.	Hed and Bellander, 2006
	2D	Outflow and heat transfer studies for the fluid flowing through the tube in the heat exchanger module and air spacer kept in the top and bottom of the module in conjunction with transient heat transfer analysis for the PCM encapsulated in the shell portion of module	The fluid domain is considered to be incompressible; density, specific heat and thermal conductivity are considered to be constant for the heat transfer fluid; density and thermal conductivity of the PCM are considered to be constant for solid and liquid phase; latent heat value of the PCM is approximated with the apparent heat capacity using the results obtained from the DSC analysis and experimental phase change temperature range.	Exp.	Raj and Velraj 2011
	2D	Energy and exergy analyses are performed for a free cooling system using a LHS unit employing multiple PCMs	Temperature variations normal to the flow direction are neglected; thermophysical properties of PCMs are independent of temperature but differ between solid and liquid phases; the air velocity profile is fully developed; the effect of the natural convection is negligible.	Exp.	Mosaffa et al., 2014
	1D	A possibility to employ latent heat of fusion in PCMs for TES in air-based solar thermal systems	No convection was considered, no voids in the PCM were considered in the simulations.	Exp.	Charvát et al., 2014
	2D	Optimization study of a PCM-Air heat exchanger as well as the development of load shifting solutions which take into account the thermal comfort of the occupants and the indoor air quality	Thermophysical properties of the PCM constant apart from specific heat. The modes takes into account advection, conduction and convective transfers and heat storage within the PCM.	Exp.	Mankibi et al., 2015

Table 2-13 Review on PCM-air heat exchanger mathematical models (continuation)

Method	Dimensional	Aims	Assumptions of the model	Validation	Ref.
Enthalpy Method	1D	Analyse the LHS system for space heating with and without fins	The thermophysical properties of the PCM and fin material are independent of temperature; The PCM is homogenous and isotropic. For 1-D, the effects of fins are considered negligible. For 2-D, the mode of heat transfer is conduction only; all PCM sub-units are identical and independent of each other	-	Costa et al., 1998
	1D	Assess the thermal performance of a ventilated panel heating	The phase change conduction dominated; convection in the melt accounted for by defining an equivalent thermal; conductivity of the liquid phase;	Exp.	Laouadi and Lacroix, 1999
	1D	Numerical analysis of the melting time	Thermal conductivity of the PCM in the direction of the HTF flow is ignored; the effects of natural convection within the melt are negligible	Exp.	Zivkovic and Fujii, 2001
	2D	Transient thermal behaviour of storage	Same as Saman et al.(2005) including the variation of the temperature of the PCM's internal and boundary nodes and also the natural convection in the melting process	Exp.	Halawa et al., 2005
	3D	Develop a enthalpy-based computational model for PCM-encapsulated heat sinks	The thermophysical properties of the phase change material are independent of temperature; the phase change material is homogenous and isotropic; the material is assumed to be thick in the z direction, so that a two-dimensional analysis can be applied; Thermal resistances across the walls confining the phase change material is neglected	Anal.	Liu and Majumdar, 2006
	1D	Simulate the thermal performance of a real scale PCM-air heat exchanger	Only conduction heat transfer inside the PCM plate in a normal direction to the air flow rate; symmetry assumption	Exp.	Dolado et al., 2011
	2D	Simulate and find out the optimum design for plate type storage filled with PCM material which is used in night ventilation systems	PCM and air flows are considered to be unsteady and laminar, the viscous dissipation term is considered negligible.	-	Darzi et al., 2013
	2D	Validation study of CFD models used to predict the effect of PCM clay boards on the control of indoor environments, in ventilated and non-ventilated situations	Non-linear enthalpy temperature relationship and hysteresis for the PCM modelling. Conduction and convection were considered. Air assumed as ideal gas.	Exp.	Gowreesunker and Tassou, 2013
	2D	Model the charging behaviour of a heat exchange devices with a zigzag configuration containing multi-phase change materials	Only conduction heat transfer inside the PCM plate in a normal direction to the air flow rate; Symmetry assumption	Exp.	Wang et al., 2015

From the studies reported in Tables 2-12 and 2-13 the following assumptions were considered in order to simplify the mathematical model without introducing significant error in the calculating of the temperature variation within the PCM and air:

- Thermophysical properties of the PCM material are independent of temperature but can be different for the liquid and solid phases (Costa et al., 1998; Halawa, 2005; Hed and Bellander, 2006; Liu and Majumdar, 2006; Halawa et al., 2010, Mosaffa et al., 2014);
- Specific heat relationship specified with temperature (Hed and Bellander, 2006; Raj and Velraj, 2011 and Mankibi et al., 2015) and enthalpy relationship with temperature (Gowreesunker, 2013; Gowreesunker and Tassou, 2013);
- Thermal resistance across the containers walls can be neglected (Zivkovic and Fujii, 2001; Zukowsky, 2007; Liu and Majumdar, 2006);
- For flat thin containers the effects of natural convection within the liquid PCM is ignored (Costa et al., 1998; Laouadi and Lacroix, 1999; Vakilaltojjar, 2000; Zivkovic and Fujii, 2001; Dolado et al., 2011; Mosaffa et al., 2014; Charvát et al., 2014, Wang et al., 2015) and
- The fluid domain is considered to be incompressible. Density, specific heat and thermal conductivity are considered to be constant (Raj and Velraj, 2011)

However, other assumptions resulted in a deviation between the numerical and experimental results such as neglecting the sensible heat. Bruno and Saman (2002) noticed that the heat transfer rate during the first hour was higher than the calculated by the model through failing to take into account the sensible heat and the natural convection.

2.5 Computational modelling on air – PCM TES systems

There are several commercial programs associated with energy simulation of buildings. These can simulate the thermal performance of TES systems with PCM such as EnergyPlus, TRNSYS, PCM express and others. These softwares may be useful for TES systems where PCMs are applied in building structures such as walls, floors or ceilings. Even though they do not present modules for the direct simulation

of PCMs, they include algorithms for PCM walls. TRNSYS software has been used to simulate the thermal behaviour of the designed space using PCM in construction such as Type 232 Ibáñez et al., 2005, Type 241 (Halawa and Saman, 2011), Type 204 (Dolado, 2011). Kuznik et al. (2010) developed a new TRNSYS named Type 206 to model the thermal behaviour of an external wall with a PCM, which was validated by the experimental data from the literature. EnergyPlus software was used by Barbour and Hittle (2005) and Pedersen (2007). However for independent TES systems numerical models continue to be needed. Most of the authors developed firstly a numerical code using FORTRAN, Maltlab, and C++ etc. and then imported them into the pretended software. An example is Arkar and Medved (2007) where a numerical model was developed to determine the optimum phase-change temperature and to form the temperature-response function. This model was then integrated into TRNSYS and analysed. Also Amin et al. (2009) used TRNSYS to calculate the energy storage density factor, defined as the critical objective in TES design, through a previously developed theoretical model. Recently, Computational Fluid Dynamics (CFD) have been used to study different PCM-air heat exchangers, although the subcooling phenomenon is not taking into account (Mehling and Cabeza, 2008). Commercial CFD codes are FLUENT and COMSOL multiphysics. Chiu and Martin (2013) Mosaffa et al. (2014) investigated the potential of multiple PCMs while modelling the phase change with COMSOL multiphysics. Ye et al. (2011) used FLUENT software which allowed the investigation of the fluid flow and heat transfer in a plate-fin unit applied for rapid heat storage/release by paraffin. Dolado (2011) developed a fluid dynamics model using FLUENT to solve all the conversation equations (mass, energy and moment) taking directly into account effects of the natural convection within the PCM.

The enthalpy method due to its numerous advantages and its common usage in the phase change study, is available in FLUENT software (ANSYS package) denominated as the Solidification and Melting model. In the recent years significant research has been carried out using the Solidification and Melting model and useful agreements have been obtained with the experimental results (Shatikian, 2004; Assis et al., 2007 and Shmueli et al., 2010). However there are limitations associated to this model, specifically via the lever rule (assuming that the enthalpy-temperature relationship is linear, the melting and solidification of the enthalpy-temperature relationship is therefore similar) (FLUENT, 2010). In other words, modelling in

FLUENT does not provide the flexibility to vary the enthalpy temperature relationships and the possibility of introducing temperature hysteresis (Susman et al., 2011). This limitation presented discrepancies between the experimental and numerical results (Susman et al., 2011; Egolf and Manz, 1994; Kuznik and Virgone, 2009). A solution was proposed by Gowreesunker (2013), treating the melting and solidification separately and by using specific enthalpy-temperature relationships of melting and solidification within the simulations. This was achieved through the addition of a heat source in Equation 2-18 to mimic the melting and solidification process. The solution calculates the energy stored/released directly from the temperature in the form of a user defined function (UFD). This eliminates the dependency of the enthalpy function on the lever rule and provides a more flexible approach. Therefore it corresponds to a semi-empirical method, requiring the experimental enthalpy-temperature relationship. The results showed an improved agreement with the experimental results over the default FLUENT results. Chiu and Martin (2012) proposed the enthalpy method through use of the specific heat capacity (c_p). This integration was considered appropriate since the phase change of the considered PCM occurs over a temperature range. Comparison of the numerical and experimental results shows accordance within 5% difference in terms of charge and discharge time in thermal cycling (Chiu and Martin, 2012). Lamberg (2004), compared the results obtained by enthalpy and effective heat-capacity formulation for two different thermal energy storages. One with internal fins and one other without fins. The author concluded that the most precise method was the effective heat-capacity. The effective heat-capacity method can also be applied to FLUENT by adopting the general energy equation. It should be further improved by coupling the cp- temperature relationship obtained commonly from the differential scanning calorimetry analysis (DSC) (Raj and Velraj, 2011 and Diarce et al., 2014). It should be noted that the scanning rate of the DSC analysis should be carried out based on the cooling rate/heating rate of the selected application, in order to obtain the correct phase change temperature range of the selected PCM (Raj and Velraj, 2011). Otherwise, there will be a difference in the temperature at which the phase change occurs, and any theoretical results may not match with the real application results (Raj and Velraj, 2011).

Overall for air-PCM heat exchangers the main challenge is the optimization of the system. Through numerical simulations it is relatively easy to perform parametric studies analysing the influence of various design and operation parameters (Charvát et al., 2014).

2.6 Experimental models on air – PCM TES systems

Different experimental apparatus were suggested in the recent years for air- PCMs TES systems. Most of the studies for building applications were related to TES in order to provide free cooling during day time in summer. There are two scales testing: laboratory tests and real life tests. For the laboratory experiments, the main purpose of the results is the validation of the mathematical model undertaken. Practical air-PCM TES can then be designed and applied into the real project. The real life test is more to evaluate the practical performance of the applied air-PCM TES and to induce the experiences for further application. Within both scales of experiment testing, the apparatus involves the measuring of the air velocity or air flow, of the outlet air temperature (after the TES unit) when the inlet air temperature is varied (the variation can be performed under controlled conditions in an environmental chamber or through real data) and the temperature within the PCM. These parameters can be measured by different types of anemometers and thermocouples and recorded by a data logger for further analysis.

2.6.1. Laboratorial scale experiments

The laboratorial sale experiments intend to calculate the major parameters influencing the thermal performance of the storage systems for different design conditions. Furthermore they are adapted numerically to the intended scale of study. Most of the air-PCM heat exchange studies listed in Tables 2-14 and 2-15 were experimentally validated. However, this conversion is only acceptable if none of the working conditions are omitted. Vakilaltojjar (2000) tested experimentally two sets of PCMs ($CaCl_2 \cdot 6H_2O$ and $KF \cdot 4H_2O$) enclosed in flat bags and conical capsules. For the flat bags, in general, the results of experiments with the materials encapsulated in these flat containers showed consistency with those obtained from the computer model,

except when the supercooling effect was involved. These sets of experiments were used to validate various numerical models such as Vakilaltojjar and Saman (2001), Halawa (2005), Halawa et al. (2005, 2010), Saman et al. (2005) and Halawa and Saman (2011). In Zalba et al. (2003) a free cooling system corresponding to an air-PCM heat exchanger installation was designed and constructed to test the performance of such systems. Other referable studies are presented in Waqas and Kumar (2009) and Butala and Stritih (2009). Some numerical studies neglect the sensible heat stored compared to the phase change enthalpy, hence, the experimental validation need to be carefully interpreted.

Common commercial PCM used in free cooling experiments are RT20, RT21, RT 22, RT25 and RT27 supplied by Rubitherm (Rubitherm GmbH) because they present melting temperatures around the acceptable comfort temperatures. Therefore various experimental works were carried out with these PCMs such as Zalba et al. (2004), Butala and Stritih (2009), and Dolado et al. (2011), using the results to validate mathematical models involving the same PCMs.

2.6.2 Real scale experiments

The full scales (also called real scale) represent the experimental rig projected for the entire intended dimension of study. The main outcomes of this work are the full thermal characterisation of the system, demonstrating the technical feasibility. Some examples are Yanbing et al. (2003), Takeda et al. (2004), Arkar et al. (2007), and Dolado et al. (2011).Yanbing et al. (2003) studied the thermal storage system applied in the space between the hung ceiling and the floor above for the consideration of space occupancy. This type of experimental setup has the advantage to percept more precisely, and in real time the behaviour and outcomes of the system in the pretended area thus avoiding the “forgetfulness” of possible external influences that may not be contemplated in a small scale testing rig. However this kind of testing is costly and time consuming. It requires the specific expertise of technicians in order to correctly set up the system and all the necessary electrical connections.

A review on air-PCM heat exchanger experimental works is listed in Table 2-14 and 2-15.

Table 2-14 Review of rectangular PCM-air heat exchanger experimental models

Ref.	Objectives of the study	Measurements	Operating Conditions	PCM	PCM structure geometry	PCM mass	Panels /air gap dimension	Type of heat exchanger	Major results
Zivkovic and Fujii, 2001	Numerical validation, Comparison of rectangular and cylindrical containers	Temperature in the centre of the PCM using thermocouples Melting time	(T_m = 29 ºC)	$CaCl_2.6H_2O$	Rectangular container	-	PCM: L=0.1m, W=0.1m, H= 0.02m. Air gap: -	Direct contact between PCM container-thermal bath	Heat conduction resistance of the container's wall can be neglected. Conduction within the PCM in the HTF direction can be ignored. For flat thin containers the natural convection within the liquid PCM can be ignored. Rectangular container requires half of the melting time as for the cylindrical container
Bruno and Saman, 2002	Prediction of the heat transfer between the air and flat sheets of encapsulated PCM	Inlet and outlet air Heat transfer rate	Air flow rate for melting= 950 m^3/h for solidification= 939.6 m^3/h	$CaCl_2 \cdot 6H2O$ (T_m= 29 ºC)	Rectangular container		6 parallel PCMs: L=1.3 m, H= 0.3 m Air: D=0.3 m	Direct contact between PCM container-air (air through PCM panels)	Tested heat transfer rate during the first hour was higher than that predicted by the model as the sensible heat was not taken into account. Due to the natural convection was not considered in the model. Heat transfer rates can be increased by increasing the flow rate or with lower inlet temperatures
Yanbing et al., 2003	Numerical validation Thermal performance	Air temperature, flow rate, flowing resistance, fan power	(T_m= 22-26 ºC)	n.a.	Plates PCM packed bed storage	150 kg	PCM panel : L= 0.15 m, W= 0.08 m, H=0.01m. Air gap: -	Direct contact between PCM container-air	The temperature decreasing effect is due to cool storage with PCM (mainly by latent heat) and from the fabric of the building (by sensible heat)
Zalba et al., 2004 and 2011	Free cooling Numerical validation Influencing parameters	Air inlet and outlet temperatures Air flow rate	T_{inlet} (melting)= 28 and 30 ºC; T_{inlet} (solidification)= 16 and 18 ºC; Air flow rate: 100 and 150 m^3/h	RT 25	Plates of encapsulated PCM	3 kg	H: 0.01 – 0.03 m Air gap:-	Direct contact between PCM container-air	Solidification process: thickness of the encapsulations, inlet temperature of air, air flow, interaction thickness x temperature; melting process: inlet air temperature has a bigger influence than thickness of the encapsulation
Butala and Stritih, 2009	Influence factors: air velocities, inlet and outlet air temperatures, and heat fluxes	Air inlet and outlet temperatures Air velocities (anemometer)	T_{inlet}= 26, 36, 40 ºC Air flow= 1.5 and 2.4 m/s	RT20 (T_m= 22 ºC)	Plates of encapsulated PCM + metallic fins (externally and internally)	3.6 kg	PCM panel: L=0.5 m W=0.22 m H = 0.09 m Air gap: -	Direct contact between PCM container-air	Airflow of 1.5 m/s guaranties lower the outlet air temperature (26 ºC). Higher heat flux was achieved with 2.4 m/s air flow and 36 ºC air inlet temperature Biggest cold storage for air flow of 2.4 m/s and air inlet temperature of 40 ºC

Table 2-15 Review of rectangular PCM-air heat exchanger experimental models (continuation)

Ref.	Objectives of the study	Measurements	Operating Conditions	PCM	PCM structure geometry	PCM mass	Panels /air gap dimension	Type of heat exchanger	Major results
Lázaro et al., 2009	Free cooling Compare two different prototypes	Air flow, inlet and outlet air temperature and humidity PCM and air channels temperatures	Varying the cooling power (5 kW) (100%, 75%, 60%, 50%, 40%, 25 %, 10 %)	- (Organic) - (Inorganic)	Aluminium Pouches Aluminium rectangular panels	-	-	Direct contact between PCM container-air	The duration time of cooling capacity of PCM heat exchanger depends on the cooling power demand; the quickest was achieved for 75 % of the total cooling power (5 kW), however even for 25 % it took an acceptable time – 5 hours
Rady, 2009	Provide basic understanding of the heat transfer process in the composite bed consisting of a mixture of multiple granular phase change composites	Air flow rate, air inlet, outlet and PCM temperatures	Inlet temperature varying from 40 °C to 50 °C, Re= 7.29	GR27, GR 41	Packed bed column		Air + PCM cylindrical tube D= 0.050 m and H= 0.2 m	Direct contact between PCM and air	The optimum mixing ratio is independent of the value of Reynolds number
Waqas and Kumar, 2011	Free cooling	Air outlet velocity, inlet and outlet dry and wet bulb temperatures, PCM temperature	Discharging: T_{inlet}= 36, 38, 40 ºC; Charging: T_{inlet}= 20, 22, 24ºC; air flow= 4 and5 m^3/h /kg	SP29	Galvanized steel plates of encapsulated PCM	13 kg	PCM panel: L=0.5 m W=0.5 m H = 0.01 m Air gap: -	Direct contact between PCM container-air	Solidification of PCM is strongly influenced by air inlet temperature and flow rate. If charging air temperature is not lower than the subcooling temperature the solidification of the PCM will not be initiated
Osterman et al., 2015	Examine experimentally the use of storage unit for heating and cooling.	Flow visualization, air and pressure drop	Air flow rate = 22 and 44 m^3/h T_{inlet}: 6- 30 °C	RT22HC	compact storage module plates	20.415 kg or 27.2 kg	PCM panel: L=0.30m,W= 0.45m, H= 0.015 m Air gap: 0.008 /0.016 m	Direct contact between PCM container-air	For 45°C, 35 °C and 30 °C, melting times resulted in 8 h, 12.5 h and 18.5 h; 3.5 h if inlet decreased from 9 °C to 4 °C. For 16 °C and 30 °C, 1.8 kWh of cold is stored, 35 °C and 10 °C 2 kWh of heat. Annual energy savings: 670 kWh for cooling/ heating of ambient air
Peiró et al., 2015	Experimental evaluation of the advantages using of using multiple PCM in TES	PCM,HTF inlet and outlet temperatures. Outlet HTF volume flow	HTF temperature = 187 °C and flow rate = 2.8 m^3/h	Hydroquinone and d-mannitol	Shell-and-tube heat exchanger	170 kg and 165 kg	Storage tank vessel volume= 0.154 m^3	Direct contact between storage vessel and HTF pipes	The outlet HTF temperature for multi PCMs has lower and more uniform values than the single PCM cases, An increase in a factor of 4 could be achieved by implements multiple PCM configuration

From the review of the rectangular PCM-air heat exchanger, it is found that the most important parameters to be measured are the air inlet and outlet temperatures, the temperatures across the PCM panels, the inlet and outlet air flow rates/velocities and in some cases the air humidity and air flowing resistance was also measured. The PCM panels share similar thickness between 0.01 m - 0.03 m. Zalba et al. (2003) concluded that the parameters influencing the solidification process were the thickness of the encapsulation, the inlet air temperature and air flow. The parameters influencing the melting process were the same as for solidification, although the inlet air temperature also plays a major role. Later on Zalba et al. (2011) stated that the process was faster when the thickness of the encapsulation was lower, the temperature difference between air and the melting temperature of the PCM was higher, and the air flow was higher. Waqas and Kumar (2011) claimed that the most important parameter affecting the solidification of the PCM was the charging air inlet temperature. Higher air flow rate will be beneficial for the accumulation of maximum cold in the PCM during the charging process, keeping in view the short Summer nights (Waqas and Kumar, 2011). However, higher air flow rates were not beneficial if the cold air temperature was not lower than the sub cooling temperature (especially for salt hydrate PCMs) and the solidification of the PCM was not initiated (Waqas and Kumar, 2011). The authors also observed that during the melting process at a higher inlet air temperature more cold is extracted from the PCM in the given time period compared to that of the lower melting temperature, due to the higher heat transfer rate and greater heat losses. Bruno and Saman (2002) concluded that the heat transfer rates can be increased by increasing the flow rate or with lower inlet temperatures. However, higher air flow rates increase the heat transfer and shorten the charging time. It increased the air outlet temperature and the amount of heat absorbed by the PCM (Mosaffa et al., 2014). Therefore, for the air-PCM unit both the melting/solidification of the PCM and the air outlet temperature have to be balanced and investigated in parallel for the available inlet conditions.

2.7 Major applications of TES in buildings

The use of PCMs has been considered for thermal storage in buildings prior to 1980. The first applications of PCMs were their use in heating and cooling applications by Telkes (1978) and Lane (1981) (Mehling and Cabeza, 2008). Recently different applications for the use of PCMs by several authors were developed. However, research into latent heat storage for solar heating systems continues and has also been considered for waste heat recovery, load levelling for power generation, building energy conservation and air conditioning (Velraj and Pasupathy, 2006). Based on Zalba et al. (2003), Regin et al. (2008) and Kenisarin and Mahkamov (2007) it is possible to summarize the main applications of TES in buildings as listed in Table 2-16. The most common TES for the heating or cooling of buildings is mainly based on sensible heat storage material. However, in recent years, several works were carried out for the heating and cooling of buildings based on LHS through PCMs (Tyagi and Buddhi, 2007). They may be classified as low temperature thermal storage technologies as presented in Figure 2-12. The TES can be encapsulated and applied in different locations within the building or applied directly in buildings materials. Also, they may classify as both short-time or annual storages. The former usually uses the daily absorb/release cycles, whilst the latter work on a season basis. In other words, for short time storages we can consider the heat storage during night-time and its release in the day time or vice versa. For annual storage, the heat is stored during the Summer for its release in colder seasons or vice versa. LHS with PCMs can be categorized as active or passive space heating/ cooling systems as shown in Figure 2-13. In passive systems, PCMs can be encapsulated in building materials such as concrete, gypsum wallboards, ceiling or floor to increase their thermal storage capacity. Alternatively, storage units using PCMs can be used with conventional active space heating and cooling systems to improve the overall thermal efficiency (Bruno, 2004). PCMs with a melting temperature between 20 and 32 °C were recommended for thermal storage in conjunction with both passive and active solar storage for heating and cooling in buildings (Tyagi and Buddhi, 2007).

Table 2-16 PCM-TES applications (Zalba et al., 2003; Regin et al., 2008 and Kenisarin and Mahkamov, 2007)

PCM – TES Applications in Buildings
Passive Storage in buildings in bioclimatic building/architecture (HDPE + paraffin)
Cooling: use of off-peak rates and reduction of installed power, ice-bank
Heating and hot water: using off-peak rate and adapting unloading curves
Thermal storage of solar energy

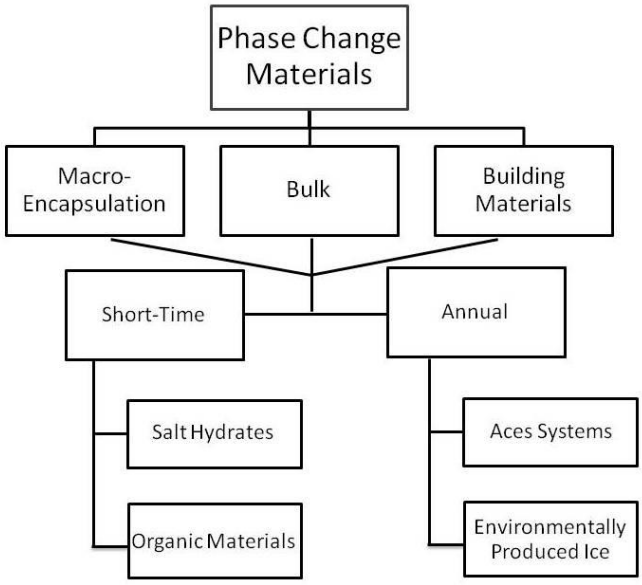

Figure 2-12 Low temperature thermal storage technology classification

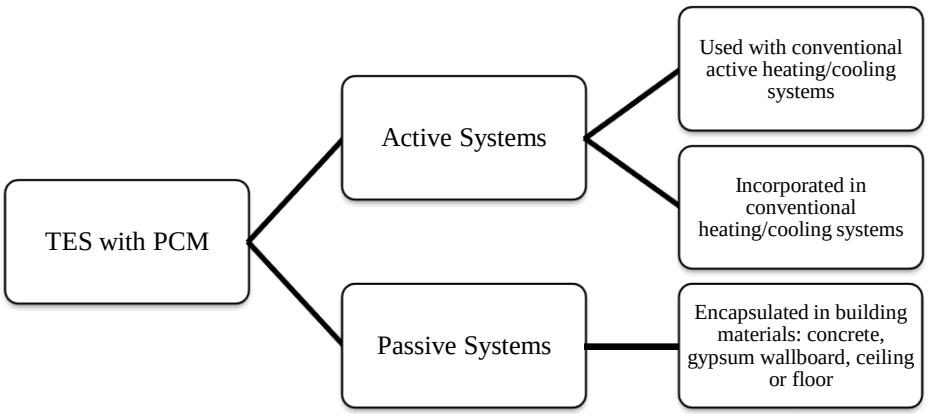

Figure 2-13 Active and passive system for TES with PCM

2.7.1 Free cooling passive methods

LHTES can be encapsulated into building materials or structures. The system is said to be passive as no electrical device is needed. The concept of PCMs integrated into buildings materials allow the PCM to absorb heat during daytime which begins the melting process, and during the night the heat is released by the solidification process of the PCM, resulting in a lower heat flow from outdoors to indoors (Castell et al., 2011). During the winter, the system can also be used for heating by utilising solar energy during the day. In passive methods, the stored heat or cold is automatically released when indoor or outdoor temperatures rise or fall beyond the melting point of PCM (Ravikumar and Srinivasan, 2008). Passive methods used for the thermal energy management of the built environment include the thermal mass, which can contribute to the downsizing of AC/heating equipment and the reduction of the AC/heating demand (Diaconu and Cruceru, 2010). Lee et al. (2015) studied experimentally the integration of a thin PCM layer into a wall via a thermal shield. It allowed the reduction of the peak heat flux in 51.3% and 29.7% for the south wall and west wall, respectively. The applications of PCM in structures of buildings have an advantage in not requiring separate plant and space. Therefore there are several studies about PCMs integrated into building materials (concrete, brick, glass, etc.) or components, such as wallboards, floors, ceilings and roofs, Tables 2-17 and 2-18 list some of them.

The main advantages of PCM wallboards are:

- Being cheap and widely used in a variety of applications (Sharma et al, 2009)
- Capable of minimising the effect of large fluctuations in the ambient temperature on the inside temperature of the building (Bruno, 2004)
- Twice greater than a room with conventional wallboards when the temperature was increased from 18.3 to 29.4 °C (Kenisarin and Mahkamov, 2007)

However, PCM wallboards also present some disadvantages:

- The heat storage is limited by the low value of the heat transfer coefficient (h_c) between the air and the wallboards (Kenisarin and Mahkamov, 2007, Liu and Awbi, 2009);
- Presence of an unpleasant odour in the room with the PCM wallboard (Feldman and Banu, 1996)
- Layer of corrosion formed on some metallic (copper and aluminium) surfaces in the room with PCM due the vaporisation of impurities from the fatty acids (Rudd, 1993);
- PCMs without the addition of fire retardants, organic PCMs had unacceptable flammability characteristics (Kenisarin and Mahkamov, 2007) and
- Any replacement of the PCM wallboards will affect the aesthetic of the room.

David et al. (2011) demonstrated that even accounting for the possibility of having mixed convection in both laminar and turbulent regimes, the use of the most common correlations available in the literature would still provide $h_c \leq 2.5 W/m^2°C$ for limited temperature differences between wall and air ($T < 2$ °C). This implies a poor heat transfer between the wallboard and the indoor environment, thus reducing the daily thermal energy storage in the PCM if compared with its storage potential (Evola et al., 2014).

Table 2-17 Passive methods: PCM integrated into wallboards

Structure	Images	Reference
Walls	This item has been removed due to 3rd Party Copyright. The unabridged version of the thesis can be	Neeper, 2000
	This item has been removed due to 3rd Party Copyright. The unabridged version of the thesis can be found in the Lanchester Library, Coventry University	Ahmad et al., 2006
	This item has been removed due to 3rd Party Copyright. The unabridged version of the thesis can be found in the	Ahmad et al., 2006
	This item has been removed due to 3rd Party Copyright. The unabridged version of the thesis can be found in the Lanchester Library	Chen et al., 2008
	This item has been removed due to 3rd Party Copyright. The unabridged	Kuznik et al., 2008
	This item has been removed due to 3rd Party Copyright. The unabridged	Xiao et al., 2009
	This item has been removed due to 3rd Party Copyright. The unabridged version of the thesis can be found in the	Lee et al., 2015

Table 2-18 Passive methods: PCM integrated into glass, floors and roofs

Others building structures	Images	Reference
Glass	This item has been removed due to 3rd Party Copyright. The unabridged version of the thesis can be found in the Lanchester Library, Coventry University	Inglas, 2002
Floor	This item has been removed due to 3rd Party Copyright. The unabridged version of the thesis can be found	Xu et al., 2005
Roof	This item has been removed due to 3rd Party Copyright. The unabridged version of the thesis can be found in the	Pasupathy and Velraj, 2008
	This item has been removed due to 3rd Party Copyright. The unabridged version	Alawadhi and Alqallaf, 2011
Solar chimney	This item has been removed due to 3rd Party Copyright. The unabridged version of the thesis can be found in the Lanchester Library, Coventry University	Liu and Li, 2015

The main problem with incorporating PCMs in the building envelope is the difficulty of exchanging a high rate of heat between the air and the PCM. Also, increasing the thermal mass of the built environment can contribute to improving the indoor thermal comfort (Diaconu and Cruceru, 2010). Passive ways for cooling may also not operate

as effectively in much warmer climates, because the outdoor ambient air temperature does not decrease sufficiently at night. Stetiu and Feustel (1996) found that for climates with relatively high ambient temperatures (above 18 °C) during the night, it would be beneficial to force the supply air along the wall surfaces to facilitate good heat exchange.

2.7.2 Free cooling active methods

Free cooling is based on the use of the freshness of a source, such as outside air, to cool down buildings. If, for example the night coldness is stored and utilized during daytime to achieve comfort temperatures in indoor spaces, mechanical ventilation can be either totally eliminated during the day time or at least can be limited only to certain periods (Waqas and Kumar, 2011). As there will be no need for energy to produce a cold source, this process is commonly known as free cooling. Free cooling may also be accomplished through LHTES systems improving the cooling potential of mechanical ventilation systems (Raj and Velraj, 2010), or even helping reduce the size of the mechanical ventilation system. This provides more favourable temperatures and therefore better thermal comfort conditions (Arkar et al, 2007). The main advantages of free cooling are: cooling with reduction of greenhouse gases and the maintenance of excellent indoor air quality within the building (Raj and Velraj, 2010). For free cooling systems, PCMs have to be selected so that the cooled air temperature is within the range of human comfort. For instance, in Summertime, the human comfort zone lies between 23 °C and 27 °C (ASHRAE, 2001). In order to achieve sufficient heat transfer, the temperature difference between the air temperature and the melting temperature of the PCM should be within the range of 3-5 °C (ASHRAE, 2001). Tables 2-19 and 2-20 list the studies on active methods for free cooling applications. An active free cooling system is said to be active because of the use of electric devices. A free source of cooling is used (the night freshness for example) and the storage of this coolness is ensured with an active system. In active methods, storage as HTF is actively moved known as forced convection. This can operate optimally in reducing the internal dry bulb temperature and can even overcome this problem. It has the potential not only to significantly impact on energy consumption, but to reduce it to a small fraction of its current level. Only the energy

consumption for a fan remains (Mehling et al., 2002). This type of systems also allows full control of the process during the charging/discharging of the PCM, thus optimizing the performance of the whole system. However, if the system is not sufficiently designed, it can be ineffective. The key benefits of using the storage system as a component of an air conditioning system can be summarised as a reduction in equipment size, capital cost savings, energy cost savings, peak power savings and improved system operation (ASHRAE, 1995). One of the first experimental works on free cooling combined with a ventilation system was from Turnpenny et al. (2000). In this study, the coldness of the night air was stored in the PCM and discharged during the daytime. The novelty was not only that the night ventilation system used LHS system, but also in the use of a reversible heat pipe embedded in the PCM (Table 2-19 and Table 2-21: Cases 1 and 2). Estimation for heat transfer rate was possible. In this study however it was possible to achieve 70-90 W for the outside air and the PCM difference temperature was around 12°C, although to melt and freeze the PCM in a practical timescales (7-10 hours) a difference above 15 °C is needed. Another innovative study with active free cooling systems was developed by Yanbing et al. (2003). For this case the LHTES (PCM Packed Bed Storage –NVP) system was mounted above the ceiling and surrounded by air ducts (Table 2-19 and Table 2-21, Case 3). At night the cooled outside air was blown through the LHTES system to solidify the PCM. During the daytime the air circulated between the LHTES system and the room, so the cold stored within the PCM was discharged into the room. The cool discharging rate in the night-time was 0-1000 W and in the daytime was 0-300 W.

Multiple PCMs have been presented as a heat transfer enhancement technique as discussed in section 2.3.6. Recently active TES including multiple PCMs have been investigated for free cooling applications as reported in Chiu and Martin (2013) and Mosaffa et al. (2012). Mosaffa et al. (2012) studied an LHS free cooling unit with several layers of PCM each containing 2 PCMs with different melting temperature and parallel air channels to provide comfort conditions for the climate in Tabriz, Iran. Multiple PCMs improved the thermal performance of the TES unit in that it reduced the time by 20 % and 40 % for the discharging and charging process (Chiu and Martin, 2013) and a nearly constant heat flux was maintained between the PCM and the HTF (Mosaffa et al., 2013) enhancing overall the free cooling applications.

Table 2-19 Summary of active systems for free cooling of buildings

Paper	Objectives of the study	Key arguments	PCM considered	Geometry of PCM structure	PCMs location	Type of heat exchanger	Methodology	Major results
Turpenny et al, 2000	Development of latent heat storage unit incorporating heat pipe (novel since it is reversible) embedded in PCM for free cooling buildings	- LHS incorporating reversible heat pipe; - incorporate of finning arrangements spiral wire fins	-	Cylindrical PCM jacket	Ceiling (Table 18, picture 1)	Heat pipe	Experimental and Mathematical (one-dimensional	- Heat transfer rate ~ 40 W over a melting period of 19h for a temperature difference between air and PCM of 5° C - Heat storage ~ 270W h over 8hours - Large temperature difference between air and PCM (15 °C or more) was needed to melt and freeze the material in a practical time scale (7-10h
Turpenny et al., 2001	Improvement of previous study through: new fins arrangement (plate fins arranged longitudinally along the PCM end of the heat pipe); guaranty of full contact between all the extend surface and the PCM gel	- Ceiling fan with model with 3 blades	-	Cylindrical PCM jacket	Ceiling (Table 18, picture 2)	Heat pipe	Experimental	- Heat transfer rate ~ 200 W – being sufficient for the summer load - Heat storage ~ 100 W h over 2-3 hours
Yanbing et al., 2003	Analyse of thermal behaviour of a proposed Night Ventilation with PCM Packed Bed Storage (NVP)	-Predict energy consumption; -Air flow resistance; -Convective heat transfer	RT 25	Plates PCM packed bed storage	Ceiling (Table 18, picture 3)	Direct contact between PCM-air	Experimental and Mathematical	- Convective heat transfer coefficient 12-19 W/m^2. °C -Air flow resistance through PCM < 20 Pa
Zalba et al., 2004	Study of free cooling with night ventilation system	-Determination of the mains influence parameters for melting/freezing of PCM	RT 25	Plates of encapsulated PCM	- (Table 18, picture 4)	Direct contact between PCM-air	Experimental, Statistical method (DOE) and Empirical	-Relative long duration of loading (4h)and unloading (8h) process -Very high power consumption of the fans
Nagano et al., 2004	Predict the heat transfer coefficient to estimate the amount of exchanged heat	-Creation of dimensional numbers to predict heat transfer coefficient	GR 25	Packed bet of PCM granules	- (Table 18, Picture 5)	Direct contact between PCM-air	Experimental, numerical and computer simulation	-Exchanged heat per unit time and unit area is proportional to the face velocity and the difference of temperature in the PCM packed bed -Heat transfer coefficient can be used to estimate the amount of exchanged heat and time required phase change to be completed
Takeda et al., 2004	Ventilation system with packed bed of granules containing PCM in air supply ducts (for cooling)	-Definition of factor "latent heat corresponding to flow rate,(D^1)"; Definition of factor load ratio (η^2)	GR 25	Plates of encapsulated PCM	Under floor (Table 18, picture 6)	-	Experimental and Computer simulation	- It was found that the benefit depends more on the range of daily temperature variation than on average temperature - Reduction of ventilation load by 62.8% (for Kyoto)
Marín et al., 2005	Improvement of previous study through: graphite compounded material with PCM to enhance heat transfer	- Designing a TES using air and porous matrix of graphite embedded into the PCM for efficient free cooling	RT 25	Plates of encapsulated PCM embedded into a graphite matrix	- (Table 18, Picture 7)	Direct contact between PCM-air	Experimental and Numerical	-Response time much lower (50% in time) -Power consumption of the fans decreased by 50% -Very low reduction of the energy stored (12 and 20%) based on the storage volume occupied by the graphite
Hed and Bellander, 2005	Free cooling of buildings	-The possibility of use of phase change materials integrated into a building is explored	-	Plates of encapsulated PCM	Ceiling (Table 18, picture 9)	Direct contact between PCM-air	Mathematical model	-Heat transfer coefficient between the airflow and the PCM increases significantly when the surface is rough compared to a smooth surface (valid for toughness of 0.02 -Heat transfer coefficient for air velocity of 4 m/s ranging from 16-30 W/m2. °C

Table 2-20 Summary of active systems for free cooling of building (continuation)

Paper	Objectives of the study	Key arguments	PCM considered	Geometry of PCM structure	PCMs location	Type of heat exchanger	Methodology	Major results
Nagano et al., 2006	Remove the cooling load in the room	- New floor supply air conditioning system; -Performance of charge/discharge experiments to simulate office air conditioning over 24 h periods	C_6H_{34} and $C_{18}H_{38}$	Packed bed of the granular PCM	Floor (Table 18, picture 8)	Direct contact between PCM-air	Experimental and Simulation	-89% of daily cooling load could be stored each night for 30 mm thick packed bed of the granular PCM -1.79 MJ/m2 heat storage by the end of each night that allowed a daytime air conditioning limited to 3h
Arkar and Medved, 2007	Free cooling of low energy building using LHTES	- LHTES integrated into a mechanical ventilation system -LHTES optimization made for selected parameters: PCM's phase change temperature range, PCM melting temperature and ratio of the PCM's mass to the air volume flow rate	RT20	Cylindrical LHTES filled with spheres of encapsulated PCM	- (Table 18, picture 10)	Direct contact between PCM-air	Numerical model (Fourier series) and Modelling (TRNSYS)	LHTES with 6.4 kg/m2 of PCM of floor area allow suitable thermal comfort conditions -LHTES can be used as heat storage during winter if the ventilation system is combined with an air solar collector or a ventilated façade element
Butala and Smith, 2009	Free cooling of buildings	- Study of the ceiling and floor free cooling principle, as well as passive cooling	RT 20	Plate incorporating fins	Ceiling (Table 18, picture 11)	Direct contact between PCM-air	Experimental model	-After 200 min the outlet air temperature equals the inlet air temperature -Bigger difference inlet temperature and environment temperature reduce time for cooling - Higher airflow reduces lightly the time for cooling
Raj and Velraj, 2011	Free cooling of buildings	-Modular heat exchanger developed in this work is a shell and tube type with phase change materials in the shell portion of the module and passage for the flow of air through the tubes. -Determine the PCM solidification characteristics and to verify the suitability of the selected geometrical dimensions	-	Cylindrical container	- (Table 18, picture 12)	Direct contact between PCM-air	Experimental and Mathematical model (CFD)	-The air spacer provided between the module increases the retention time of the air for better heat transfer -The increase in the surface heat transfer coefficient on the tube side due to an increase in the frontal velocity has a considerable effect in reducing the time for solidification -The PCM present adjacent to the inner ring of the tubes is sub cooled when the PCM present in the region between the two outer rings of tubes attains the solidus temperature
Waqas and Kumar, 2011	Free cooling of buildings	-Storage unit for building ventilation in dry and hot climates -Experimentally investigate the influence of air flow rate and the air inlet temperature on cold accumulation in PCM.	SP29	Plates of encapsulated PCM	- (Table 18, picture 13)	Direct contact between PCM-air	Experimental model	-The experimental results indicate that the PCM storage can be used to keep the hot air within the defined temperature limits during day time by releasing the cold stored in PCM during night-time
Evola et al. 2014	Improve summer thermal comfort in buildings	-Identify the temperature distribution along the ventilated cavity -Efficiency is evaluated through a case study, based on simulations	Micronal T23	Plates of encapsulated PCM	Wall (Table 19, picture 14)	Direct contact between PCM-air	Mathematical model (EnergyPlus)	-Allowed reduction of the average room operative temperature in July of about 0.4 ◦C with respect to the common practice of attaching PCM wallboards directly on the partition wall -Indoor conditions were kept for a longer time in a comfortable range, and occasional discomfort sensations are less intensive

Table 2-21 Active systems for free cooling of buildings

	Active systems	Reference
Case 1	This item has been removed due to 3rd Party Copyright. The unabridged version of the thesis can be found in the Lanchester Library, Coventry University	Turnpenny et al., 2000
Case 2	This item has been removed due to 3rd Party Copyright. The unabridged version of the thesis can be found in the	Turnpenny et al., 2001
Case 3	This item has been removed due to 3rd Party Copyright. The unabridged version of the thesis can be found in the Lanchester Library, Coventry University	Yanbing et al., 2003
Case 4	This item has been removed due to 3rd Party Copyright. The unabridged version of the thesis can be found in the Lanchester Library, Coventry University	Zalba et al., 2004
Case 5	This item has been removed due to 3rd Party Copyright. The unabridged version of the thesis can be found in the Lanchester Library,	Nagano et al., 2004
Case 6	This item has been removed due to 3rd Party Copyright. The unabridged	This item has been removed due to 3rd Party Copyright. The unabridged version of the	Takeda et al., 2004

Table 2-22 Active systems for free cooling of buildings (continuation)

	Active systems	Reference
Case 7	This item has been removed due to 3rd Party Copyright. The unabridged version of the thesis can be found	Marín et al., 2005
Case 8	This item has been removed due to 3rd Party Copyright. The unabridged version of the thesis can be found in the Lanchester Library, Coventry University	Hed and Bellander, 2005
Case 9	This item has been removed due to 3rd Party Copyright. The unabridged version of the thesis can be found in the Lanchester Library, Coventry University	Nagano et al., 2006
Case 10	This item has been removed due to 3rd Party Copyright. The unabridged version of the thesis can be found in the Lanchester Library, Coventry University	Arkar and Medved, 2007
Case 11	This item has been removed due to 3rd Party Copyright. The unabridged version of the thesis can	Butala and Stritih, 2009
Case 12	This item has been removed due to 3rd Party Copyright. The unabridged version of the thesis can be found in the Lanchester Library,	Raj and Velraj, 2011
Case 13	This item has been removed due to 3rd Party Copyright. The unabridged version of the thesis can be found in the Lanchester	Waqas and Kumar, 2011
Case 14	This item has been removed due to 3rd Party Copyright. The unabridged version of the thesis can be	Evola et al., 2014

Some studies present in Tables 2-19 ad 2-20 were patented as listed in Table 2-23.

Table 2-23 Publication of patents related with PCM-air exchange in the recent years (Dolado, 2011).

There are a few technologies of active methods with TES for free cooling available on the market (Table 2-24) .Some of them are related with the patents listed in Table 2-23, as the cool-phase developed and patented by Nottingham University and Monodraught. The same company presents different low energy technologies applied to ventilation and to air conditioning systems. Units represented as a) and c) in Table 2-24 represent independent air-PCM TES systems. The outside air is supplied directly to the system and released after crossing the phase change material. Unit b) represents a simple panel containing a PCM that can be mounted directly in the ceiling and once again the air is cooled by passing through the solidified panel. Another example is Napevomo, a prototype that has been set in a positive-energy house which participated to an international competition called "Solar Decathlon Europe". It contains an air-cooling system designed by Ango et al. (2011) integrated inside the house floor between its structure poles. The system is composed of four LHTES devices each containing a horizontal energy storage device, namely a box-section tube bundle filled with paraffin wax. Two paraffin waxes were used, one with a 245,000 J/kg latent heat capacity (Rubitherm RT28 HC) and a melting temperature range spread around 28 °C, the second with a 134,000 J/kg latent heat capacity and a melting point of around 21 °C (Rubitherm RT21) (Rouault et al., 2014).

Table 2-24 Commercial technologies of free cooling

a) Cool-phase (Monodraught)	This item has been removed due to 3rd Party Copyright. The unabridged version of the thesis can be
b) CoolDeck (Climator)	This item has been removed due to 3rd Party Copyright. The
c) Emcovent (Emco)	This item has been removed due to 3rd Party Copyright. The unabridged
d) Napevomo	This item has been removed due to 3rd Party Copyright. The unabridged version of the thesis can be found in the Lanchester Library.

2.7.3 Space heating (using auxiliary source) active methods

A concept similar to active free cooling has been developed for space heating. However, for heating purposes the PCM TES usually needs to be linked to auxiliary heat sources such as heat pumps or solar collectors as the desirable warm air temperature are not freely available during the winter. This will again allow the reduction of the cooling system capacity and the annual running costs respectively. Space heating is possible through building different layers of PCMs with different change phase temperatures in order to fit with different auxiliary heat sources. These are provided mostly by solar collector panels, air conditioning and heat pumps. Vakilaltojjar (2000) designed and developed a thermal storage system consisting of two phase change materials for use with a reverse cycle air conditioner. The feasibility for use in residential houses was investigated (Figure 2-14). The aim of this type of storage system was to be used for both space heating in winter and space cooling in summer. The chosen PCM layers were calcium chloride hexahydrate ($CaC_{12}.6H_20$) and potassium fluoride tetra hydrate ($KF.4H_20$). Three different configurations were used for encapsulating these materials: flat plain plastic bags, flat plastic bags with dimples, and conical capsules.

Yamaha and Misaki (2006) investigated the use of paraffin mixture containers in the air ducts as storage devices for air-conditioning equipment. The air passed through a closed loop of the PCM tank and the air conditioner during the charging operation (Figure 2-15 (1)). Once the charging was finished, the air conditioning ran at its normal operation mode and the air bypassed the storage tank (Figure 2-15(2)). The tank was completely discharged from 13:00 to 16:00 h when the air flowed through the storage tank and cooled down the inlet temperature of the room (Figure 2-15(3)). Real et al. (2014) focussed on improving the performance of a heat pump based HVAC system with two thermal storage tanks using phase change materials (PCM). A cold tank was used to take advantage of the low outside temperatures at night to cool the PCM with a high COP and it is used later to cool the building when the outside temperature rises. The second tank was operated as an alternative hot reservoir which provided the system with the flexibility to dissipate the heat to the tank at a constant temperature preventing the reduction of the COP below a minimum value. The HVAC system catered for the needs of the house during the required period and successfully kept the temperature within the established limits. The heat pump coupled to TES was also investigated by Moreno et al. (2014). In this study the cold TES tank was used for shifting the cooling load of a small house-like structure. The PCM tank was able to supply 14.5% more cold and to maintain the indoor temperature within the comfort zone of 20.65 % longer than

the water tank. An experimental study was conducted to investigate a suitable PCM to take advantage of an off-peak electricity tariff while a heat pump was in use (Agyenim and Hewitt, 2010). Results demonstrated that with an improvement in heat transfer techniques, the store size of the heat pump can be reduced by 30%. An extensive review on PCMs in domestic heat pump and air conditioning can be found in Moreno et al. (2014). Chaiyat (2015) also investigated the use of PCM to improve the cooling efficiency of an air conditioner (Figure 2-16) under Thailand's climate. The electrical power of the modified system could save around 9% or 3.94 kWh/day compared to the normal system at around 39.36 kWh/day. The payback period was around 4.12 years.

Figure 2-14 The proposed storage system for storing heat and coolness using two phase change materials (Vakilaltojjar, 2000).

Figure 2-15 Diagrams of air conditioning system allied with PCM (Yamaha and Misaki 2006)

Figure 2-16 Prototype of the air-conditioner integrating with the PCM bed (Chaiyat, 2015)

Extensive efforts have been made to apply TES to solar energy systems where heat is required to be stored during the day for use at night. This solution has also been investigated due to the high operating temperatures that induce a loss of efficiency in solar photovoltaic and thermal panels (Biwole et al., 2013). One of the first air-based heating systems was carried out by Morrison and Abdel Khlaik (1978). Halawa (2005) developed a similar storage

system incorporating different layers of PCMs, but for use with a solar collector. The experimental data was collected from Vakilaltojjar (2000) and further developed the theoretical model. The study showed that the PCM with melting temperature of 29 °C was suitable for space heating, as thermal comfort levels were found to be acceptable during the discharge tests. When the energy storage unit was discharged at a flow rate of 16 m^3/h, the heat transferred was initially 2.75 kW and then reduced from 1.5 kW to 1 kW over the next 6 hours.

Figure 2-17 Schematic diagram of the air-based system used with storage (Halawa, 2005)

Biwole et al. (2013) numerically investigated a system composed of an impure phase change material situated in the back of a solar panel (SP) Results show that adding a PCM on the back of a solar panel can maintain the panel's operating temperature under 40 °C for 80 min under a constant solar radiation of 1000W/m^2. Arkar and Medved (2015) studied a solar air heating system composed of a vacuum tube air solar collector and a TES. The system performance for the different intensities of solar irradiation throughout the day has shown that 54-67% of the heat produced by solar air heating systems in the daytime can be delivered during the night-time for building heating.

2.8 Conclusions and scope of the present work

The present literature review allows the understanding of TES systems, especially the LHS using PCMs. PCMs were classified and their thermophysical, chemical and kinetic properties are presented. Organic and inorganic compounds are the two most common groups of PCMs and in general they present low thermal conductivity. This aspect can be improved through the geometry of the container and also through heat transfer enhancement techniques. The most common geometry of the containers are cylindrical or rectangular, the latter one presents some advantages in the uniformity of the thickness and its simplicity of manufacture. On the other hand, heat transfer techniques are mainly associated with conductivity of metallic structures such as finned tubes, matrixes, honeycomb structures, heat pipes, through composites of PCMs, high conductive particles or through the use of multiple PCMs. The thermal performance and optimization of TES has been studied by mathematical formulation, computational modelling or experimental analysis. Several experimental models on air –TES systems have been carried out, mostly involving parallel plates containing PCMs in contact with air in order to promote the heat transfer and respectively the melting and solidification of the PCMs. The most important parameters to be measured are the temperature of the inlet and outlet air, temperature across the PCM panels, inlet and outlet air flow rate/velocity, in some cases also the air humidity and air flowing resistance was measured. For the mathematical formulation, the enthalpy method and the effective heat capacity were shown as the most appropriate and common methods to be used. Both methods can be applied in computational softwares such as Matlab and ANSYS and further improved by coupling the enthalpy-temperature or heat capacity –temperature relationship. This relationship is commonly obtained using DSC analysis. Different designs of air-PCM systems for free cooling and heating can be found in the literature. Most of the works related with the heating of buildings have been studied using auxiliary sources such as air conditioning, heat pump and solar collectors. Free cooling applications using the night-time air ambient temperature were studied and successfully utilised. Multiple PCMs TES for free cooling applications have been recently proposed in the literature and hence not yet brought into the market. These units have been studied experimentally and numerically but always under constant HTF temperature conditions. Therefore, air-multiple PCMs units for free cooling and ventilation application relying on real climatic conditions and upon the daytime and night-time temperature difference have not yet been explored. Consequently this was identified as a gap in the current knowledge, requiring further investigation in the present research.

CHAPTER 3 – RESERACH METHODOLOGY OVERVIEW AND EXPERIMENTAL STUDY

3.1 Research methodology overview

The present work intends to develop an air-multiple unit for the free cooling of buildings. The study is carried out firstly through the experimental testing of a small scale prototype of an air-single PCM unit. The influence of the air inlet temperature and velocity is investigated on the charging/discharging time of the PCM, air outlet temperature, cooling/heating load and effectiveness over the phase change. The selected PCM is then thermally characterised through DSC, namely the phase change temperature range, the specific heat relationship with temperature and enthalpy relationship with temperature. Other two PCMs with different melting points are also thermally characterised for the investigation of multiple PCMs furthermore. Two heating/cooling rates for the DSC testing are investigated: the one recommended by the standard and another related to the experimental testing. This is followed by the experimental validation of a CFD model including the two most common numerical methods: enthalpy method and the effective heat capacity method. The method presenting better agreement with the experimental results is selected and applied into a CFD model to further investigate the use of multiple PCMs. A parametric study is conducted to investigate the effect of the selection of the PCMs, geometry of the PCM panels (height and length) and the air mass flow rate. The best solution is then adapted to a case study.

3.2 Introduction

This chapter aims to research the thermal performance of the air- PCM unit in laboratory conditions. It will also provide experimental data to validate the computational model that follows in Chapter 6. Several important factors e.g. air temperature differential, air velocity/mass flow rate, ambient air inlet/outlet temperature and mass of the PCM are considered important in designing the experimental rig. Based on the literature review (Chapter 2) for air-PCM units, the two air inlet temperature and velocity are identified as the major factors. Hence these factors are analysed with respect to melting/solidification times and to air temperature differences. Several temperature measuring thermocouples were used to measure the temperatures along the PCM panels, at the air inlet and outlet. In this chapter,

detailed experimental findings are discussed and facts are established regarding the dynamics of TES storage for the system under investigation. Free cooling applications can be achieved by charging the PCM during night-time, i.e. solidification of the PCM in order to cool the inlet air by means of the discharging of the PCM i.e. melting of the PCM. To summarise, this chapter will also establish experimental findings on i) charging/discharging time of TES and air temperature difference between inlet and outlet, ii) heating/cooling load in charging (discharging) process iii) effectiveness over the phase change process. These key findings will be brought into the research of numerical and case study. The experimental heating/cooling rates are to be used in the Differential Scanning Calorimetry (DSC) testing presented in Chapter 4.

3.3 Design of the air- PCM heat transfer unit

3.3.1 Selection of the working materials

Several PCMs are discussed on the literature (Raj and Velraj, 2010, Cabeza et al., 2011, Iten and Shuli, 2014). As discussed in Chapter 2, the selection of the PCM depends on many factors including melting point, cost, energy density for thermal energy storage, availability, suitability for the application. For the present TES-PCM air system, paraffin was considered due to the following reasons:

(i) Available in several commercial types;
(ii) Low cost;
(iii) Compatibility with metals
(iv) Excellent thermal stability and
(v) Match with the thermal energy storage density.

Several paraffins are available on the market, however suitable melting temperature should be selected for the appropriate application. For the cooling of buildings, RSECE (2006) and ASHRAE (2010) suggest indoor temperatures within 23-26 °C in order to achieve the thermal comfort of occupants. A commercial paraffin RT25 (Rubitherm, 2015) with phase change temperature from 23 °C to 25 °C has been selected to fulfil the comfort temperatures.

The thermophysical properties of the selected paraffin were provided by the manufacturer and listed in Table 3-1.

Table 3-1 RT25 properties (Rubitherm, 2015)

The commercial paraffin RT25 is a mixture of compounds and therefore the melting occurs across a range of temperature: 23-25 °C. For the present study the RT25 was assumed to be completely discharged at 25 °C and completely charged at 23 °C. Air is considered as working fluid for ventilation application.

3.3.2 Selection of the geometry and dimensions

(i) PCM panel encapsulation

There are three typical options for the selection of the shape of the encapsulation: plates, cylinders and spheres (Dolado et al., 2011). Plates are selected due to the advantages such as:

- Uniformity of the PCM thickness and therefore, of the phase change process;
- Melting and freezing process on a plate surface is symmetric in relation to all sides of the plates;
- Heat transfer in the PCM can be controlled with selected thickness of the encapsulation;
- High ration area/volume storage;
- Less pressure drop in the air;
- Simplicity of the manufacturing process and versatility of handling (transportation, installation and maintenance);
- Applicability to various applications and

- Easy to control the PCM thickness which is a crucial design factor influencing the melting and solidification time.

Rectangular containers were also selected in similar applications due to their much shorter melting time (half) than the cylindrical container of the same volume and heat transfer (Zivkovic and Fujii, 2001). In section 2.3.3 the corrosion of the PCMs and compatibility with the container was discussed, plastic materials were not recommended to be in contact with organic compounds i.e. paraffins as discussed in Castellón et al. (2011). In that sense, metallic containers were chosen to assure the compatibly with the paraffins and also to enhance the heat transfer between the air and the PCM panels (Ismail and Henriquez, 2002).

(ii) Dimensions of air- PCM heat transfer unit

Several experimental tests on rectangular air-PCM heat exchangers have been reported in Chapter 2. For the present study, the chosen PCM thickness was 0.02 m (H_{panel}) as it was presented as one of the most suitable dimensions for air-PCM TES systems (Laouadi et al., 1999; Vakilaltojjar and Saman, 2001; Silva et al., 2002; Liu and Majumdar, 2006; Amin et al., 2009; Halawa and Saman, 2011). Halawa and Saman (2011) stated that if the mass of the PCM and the thickness of the panel were constant, the other two dimensions (width and length) do not play an important role in the heat transfer. Thus, the chosen length and width of the panels were fixed on 0.5 m and 0.25 m respectively meeting the requirements of a small prototype scale. The dimensions of the rectangular air channels corresponded to $L_{channel}$ x $W_{channel}$ x $H_{channel}$ in which L was the same length as the PCM panels (L_{panel}), W was the same as the width of the PCM panels (W_{panel}) and $H_{channel}$ was the air gap height. Different air gap heights have been investigated for rectangular air-PCM units: 0.05 m (Saman et al., 2005 and Halawa and Saman, 2011), 0.01 m (Dolado, 2011), 0.08 m and 0.016 m (Gowreesunker, 2013 and Osterman et al., 2015), 0.02 m (Charvát et al., 2014) and 0.035 m (Osterman et al., 2013). Too small dimension will make the construction delicate, and the number of panels will have to be increased leading to a higher pressure drop across the unit. Thus, for the present study an air gap of 0.02 m for each PCM panel was chosen.
The experimental setup included an arrangement of three PCM panels and to fulfil the 0.02 m air gap for the top and bottom of each panel, the middle air gaps height correspond to 0.04 m. Specification of the TES systems dimensions are listed in Table 3-2. The air-PCM heat transfer unit was inserted in rectangular air duct built in wood with thickness of 0.01m.

Table 3-2 Specification of the air-PCM TES system

Internal height of the PCM panels (H_{panel})	0.02 m
PCM encapsulation thickness (steel plate)	0.003 m
Air channels height ($H_{channel}$)	0.02 m 0.04 m
Length of the PCM panels (L_{panel})	0.5 m
Width of the PCM panels (W_{panel})	0.25 m
Air duct thickness (wood layers)	0.01 m
Total internal height of the air – PCM TES unit (H_{total})	0.198 m

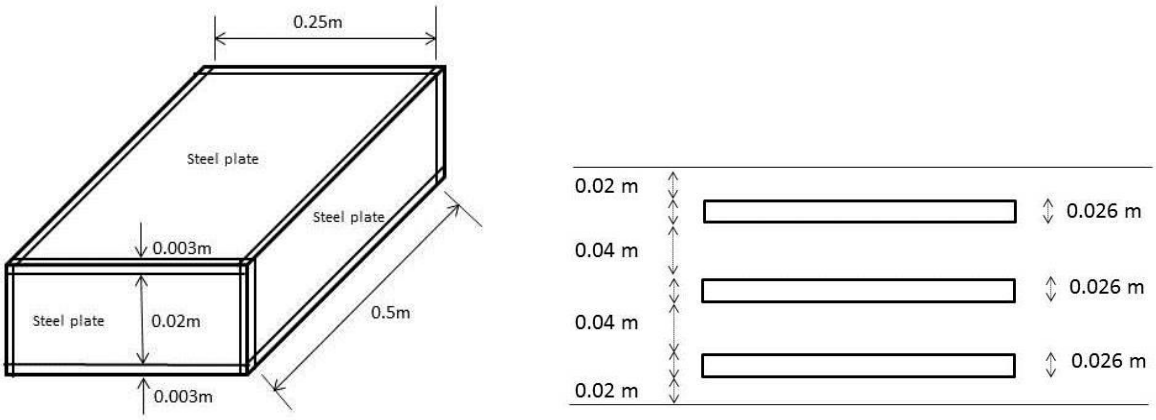

a) Single PCM panel dimensions

b) PCM panels and air channel heights arrangement

Figure 3-1 PCM panel and air gap dimensions

(iii) Mass and volume of the PCM panels and air channels

Each panel with an internal volume of 0.0025 m^3 was filled to the top with a liquid PCM in order to prevent any overflow due to volume expansion corresponding to a total mass of 1.8 kg per panel as display in Figure 3-2. The total volume of air channels corresponds to 0.07425 m^3 corresponding to a mass of 0.09 kg.

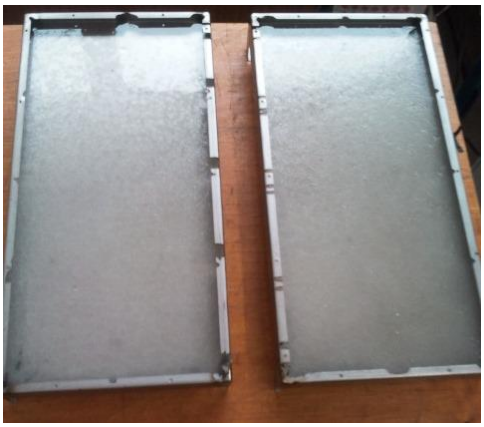

Table 3-3 PCM panels specifications

Panel internal volume	0.0025 m^3
PCM mass	1.8 kg
Panel mass	1.8 kg
Total mass per panel	3.6 kg

Figure 3-2 Mass and volume of PCM panels

3.4 Experimental setup

The experimental setup consists of an air duct made from wood due to its low thermal conductivity, aiming to reduce the heat losses to the surroundings. The main air duct presents a length (L), width (W) and height (H) of 2.2 m, 0.25 m and 0.218 m respectively. The air duct includes an air-PCM heat transfer unit coupled to a heating/cooling unit, exhaust fan and to a range of measuring equipment as presented in Figure 3-3. A photographic view of the experimental setup is also presented in Figure 3-4.

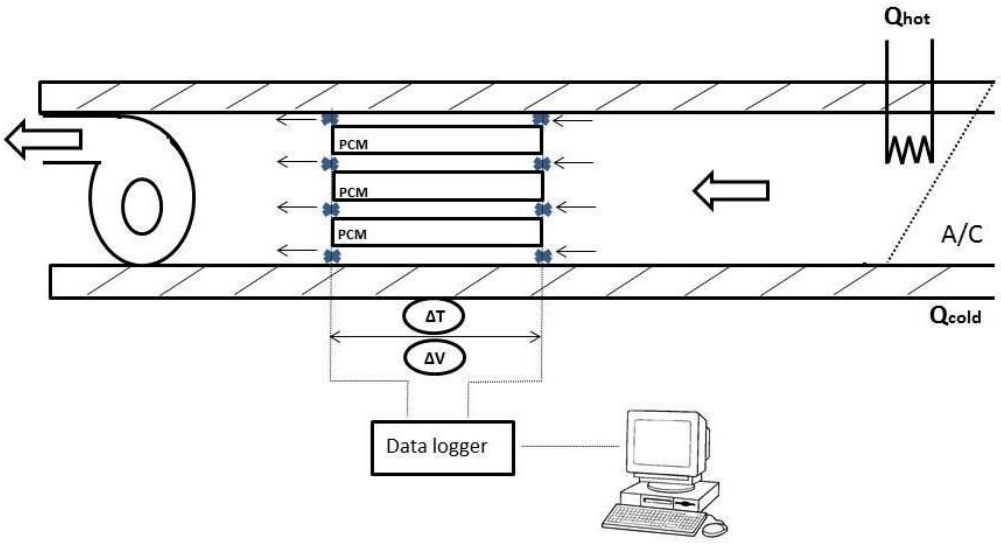

Figure 3-3 Experimental Setup

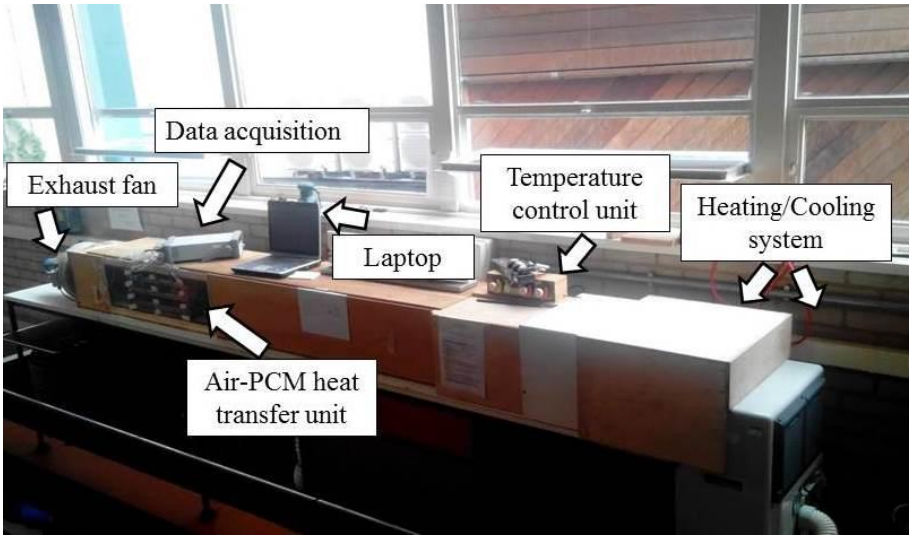

Figure 3-4 Experimental Setup

3.4.1 Components of the testing rig

(i) Exhaust fan

The air is pulled through a centrifugal exhaust fan with an electrical power and volumetric flow rate of 0.11 kW and 147 m^3/h, respectively. Varying the air velocity plays a very important role in the heat transfer between the air and the PCM panels to be analysed in this experiment. A variable speed device was coupled to the exhaust fan in order to vary the air inlet velocity. The air velocity at the main air duct can be varied from 0.6 m/s until 2.5 m/s as used for the experimental proposes and further described in section 3.3.

(ii) Air –PCM heat transfer unit

An air- PCM heat transfer unit was composed by three panels "filled" with RT25 PCM into rectangular plate and each panel was surrounded on the top and bottom by air channels. As there is no limitation in terms of space or a particular application, the plates were arranged horizontally to reduce the pressure drop and the electrical consumption of the fan. The air-PCM heat transfer unit was coupled downstream to a heating/cooling unit on one side and an exhaust fan on another side. Contrary to Zivkovic and Fujii (2001), Butala and Stritih (2009) and Waqas and Kumar (2011), three parallel plates have been arranged instead of a single panel in order to replicate the melting and solidification phenomena for the same conditions

and to achieve converged results when comparing the three panels. In other words, unexpected anomalies can be easily identified when comparing the results obtained by the three panels.

(iv) Heating/Cooling unit

The construction of the heating unit involved four electrical heating coils (2.5 kW, 2 kW, 2 kW, 2 kW) enclosed into a metal tube structure and connected to a wood box (Figure 3-5). The safety issues were guaranteed as the electric coils did not increase the temperature beyond 80 °C a lower temperature than the conventional wood burning temperature of 250 °C. Each electrical coil thermostat, except for the 2.5 kW coil with two thermostats, were connected to an adjust control, allowing six different setting temperatures (Figure 3-5). The cooling unit corresponds to a portable air conditioner (Electro-Aire) with a cooling capacity of 2.6 kW.

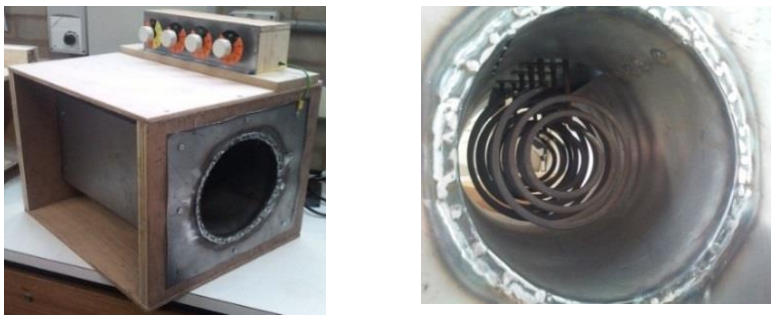

Figure 3-5 Heating unit

3.4.2 Measurement instrumentation

The instrumentation used in this study included an anemometer for the air velocity measurement, thermocouples for the PCM and air inlet/outlet temperature measurements and a data acquisition system to record the temperatures.

(i) Air velocity meter (anemometer)

The air velocity was measured at the inlet of the air duct at 25 points (Figure 3-6) as suggested in ASHRAE (1993) and TSI (2014) using an air velocity meter (TSI, model TA440A). The air velocity was also measured at the outlet and at the centre of each air channel for experimental validation purposes (Chapter 5). The accuracy and resolution of the equipment were ±0.015 m/s and 0.01 m/s respectively. The measured velocities are attached in Appendix B.

(ii) Thermocouples

The chosen thermocouples were K-type provided by RS Components and with an accuracy of ± 0.3 ºC. The air temperatures were measured at the inlet and outlet of each PCM panel by eight thermocouples as presented in Figure 3-3 (blue crosses). The temperatures were also measured along each PCM panel (15 thermocouples for each PCM panel) as presented in Figures 3-7 and 3-8. All of them were located at the centre of the panel as the panel presents a minimum height of 0.02 m and no significant variation was expected along the height.

Anemometer (TSI)

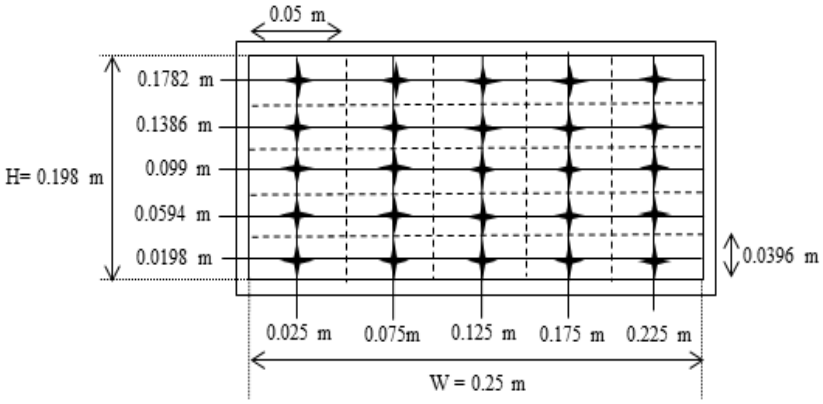

Air velocity measuring points for rectangular duct traverse

Figure 3-6 Air velocity measurement

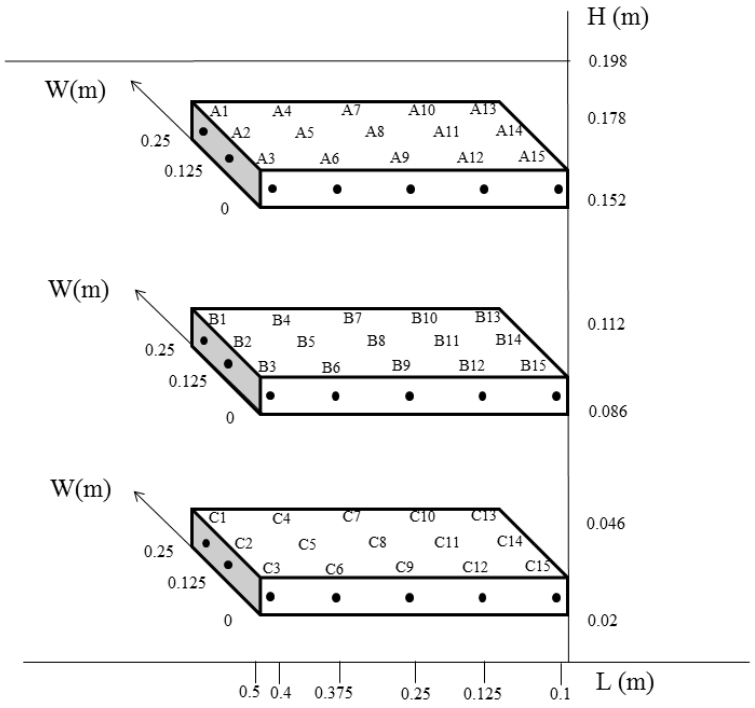

Figure 3-7 Schematic view of the thermocouples distribution

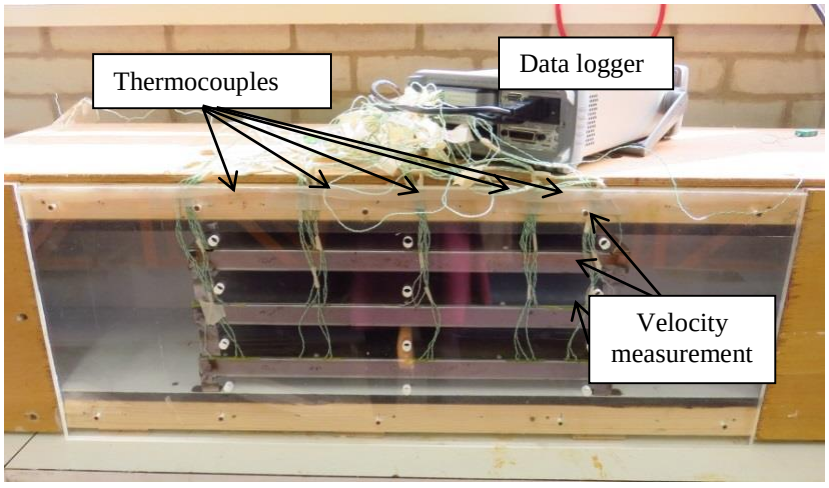

Figure 3-8 Thermocouples distribution

The thermocouples which are used in the present work are made of Nical-chromium –Alumel ((NiCr / NiAl)) (K type), of 0.2-mm wire diameter. Each wire is insulated. Thermocouples are used for measuring the water flow temperature inside the test section. The direct comparison calibration method is used to calibrate these thermocouples by using standard

thermometer with scale from 0 ºC to 100 ºC. In this method, the hot junction of the thermocouple and mercury thermometer was submerged into water in a tank. The used water was heated very slowly with small increment of temperature. The water in the tank was stirred by a mechanical stirrer. The reading of thermocouples and the thermometer were recorded at different temperatures, while heating the oil very slowly up to 100 ºC.

(iii) Data acquisition

The thermocouples were connected to a digital temperature recorder model 3470A by Agilent Technologies, UK. They included two cards that allowed coupling to a maximum of 62 thermocouples. The provided software has been used to record the temperature data in a database format with a personal computer. Time steps of 10 seconds were used for temperature monitoring.

Table 3-4 Instrumentation for experimental study and their technical information

Variable	Instrument	Model/Brand	Measurement range	Sensitivity	Quantity
Air velocity	Air flow meter	TA440A/ TSI	0 – 30 m/s	± 0.001 m/s	1
PCM/air temperatures	Thermocouples	K-type / RS Components	-50 ℃ – 1100 ℃	±0.1 ºC	55
	Data logger	3470A/ Agilent Technologies	-100 °C to 1200 °C	±0.1 ºC	1

iv) Experimental Uncertainty

The PCM and air temperatures and air velocities were measured with appropriate instruments clarified in Table 3-4 The uncertainty of the experiment was calculated by Equation 3-1 (Zhou and Zhao, 2011).

$$U = \pm \sqrt{\left(\frac{\Delta T_{TC}}{T_{TC}}\right)_{PCM}^{2} + \left(\frac{\Delta T_{TC}}{T_{TC}}\right)_{air}^{2} + \left(\frac{\Delta V}{V}\right)^{2}} \times 100\% \qquad (3\text{-}1)$$

The uncertainty was first estimated separately based on the sensitivity values specified in Table 3-4. Because the sensitivity of thermocouples and the data logger are set at ± 0.1 °C, the reading errors for PCM and air temperature measurements are assumed as ±0.2 ˚C (ΔT_{TC}). The sensitivity of the anemometer used in measuring the velocity of the air is ±0.001 m/s and reading errors are ±0.001 m/s (ΔV) respectively.

The relative uncertainties of the PCM temperature considering the minimum and maximum temperatures are:

For T_{min} = 15°C, the uncertainty becomes:

$$\left(\frac{\Delta T_{TC}}{T_{TC}}\right)_{PCM} = 1.3\ \%$$

For T_{max} = 35°C, the uncertainty becomes:

$$\left(\frac{\Delta T_{TC}}{T_{TC}}\right)_{PCM} = 0.57\ \%$$

The relative uncertainties of the air temperature considering the minimum and maximum temperatures are:

For T_{min} = 12 °C, the uncertainty becomes:

$$\left(\frac{\Delta T_{TC}}{T_{TC}}\right)_{air} = 1.6\ \%$$

For T_{max} = 38 °C, the uncertainty becomes:

$$\left(\frac{\Delta T_{TC}}{T_{TC}}\right)_{air} = 0.52\ \%$$

The relative uncertainties of the air velocity considering the minimum and maximum velocities are:

For V_{min}= 0.6 m/s, the relative uncertainty of the velocity of the air is:

$$\left(\frac{\Delta V}{V}\right)_{air} = 0.16\ \%$$

For V_{max}= 2.5 m/s, the relative uncertainty of the velocity of the air is:

$$\left(\frac{\Delta V}{V}\right)_{air} = 0.04\ \%$$

The maximum uncertainties reached for each parameter are summarized in Table 3-5

Table 3-5 Experimental uncertainty

Parameter	Equipment	Uncertainty
PCM temperature	K-type thermocouples (ΔT_{TC}) Data logger (ΔT_{DT})	1.3%
Air temperature	K-type thermocouples (ΔT_{TC}) Data logger (ΔT_{DT})	1.6 %
Air velocity	Anemometer (ΔV)	0.16 %

The total uncertainty is obtained by applying Equation 3-1 for the uncertainties listed in Table 3-5. Thus, the experimental uncertainty is estimated at 2.1 % and it guarantees the credibility of the experimental data.

3.5 Experimental procedure

The experimental procedure involves the charging and discharging of the panels for different air inlet velocity and temperature conditions (Table 3-6). The charging and discharging processes corresponded to the solidification and melting of the PCM panels respectively.

In the discharging process, hot air flowed at a constant flow rate through the air-PCM heat transfer unit in order to melt the PCM panels. The process was continued until the PCM

reached 30 °C, beyond the melting temperature of 25 °C. In the charging process, cold air at a lower temperature than the PCM solidification temperature was supplied at a constant flow rate until the whole PCM was solidified below 23 °C.

Table 3-6 Experimental procedures

Experiment		Air inlet temperature (°C)	Air inlet velocity (m/s)	Air mass flow rate (kg/s)
Variable inlet velocity	Discharging process	38	0.6	0.036
			1.6	0.097
			2.5	0.152
	Charging process	12	0.6	0.036
			1.6	0.097
			2.5	0.152
Variable air inlet temperature	Discharging process	30	1.6	0.097
		34		
		38		
	Charging process	12		
		16		
		18		

3.6 Results and discussion

To estimate the charging and discharging time, a total of 15 thermocouples have been fixed in each panel to understand the temperature variations along the panels. However, the analysis can be simplified by identifying the critical points. These critical points corresponded to last points from the inlet where melting or solidification took place and assuring that these points were fully melted or solidified, the entire panel was assumed completely charged or discharged. In order to identify these critical points, Figure 3-9 presents three scenarios (1, 2 and 3) of a single panel containing the PCM completely solidified and in contact with a heat source. For all scenarios over the time that the PCM started to melt with associated liquid fraction; the increase of the liquid fraction was identified by the interfaces numbered from 1 to 4. For scenario 1, the panel was heated from the top and bottom and over time the liquid

fraction increases from interface 1 to 4. In this case, the melting fractions increased symmetrically. The last part that melted was at the centre of the panel and delimited by interface 4. For scenario 2, the panel was heated from the top and bottom and also from the right end. The melted fraction was increased symmetrically in the vertical direction. However, for the horizontal direction a higher rate of melting fraction was noted at the right end as it was closer to the heat source. Over time the interface moved from 1 to 4 and it was observed that the left end was the last part that melted, represented by interface 4. Scenario 3 represents the current experiment, similar to the previous case however the heat source was from the convection of hot HTF surrounding the panel. Hence, additionally to the previous case, the left and right ends were surrounded by a high convective heat coefficient of the surrounded HTF benefiting the heat transfer at these last two ends. Therefore the melting of the last part is not expected to occur at the left end, but between the centre and the left end.

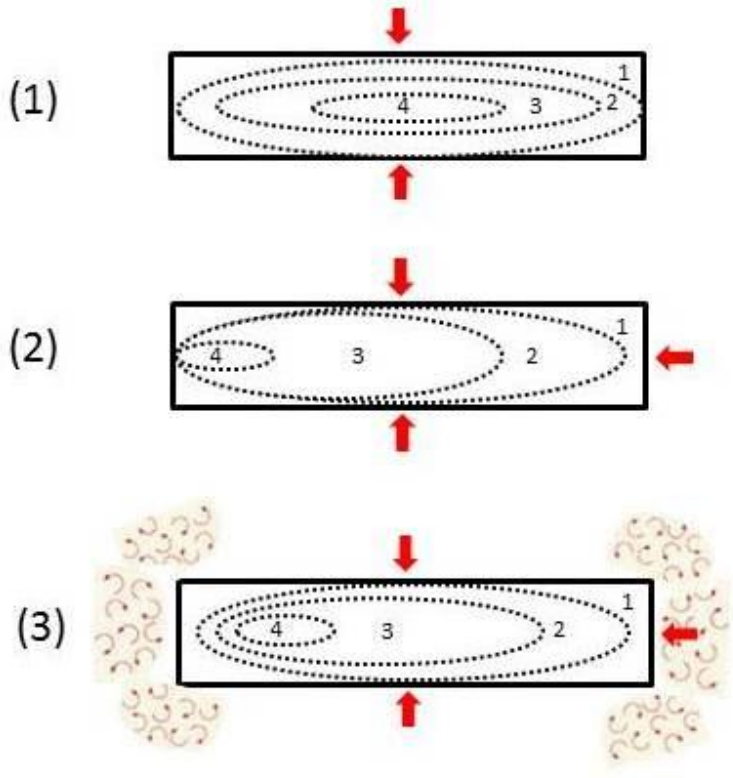

Figure 3-9 Melting process of single PCM panel in contact with heat source

The analogy presented in Figure 3-9 was confirmed experimentally and shown in Figure 3-10 The complete charging and discharging time for each panel was assumed with respect to

thermocouples A5, B5 and C5. Also, by comparing these three thermocouples it was observed that the complete melting time of the bottom panel – C5 took slightly longer when compared with the top panel- A5 and the middle panel - B5 (Figure 3-10). The more reasonable explanation for this slight discrepancy was related to a minimal thermal buoyancy effect that occurred in the experimental apparatus benefiting the upper panels.

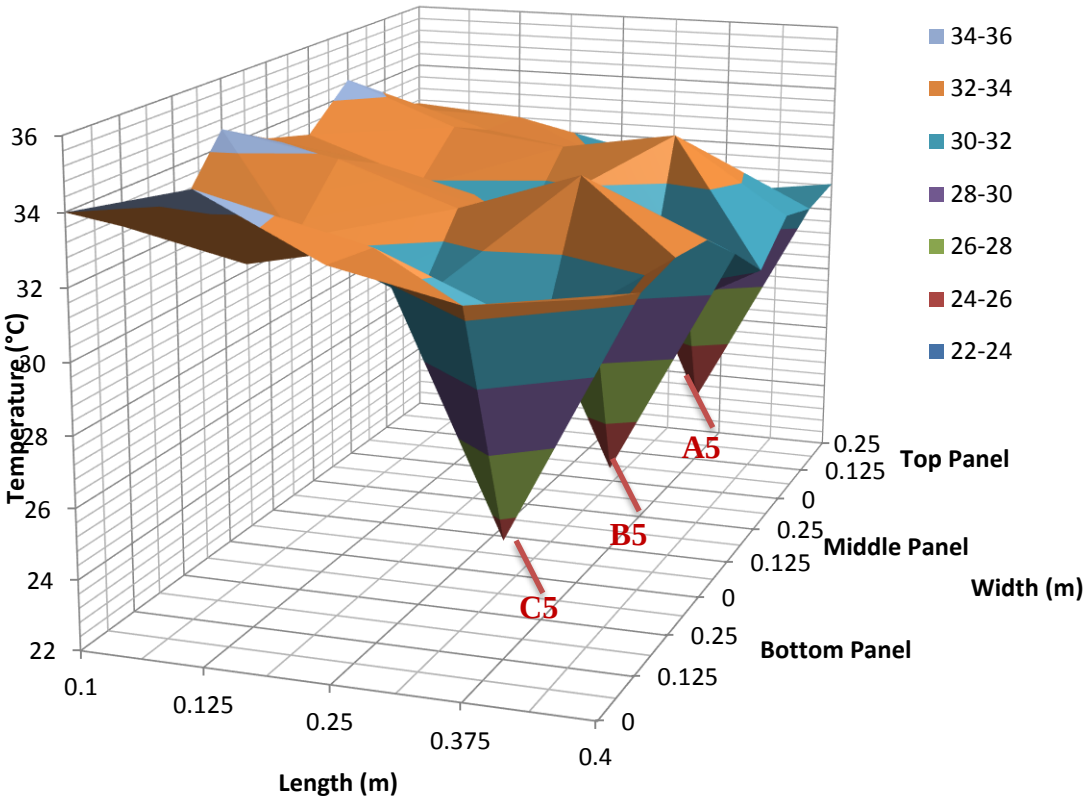

Figure 3-10 Temperature profile across the PCM Panel

Typical melting and solidification curves can be visualized in Figures 3-11 and Figure 3-12. For each curve it was possible to visualize three different shapes. The first one corresponding to a "sharp" increasing trend, reflected the sensible heat due to the increase of the initial PCM temperature until the beginning of the melting temperature (approx. 23°C), followed by the phase change process (23 – 25 °C). This was represented by an increasingly smooth curve with a nearly constant temperature. Afterwards a third curve was noticed with a rapid increase in temperature corresponding to the sensible heat after the phase change was completed. Hence, charging and discharging processes were assumed complete at 23 °C and 25 °C respectively.

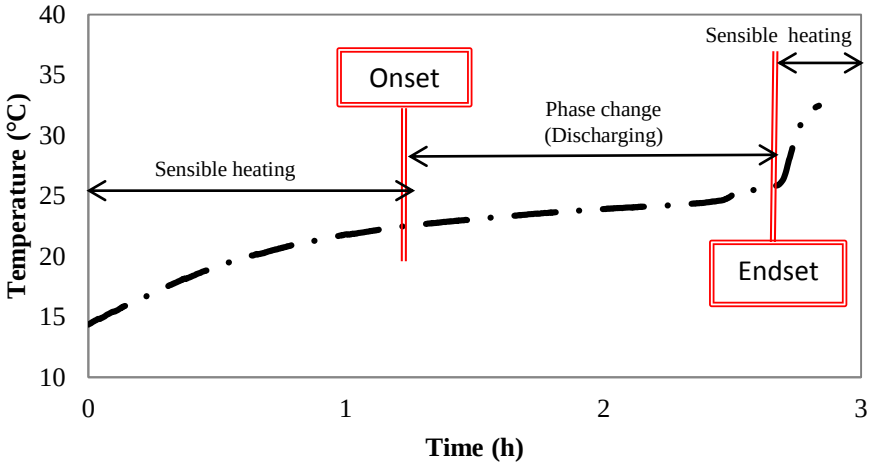

Figure 3-11 Typical PCM discharging process curve

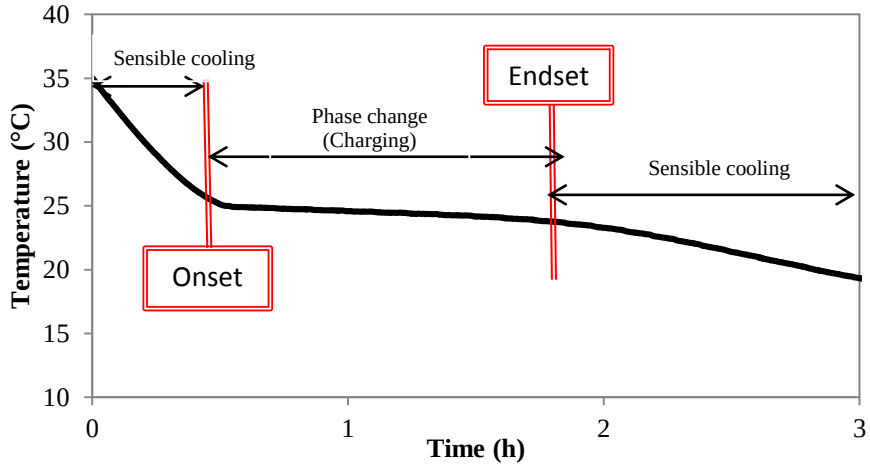

Figure 3-12 Typical PCM charging process curve

Similar curves were presented in the literature namely Tay et al., 2001 and Castell et al., 2011.

3.6.1 Influence of air inlet velocity

The influence of the air inlet velocity on the discharging time was analysed for three velocity variations of 0.6 m/s, 1.6 m/s and 2.5 m/s for the inlet temperature of 38 °C (Table 3-6)

i) Charging/discharging time and air temperature difference

For the discharging process the air temperature was fixed at 38 °C and the influence of the air velocity was analysed through varying the velocity from 0.6 m/s, 1.6 m/s and 2.5 m/s. The initial temperature of the whole system was at 16 °C and the average ambient temperature at 19 °C. The transient PCM temperatures for the different conditions were presented in Figure 3-13 to 3-15. The phase change was considered to start at 23 °C based on Table 3-1 and also, as observed in Figures 3-11 and 3-12, from this temperature onwards, the curves start to become horizontal translating the beginning of the phase change. The black line represents the melting temperature, i.e. temperature at which the phase change was complete and the PCM was completely liquid (25 °C). The period of time for the PCM to increase its initial temperature until it reached the melting temperature was represented by t_1, t_2 and t_3 for 0.6 m/s, 1.6 m/s and 2.5 m/s respectively.

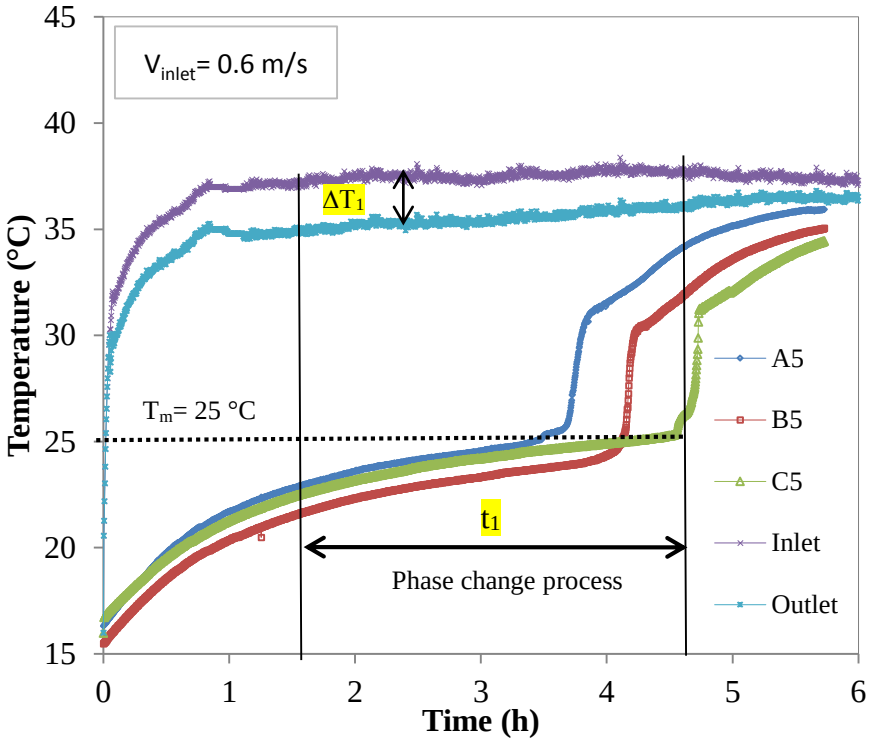

Figure 3-13 Influence of air inlet velocity (0.6 m/s) on the PCM and air outlet temperature for the discharging process

Following the analogy presented in Figures 3-9 and 3-10, the complete charging and discharging time for each panel was assumed with respect to thermocouples A5, B5 and C5.

Figure 3-13 displays these curves and a similar trend was presented for the thermocouples A5 (top panel), B5 (middle panel) and C5 (top panel) showing a good agreement of the results. Discharging took place after 3.7h, 4.1h and 4.6h for the thermocouples A5, B5, and C5 respectively. Due to the minimal thermal buoyancy effect occurring in the experimental apparatus the last thermocouple reaching the melting temperature was C5. Hence the panels were assumed completely discharged when the thermocouple C5 registered the melting point (25 °C), corresponding to period of time t_1. For the air inlet velocity of 0.6 m/s the discharging time for C5 was 4.6h. The temperature difference corresponded to an average of 2.4 °C (ΔT_1).

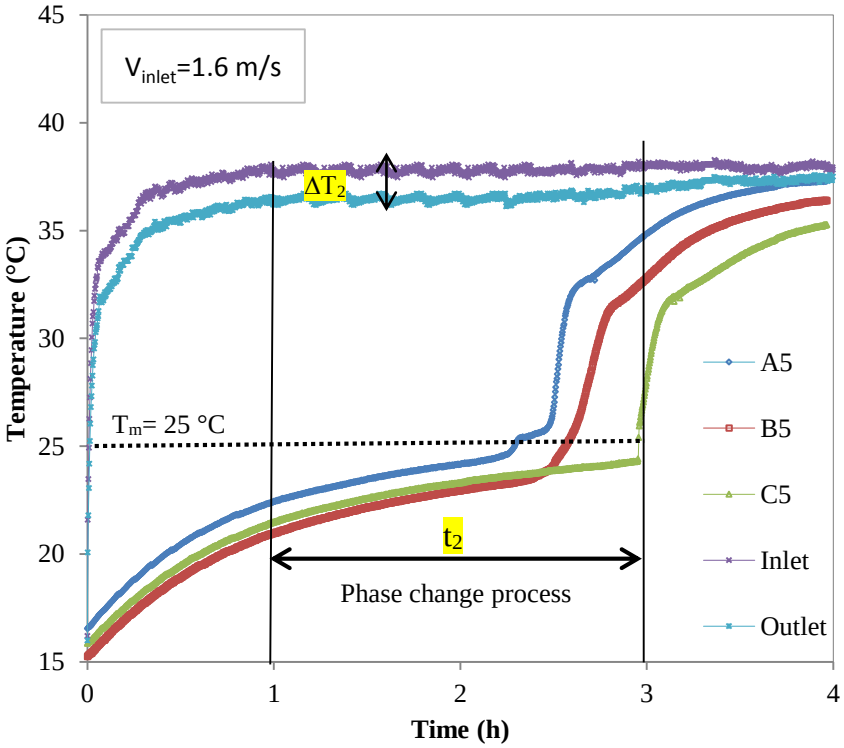

Figure 3-14 Influence of air inlet velocity (1.6 m/s) on the PCM and air outlet temperature for the discharging process

Figure 3-14 displays the same curves and a similar trend was presented for the thermocouples A5 (top panel), B5 (middle panel) and C5 (top panel) showing good agreement of the results. The discharging time took place after 2.7h, 2.7h and 3h for thermocouples A5, B5, and C5 respectively. The panels were completely discharged after 3h (t_2). For the air inlet velocity of 1.6 m/s the air temperature difference was 1.3 °C (ΔT_2).

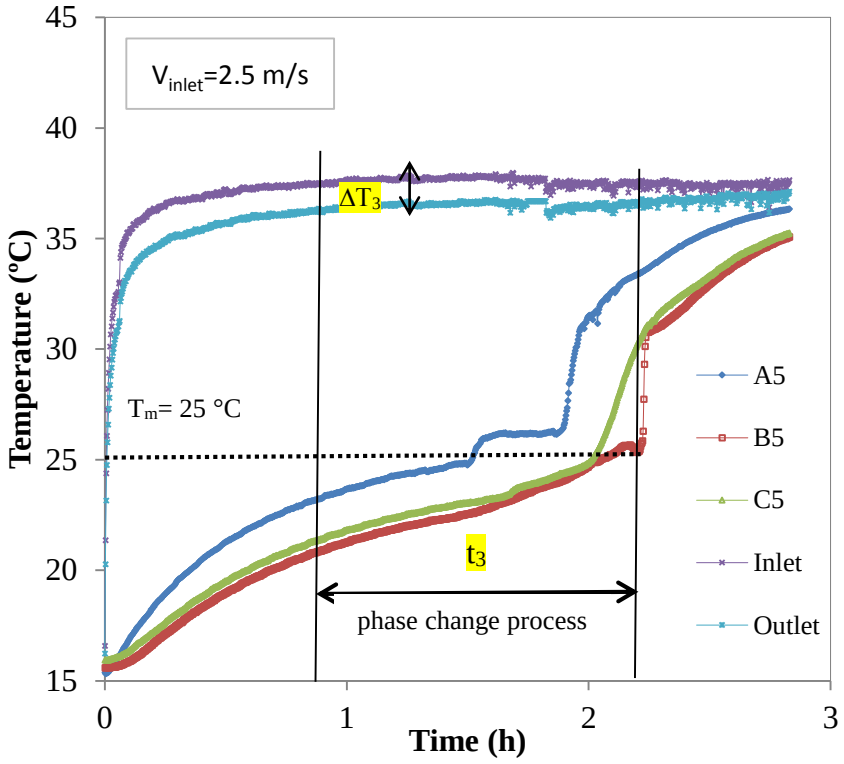

Figure 3-15 Influence of air inlet velocity (2.5m/s) on the PCM and air outlet temperature for the discharging process

For air inlet velocity of 2.5 m/s the panels were completely discharged after 1.9 h, 2 h and 2.2 h for thermocouples A5, B5, and C5 respectively and the air temperature difference was 0.7 °C (ΔT_3). From Figure 3-13 to Figure 3-15 it was observed that firstly the PCM temperature increased very rapidly (sensible heating) followed by a slow temperature increase from 23 - 25 °C (phase change). Afterwards the PCM temperature increased very sharply meeting the air inlet temperature (38 °C) in a very short period of time (sensible heating). Overall, it was possible to visualise that increasing the air inlet velocity decreases the time for the PCM panels to be completely discharged. However, this increase was not proportional. For instance increasing the air inlet velocity from 0.6 m/s (t_1) to 1.6 m/s (t_2) significantly reduced the melting time by approximately 1.6h, however, a further increase to 2.5 m/s reduced the time only in 0.8h. It was also observed that for the discharging process, increasing the air inlet velocity decreases the temperature difference between the air inlet and air outlet temperatures, ΔT and thus enabled faster heat transfer. From the graph, it was observed that for the air inlet velocity of 2.5 m/s an average temperature difference of 0.7 °C was registered. For 1.6 m/s the temperature difference reaches 1.3 °C. For an air inlet velocity of

0.6 m/s, the average temperature difference corresponded to 2.4 °C. For a lower air inlet velocity, there is a longer contact time between the air and the PCM, enhancing the heat transfer and consequently the air temperature difference. Again, it was observed that the air inlet difference did not vary proportionally. For both parameters (discharging time and air temperature difference) the first increment of velocity (0.6 m/s to 1.6 m/s) reached twice the value than that observed for the second increment (1.6 m/s to 2.5 m/s).

For the charging process the air temperature was fixed at 12 °C and the influence of the air velocity was analysed by varying the velocity from a minimum of 0.6 m/s, 1.6 m/s to a maximum of 2.5 m/s. The initial temperature of the PCM panels was at 30 °C, the average ambient temperature was at 19 °C. The transient PCM temperatures for the different velocities (Figures 3-16 to Figure 3-18) corresponded to the charging time t_1, t_2 and t_3 of the PCM panels for 0.6 m/s, 1.6 m/s and 2.5 m/s respectively.

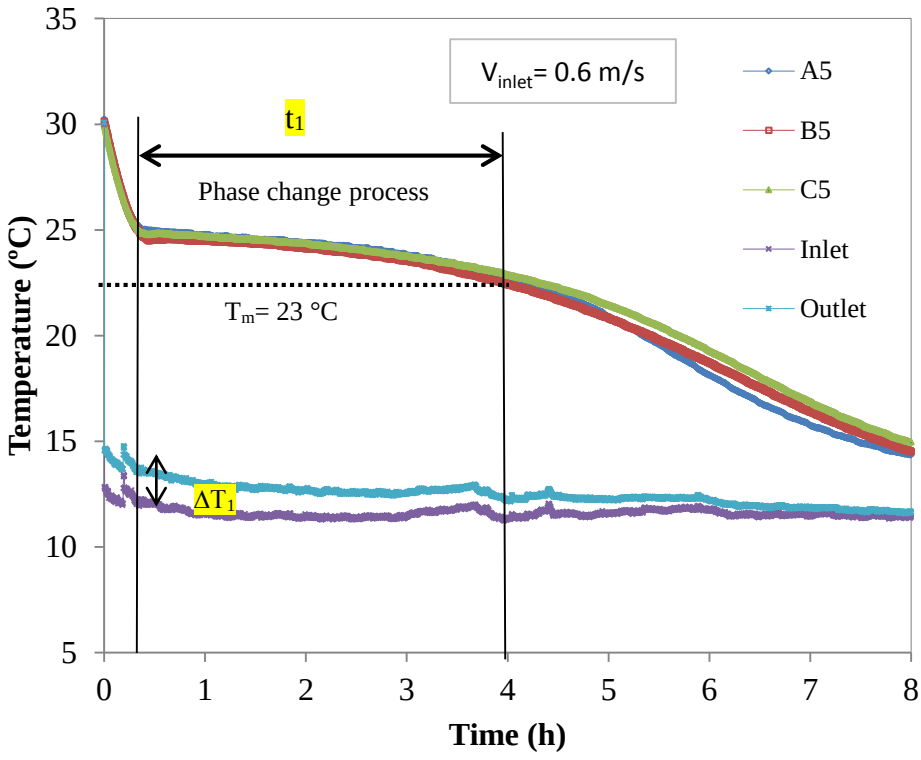

Figure 3-16 Influence of the air inlet velocity (0.6 m/s) on the PCM and air outlet temperature for the charging process

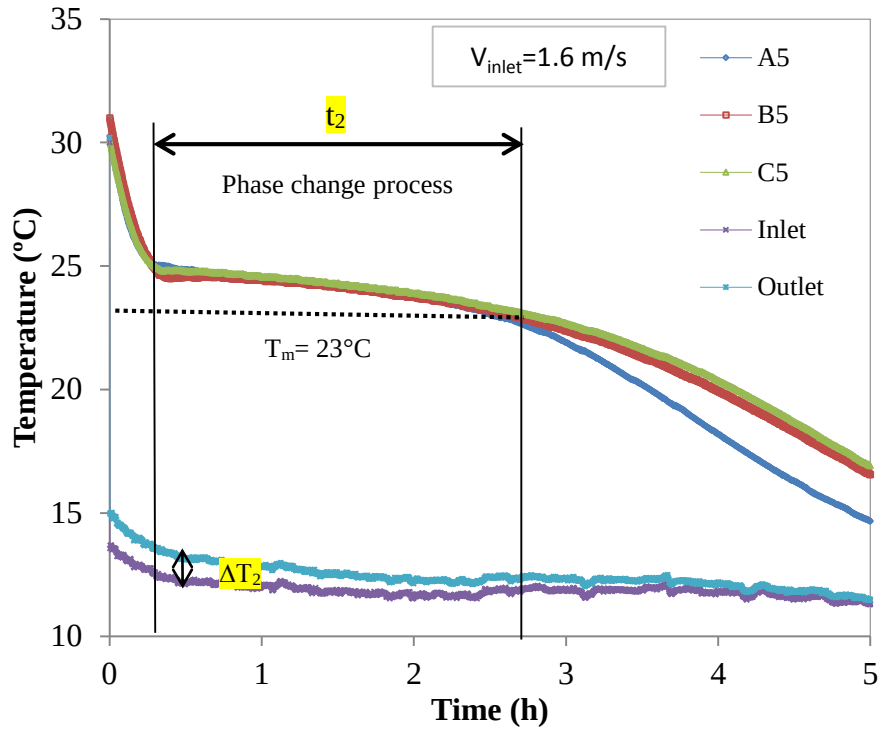

Figure 3-17 Influence of the air inlet velocity (1.6 m/s) on the PCM and air outlet temperature for the charging process

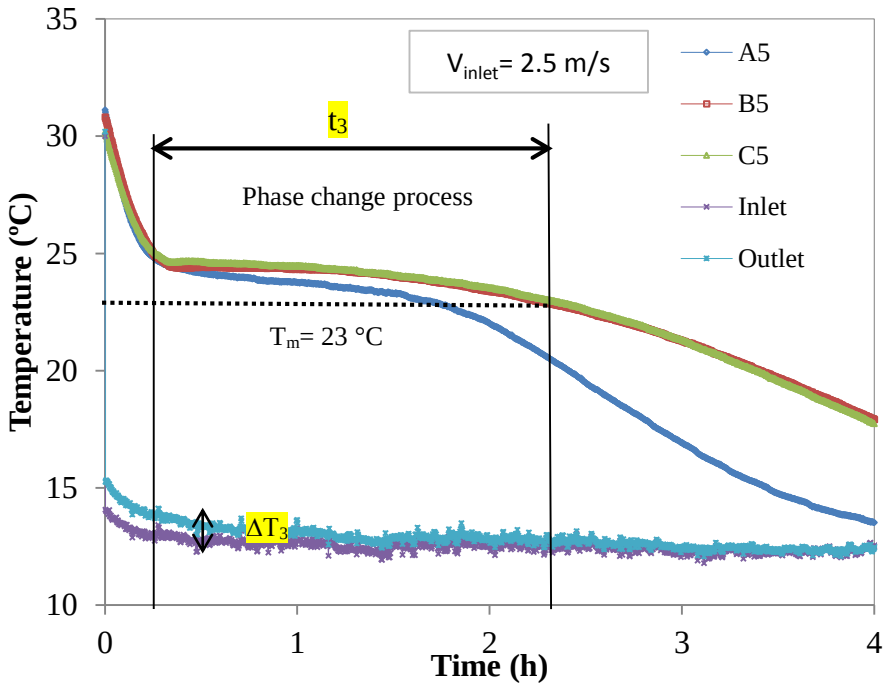

Figure 3-18 Influence of the air inlet velocity (2.5 m/s) on the PCM and air outlet temperature for the charging process

For the velocity of 0.6 m/s, 1.6 m/s and 2.5 m/s, the complete phase change took 4h (t_1), 2.8h (t_2) and 2.3h (t_3) respectively. Through increasing the air inlet velocity from 0.6 m/s to 1.6 m/s the solidification time was reduced by over 1 hour. Increasing the velocity further to 2.5 m/s reduced the time in nearly half an hour. Another observation was that the temperatures at A5, B5 and C5 become similar as the velocity increases. This is because the air inlet temperature for higher velocities becomes uniform along the height, contrary to smaller velocities when the buoyancy effect was more evident. For smaller velocities, the temperature was higher at the top and bottom due to the stack effect.

It was observed that for the charging process of the PCM, the increase in the air velocity reduced the difference between inlet and outlet air temperatures and also the time at which they become equal. This was because of the increase in heat transfer between air and energy stores in PCM panels. For instance, for 0.6 m/s the temperature difference (ΔT_1) remained around 1.2 °C. During the phase change however, for a higher air inlet velocity of 2.5 m/s, ΔT_2 it reduces to 0.3°C. Again, this was due to the longer contact time between the PCM and air inlet temperature for the lower velocity: 0.6 m/s. As for the discharging process, the charging time and air temperature difference reached half magnitude for the second increment (1.6 m/s to 2.5 m/s) compared to the first increment (0.6 m/s to 1.6 m/s) of the air velocity. Table 3-7 summarizes the influence of the air inlet velocity on the charging and discharging process.

Table 3-7 Summary of the air inlet velocity influence on the charging and discharging process

	0.6 m/s (t_1)	1.6 m/s (t_2)	2.5 m/s (t_3)
Discharging process (T= 38°C)	4.6h	3h	2.2h
Charging process (T= 12°C)	4h	2.8h	2.3h

From Table 3-7, comparing the overall time for the charging and discharging processes, it can be seen that for the selected air inlet temperatures of any air inlet velocities the discharging process takes slightly longer than the solidification process ≈ 0.5h. Looking closely at the discharging process, increasing the air inlet velocity from 0.6 m/s to 1.6 m/s reduces the

melting time in 1.6h and by increasing the velocity further the velocity to 2.5 m/s reduced the melting time in only another 0.8h. For the charging process, increasing the velocity from 0.6 m/s to 1.6 m/s reduced the melting time in 1.2h and further increasing the velocity to 2.5 m/s reduced the melting time in 0.5h. For both the charging and discharging process, it was concluded that increasing the air velocity from 0.6 m/s to 1.6 m/s significantly reduces the phase change time, hence 1.6 m/s was selected as the air inlet velocity to be used for the following analysis: air inlet temperature influence on the charging and discharging time.

Table 3-8 summarizes the influence of the air inlet velocity on the air temperature for both the charging and discharging processes.

Table 3-8 Summary of the air temperature difference

	0.6 m/s (ΔT_1)	1.6 m/s (ΔT_2)	2.5 m/s (ΔT_3)
Discharging process (T= 38°C)	2.4 °C	1.3 °C	0.7 °C
Charging process (T= 12°C)	1.2 °C	0.6 °C	0.3 °C

Overall, for the selected velocities it was observed that the air temperature difference between the air inlet and outlet was higher for the discharging processes. For both processes the air temperature difference decreased as the air velocity was increased. The temperature difference decreased most significantly for the first increment 0.6 m/s to 1.6 m/s for both processes. For instance, for the charging process the temperature difference corresponded to only 0.3 °C for an air inlet velocity of 2.5 m/s.

ii) Heating/cooling load

During the discharging process of the PCM panels, air was cooled down to corresponded to a certain cooling load (Q_c). The cooling load during the discharging process was calculated using the measured values of the air temperature at the inlet and outlet of the air-PCM heat transfer unit. The cooling load of the unit can be calculated as follows:

$$Q_c = \int_0^t m_{air}\, c_{p,air}(T_{in} - T_{out})\, dt \qquad (3\text{-}2)$$

where T_{in} and T_{out} correspond to the air inlet and outlet temperatures respectively for each time step, t.

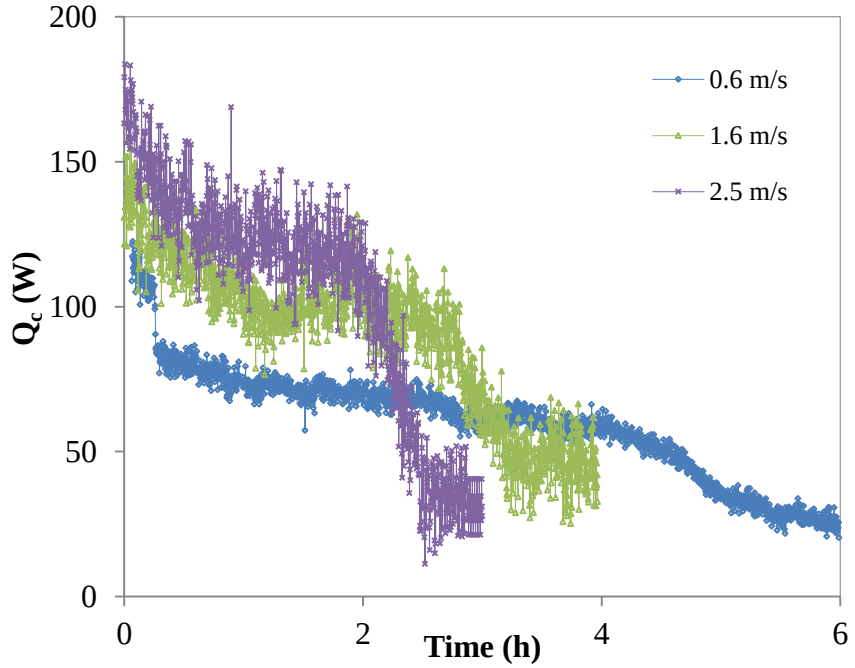

Figure 3-19 Influence of the air inlet velocity on the cooling load for the discharging process (Q_c)

Generally for all air inlet velocities during the first hours, a high cooling load was observed related to the air sensible cooling (i.e. PCM sensible heating) followed by a nearly constant load during the phase change followed again by air sensible cooling (i.e. PCM sensible heating) that drastically reduced the cooling load. Figure 3-19 shows that at a higher air inlet velocity, the cooling load achieved higher values but reached the minimum value in a shorter time period, showing and confirming that the discharging process of the PCM was completed earlier at a higher air inlet velocity. On the other hand for lower air inlet velocities, the cooling load (Q_c) reached lower values. However, it stayed above the minimum value for a longer period of time. An average cooling load corresponded to 70 W, 110 W and 130 W for air velocities of 0.6m/s, 1.6 m/s and 2.5m/s respectively for designed test rig.

While the PCM panels were charged the air was heated up and the heating load during the process was determined as follows:

$$Q_h = \int_0^t m_{air}\, c_{p,air}(T_{out} - T_{in})\, dt \qquad (3\text{-}3)$$

where T_{in} and T_{out} correspond to the air inlet and outlet temperatures respectively for each time step, t.

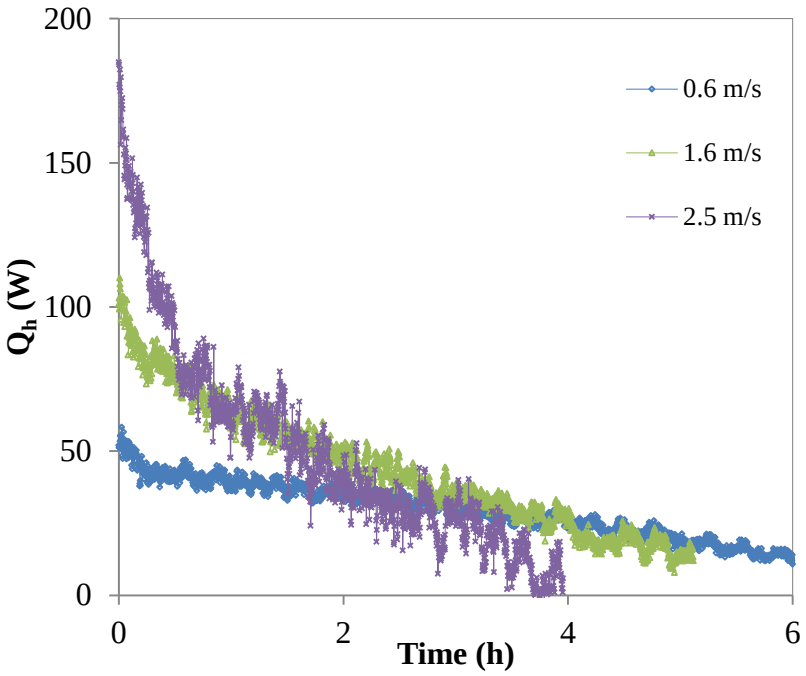

Figure 3-20 Influence of the air inlet velocity on the heating load for the charging process (Q_h)

As for the cooling load, for the heating load it was observed that the for higher air inlet velocities the heating load reached the minimum value in a shorter period of time, translating to a quicker charging time of the panels. Lower air inlet velocity translated lower heating load. However, it remained nearly constant over 8h. The average heating load corresponded to 30 W, 40 W and 50 W to air velocity of 0.6m/s, 1.6 m/s and 2.5m/s respectively.

iii) Effectiveness over the phase change process

The effectiveness over the phase change process can be determined by the average inlet and outlet temperature during the process (Tay et al., 2012). This parameter gives an indication of the performance of the effectiveness.

$$\varepsilon = \frac{T_{in} - T_{out}}{T_{in} - T_{m,PCM}} \quad (3\text{-}4)$$

The Equation 3-4 formulation was adapted from the theoretical (general) heat exchanger temperature transfer efficiency with the phase change material taken as the ideal outflow temperature (Chiu and Martin, 2013). Figure 3-21 and Figure 3-22 display the effectiveness of the discharging and charging process respectively for different air inlet velocities.

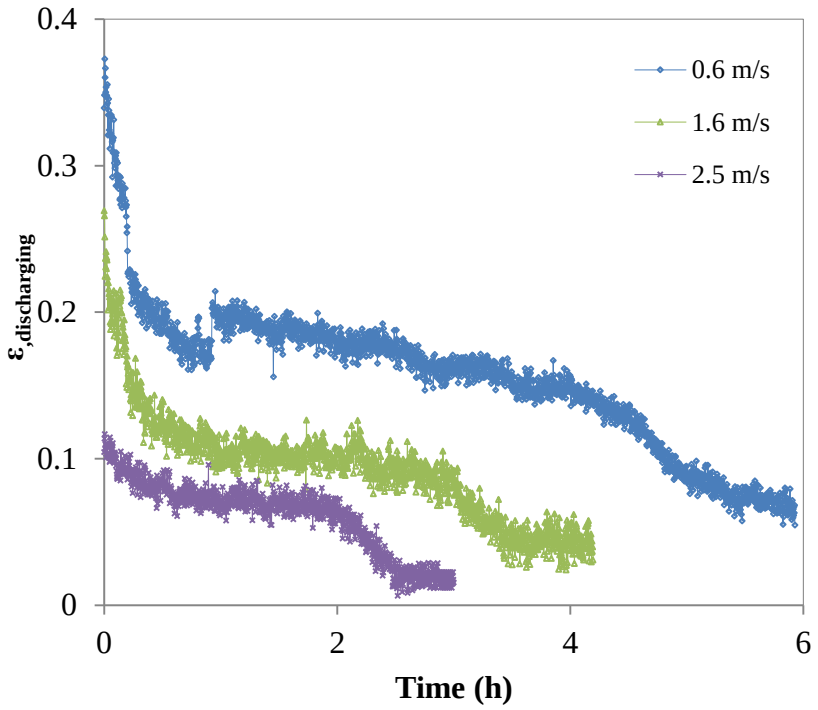

Figure 3-21 Influence of the air inlet velocity on the effectiveness for the discharging process

Overall the average effectiveness of the discharging process ranged between 0.18 and 0.08. The typical values of effectiveness vary between 0 and 1, representing minimum and maximum value. While difference between temperatures (inlet and outlet) is low effectiveness will tend to have lower value and vice versa. More importantly the objective is to define effectiveness is to understand how the air inlet temperature and velocity influence the effectiveness trend over the time.

Higher effectiveness was achieved for lower air inlet velocity due to the longer contact time of the PCM with the air. For, a lower velocity, the panels were in contact with the air source for longer enhancing the transfer process and hence the air temperature difference directly proportional to the effectiveness.

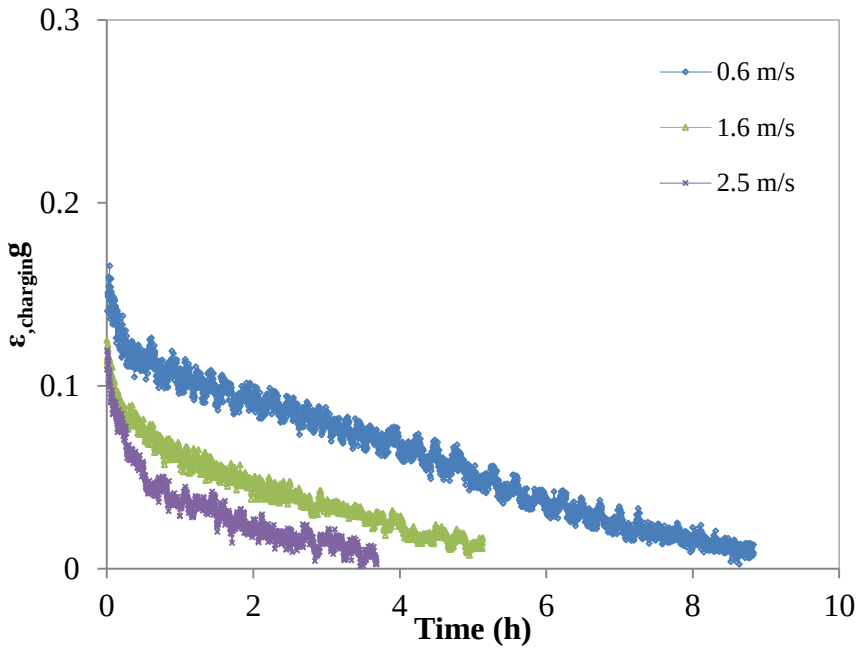

Figure 3-22 Influence of the air inlet velocity on the effectiveness for the charging process

The charging process was represented by an effectiveness ranging between 0.1 and 0.05. As for the discharging process, as the air inlet velocity was decreased, the effectiveness over the phase change was increased. Overall, the effectiveness was higher for discharging than for the charging process. This was due to the higher air temperature difference achieved. For the selected temperatures, the discharging process presented higher temperature difference (Table 3-8) translating to a higher effectiveness.

3.6.2 Influence of air inlet temperature

The influence of the air inlet temperature was evaluated by fixing the air inlet velocity at 1.6 m/s and varying the air inlet temperature from 30 °C, 34 °C and 38 °C. The initial temperature of the PCM was at 16 °C, i.e. fully solidified. Figures 3-23 to 3-25 display the discharging time and air temperature difference for an air inlet temperature of 30 °C, 34 °C and 38 °C respectively.

i) Charging/ discharging time and air temperature difference

For the discharging process, the air velocity was fixed at 1.6 m/s and the influence of the air temperature was analysed by varying the temperature from 30 °C, 34 °C and 38 °C. The initial temperature of the whole system was at 16 °C and the average ambient temperature at 19 °C. The transient PCM temperatures for the different conditions are presented in Figures 3-23 to 3-25. The black line represents the melting temperature, i.e. temperature at which the phase change was complete and the PCM was completely liquid (25 °C). The time taken by the PCM to increase its initial temperature until it reaches its melting temperature was represented as t_1, t_2 and t_3 for 30 °C, 34 °C and 38 °C respectively.

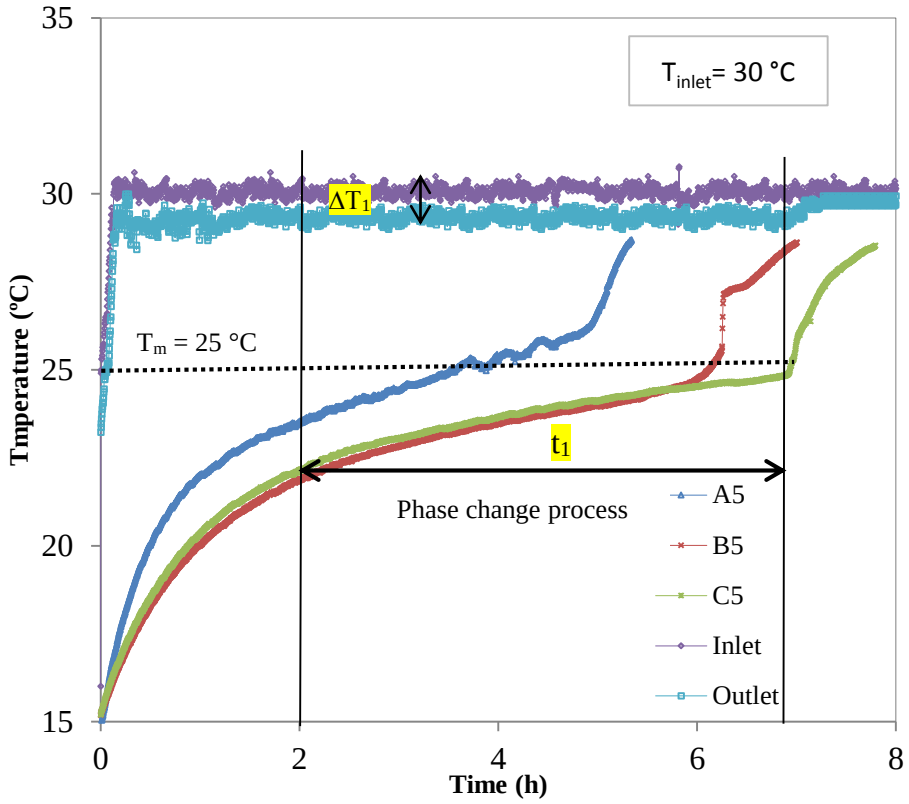

Figure 3-23 Influence of the air inlet temperature (30 ºC) on the PCM and air outlet temperature for the discharging process

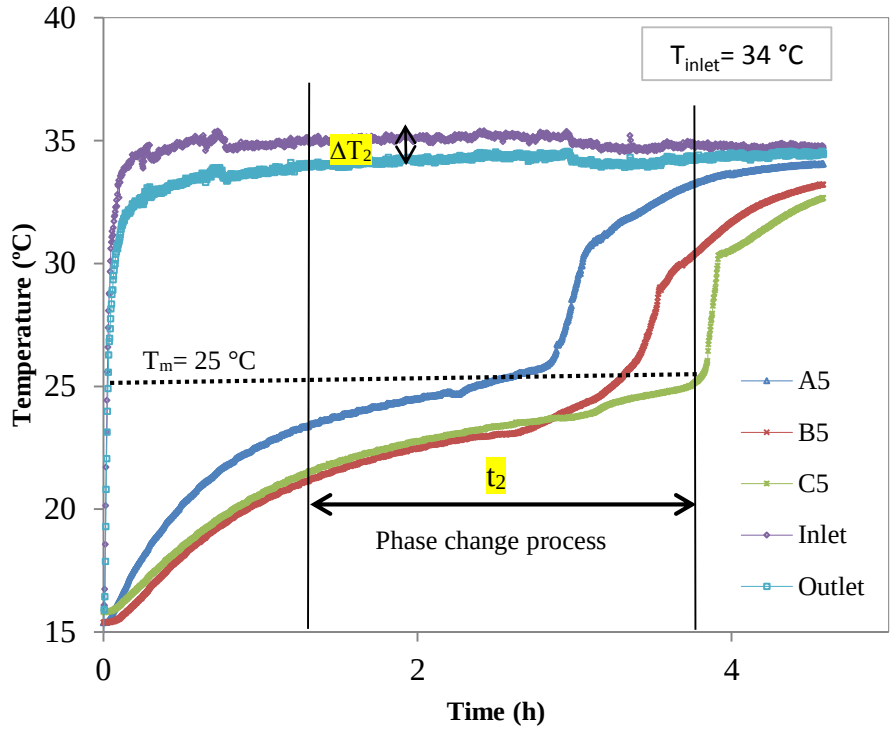

Figure 3-24 Influence of the air inlet temperature (34 ºC) on the PCM and air outlet temperature for the discharging process

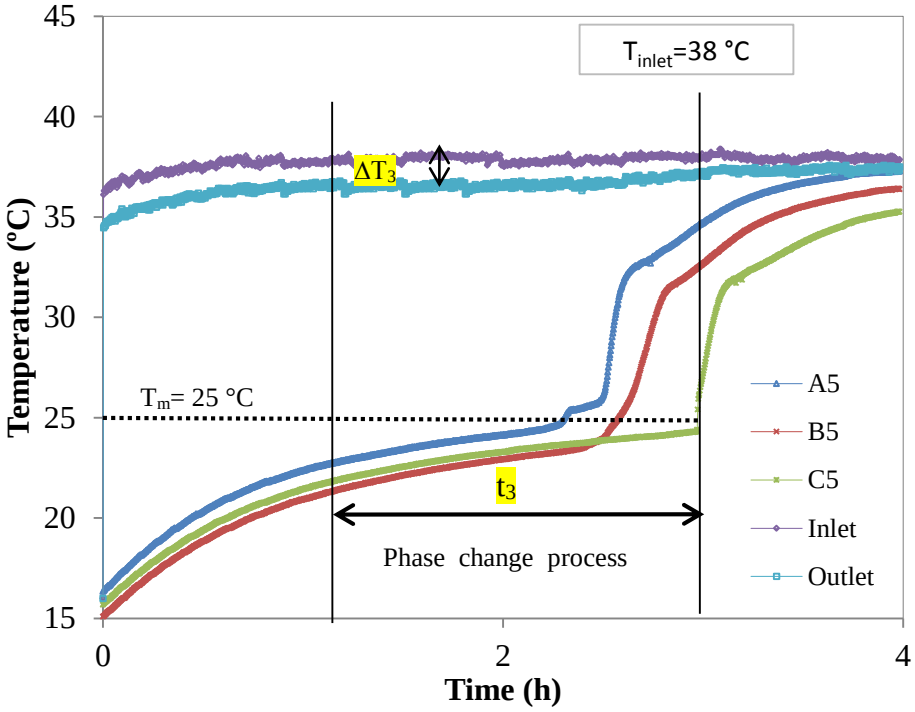

Figure 3-25 Influence of the air inlet temperature (38 ºC) on the PCM and air outlet temperature for the discharging process

Figure 3-23 shows that for the minimum inlet temperature (30 °C) the melting process took around 6.9h. This time was reduced by three hours for the inlet temperature of 34 °C and reduced in only 0.8h for the maximum temperature (38 °C). The results suggest that increasing the air inlet temperature from 30 °C to 34°C significantly affects the discharging time. Increasing further to 38 °C reduced the time in 0.8h. In all cases, after the discharging was complete, the PCM temperature increases very sharply to meet the air inlet temperature (heat source input) in a very short period of time. For the air temperature difference, it was observed that increasing the air inlet temperature achieved a linear relationship of the air outlet temperature. In fact, there was an air temperature difference of only 0.2 °C between each increment.

For the charging process, the air velocity was fixed at 1.6 m/s and the influence of the air temperature was analysed by varying the air temperature from 12°C, 16 °C and 18 °C. The transient temperatures for the three conditions are presented in Figures 3-26 to 3-28.

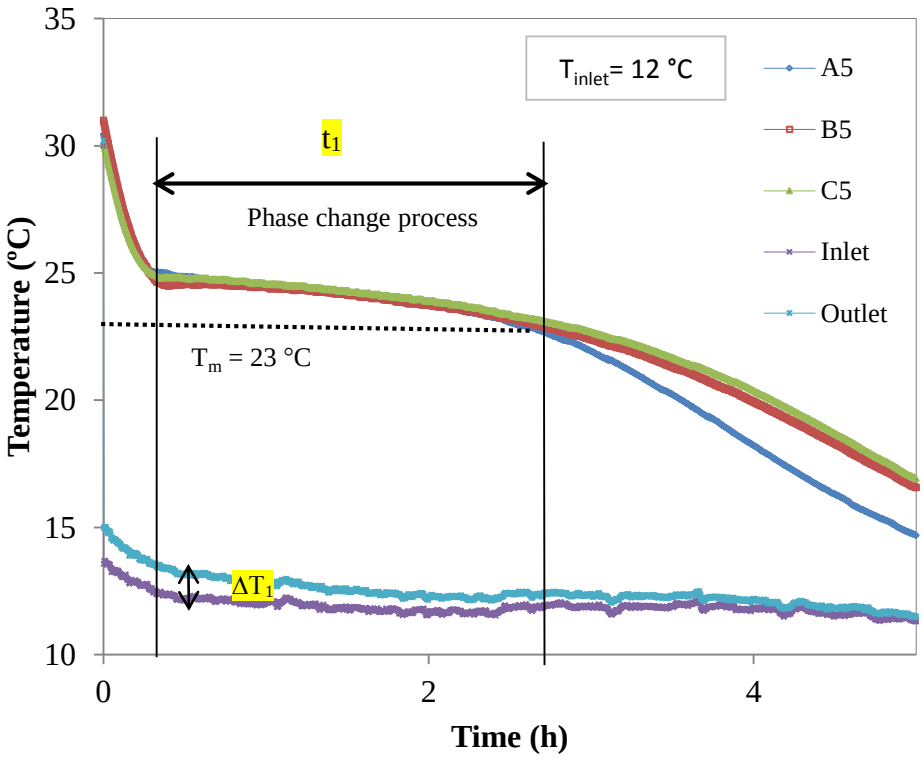

Figure 3-26 Influence of the air inlet temperature (12ºC) on the PCM and air outlet temperature for the charging process

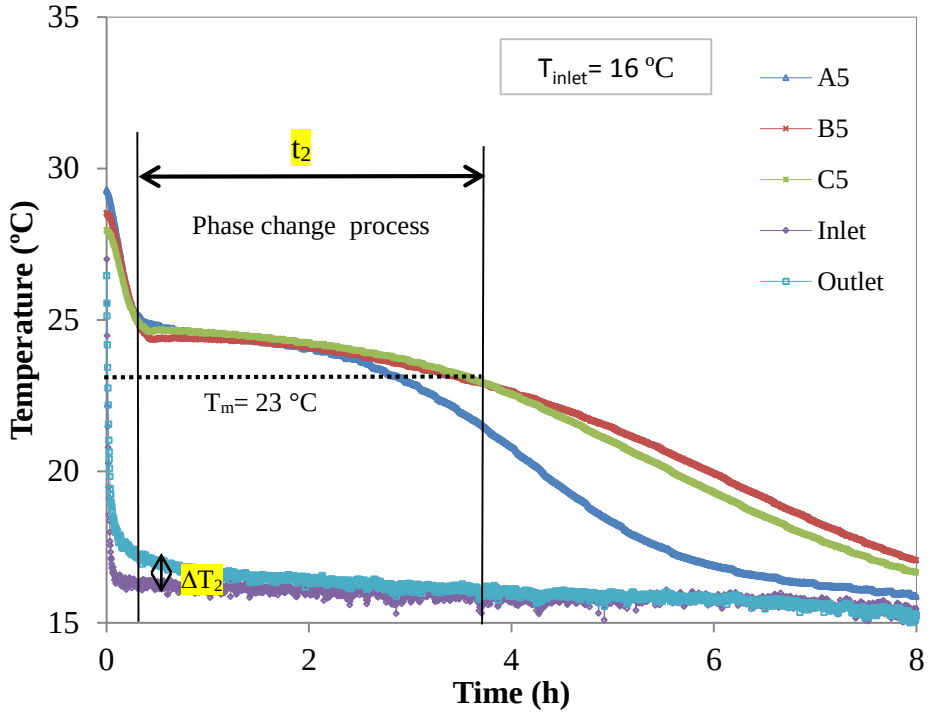

Figure 3-27 Influence of the air inlet temperature (16 ºC) on the PCM and air outlet temperature for the charging process

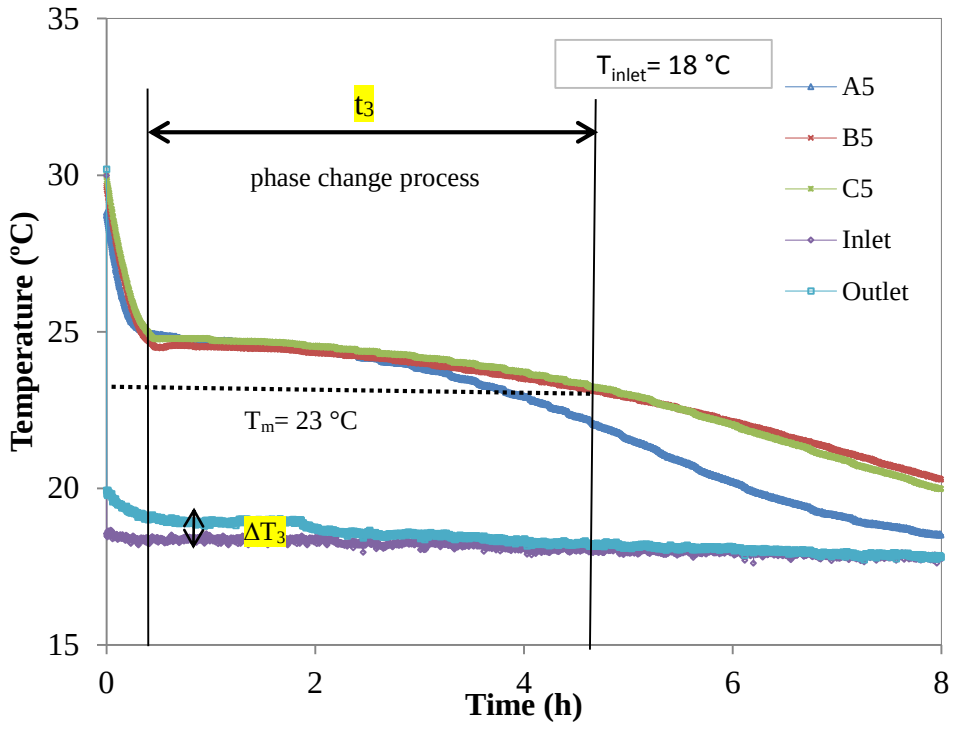

Figure 3-28 Influence of the air inlet temperature (18 ºC) on the PCM and air outlet temperature for the charging process

As can be seen in Figure 3-26, 3-27 and 3-28, the charging time was reduced for smaller air inlet temperatures. This reduction was proportional. Reducing the air inlet temperature from 18 ℃ to 14 ℃ decreased the charging time by an hour and the further decreasing of the temperature to 12 ℃ reduced the process by another hour. The air temperature difference increased for a lower air inlet temperature. A maximum air temperature difference of 0.6 °C was observed for air inlet of 12 °C. Tables 3-9 and 3-10 summarize the charging and discharging time and air outlet difference for the different scenarios.

Table 3-9 Summary of the air inlet temperature influence on charging and discharging time

	30 ℃ (t_1)	34 ℃ (t_2)	38° (t_3)
Discharging process (V= 1.6 m/s)	6.9h	3.8h	3h
	12 ℃ (t_1)	16 ℃ (t_2)	18 ℃ (t_3)
Charging process (V= 1.6 m/s)	2.8h	3.8h	4.8h

Table 3-10 Summary of the air inlet velocity influence on air outlet temperature

	30 ℃ (ΔT_1)	34 ℃ (ΔT_2)	38° (ΔT_3)
Discharging process (V= 1.6 m/s)	0.7 °C	0.9 °C	1.1 °C
	12 ℃ (Δt_1)	16 ℃ (Δt_2)	18 ℃ (Δt_3)
Charging process (V= 1.6 m/s)	0.6 °C	0.4 °C	0.3 °C

ii) Heating/cooling load

The cooling load of the PCM during the discharging processes was calculated using Equation 3-2 based on the measured air temperature at the inlet and outlet of the air-PCM heat transfer unit.

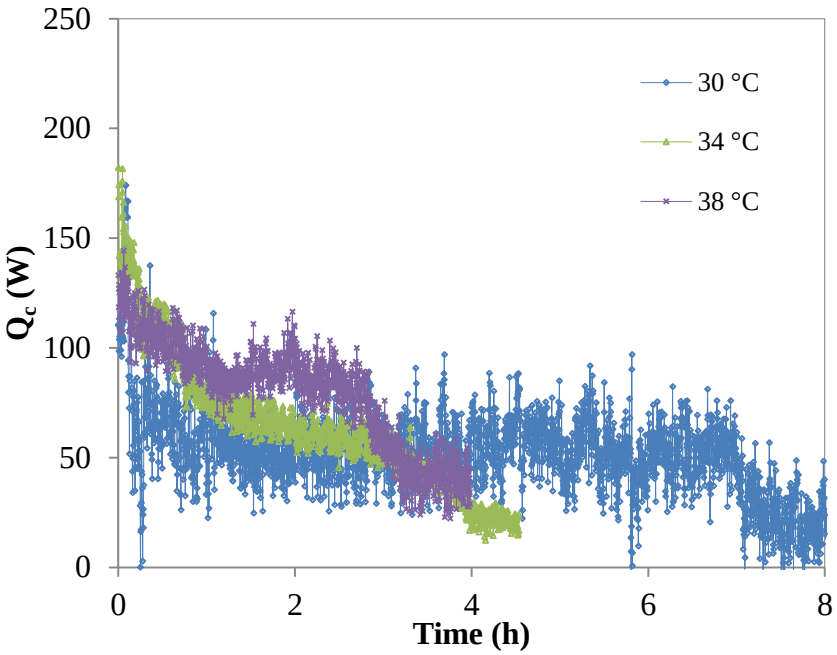

Figure 3-29 Influence of the air inlet temperature on the cooling load for discharging process

The cooling load remained at approximately 80 W for an air inlet temperature of 38 °C, dropping to a minimum value after 3h. This drop was associated with the end of the phase change. For 34 °C, the cooling load remained at approximately 60 W, reducing after 3.8h. At last for air inlet of 30 °C the cooling load remained at 50 W till 6.8h. Overall, for a higher air inlet temperature, the heat flux reached the minimum value in a short time period, showing that the discharging process of the PCM was completed earlier at higher air inlet temperatures. On the other hand, for lower air inlet temperatures, the heat transfer rate reached lower values. However, it stayed above the minimum value of 50 W for a longer period of time. The heating load was estimated using Equation 3-3 and displayed in Figure 3-30.

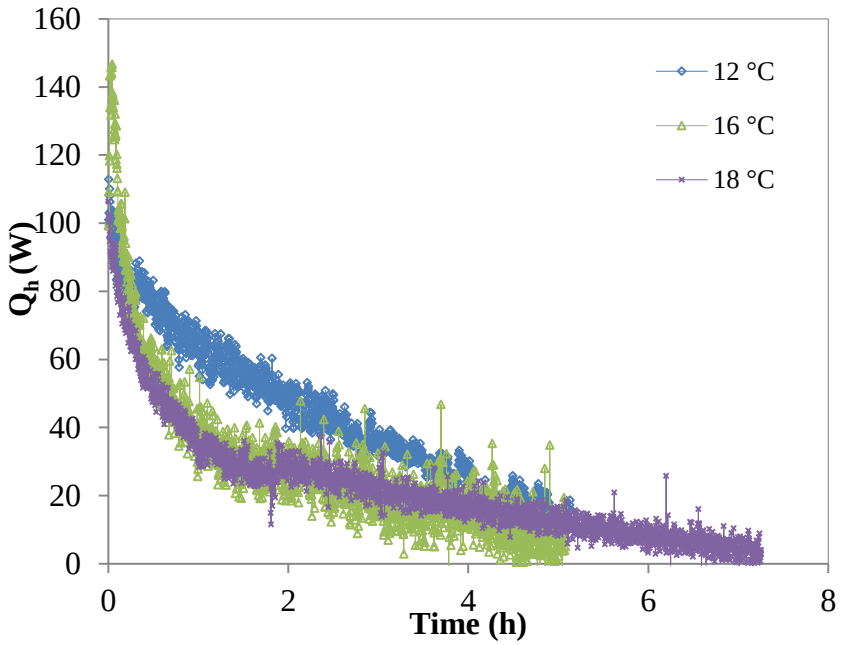

Figure 3-30 Influence of the air inlet temperature on the heating load for charging process

Similar heating loads were observed for 16 °C and 18 °C (30 W) due to the similar air temperature difference observed for both cases. This figure increased slightly for an air inlet temperature of 12 °C to 50 W, but it decreased drastically after 2.5h due to the end of the phase change and became approximate to the other two curves. The effectiveness of the lower air inlet temperature was highest during the discharging process. For higher inlet temperatures, greater effectiveness was achieved for the charging process.

iii) Effectiveness over the phase change process

The average effectiveness over the phase change was calculated for the discharging and charging process through Equation 3-4 and displayed in Figure 3-31 and Figure 3-32. From Figure 3-31, the average effectiveness ranged between 0.17 and 0.09 for the discharging process. The highest value was registered for the air inlet temperature of 30 °C followed by inlet of 34°C and 38 °C. This was due to the temperature difference between the air inlet temperature and the discharging temperature represented in the nominator of Equation 3-4.
For the charging process (Figure 3-12) the average effectiveness registered a higher value for an air inlet of 18 °C and was reduced for the lower air inlet temperatures. Again, this was due to the temperature difference between the air inlet and the melting temperature of the PCM.

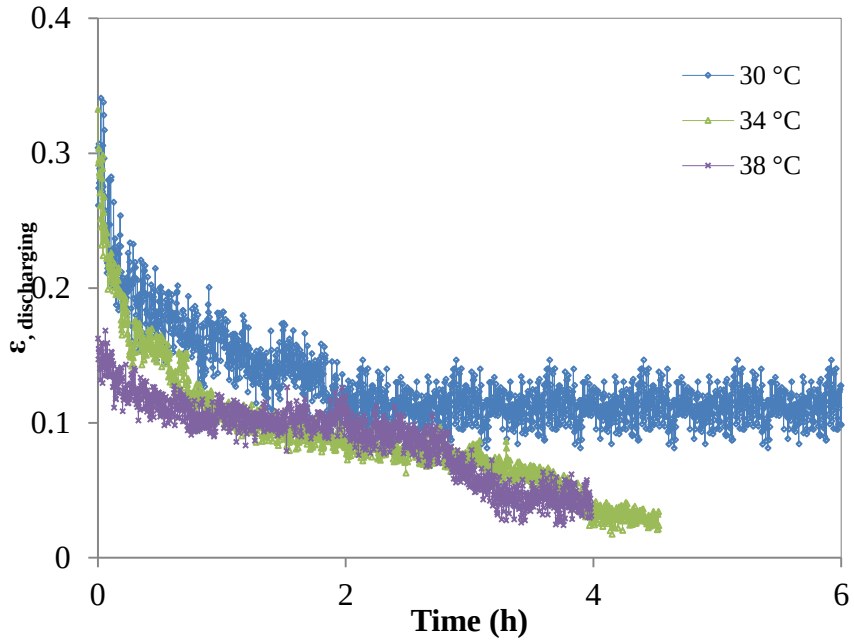

Figure 3-31 Influence of the air inlet temperature on the effectiveness for discharging process

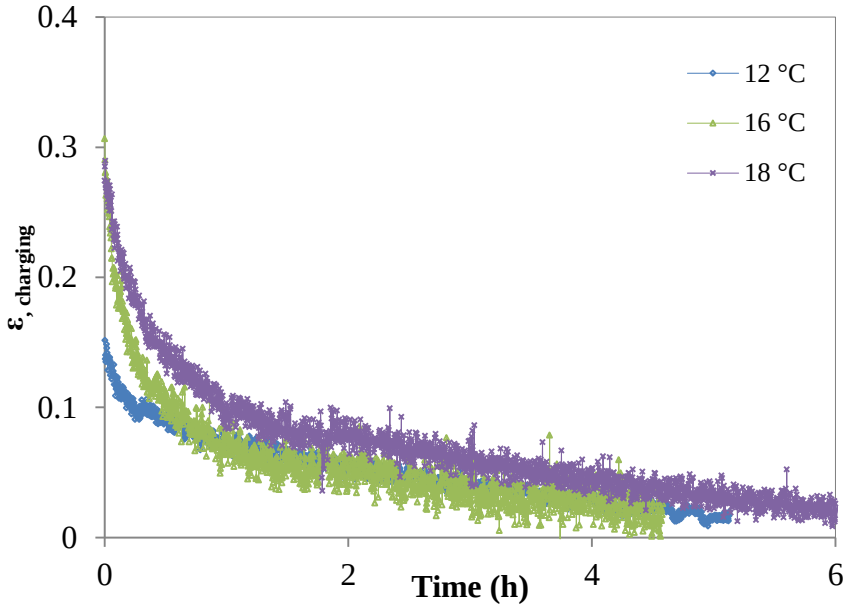

Figure 3-32 Influence of the air inlet temperature on the effectiveness for charging process

3.7 Conclusions

Both the charging and discharging processes were influenced by the air inlet velocity. It was observed that for the selected temperatures, the increase of the air inlet velocity reduced the charging and discharging time. However, this reduction was more significant when the velocity was increased from 0.6 m/s to 1.6 m/s. Overall, the air temperature difference was higher for the discharging process than for the charging process. Similarly the air temperature difference reduced more effectively from 0.6 m/s to 1.6 m/s for both processes. Increasing the velocity to 2.5 m/s represented a temperature difference of only 0.7 °C and 0.3 °C for the discharging and charging processes respectively.

The air inlet temperature proved to be the most important parameter affecting the discharging time. The discharging time was reduced when the air inlet temperature was increased from 30 °C to 34 °C. However, the charging time presented a linear reduction with the decrease of the air inlet temperature.

Overall, the air temperature difference achieved higher values for the discharging process than for the charging process. The air temperature difference was more significantly influenced by the air inlet velocity rather than for the air inlet temperature. For both processes, the air outlet temperature difference was reduced by approximately half for the second increment of the air velocity (1.6 m/s to 2.5 m/s). However, the air temperature difference reduced closely to the air inlet temperature in both processes.

The cooling load associated with the discharging of the PCM panels was in average 70 W, 110 W and 130 W for an air inlet temperature of 38 °C and an air inlet velocity of 0.6 m/s, 1.6 m/s and 2.5 m/s respectively. The heating load related to the charging of the PCM panels achieved 30 W, 40 W and 50 W for velocity of 0.6 m/s, 1.6 m/s and 2.5 m/s respectively.

The cooling load (i.e. the discharging process) decreased for lower air inlet temperatures corresponding to 50 W and 60 W and 80 for 30°C, 34 °C and 38 °C respectively. The heating load (i.e. charging process) was the same for 16 °C and 18 °C (30 W) increasing slightly for 12 °C (50 W). For the higher velocities the cooling and heating load reached higher values but dropped sharply as the phase change of the PCM was completed. Although for lower air

inlet velocities both loads achieved lower values, they remained nearly constant over a longer period of time due to the longer phase change time. The effectiveness reached its highest values for a velocity of 0.6 m/s for both the charging and discharging processes, due to a longer contact between the air and the PCM panels.

Free cooling applications that rely on the daytime and night-time temperature differences face two challenges, the charging of the PCM over a short period of time (overnight) and the discharging of the PCM during the daytime. These results suggest that the further increase of the air inlet velocity will not reduce the charging time. Instead, a lower temperature will be required for that end. Therefore, to accomplish the required charging time, the PCM thermophysical properties (namely the melting temperatures) need to be considered taking into account the night-time temperature profile. For the discharging time, it can be extended over a certain period of time by reducing the air inlet velocity even for higher air inlet temperatures. However, the increase of the air inlet velocity has to be carefully balanced to achieve the intended air temperature difference.

The data for these experiments have been used to validate a CFD model developed to further investigate the use of multiple PCMs for free cooling application (Chapter 5 and 6).

CHAPTER 4 - CHARACTERISING PCM BY DIFFERENTIAL SCANNING CALORIMETER (DSC)

4.1 Introduction

Generally, PCMs are thermally characterised by calorimetric experiments such as the Differential Scanning Calorimetry (DSC) for small samples of PCM materials. This chapter intends to characterise the phase change temperatures, the specific heat and the enthalpy of a RT25 paraffin sample. Firstly the recommended rate of 10 ° C/min is used (ASTM D 4419, 1990) for the DSC analysis. Secondly, the experimental heating and cooling rate of 0.2 °C/min is used for the DSC. The temperature range, specific heat and enthalpy values obtained for both heating/cooling rates are discussed and moreover applied into the CFD model developed in Chapter 5, with regards to the experimental results. Furthermore, the properties obtained by DSC for RT25 are adapted for paraffins RT18 and RT20 based upon Chiu and Martin's (2013) approach and applied in the multiple PCM analysis described in Chapter 6.

4.2 The Differential Scanning Calorimeter (DSC)

The DSC is a known technique for the measurement of the quantity of heat absorbed or released by a substance during temperature transitions. It also measures the occurrence of heat flux. The calorimetry depends on the thermodynamic conditions that should occur in the process. Thus, the classification of the calorimetry is based on three criteria to be used in the (i) the measurement, (ii) the operation mode and (iii) the constructive aspects of the calorimeter (Silva, 2001; Netzsch, 2009; Pires, 2010) and described as follows:

(i) The measurements depend on the way the heat is transferred by the sample containing the substance. This evaluation can be done by *compensation*, *storage* or *exchange*. For the first method, any change in the temperature of the sample is compensated by supplying or removing energy to or from the sample by the calorimeter. In this case, the compensated energy is measured. Another way to quantify the transferred energy is to measure the temperature variation between the sample to be tested and a sample with a known

behaviour (both samples are in contact). The *stored* energy is measured in this process. For the *exchange* method the transferred energy is measured by directly measuring the sample temperature and the surrounding temperature. Due to the complex mechanism involved in the heat transfer, the thermal differential between the sample, the surroundings and the heat transfer flux is in fact made by the calibration.

(ii) The second criterion for the calorimeter classification is the operation mode. There are mainly two modes: *static readings* and *dynamic readings*. The *static reading* uses a constant heating/cooling rate contrary to the dynamic reading, where a variable heating rate is used. The dynamic reading, as shown in Figure 4-1 (Barreneche et al., 2013), presents a smooth curve along the heating and cooling process contrary to the static mode where the curve is represented as a "steps" line. The static mode therefore is also dominated by the step mode. This may be useful to evaluate a specific parameter as for example the sub-cooling effect that is present in some phase change materials such as salt hydrates. However, for other materials such as paraffins, where this phenomenon does not appear, dynamic readings should be selected.

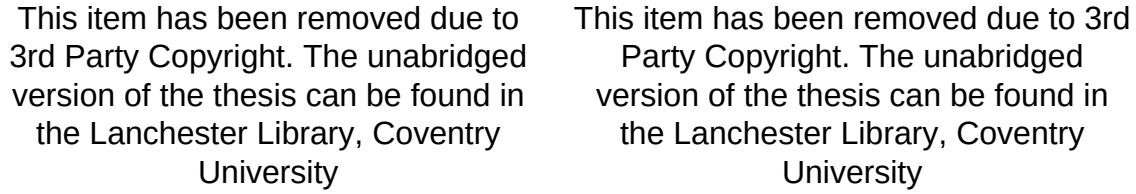

Figure 4-1 Typical DSC response when performing dynamic mode (left) and static mode (right) (Barreneche et al., 2013)

(iii) The constructive aspects of the calorimeter are classified as *simple* and *differential* measurements. The *differential* measurement is also denominated as a *double construction* as it does not only involve a holder for the sample of interest, but additionally another holder for a reference sample. This one is more advantageous than the simple measurement because a differential signal allows the replication of

irregularities that otherwise would not be detected. Additionally, an external influence for example the ambient temperature variation can be ignored, as it affects both samples in the same way (the studied and the reference sample).

The DSC working under the *compensation* method and the *double construction* implies two separate systems of heating and measurement, separate chambers for each holder and thermally isolated from each other. During the operation of the calorimeter both holders are maintained at the same temperature. Varying the heat flux of the transferred energy in each holder will allow the compensating of the temperature variation that occurrs during the process. In practice, the compensated energy in each holder is equal to the sum of the transferred energy by the sample and the associated heat losses. To perform the *differential* measurement it is necessary to have equal heat losses from each chamber, depending on the precision of the measurements. The *differential* calorimeter by *compensation* does present reduced chambers, characterized by a smaller thermal inertia and therefore quicker responses. However, it presents a higher cost and most applications do not strictly require this sort of potentiality, making it one of the less used methods.

Moreover, the calorimeter by *exchange* presents more simplified configuration because it includes only one calorimetric chamber that is shared between the two holders. In this type of calorimeter the *double construction* has the advantage of making it unnecessary to know the thermal differential between the sample and the surrounding. The *differential* measurements are carried out between the two holders and following the calibrations it quantifies the transferred energy. Thus, in the present work the differential calorimeter by exchange is used.

4.3 DSC equipment specification

The DSC equipment used in the present work is the Netzsch brand and the DSC 204 Phoenix model (Netzsch, 2015). The equipment includes a calorimetry chamber, a control temperature module, a cooling unit and an acquisition and control system with corresponding software. It allows temperature measurement between -170 °C and 600 °C. The heating of the chamber is accomplished with thermal resistances integrated in the chamber wall and the temperature is measured by E-type thermocouples. The available heating rate ranges from 0.1 to 99.9 Celsius (°C)/min. The temperature control of the calorimetry chamber and the temperature defined by the user is achievable by control modules (TASC 414/3^{a}, Netzsch) with a

precision of ±0.5 and a response time of 0.6 seconds. The cooling of the chamber is performed by the use of an external unit (CC 200, Netzsch). Nitrogen is supplied in the chamber for cooling at a pressure of 0.5 bar and with a volumetric flow varying between 5ml/min and 70 ml/min. The maximum cooling rate allowed for a cooling until ambient temperature is 70 °C/min and 40°C/min for temperature as low as -140 °C. The DSC was completed with standard samples, aluminium crucibles and a cold press to seal the crucibles. The DSC equipment and the accessories are presented in Figure 4-2 and 4-3 respectively.

Figure 4-2 DSC (top) and temperature control unit (bottom)

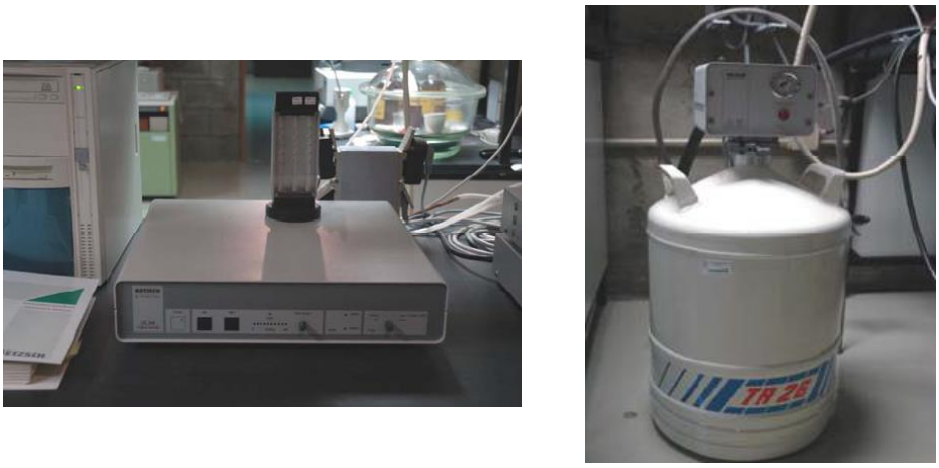

Figure 4-3 Calorimeter cooling unit

4.4 DSC calibration

Due to the complexity associated with the heat transfer mechanisms occurring within the calorimeter chamber, the evaluation of the thermal behaviour of a certain sample is achieved by the previous calibration of the calorimeter. The conditions in which this calibration is carried out should be similar with the samples for analysis. Normally, the process of calibration is based upon the substance with known thermal behaviour (standard sample). Hence, the standard sample calorimetry properties have to be known with precision, namely the phase change temperature, the heat involved in the phase change and the specific heat. The temperature and sensitivity calibration need to be carried out in order to use the calorimeter. The temperature has to be calibrated due to the temperature sensor being located in the holder rather than in the sample. In the calibration process, the temperature deviation by the sensor and the sample is quantified in order to build a correction curve. The procedure of calibration consists in submitting the different standard samples provided by the manufacturer, to similar test conditions intended for later use. In this specific case, the equipment program that allows the building of the calibration curves, requires at least the reading of five standard samples. Table 4-1 presents the characteristics of the samples used for the calibrating of the equipment. More details related with the calibration of the DSC can be found in Silva (2001).

Table 4-1 Characteristics of the standard samples used for the calibration of the DSC

Sample	Temperature of fusion (°C)	Enthalpy of fusion (J/kg)
C6H12	-87.0	-79400
Hg	-38.8	-11440
KNO3	128.0	-50500
In	156.6	-28590
Sn	231.9	-60620
Bi	271.4	-53300

4.5 Governing equations

The DSC provides a convenient and moderately accurate method of measuring heat capacities and enthalpy changes. The enthalpy changes (ΔH) and specific heat (c_p) determination are described in ASTME 1269 (1995) and presented by Equations 4-1 and 4-5.

$$\Delta H = \int_{T_1}^{T_2} c_p \, dT \tag{4-1}$$

Therefore the first step is to determine the specific heat. The specific heat is based on the fact that the DSC signal (V^{DSC}) is proportional to the heat capacity of the set, formed by the sample and the crucible in the region where only sensible heat is involved, allowing the following equation to be written:

$$V^{DSC} = A_0\left(mc_p + c_{p,cru}\right) \tag{4-2}$$

The term related to the crucible characteristics can be eliminated from Equation 4-2 if the measurements are run for the sample and for the empty crucible under the same testing conditions. The specific heat of the sample can be expressed as

$$c_p = \frac{V^{DSC} - V_{ref}^{DSC}}{mA_0} \tag{4-3}$$

The constant A_0 can be calculated using a standard sample. Hence, the constant value is determined as

$$A_0 = \frac{V_{sp}^{DSC} - V_{ref}^{DSC}}{m_{sp}c_{p,sp}} \tag{4-4}$$

Combining Equation 4.3 and 4.4 resulted into

$$c_p = \frac{m_{sp}}{m}\frac{V^{DSC} - V_{ref}^{DSC}}{V_{sp}^{DSC} - V_{ref}^{DSC}}c_{p,sp} \tag{4-5}$$

The ASTM E 1269 (1995) procedure involves running measurements for an empty crucible (V_{ref}^{DSC}), a crucible with standard sample (V_{sp}^{DSC}) and a crucible with the substance whose specific heat needs to be determine (V^{DSC}). The testing must be carried out consecutively and in the same experimental conditions.

4.6DSC experimental procedure

Desired conditions for the testing are very important for DSC measurement such as the temperature range and heating/cooling rates. ASTM D 4419 (1990) recommends that the sample is exposed to a heating rate of 10 °C/min and ventilation inside the calorimetry chamber provided by an inert purge gas with a volumetric flow between 10 and 50 ml/min. The selected temperature range was the same for all samples, for the heating process the initial temperature was setup at -20 °C and the final temperature at 40°C. The reverse process was adopted for the cooling process. A heating/cooling rate of 10 °C/min and 0.2 °C/min with a purge gas flow rate of 25 ml/min was used after the DSC calibration to test the paraffin samples listed in Table 4-2. Two heating and cooling cycles were performed for each testing and the second cycle was selected due to the better stabilization of the system at the second run.

Table 4-2 Mass of the samples and the crucibles

Sample	m (mg)	m_{cruc} (mg)	m_{total} (mg)
Reference	0	38.6	38.6
RT25	7.1	38.5	45.6

4.7DSC results

4.7.1 Heating and cooling rate recommended by ASTM D 4419 (1990)

Figure 4.4 presents the heat flow signal (mW/mg) obtained from the DSC testing for a heating rate of 10 °C/min. The heat flow variation with temperature allowed the identification of the region where the transition occurred between the solid and liquid paraffins. The onset, T_{on} and endset, T_{end}, temperatures were the temperatures at which the DSC heat flow curve

separated from the baseline and the phase change occurred. T_{peak} corresponded to the temperature at which the maximum heat flow was registered. The calorimeter also included a calculation program that allowed the determination of the temperatures associated with the phase transition region, following the same procedure (ASTM D 4419, 1990).

The T_{on}, T_{end} and T_{peak} were slightly different for melting and solidification due to the apparent hysteresis allied to any phase change process. Table 4-3 presents a summary of the T_{on}, T_{end}, T_{peak}, C_p and H for the selected paraffin.

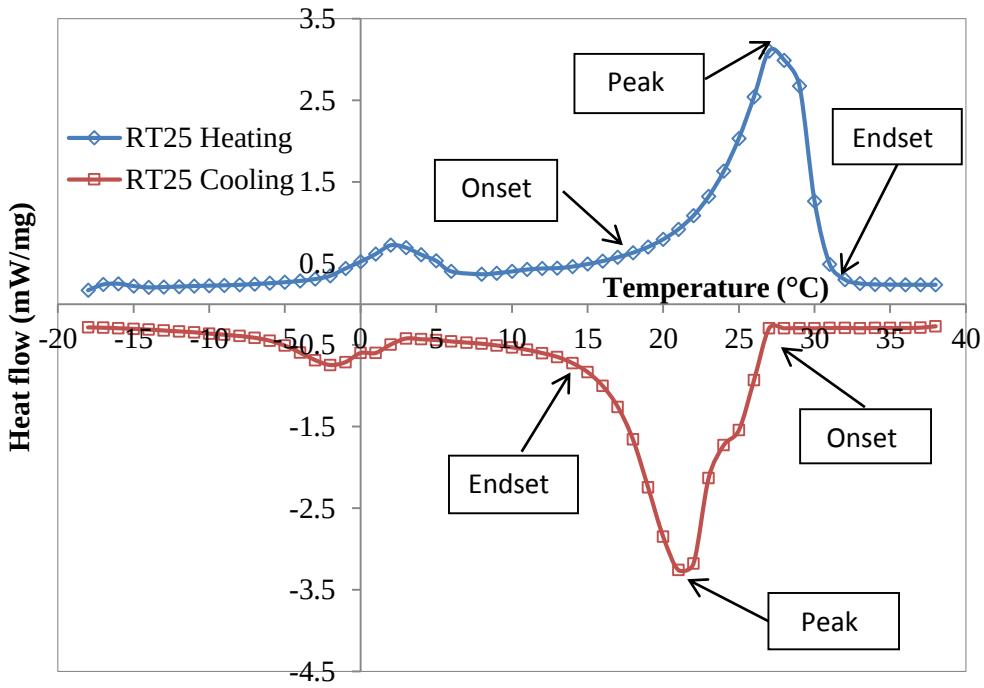

Figure 4-4 DSC curve for RT25

Figure 4-4 shows that the phase change of RT 25 was comprehended between 18 and 31 °C for the melting process and 15 °C – 26 °C for the solidification process. The peak temperature (T_{peak}) occurs at 27 °C for the melting and at 21 °C for the solidification with heat flow peak (DSC_{peak}) corresponding to approximately 3.2 mW/mg for both processes. From the measured heat flow, the C_p was calculated applying Equation 4-5 followed by the enthalpy (H) calculation applying Equation 4-1. Figure 4-5 presents the Cp-T and H-T curves for RT25 material.

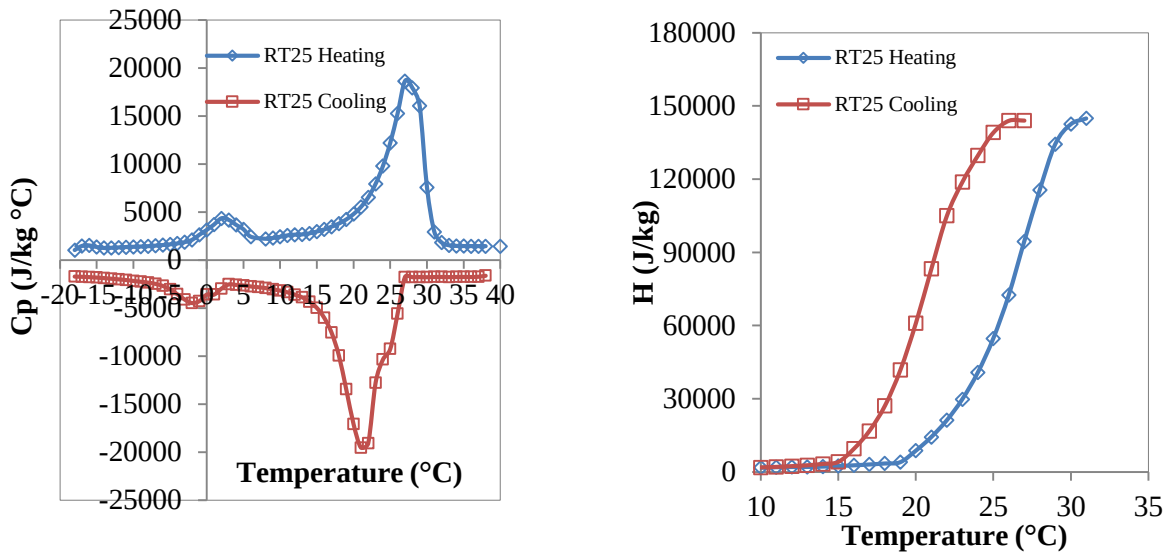

Figure 4-5 Specific heat and enthalpy curve for RT25

Table 4-3 Summary of the onset (T_{on}), endset (T_{end}), peak temperature (T_{peak}), specific heat (C_p), peak specific heat ($C_{p,peak}$) and enthalpy (H) for heating rate of 10°C/min

PCM		T_{on} (°C)	T_{end} (°C)	T_{peak} (°C)	C_p (J/kg °C)	$C_{p,\ peak}$ (J/kg °C)	H (J/kg)
RT25	Heating	18	31	27	3000	17590	145874
	Cooling	26	15	21	3000	17831	144012

The specific heat (C_p) corresponds to the material when it is completely solid or liquids, i.e before/after the phase change starts. The enthalpy (H) is represented in Equation 4-1 as a cumulative variable corresponding to the cumulative value obtained through the phase change. It observed that the C_p determined by DSC corresponds to 3000 J/kg. °C and slightly higher than the value proposed by the manufacturer of 2000 J/kg. °C (Table 3-1). The value determined by DSC will be used in simulations carried out in Chapter 5.

4.7.2 Experimental heating and cooling rate

Raj and Velraj (2012) claimed that if the experimental phase change temperature range for the given application is available, the apparent heat capacity model based on this range will provide accurate results. It makes sense that an accurate validation of the CFD results with the experimental results inferred that the scanning rate of the DSC analysis should be as close as possible to the heating/cooling rate of the selected application. Otherwise, there will be a difference in the temperature at which the phase change occurs, and any theoretical results may not match with the real application results. From Chapter 3 the experimental heating was determined and displayed in Figures 4-6 to Figure 4-9.

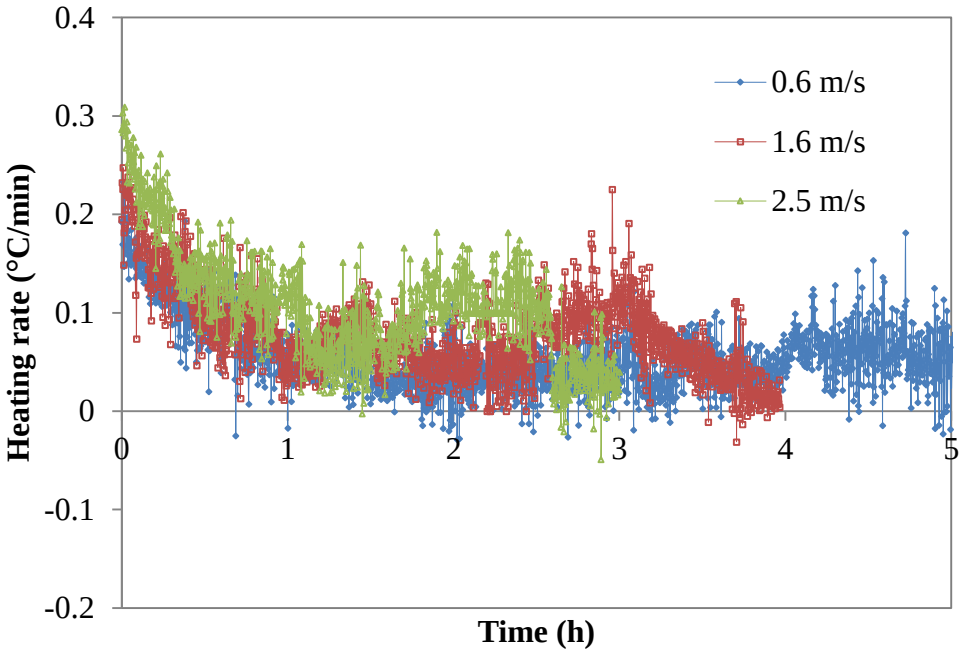

Figure 4-6 Experimental heating rate for discharging process under different air inlet velocities

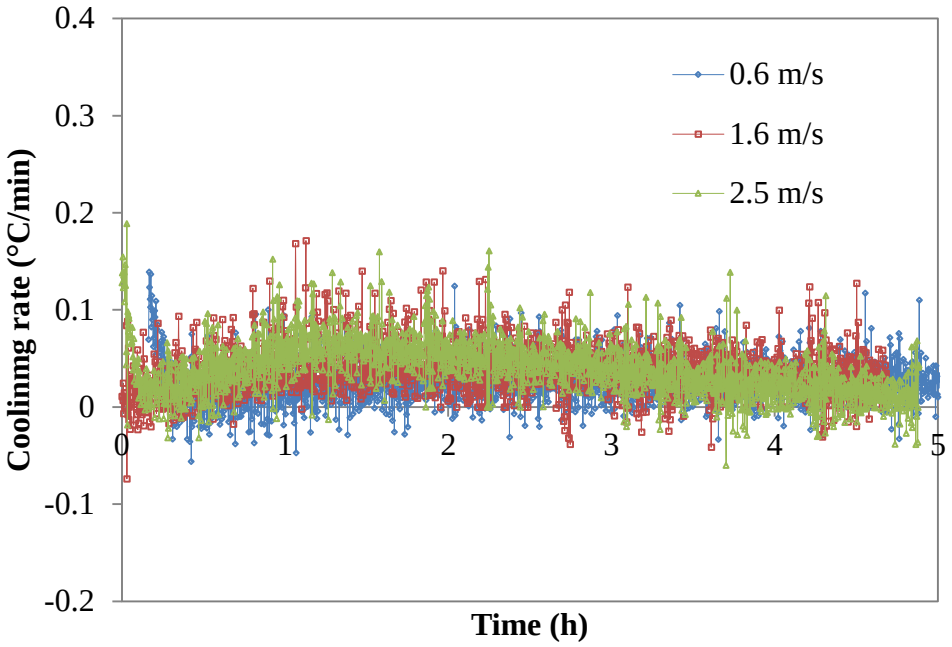

Figure 4-7 Experimental cooling rate for charging process under different air inlet velocities

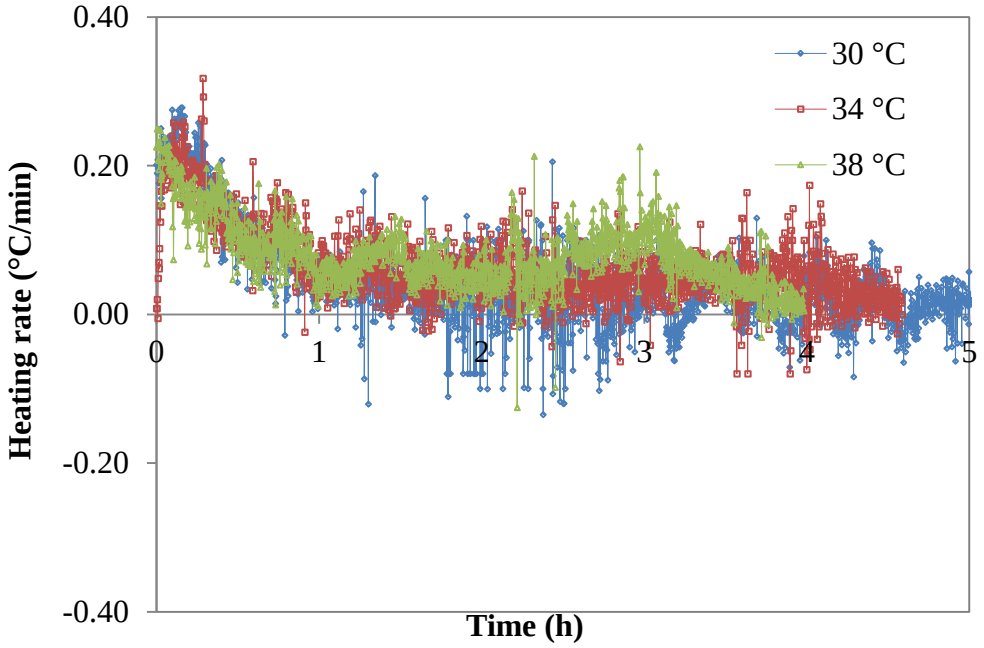

Figure 4-8 Experimental heating rate for discharging process under different air inlet temperatures

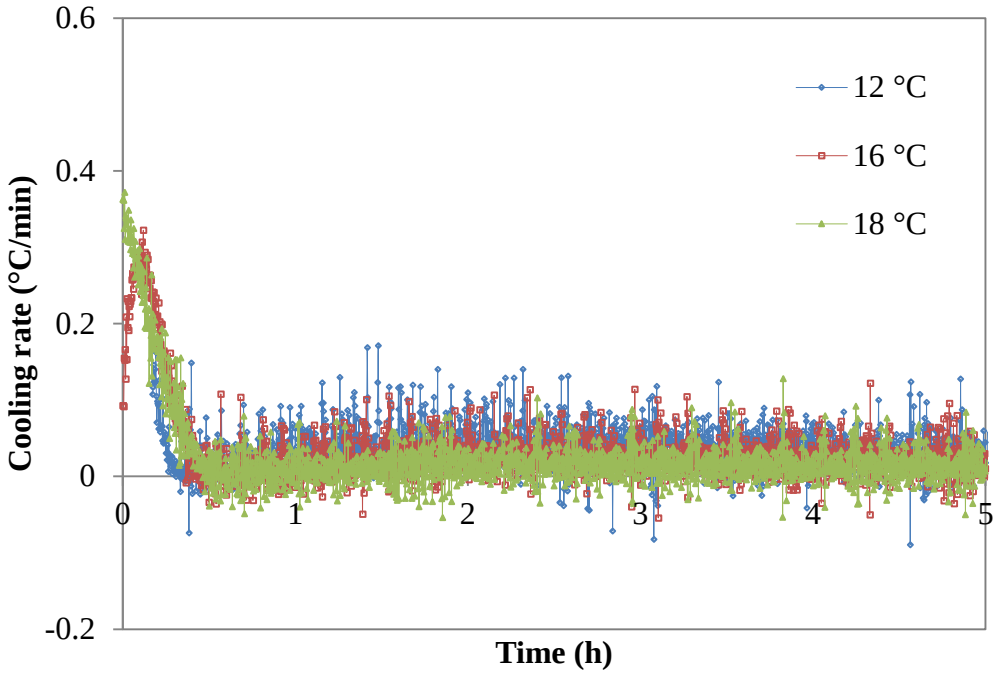

Figure 4-9 Experimental cooling rate for charging process under different air inlet temperatures

Overall, the heating and cooling rates for the discharging (i.e. melting) and charging (i.e. solidification) processes varied between 0.2 °C/min and 0.01 °C/min under different air inlet temperatures and velocities studied in Chapter 3. The DSC equipment used for the testing allows a minimum heating/cooling rate of 0.2 °C/min, therefore it was not possible to investigate lower heating or cooling rates. From the measured heat flow using the heating/cooling rate of 0.2 °C/min applying Equation 4-5, it was possible to determine the specific heat capacity. The heat flow, apparent specific heat capacity and the enthalpy of RT 25 DSC measurement for a heating and cooling rate of 0.2 °C/min were displayed in Figures 4-10 to Figure 4-12.

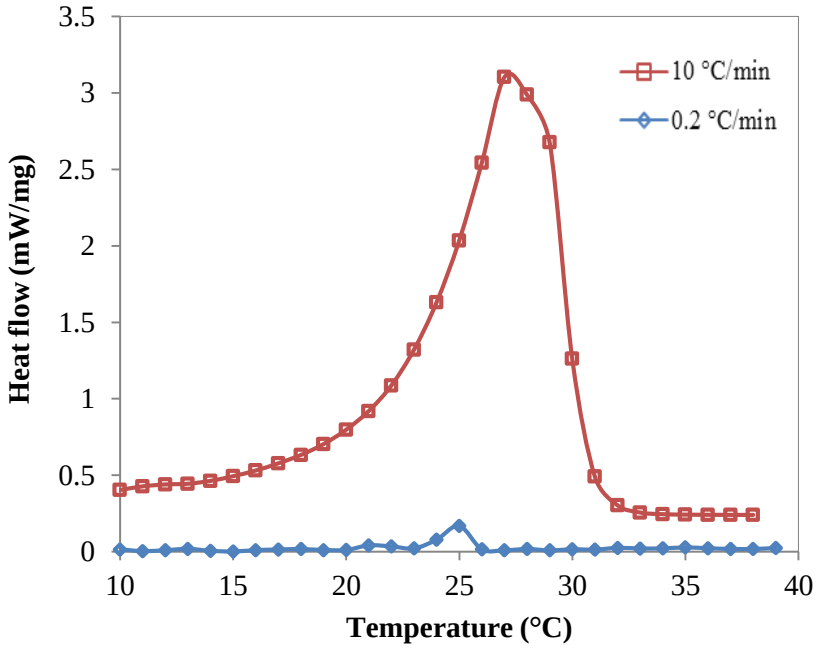

Figure 4-10 DSC measurements for 0.2 and 10°C/min heating rates of RT25 paraffin

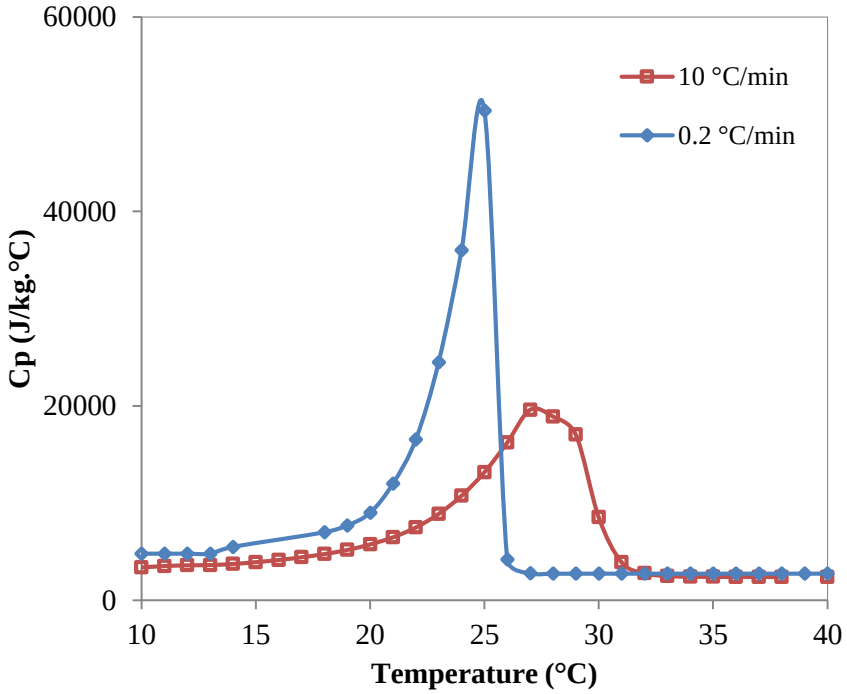

Figure 4-11 Specific heat for 0.2 and 10°C/min heating rates of RT25 paraffin

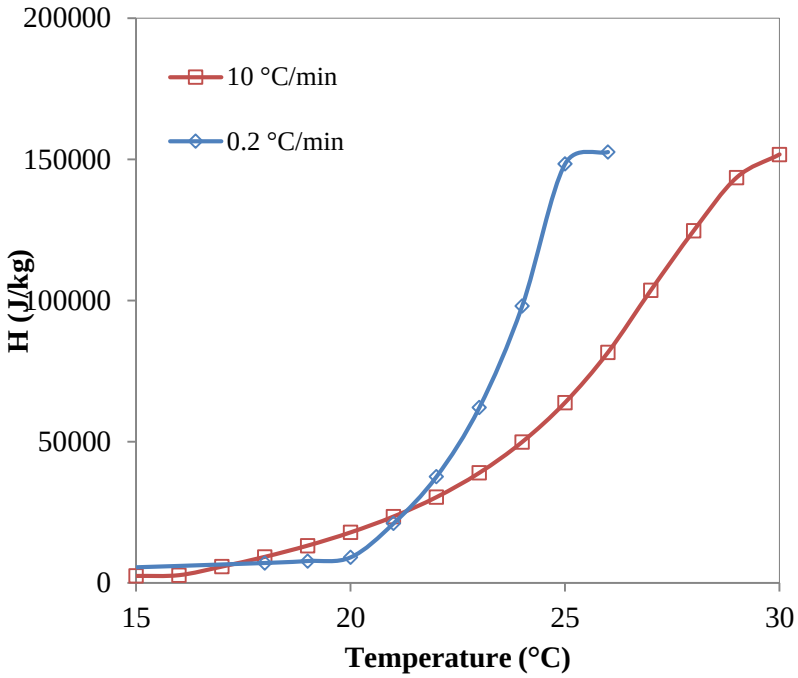

Figure 4-12 Enthalpy for 0.2 and 10°C/min heating rates of RT25

Overall it was observed that for a smaller heating rate the phase change range narrowed down and the heat flow was lower, reaching the peak value of 0.2 mW/mg (Figure 4-10). On the other hand with a smaller heating rate higher specific heat values were achieved (Figure 4-11). However, the enthalpy remained the same for both heating rates (Figure 4-12). Table 4-4 summarized the phase change temperatures, specific heat and enthalpy registered for heating rates of 0.2 and 10 °C/min respectively.

Table 4-4 Parameters values determined from the DSC measurements for melting process

Heating rate (°C/min)	T_{on} (°C)	T_{end} (°C)	T_{peak} (°C)	$C_{p,peak}$ (J/kg.°C)	H (J/kg)
0.2	22	26	25	50349	152599
10	18	31	27	17590	154066

The shapes of the specific heat curves differ considerably for the different heating rates. For lower heating rate, the T_{on} and T_{end} narrow and consequently the T_{peak} shifts towards a lower temperature. On the other hand, the $Cp_{,peak}$ increased with a smaller heating rate. Moreover, the enthalpy values were similar for any heating rate, as expected.

The same testing was performed for the cooling of the RT25 samples. The specific heat values for the cooling process were presented in symmetrical graphs for convenience and in order to differentiate the two processes.

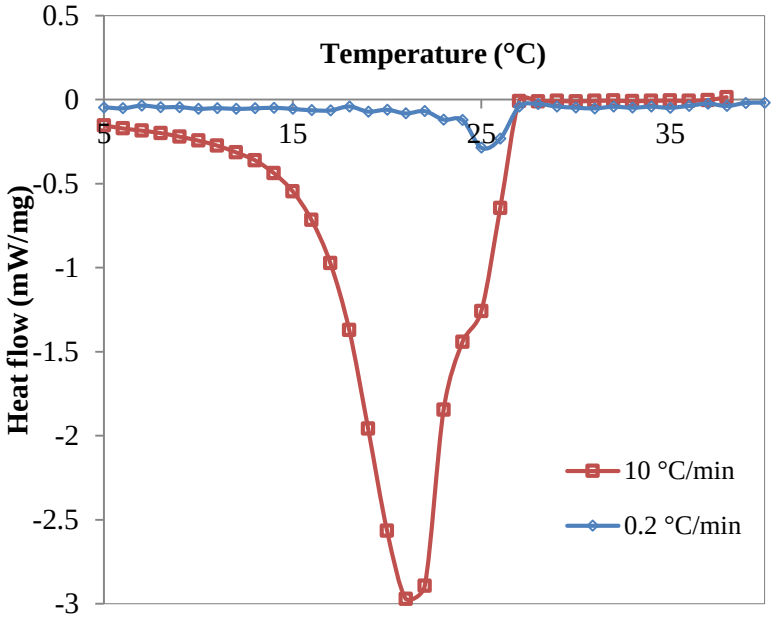

Figure 4-13 DSC measurements for 0.2 and 10°C/min cooling rates of RT25 paraffin

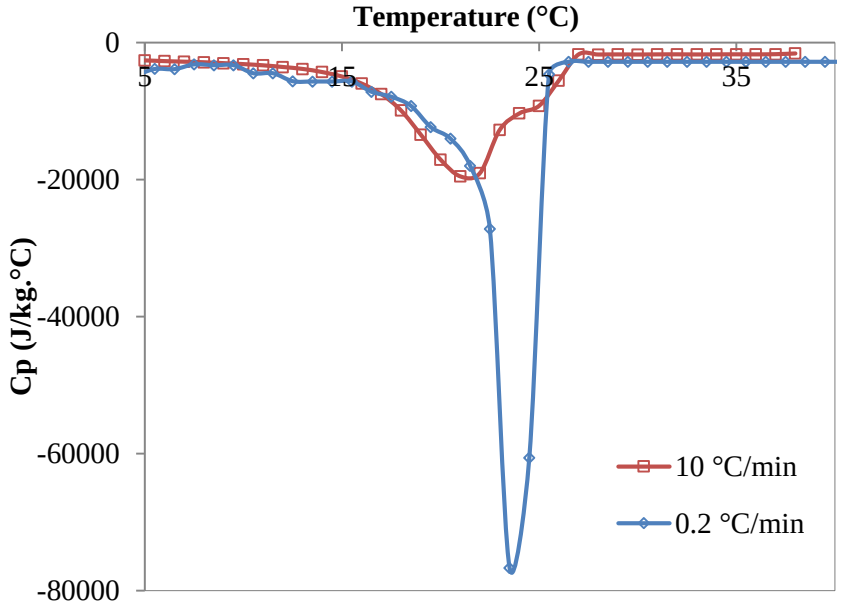

Figure 4-14 Heat capacity for 0.2 and 10°C/min cooling rates of RT25 paraffin

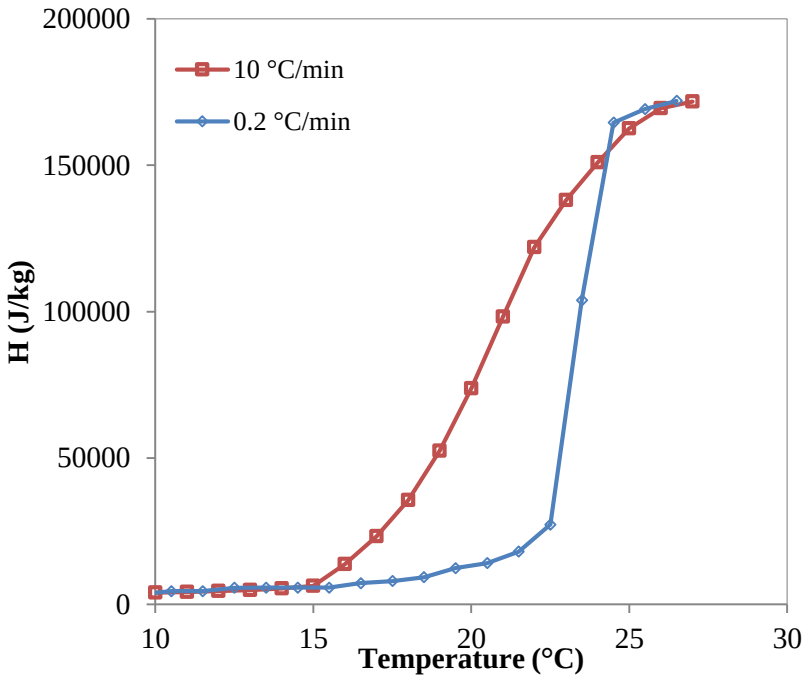

Figure 4-15 Enthalpy for 0.2 and 10°C/min cooling rates of RT25 paraffin

Similar results were observed for the cooling process with a cooling rate of 0.2 °C/min and 10 °C/min, listed in Table 4-5. It was observed that a lower cooling rate, the phase change temperature narrowed and the specific heat achieved a much higher value. The enthalpy however, remained nearly the same for both rates.

Table 4-5 Parameters values determined from the DSC measurements for solidification process

Cooling rate (°C/min)	T_{on} (°C)	T_{end} (°C)	T_{peak} (°C)	$C_{p,peak}$ (J/kg.°C)	H (J/kg)
0.2	26	23	25	60633	174849
10	26	15	21	17094	171708

The phase change temperatures obtained with a heating rate of 0.2 °C/min were in good agreement with the phase change temperatures presented in Chapter 3. This shows that using a DSC heating/cooling rate similar to the experimental heating/cooling rates translated similar thermophysical properties and therefore was selected for the analysis of other PCMs. In Chapter 6 the potential of multiple PCM is investigated requiring the specific heat and

enthalpy values for the two other selected PCMs: RT18 and RT20. Specific heats of both paraffins were determined using a similar approach presented in Chiu and Martin (2013). Chiu and Martin (2013) estimated the specific curves of the other two PCMs by taking the same specific heat curve of the analysed sample and shifting the peak temperature to their peak melting temperature. Therefore all the PCMs had the same enthalpy (i.e. latent heat) over the same temperature range, but centred on their peak phase change temperatures. In this study, the specific heat curve profiles of RT18 and RT20 have been assumed to be trending the same as the RT25 curve for a heating and cooling rate of 0.2 °/min but with the peak temperature shifted to 18 °C and 20 °C respectively. Figures 4-16 to 4-19 display the specific heat and enthalpy for the melting and solidification respectively.

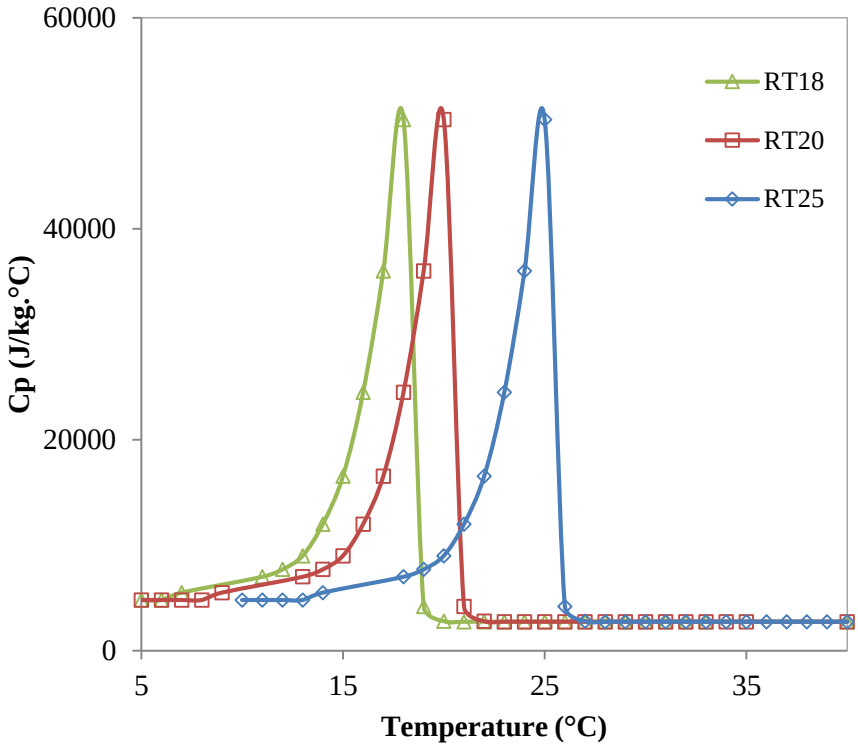

Figure 4-16 Specific heat curves for the heating of samples RT18, RT20 and RT25 (heating rate of 0.2 °C/min)

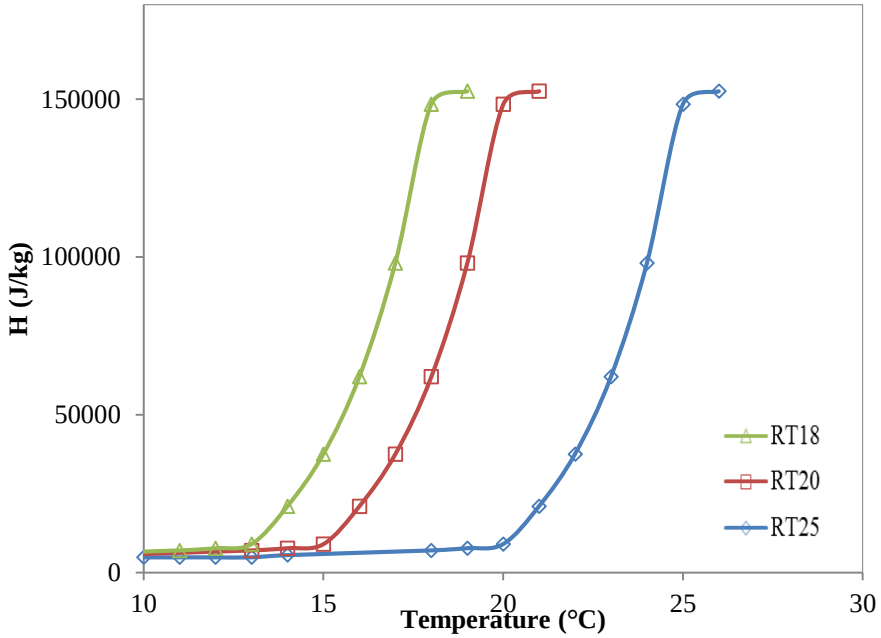

Figure 4-17 Enthalpy curves for the heating of samples RT18, RT20 and RT25 (heating rate of 0.2 °C/min)

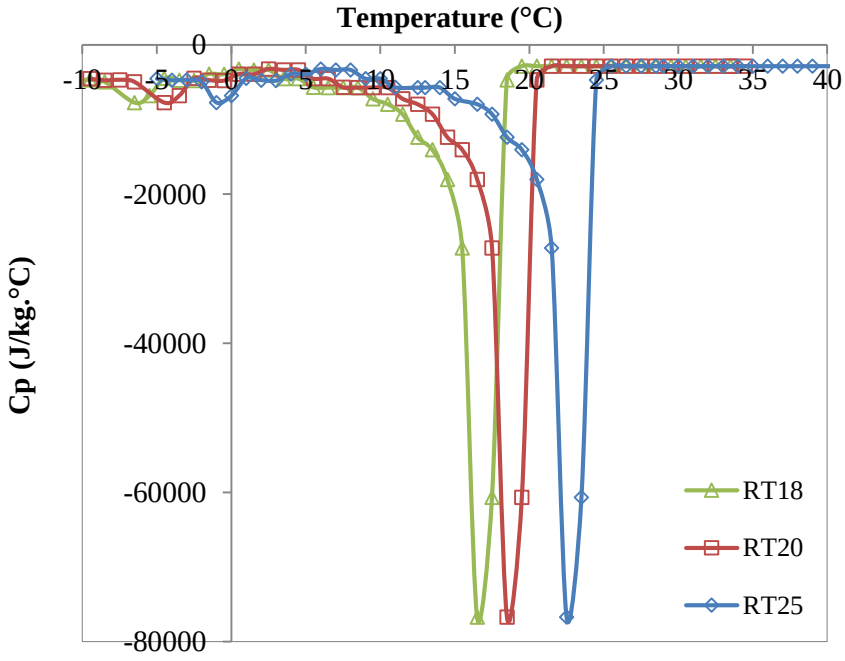

Figure 4-18 Specific heat curves for the cooling of samples RT18, RT20 and RT25 (cooling rate of 0.2 °C/min)

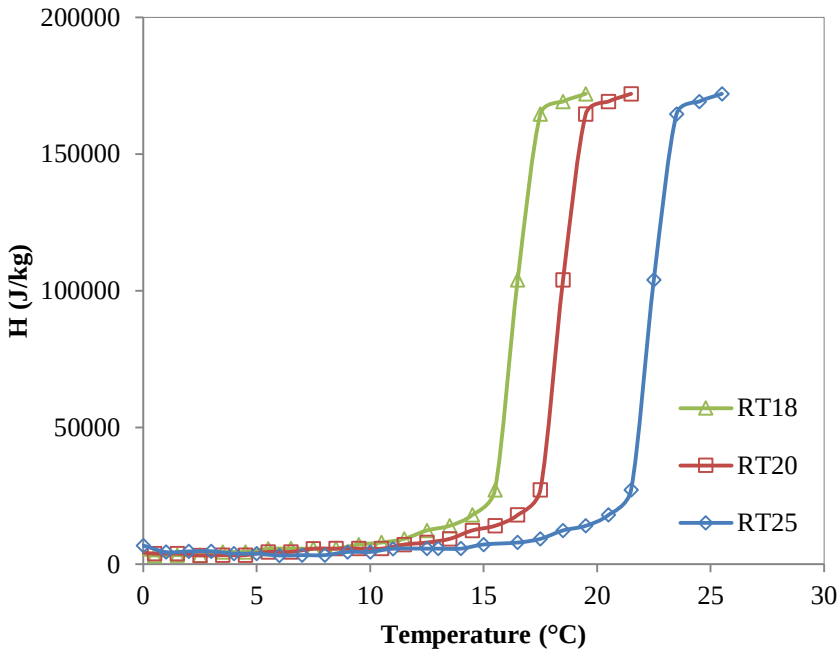

Figure 4-19 Enthalpy curves for the cooling of samples RT18, RT20 and RT25 (cooling rate of 0.2 °C/min)

A summary of the phase change temperatures, specific heat and enthalpy are listed in Tables 4-6 and 4-7 for the heating and cooling processes respectively.

Table 4-6 Parameter values determined from the DSC measurements for RT18, RT20 and RT25 for heating process

Heating	T_{on} (°C)	T_{end} (°C)	T_{peak} (°C)	$C_{p,peak}$ (J/kg.°C)	H (J/kg)
RT18	14	19	18		
RT20	16	21	20	50349	152599
RT25	22	26	25		

Table 4-7 Parameter values determined from the DSC measurements for RT18, RT20 and RT25 for cooling process

Cooling	T_{on} (°C)	T_{end} (°C)	T_{peak} (°C)	$C_{p,peak}$ (J/kg.°C)	H (J/kg)
RT18	15	18	18		
RT20	17	20	20	60633	174849
RT25	22	25	25		

4.8 Conclusion

The DSC analysis allowed the thermal characterisation of a sample of RT25 for the two heating and cooling rates of 10 °C/min and 0.2 °C/min. The first one was recommended by ASTM D 4419 (1990), followed by the heating rate approximated to the experimental heating and cooling rates observed in Chatter 3. It was observed that the melting temperatures', specific heat varied for the two heating and cooling rates, however the range of enthalpy remained the same. The results show that for smaller heating/cooling rates, the phase change temperature narrows down and the specific heat reaches a higher value. The onset and endset temperatures (T_{on}, T_{end}) for a heating/cooling rate of 0.2 °C/min were in good agreement with the experimental results presented for the charging and discharging processes in Chapter 3. Based on Chiu and Martin's (2013) approach, the specific heat and enthalpy were determined for paraffins RT18 and RT20. The specific heat and enthalpy values of RT25 obtained for both heating/cooling rates were introduced into the CFD model, later developed in Chapter 6 for the experimental validation. This was followed by the investigation of multiple PCMs for free cooling application (Chapter 7), including RT18 and RT 20 c_p and enthalpy values into the verified CFD model.

CHAPTER 5 – EXPERIMENTAL VALIDATION

5.1 Introduction

The present chapter studies the development of a CFD model for the air-PCM unit that was experimentally tested and presented in Chapter 3. Numerical simulations are carried out in order to calculate the PCM and air outlet temperatures for the similar boundary conditions used in the experimental testing. Commercial CFD package FLUENT (FLUENT, 2013) has been used for the simulations. The two most common methods for phase change problems (Chapter 2) are applied: the enthalpy method and the effective heat capacity method. The first one is available in FLUENT by the denominated Solidification and Melting model. This model requires the input of the phase change temperatures and the enthalpy value of the PCM. The second method is applied by including the c_p-T curve obtained from the DSC analysis (Chapter 4). The effective heat capacity shows better agreement with the experimental results. Hence, the verified model using the effective heat capacity method will allow further investigation of the potential of multiple PCMs for free cooling and ventilation application in Chapter 6.

5.2 Computational Fluid Dynamics (CFD) procedure

The use of CFD to simulate flow problems has risen dramatically in the past three decades and become a fairly well established discipline shared by a number of engineering and science branches (Ardejani et al., 2011). There are many advantages of CFD: it gives the perfect opportunity to study specific terms in the governing equations in a more details fashion (Tu et al., 2013). It gives an insight into flow patterns that are difficult or expensive to study using experimental techniques. It supplements the experimental/ numerical studies, providing a cost effective solution in simulating real fluid flow conditions. Also provides a thorough visualization and comprehensive information when compared to the analytical and experimental fluid dynamics. CFD allows the calculation of the fluids' flow, often associated with complications of simultaneous flow of heat, mass transfer, phase change, chemical reaction, mechanical movement, stresses and displacement of immersed or surrounding solids. However, the results of CFD may not be sufficiently accurate, if the input data involves much estimation and imprecision also, if the mathematical model of the problem is

inadequate or if the accuracy of the results is limited by the computing power. In the current numerical analysis, experimental data has been used to provide the boundary conditions, enabling to develop an accurate simulation model for the analysis. Commercial CFD package FLUENT has been used for the analysis (FLUENT, 2013). All commercial CFD packages include the input of problem parameters at user interfaces to examine the result. Hence all codes contain three main stages: pre-processor, solver and post-processor. The stages associated with the CFD procedure are displayed in Figure 5-1.

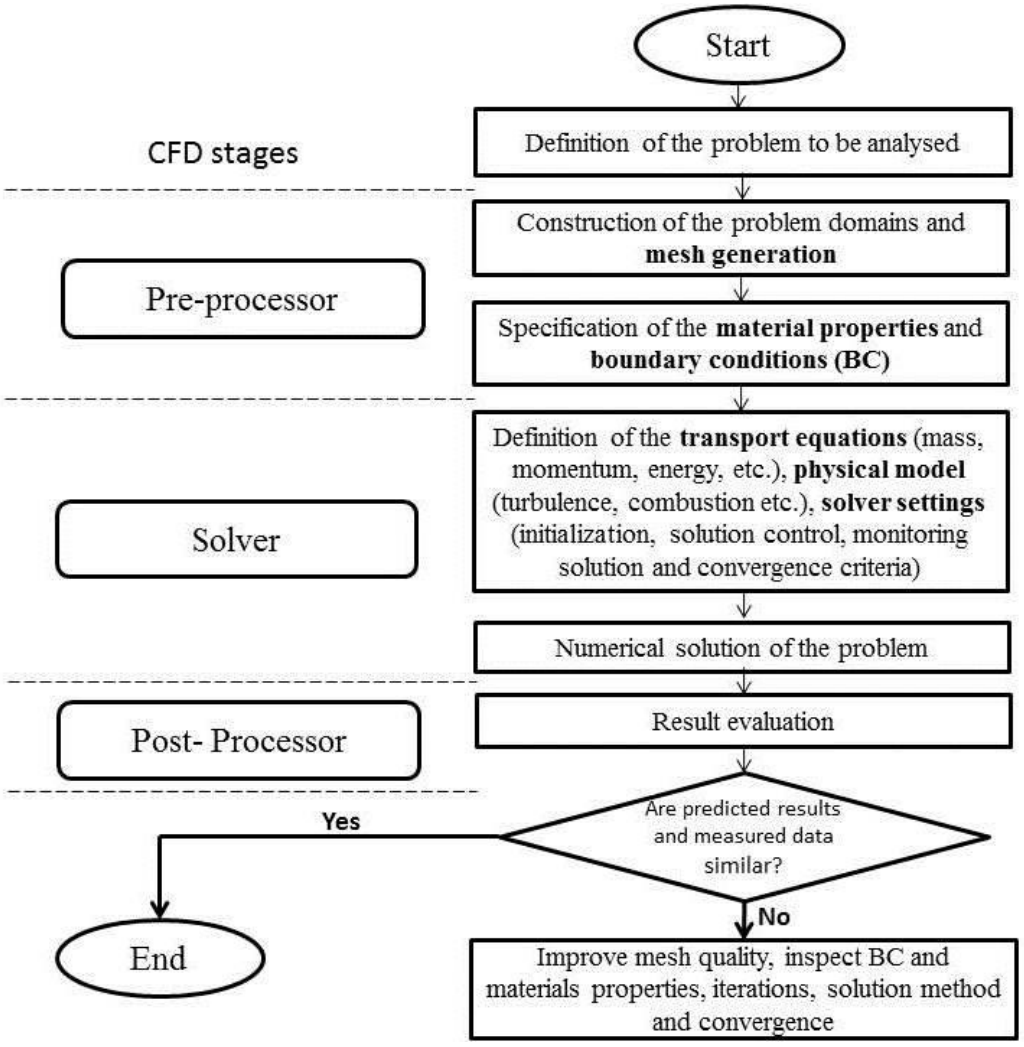

Figure 5-1CFD procedure

5.3 Geometry of the air-PCM unit

The model intends to accurately calculate temperature solutions in the domains considered in the analysis. This will be studied under different boundary conditions selected prior to the experimental testing. Thus the PCM melting and solidification time and the air outlet temperatures were determined. The experimental setup consisted mainly on an air-PCM unit including metallic rectangular panels filled with commercial paraffin RT25 surrounded by air channels (Figure 5-2). The thickness of the air duct walls and the PCM encapsulation were 0.01 m and 0.003 m respectively giving a total internal height of the unit of 0.198 m.

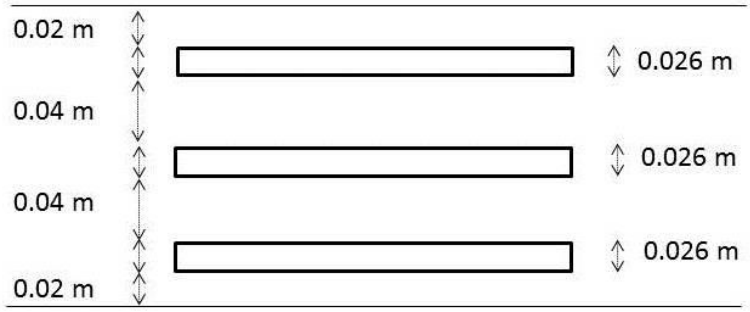

Figure 5-2 Schematic diagram of the two dimensions model

5.4 Mesh generation

CFD requires the splitting of the geometry domain into a number of smaller subdomains, denominated as meshes. Moreover, CFD enables the determination of the flow physics solutions at these meshes, as further discussed in section 5.6. The majority of time spent on the CFD study is usually devoted to successfully generating a mesh for the domain geometry (Jinyuan et al., 2006). A base 2D model was developed to reflect the dimensions of the air-unit used in the experiment. Similar to the Guo et al., (2013) approach, the current geometry of the model can be divided into three connected zones as presented in Figure 5-3 a. The experimental study established that the main heat transfer occurs in zone 2 and this zone proves a vital importance for the present research. In order to have an accurate analysis, a denser mesh has been performed for zone 2. The meshes were designed using the in-built ANSYS design modeller and all comprised hexahedral elements for improved heat transfer

phenomena (Tay et al., 2012) in the near-wall layers, wall domains and in the air domain. Three meshes resolutions denominated as coarse, medium and fine meshes were created with 3701 (Figure 5-4 a), 12160 (Figure 5-4 b) and 194560 (Figure 5.4 c) elements respectively. All meshes included a refined mesh in the near-wall zones where more complex fluid structures and heat transfer processes were foreseen to occur. The mesh refinement was performed by varying all mesh sizes by the same ratio through the adapt region tool available on FLUENT 15.0. Table 5-1 summarized the three meshes to be investigated for the experimental validation.

Table 5-1 Summary of set of CFD simulations performed

Mesh	Number of elements in total domain
Coarse	3071
Medium	12160
Fine	194560

a)

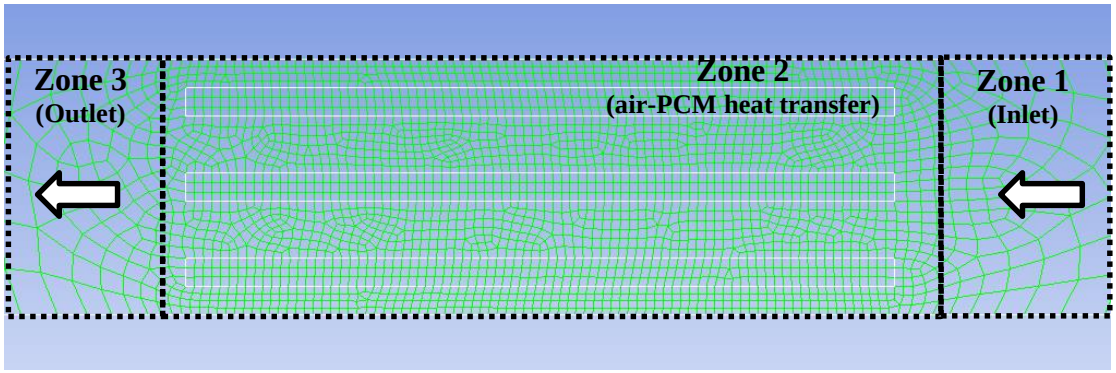

b)

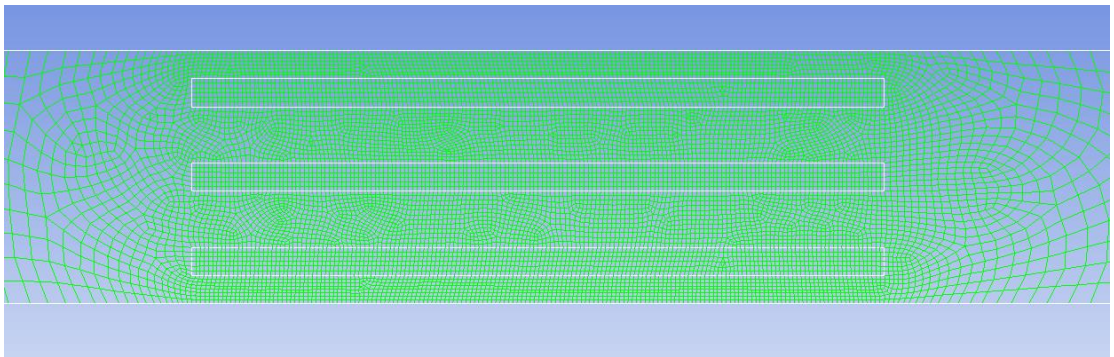

c)

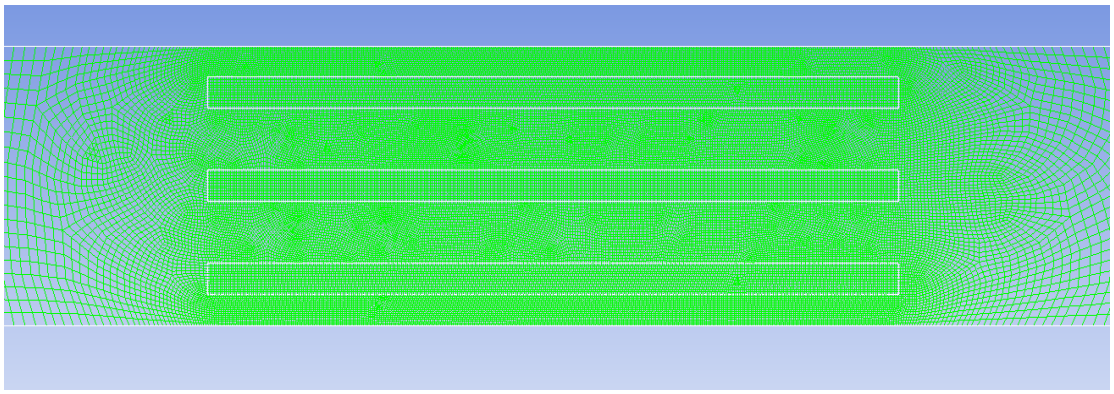

Figure 5-3 Computational meshes, a) coarse mesh (3701 elements), b) medium mesh (12160 elements) and c) fine mesh (48460 elements)

5.5 Material properties

The material properties used in the simulations were based upon the following experimental materials: RT25, steel as encapsulation material and air as the working fluid. All the properties were available in FLUENT database apart for RT25. The density, thermal conductivity and dynamic viscosity of RT 25 were obtained from the manufacturer data sheet (Appendix C) and the enthalpy and specific heat of RT25 were determined experimentally using the DSC analysis presented in Chapter 4. The values of C_p with temperature (C_p-T) for the charging and discharging process were taken from Figure 4-11 and 4-14 and introduced using the piecewise-linear option available in FLUENT.

The physical properties of the air were assumed to be independent of temperature. For fluid flows downstream of turning vanes, perforated plates, etc., the inlet turbulence is specified in terms of intensity (I_T) and length scale (L_T) (FLUENT, 2012). The turbulent intensity (I_T) is defined as the ration of the root-mean-square of the velocity fluctuations, v' to the mean flow velocity v_{avg} (FLUENT, 2006).

$$I_T = \frac{v\prime}{v_{avg}} = 0.016 {R_e}^{-\frac{1}{8}} \quad (5\text{-}1)$$

The turbulent length scale (L_T) is a physical quantity related to the size of the large eddies that contains the energy in turbulent flows and presented as (FLUENT, 2006)

$$L_T = 0.07\, D_h \quad (5\text{-}2)$$

Table 5-2 Materials properties

Material		Density (kg/m^3)	Thermal Conductivity (W/m°C)	Specific heat (J/kg °C)	Dynamic viscosity (kg m/s)	Melting point (°C)	Latent Heat (J/kg)
RT25	Enthalpy model	Solid: 880 Liquid: 760	0.2	Solid: 3000 Liquid: 3000	0.0072	23-25	Solid: 174,849 Liquid: 152,599
	Effective heat model			Figure 4-11 and Figure 4-14	-	-	-
Steel		8030	16.27	502.48	-	-	-
Air		1.225	0.0242	1006.43	0.0000179	-	-

5.6 Boundary and initial conditions

Specific boundary conditions must be provided in order to simulate the conditions observed in the experiments. These include the inlet velocity and temperature, the heat flux through the walls, the full set of conditions imposed on the flow field and the thermal conditions imposed on the temperature field as displayed in Figure 5-5. Overall, the geometry presented six boundary conditions: inlet, outlet, duct walls, PCM panel walls, air and PCM domains as shown in Figure 5-4.

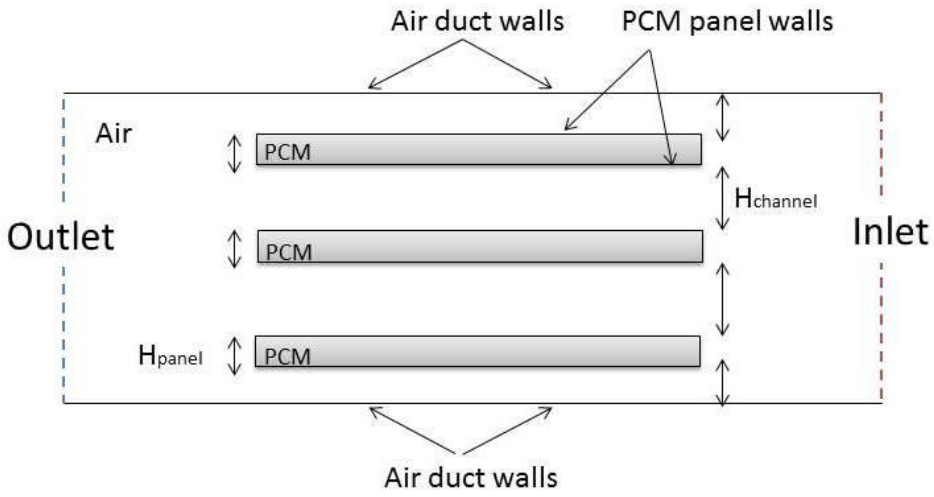

Figure 5-4 Boundary conditions of the geometry

i) Air duct and PCM walls,

The air duct walls were defined as solid wall. While in contact with the surrounding ambient air, the convection process was enabled with the appropriate thermal conditions. The thermal conditions required the definition of the convective heat transfer coefficient (h_c) and the free steam temperature. The convective heat transfer coefficient of the ambient air in contact with the air duct wall was determined as follows:

$$h_c = 10.45 - v + 10\ v^{1/2} \tag{5-3}$$

where v is the relative speed of the object through the air (m/s). The relative speed was measured and assumed as static (v= 0 m/s) and consequently the convective heat transfer coefficient corresponded to 10 W/m^2°C. The temperature of the air duct walls were set at 19 °C that corresponded to the average ambient temperature registered in the laboratory room. The thicknesses of the walls were defined as 0.01 m and wood was selected as the material.

The PCM walls were defined as coupled in order to allow the heat transfer between the air and the PCM domain as presented in Equation 5-4 and with the wall thickness specified as 0.003 m.

$$\underbrace{m_{air}c_p\left(\frac{\partial^2T}{dx^2}+\frac{\partial^2T}{dy^2}\right)}_{\text{Convective air}} = \underbrace{\pm\, h_cA_{air\ duct}\left(\frac{\partial^2T}{dx^2}+\frac{\partial^2T}{dy^2}\right)}_{\text{Heat gain/losses through the air duct}} \pm \underbrace{k_{airduct}\left(\frac{\partial^2T}{dx^2}+\frac{\partial^2T}{dy^2}\right)}_{\text{Conduction through the air duct}} \pm \underbrace{k_{panel}\left(\frac{\partial^2T}{dx^2}+\frac{\partial^2T}{dy^2}\right)}_{\text{Conduction through the PCM panel}} + \underbrace{\frac{\partial^2T}{dy^2}\Big) \pm k_{PCM}\left(\frac{\partial^2T}{dx^2}+\frac{\partial^2T}{dy^2}\right)}_{\text{Conduction within the PCM}} \tag{5-4}$$

ii) Air and PCM domains

The air and PCM domains were automatically setup as interiors domains. Figure 5-5 and Table 5-3 list the presented boundary conditions.

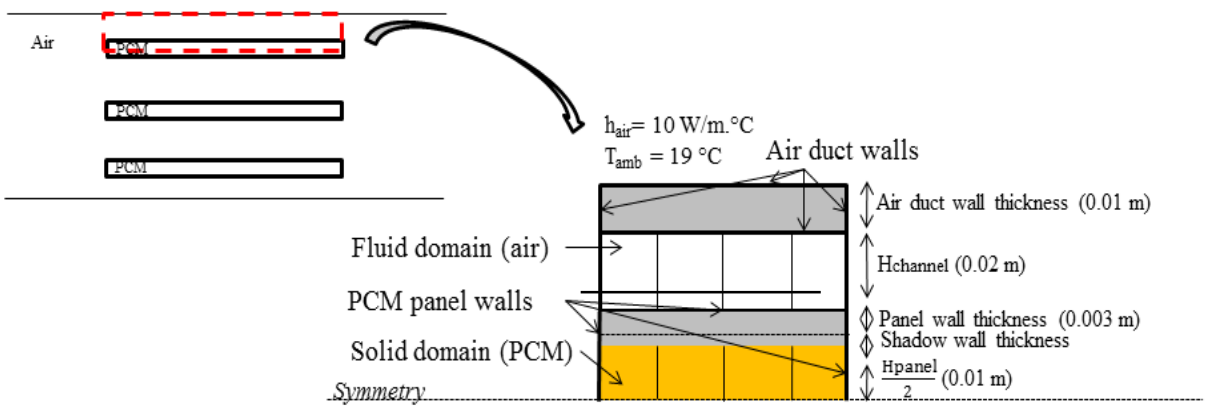

Figure 5-5 Boundary conditions (cross sectional view)

iii) Inlet and outlet

The air flow passing through the air channels was treated as a velocity inlet. The velocity inlet was specified in terms of velocity and temperature. The air velocity was assumed at a constant value based on the average velocity taken along the cross sectional area of the air duct. The air inlet temperatures corresponded to the experimental average inlet temperature at the entrance of the four channels and introduced into the model by a tabulated data. The outlet air flow was considered as outlet pressure with gauge pressure equal to 0 Pa. The boundary conditions imposed are listed in Table 5-3.

Table 5-3 Boundary conditions for the flow and thermal fields

	Boundary conditions	
	Thermal	Flow
Air inlet	12 °C, 16 °C, 18 °C (charging process) 30 °C, 34 °C, 38 °C (discharging process)	Uniform velocity inlet: 0.6 m/s, 1.6 m/s and 2.5 m/s Direction: Normal to boundary
Air outlet	-	$P_{outlet} = 0$
Air duct and PCM walls	Equation 5-4	Stationary wall, no slip shear condition

As with any numerical simulation, the setup of the initial values for the principal variables was required. For the present study the initial temperature (T_i) at t=0 was the same for all domains: PCM temperatures, air duct and encapsulation walls and air. For the discharging process the initial temperature corresponded to a temperature below the melting temperature of the PCM (T_m) as expressed in Equation 5-5 and Equation 5-6.

$$T(x, y, 0) = T_i \tag{5-5}$$

$$T_i < T_m \tag{5-6}$$

For the charging process, the initial temperature was assumed above the melting point as expressed in Equation 5-7 and Equation 5-8.

$$T(x, y, 0) = T_i \tag{5-7}$$

$$T_i > T_m \tag{5-8}$$

5.7 Governing Equations

The investigation of a two-dimensional numerical simulation of the conjugate heat transfer was conducted using CFD code FLUENT 15. The simulations were carried out in order to calculate the experimental observations. The CFD modelling employs the finite volume method for solving the common continuity, momentum and energy equations in particular domains. These equations are known as the Navier-Stokes set of equations and described in Equation 5-9, Equation 5-10 and Equation 5-11.

Momentum equation:

$$\frac{\partial}{\partial t}(\rho\vec{v}) + \nabla(\rho\vec{v}) = \nabla\left[\mu\left(\nabla\vec{v} + \nabla\overrightarrow{v^T}\right)\right] - \nabla P + \rho\vec{g} \tag{5-9}$$

Where ρ corresponds to the density, $\vec{v}$ corresponds to the vector of velocity, μ corresponds to the molecular (dynamic) viscosity and P to the static pressure.

Continuity equation:

$$\frac{\partial \rho}{\partial t} + \nabla(\rho \vec{v}) = 0 \tag{5-10}$$

Equation 5-10 states that the net accumulation of the mass must be equal to zero, i.e. mass is conserved. Equation 5-9 and Equation 5-10 characterize the fluid flow but no the heat transfer, hence an additional equation is required. Equation 5-11 describes the conservation of energy, describing the heat transferred and hence the temperature distribution.

Energy equation:

$$\frac{\partial}{\partial t}(\rho E) + \nabla[\vec{v}(\rho E + p)] = \nabla\left[k\nabla T - \sum_j h_j + \vec{J}_j + (\bar{\bar{\tau}}\vec{v})\right] + S \tag{5-11}$$

In Equation 5-11 the first term represents the rate of change of energy with time. In other words how quickly energy is stored. The second term is related to the net convection of energy leaving the system. The third term on the right-hand side represents the net diffusion of energy (energy transfer) into the system due to conduction, species diffusion and viscous dissipation respectively. The last term is related to the generation within the system by chemical reaction or any other heat source.

Overall these equations are difficult to solve through conventional mathematical methods. They are firstly discretised, then linearised and finally solved with a CFD solver through iterative methods as explained further on. In contrast to an analytical solution (which allows for solution determination at any point of interest in a medium), the CFD solution enables the determination of the solution at only discrete volumes (meshes). Discretisation is the process of breaking down the terms of governing equations for these meshes enabling simpler algebraic forms. Figure 5-6 displays the mesh discretization schematic of the air and PCM domains for subsequent derivation of the governing equations. For the finite volume method, the solution domains were subdivided into certain number of small control volumes (denominated as elements) by a mesh. The mesh defined the boundaries of the control volumes while the computational nodes lay at the center of each control volume.

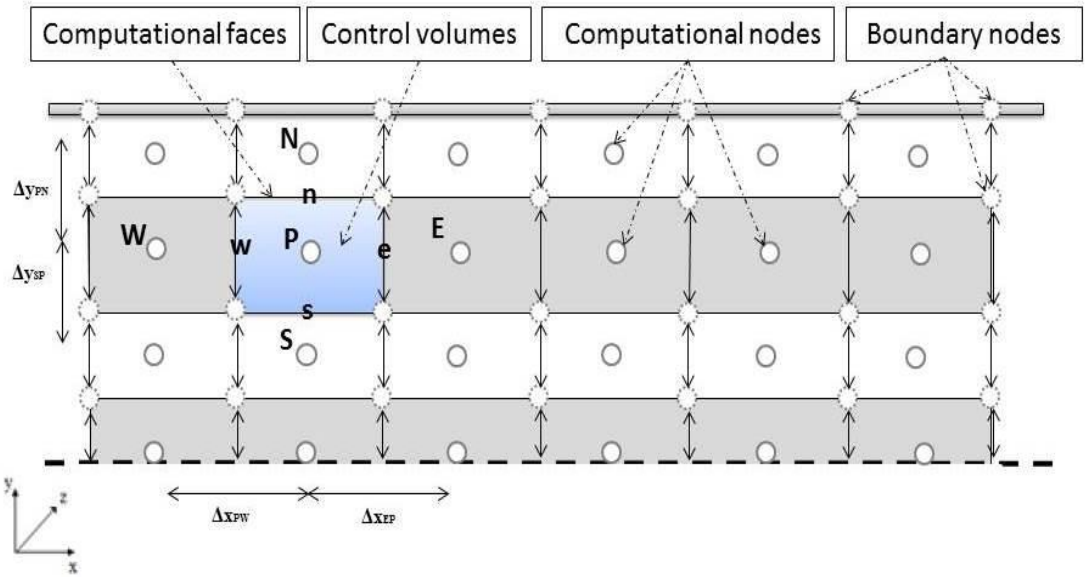

Figure 5-6 Air and PCM domains discretisation schematic

Figure 5-6 displays two types of elements. The center values element are denoted by capital letters (P, E, N, W, S) and the face values denoted by the small case letters (e, n, w, s). The governing equations are then applied to each control volume and the temperature solutions are obtained. An example is shown below for the diffusion term. It represents the net influx of energy through the perpendicularly-direction faces for the control volume in Figure 5-6 (Beausoleil-Morrison, 2010).

$$\int_{\Delta V} \frac{\partial}{\partial y}\left(k\frac{\partial T}{\partial y}\right) dV = \iiint_{x\,y\,z} \frac{\partial}{\partial y}\left(k\frac{\partial T}{\partial y}\right) dxdydz = (dxdz)\left[\left(k\frac{\partial T}{\partial y}\right)_n - \left(k\frac{\partial T}{\partial y}\right)_s\right] \quad (5\text{-}12)$$

In CFD the face values have to be computed from the element center values (FLUENT, 2011). Therefore Equation 5-11 was given in terms of face values that have to be linearized. This simplifies the governing equation into linear algebraic terms (Gowereensunker, 2013). Beausoleil-Morrison (2000) proposed a piecewise-linear variation of T in y to evaluate the temperature profile at the s and n faces.

$$\left(k\frac{\partial T}{\partial y}\right)_n \approx \frac{k_n}{\Delta y_{PN}}(T_N - T_P) \quad (5\text{-}13)$$

$$\left(k\frac{\partial T}{\partial y}\right)_s \approx \frac{k_s}{\Delta y_{SP}}(T_P - T_S) \quad (5\text{-}14)$$

Taking Equation (5-13) and (5-14) into Equation (5-12) results in

$$\int_{\Delta V} \frac{\partial}{\partial y}\left(k\frac{\partial T}{\partial y}\right) dV = (dxdz)\left[\left(\frac{k_n}{\Delta y_{PN}}(T_N - T_P)\right) - \left(\frac{k_s}{\Delta y_{SP}}(T_P - T_S)\right)\right] \quad (5\text{-}15)$$

After linearising Equation 5-15,

$$\int_{\Delta V} \frac{\partial}{\partial y}\left(k\frac{\partial T}{\partial y}\right) dV = a_N T_N + a_S T_S - a_P T_P \quad (5\text{-}16)$$

Where $a_N = (dxdz)\frac{k_n}{\Delta y_{PN}}$, $a_P = (dxdz)\left(\frac{k_n}{\Delta y_{PN}} + \frac{k_s}{\Delta y_{SP}}\right)$ and $a_S = (dxdz)\left(\frac{k_s}{\Delta y_{SP}}\right)$ and Equation 5-16 is presented as the general form of the discretized equation in FLUENT (2010) as

$$a_P \phi_P = \sum_{nc} a_{nc}\phi_{nc} + b \quad (5\text{-}17)$$

Where nc denotes the neighbours elements of element P, *a* the linearised coefficients, φ the scalar quantity at the element centre and b the discretization coefficient.

The discretisation and linearisation presented above allows the solving non-phase change problems. When it involves a phase change however, an additional boundary condition appears related to the interface between the solid and liquid phase of the material. Over the years several methods have been suggested to explicitly avoid tracking the phase change interface (Chapter 2). The most common non- explicit phase change tracking methods are denominated as enthalpy and effective heat capacity methods described in sections 5.6.2 and 5.6.3.

5.7.1 Model assumptions

The following assumptions were made in creating the model:

i. Two dimensional problem;
ii. The air was considered to be incompressible;
iii. The air velocity profile is turbulent and fully developed;

iv. The air inlet temperature corresponded to the average inlet temperature at the four air channels;
v. The heat transfer in the PCM by convection was negligible compared to the heat transfer due by conduction;
vi. Gravity effect was not taken into account;
vii. The density of the PCM in both phases were considered to be constant, independent with temperature but different for solid and liquid state;
viii. The latent heat value of the PCM was taken as a constant value for the enthalpy method and approximated to the specific heat capacity-temperature relationship for the effective heat capacity method and
ix. The internal thermal resistances and across the panel wall were neglected.

Based on the experimental results, a two dimensional problem was justified. It was shown that for a given height, the temperature difference along the width of the PCM panels and air channels was symmetrical. The air was considered incompressible as the change of the density was negligible during the flow and specific heat and thermal conductivity were considered constant (Costa et al., 1998; Raj and Velraj, 2011). The air velocity is assumed to be fully developed which is reasonable, since the air inlet velocity profile has been shown to have little influence on the air outlet temperature (Vakilaltojjar and Saman, 2001; Mosaffa et al., 2014). The thermophysical properties of the PCM were considered independent of temperature but different for solid and liquid states similar to Costa et al. (1998), Halawa (2005), Hed and Bellander (2006), Liu and Majumdar (2006), Halawa et al. (2010) and Mosaffa et al. (2014). For the effective capacity method the specific heat capacity-temperature relationship was given into the model as specified in Hed and Bellander (2006), and Raj and Velraj (2011). The heat transfer in the PCM by convection is negligible due to the minimal height of the panels – 0.02 m and therefore approximated to be a conduction problem. The same approach was adopted by Costa et al. (1998), Vakilaltojjar (2000), Zivkovic and Fujii (2001), Dolado (2011), Mosaffa et al. (2014), Charvát et al. (2014) and Wang et al. (2015). Laouadi and Lacroix (1999) also stated that the effect of natural convection is significant only when the PCM slabs are in the verticial position. This assumption did not introduce significant error in the calculation of the temperature variation with time within the PCM. This was accomplished by running only the energy equation in the transient analysis. The thermal resistances across the panel walls were neglected due to the smooth surface. This is also assumed in Zivkovic and Fujii (2001), Zukowsky (2007), Liu

and Majumdar (2006) and Raj and Velraj (2011) showing good agreements with the experimental results.

5.7.2 Enthalpy method

The enthalpy method is based on the enthalpy formulation, detailed in Voller and Shadabi (1984) and described in Chapter 2. For this method, the first term in Equation 5-11 is approximated to the enthalpy and taking into account the assumptions described in section 5.6.1, it is simplified as:

$$\frac{\partial}{\partial t}(\rho H) = k\,\nabla T \tag{5-18}$$

The total enthalpy (H) corresponds to the sum of the sensible heat and latent heat

$$H(T) = \int_{T_m}^{T} \rho\ c_p\ dT + \ \rho\ f_l\ L \tag{5-19}$$

where ρ corresponds to the density and L to the latent heat of the PCM. The latent heat (L) was associated with the liquid fraction, f_l, that allowed the computation of the change in enthalpy from the energy in the material during the phase change (FLUENT, 2010). The general form of f_l and can be written as:

$$f_l = \begin{cases} 0 & if\ \ T < T_s\ (solid) \\ \frac{T-T_s}{T_l-T_s} & if\ T_s < T < \ T_l (mushy) \\ 1 & if\ T > \ T_l (liquid) \end{cases} \tag{5-20}$$

In this model, the melting interface was not tracked explicitly. Instead the porosity was set equal to the liquid fraction, f_l in that element. The liquid fraction was computed for each iteration, based on an enthalpy balance. The mushy zone was the region in which the liquid fraction lies between 0 and 1 and so for instance if the material was fully solidified in an element, the porosity became zero. Replacing the liquid fraction defined in (Equation 5-20) into (Equation 5-19) the enthalpy of PCM corresponds to:

$$H = \int_{T_s}^{T} \rho\, c_{p,s}\, dT \qquad T < T_s(solid) \qquad (5\text{-}21a)$$

$$H = \rho \frac{T - T_s}{T_l - T_s} L \qquad T_s < T < T_l\ (mushy) \qquad (5\text{-}21b)$$

$$H = \int_{T_l}^{T} \rho\, c_{p,l}\ dT + \rho L \qquad T > T_l(liquid) \qquad (5\text{-}21c)$$

In summary, the method solves the temperatures by iterating between the energy (Equation 5-18) and the liquid fraction (Equation 5-20). The enthalpy method is available in the FLUENT package denominated as the Solidification and Melting model.

5.7.3 Effective heat capacity method

The effective heat capacity method was proposed by Poirier and Salcudean (1988) in to order to solve the phase change. This method takes into account the phase change as a sensible process with an increased (effective) heat capacity. For this method, the first term in Equation 5-11 is approximated to the specific heat. Taking into account the assumptions described in section 5.6.1 it is simplified as:

$$\frac{\partial}{\partial t}\left(\rho c_{eff}\right) = k\, \nabla T \qquad (5\text{-}22)$$

The effective heat capacity method as the enthalpy-porosity method defines a new parameter known as the effective heat capacity (c_{eff}) as follows (Yang and He, 2010):

$$c_{eff} = \int_{T_s}^{T_l} \rho c_p\, dT \qquad (5\text{-}23)$$

and,

$$c_p = c_{p,s} \qquad if\ \ T < T_s \qquad (5\text{-}24a)$$

$$c_p = (1 - f_l)\, c_{p,s} + f_l c_{p,l} + \frac{L}{T_{l-T_s}} \qquad if\ T_s < T < T_l \qquad (5\text{-}24b)$$

$$c_p = c_{p,l} \qquad if \quad T > T_l \qquad \text{(5-24c)}$$

As for the enthalpy method, the effective heat capacity method solves the temperatures by iterating between Equation 5-22 and Equation 5-23. Both methods were applied in the experimental validation and the transient profiles for the PCM temperature outputs and air outlet were compared.

5.8 Turbulence model

The geometry includes the air domains that require an adequate definition of the flow nature. Due to the turbulent nature of the airflow, it is essential to determine a reliable turbulence model. The turbulence modelling allowed the correct definition of the velocities and stresses involved in the flow, translating into the overall flow movement. The choice of the turbulence model depend on multiple considerations, including the physics of the flow, the level of accuracy required, the available computational resources and the amount of time available for the simulation (Diarce et al., 2014). In summary, CFD calculates the turbulent flows through three approaches: DNS (Direct Numerical Simulation), LES (Large-Eddy Simulation) and RANS (Reynolds–Averaged Navier–Stokes) equations simulation (Zhai et al., 2007). DNS and LES methods require large computational resources and simulation times therefore are frequently considered unsuitable for analysis. Contrary, the RANS equations govern the transport of the averaged flow quantities and model the whole range of the scales of turbulence, greatly reducing the computational effort and resources (Diarce et al., 2014). For RANS, FLUENT includes the following turbulence models: Spalart- Allamaras model, k-ε model and k-ω model. The k-ε model and k-ω model have been extensively studied over the years and reported in the literature. The k- ε model is a semi-empirical model based on the transport equations for the turbulence kinetic energy (k) and for its dissipation rate (ε). It can be either standard or Re-Normalization Group (RNG). RNG k-ε model includes several refinements over a wider class of flows, making it more accurate and reliable (FLUENT, 2006). The k-ω model is an empirical model based on model transport equations for the turbulence kinetic energy (k) and the specific dissipation rate (ω), which can also be considered as the ratio of ω to k (FLUENT, 2006). RNG k-ε has frequently been recommended in literature due to its accuracy and solving time. It has allowed the extensive validation of channel flow case studies. Gebremedhin and Wu (2003) simulated a ventilated

facility comparing the RANS models. The RNG k-ε model was presented as the most suitable for flow field modelling. From the above literature survey on turbulence models, standard k–ε and RNG k–ε are the most commonly used models. The standard k–ε model presents disadvantages, namely the ε equation contains a term which cannot be calculated at the wall and therefore a wall function must be used (FLUENT, 2006). Also it generally performs poorly for flows with strong separation, large streamline curvature and large pressure gradient (FLUENT, 2006). The RNG k-ε model is a further development from the standard k-ε model and it improved the calculations for the high streamline curvature and strain rate, the transitional flows and the wall heat and mass transfer (Bakker, 2005). Rohidin and Moshfegh (2007) employed the standard k-ε and the RNG k-ε to simulate a forced ventilation system for a packing facility and stated that RNG k-ε provided more reliable results in relation to experimental results. RNG k-ε model has been selected in Raj and Velraj (2011), showing good agreement with experimental data of the flow and heat transfer in a modular heat exchanger selected for free cooling application. Diarce et al. (2014) compared RNG k–ε and Standard k–ω models for calculating the flow and heat transfer within a ventilated layer and RNG k-ε showed the best accuracy when compared to the experimental data. Overall, RNG k–ε presented better agreements through allowing several refinements over a wider class of flows and therefore has been chosen for the present study.

5.9 Validity of the CFD model

The validation study was conducted for the charging and discharging times and the air outlet temperature for the boundary conditions listed in Table 5-3. The simulations were run for the medium mesh described in section of 5.8.1 and shown in Figure 5-3b. Firstly the simulations began solving the flow and turbulence equations for a steady state until the convergence was reached, followed by an unsteady energy balance equation. Convergence corresponds to the repetitive iterative process until the change in the variable from one iteration to the next significantly lessens. This small change can be customised by tracking the mass imbalance between successive iterations, or most commonly by calculating the equation residuals for each point. This standardises how well the discretised equation is satisfied. The residual value of 10^{-4} was set for continuity, velocity and turbulence. 10^{-8} was set for energy. Each iteration and convergence was checked and monitored. Beyond these values no significant changes were observed for the velocity, turbulence and temperature fields.

A pressure-based double precision solver was selected to solve the set of equations with SIMPLE pressure-velocity coupling scheme. The second-order upwind discretization scheme was imposed on the pressure, momentum, density, energy and first-order upwind for the kinetic and dissipation turbulence. The maximum number of iteration for every time step was twenty as recommended by Fluent (FLUENT, 2011). Two methods were applied to characterise the transient phase change of the PCM panels: the enthalpy method and the effective heat capacity method.

The validation errors were quantified in terms of the percent error for thermocouple C5 and for the air outlet temperature and calculated as follows:

$$Average\ percent\ error\ (\%) = \left[\frac{\sum\left(\frac{T_{exp}-T_{num}}{T_{exp}}\right)_t}{N_t}\right] \times 100 \qquad (5\text{-}25)$$

where:

T_{exp}: Experimental Temperature (°C)

T_{num}: Numerical Temperature (°C)

t: time (s)

N_t: Number of time-steps

5.9.1 Mesh independence study

.

The mesh independence was evaluated by comparing the numerical PCM temperatures and air outlets with the experimental results obtained for both the thermocouple C5 (PCM) and the air outlet temperature (Chapter 3). Simulations were run with the three meshes (Figure 5-3) for selected boundary conditions with an average air inlet temperature of 38 °C and an air inlet velocity of 2.5 m/s. Firstly, a steady solution was calculated for the flow equation with the energy equation deactivated to obtain a fully developed flow field. As the flow field reached convergence, the energy equation was enabled to solve the temperature solutions. This approach was valid as the energy equation was approximated as a pure conduction problem, neglecting the convection related with the motion of the liquid PCM. The simulations comprised the effective heat capacity method for the PCM solution. As elaborated in section of 5.7, the RNG k- ε model has shown to be appropriate and will thus be employed in this study. Moreover this model requires the selection of the most suitable near-

wall treatment based on the wall y^+. The wall y^+ is a non-dimensional distance that describes how coarse or fine a mesh is for a particular flow. Very close to the wall, viscous damping reduces the tangential velocity fluctuations, while kinematic blocking reduces the normal fluctuations (Salim and Cheah, 2009). However, towards the outer part of the near-wall region the turbulence is rapidly augmented by the production of turbulent kinetic energy due to the large gradients in mean velocity (Salim and Cheah, 2009). As mentioned in section 5.7, for the RNG k-ε model the ε equation contains a term which cannot be calculated at the wall and therefore the wall function must be carefully selected. For the RNG k-ε model, FLUENT offers four near- wall treatments. There are the standard wall function, the non-equilibrium wall function, the enhanced wall treatment and the user-defined wall function. The mesh density in the near wall-wall regions has been determined using the y+ characteristic parameter to resolve the near-wall region all the way to the wall. The meshes presented y^+ of 166.6, 90.62 and 30.6 for the 3701, 12160 and 194560 elements respectively. As all three meshes present $30 < y^+ < 300$ hence a standard wall function was selected (FLUENT, 2013). Figure 5-7 and Figure 5-8 display the numerical results for the three meshes and the respectively experimental results for the PCM temperature with respect to thermocouple C5 and the air outlet temperature.

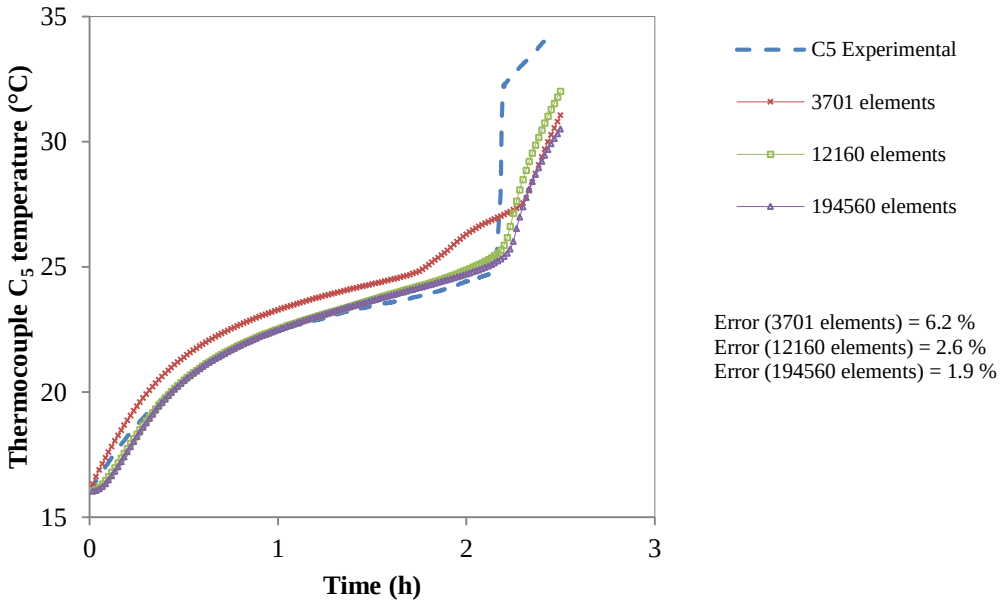

Figure 5-7 Mesh size evaluation for coarse (3701 elements), medium (12160 elements) and fine (194560 elements) (PCM temperature – thermocouple C5 and t=360 sec)

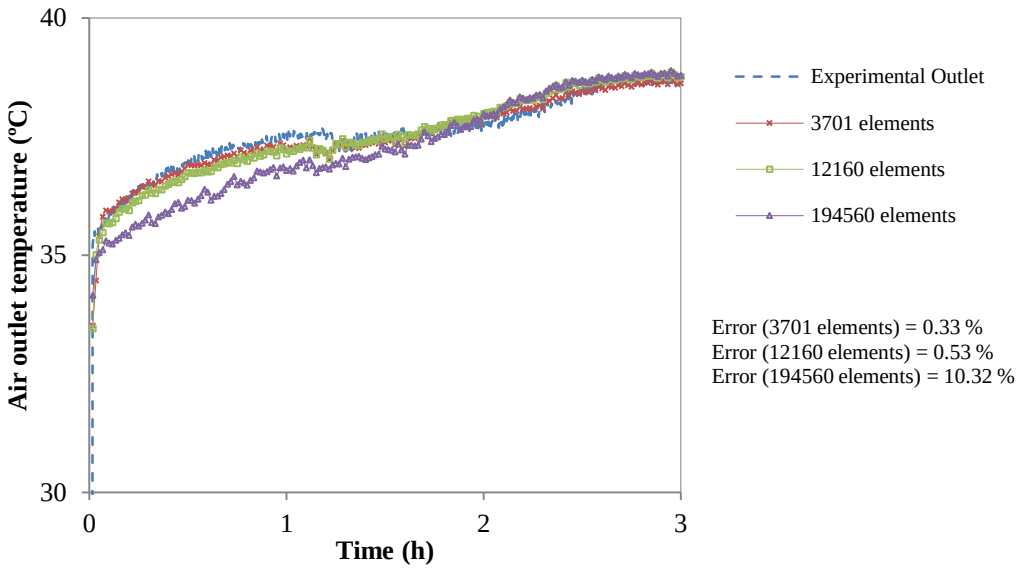

Figure 5-8 Mesh size evaluation for 3701, 12160 and 48460 elements (air outlet temperature and t=60 sec)

Figure 5-7 presents the experimental PCM temperature with the PCM temperature obtained numerically from the three modelled meshes. It is observed from Figure 5-7 that the numerical result for the coarse mesh diverged from the experiments from 1.7h onwards, however the medium and fine mesh show a similar trend with the experimental results over the 2.5 h. The percent error reduced significantly for the medium mesh (2.6 %) and slightly more for the fine mesh (1.9 %).

Figure 5-8 presents the experimental and numerical air outlet temperature for the three meshes. The coarse and medium meshes presented a similar trend and were in good agreement with the experimental result. From the above results, the medium mesh was selected for further analysis as it has shown good agreement with both experimental results: the air outlet temperature and PCM temperature. In addition it requires less computation time than the fine mesh. The time step was not investigated because only the energy equation was selected for the transient analysis and it was approximated to a pure conduction problem consequently allowing a large time step (Tay et al., 2012).

5.9.2 Flow validation

The air flow profile along the air duct was validated for six locations displayed in Figure 5-9. The positions 1 and 6 corresponded to the main air inlet and outlet and positions 2-5 to the centre of each air channel. The average air velocity was experimental measured and compared to the numerical results for 0.6 m/s, 1.6 m/s and 2.5 m/s, displayed in Figure 5-10 and Figure 5-11.

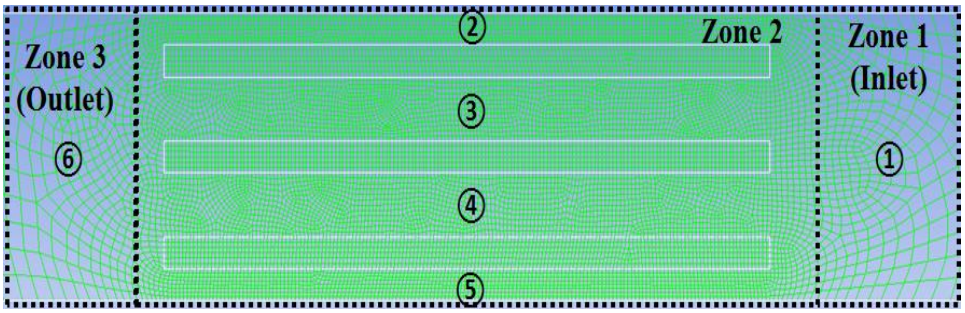

Figure 5-9 Experimental validation locations for the air velocity

Applying the above settings, the air velocity contours were obtained for a steady state condition until convergence was reached (fluid was fully developed), displayed in Figure 5-10 and Figure 5-11. It was observed that the air velocity flowing through the air channels was on average two times higher than the velocity at the main inlet, due to the smaller cross sectional area.

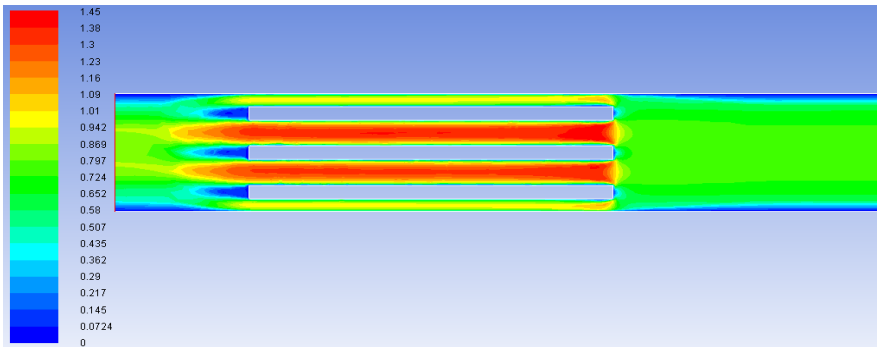

a) 0.6 m/s

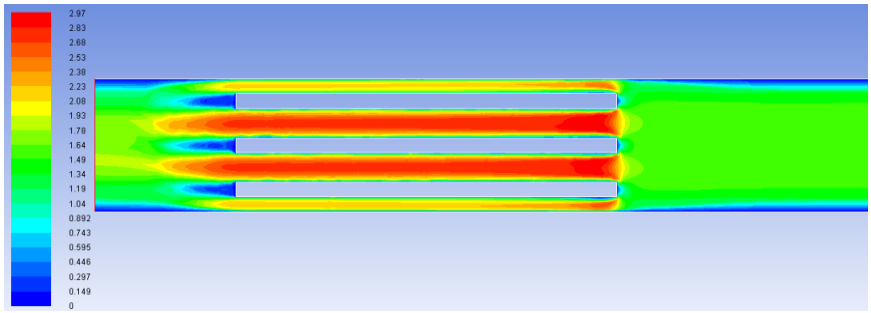

b) 1.6 m/s

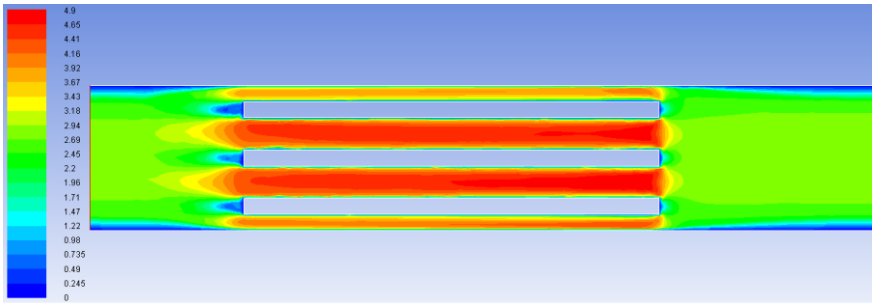

c) 2.5 m/s

Figure 5-10 Velocity contours

Figure 5-10 and 5-11 show the experimental and numerical results at the positions 1- 6 for air inlet velocities of 0.6 m/s, 1.6 m/s and 2.5 m/s. The results were obtained by running a steady state for the flow and turbulence equations with the settings previously described, until the convergence was reached.

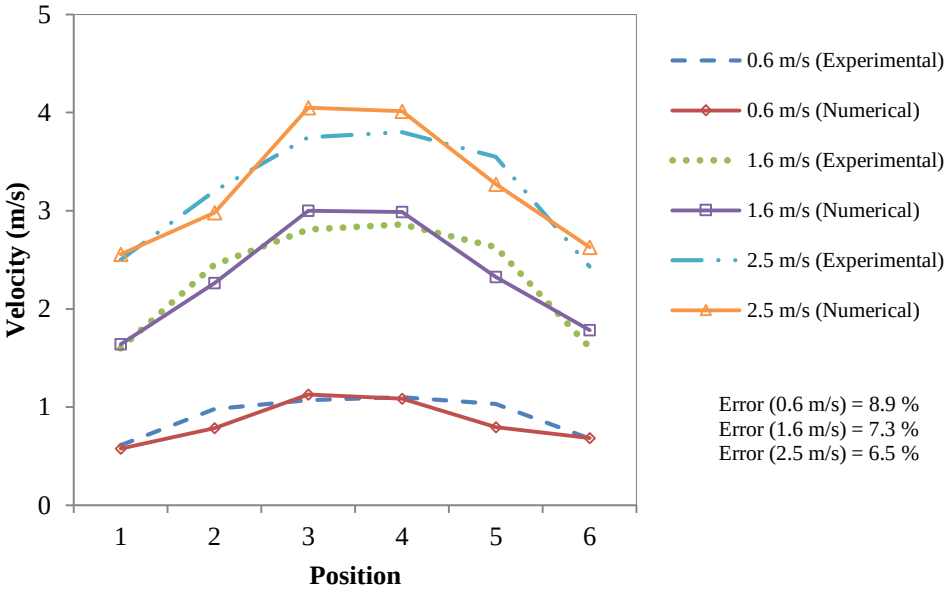

Figure 5-11 Experimental and numerical air velocities for 0.6 m/s, 1.6 m/s and 2.5 m/s

In general, both numerical and experimental results share the same velocity profile. Similar air velocity at the inlet and outlet (positions 1 and 2) is due to the mass conservation of the air along the air duct and maximum velocity at positions 3 and 4 is due to the reduction of the cross sectional area at the air channels. The differences between the experimental and numerical results were due to the uncertainties of the air velocity measurements (maximum of 0.16 %), the roughness of the air ducts built in wood (which is not specified in the model) and the location of the thermocouple in the rig. The main duct walls went through a process of sanding and paint coating in order to reduce the roughness of the walls. However, the actual roughness was not measured and therefore not introduced into the model. Even so the maximum velocity difference between experimental testing and numerical model was 0.3 m/s (position 3) for the 2.5 m/s velocity and with maximum overall error of 8.9 % for velocity of 0.6 m/s, showing a good agreement between experimental and numerical results. For the current study, the numerical simulations are carried out for position 6 (outlet), which shows very good agreements with the experimental data (Figure 5-11).

5.9.3 Validation using the enthalpy method

The enthalpy method was described in section 5.6.2 and was the first method adopted to solve the phase change process of PCM. FLUENT includes the Solidification and Melting model that is based on the enthalpy method. The model solves the temperature by iterating between the energy (Equation 5-18) and the liquid fraction (Equation 5-20). A similar set of governing equations were used in Shatikan et al. (2005) to simulate the melting of the PCM. The validity of the present method was verified by comparing the temperature-time history of the PCM and the air outlet during the charging and discharging process with the experimental data presented in Chapter 3.

The PCM temperature contours of the PCM panel during the charging and discharging process, with an air inlet velocity of 2.5 m/s, were displayed in Figure 5-12 and Figure 5-13. The contours show an increase on the PCM temperature from 16 °C to 25 °C over the 2h.

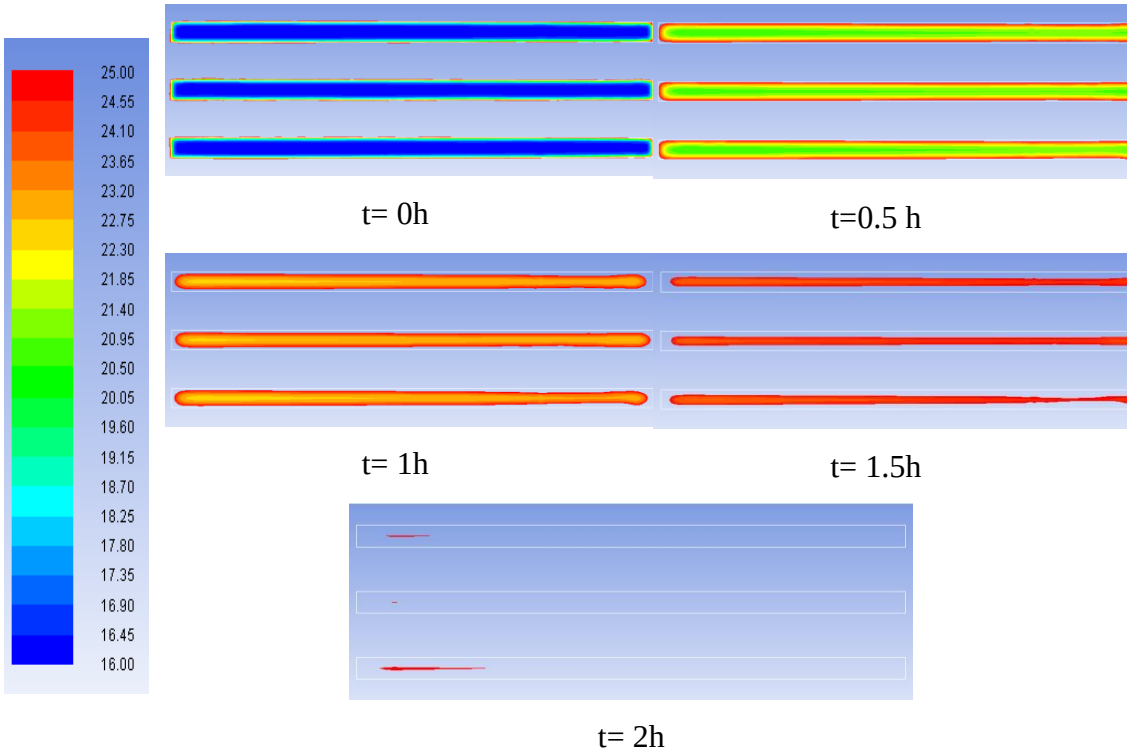

Figure 5-12 Temperature contours for discharging process (T_{inlet}= 38 °C and V_{inlet}= 2.5 m/s)

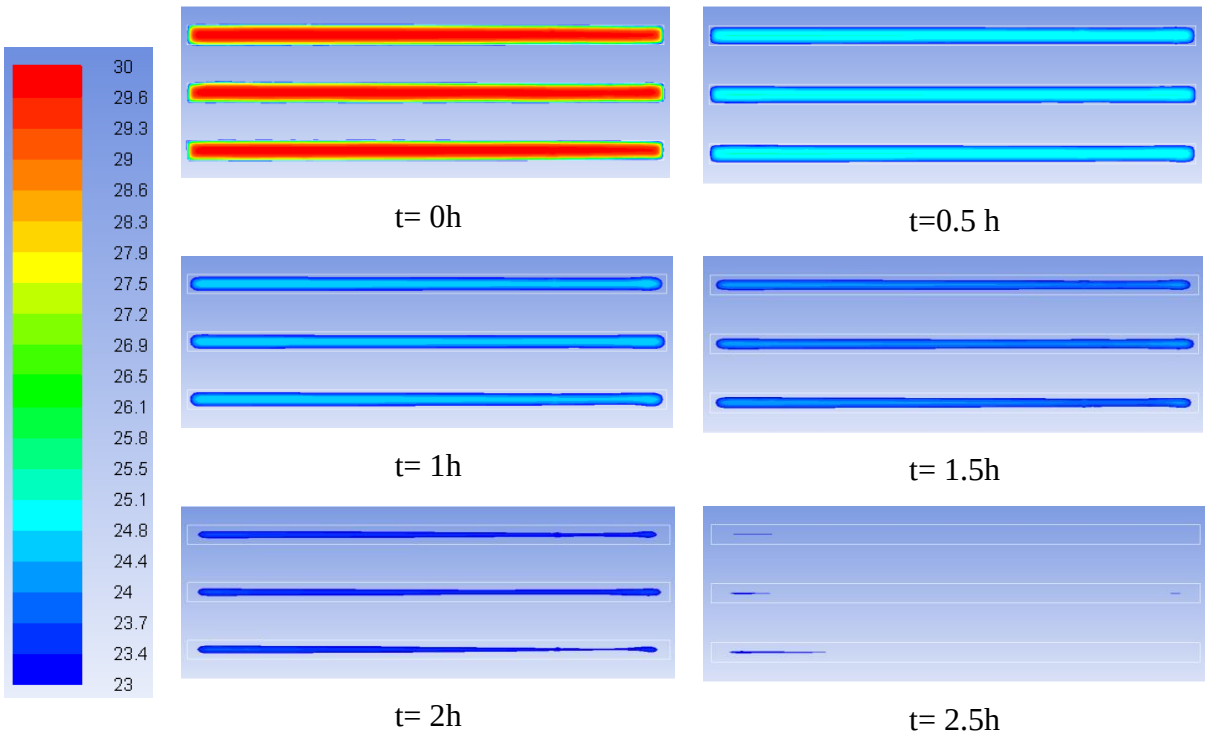

Figure 5-13 Temperature contours for charging process (T_{inlet}= 12 °C and V_{inlet}= 2.5 m/s)

The computational result confirms the scenario three described in section 3.4 (Chapter 3) and observed in the experimental results (Figure 3-10). The last location where melting took place was between the left end and centre of the panel. In the numerical model, the temperatures at this location were similar at the top, middle and bottom panel because the minimal stack effect observed in the experiments was not included in the model.

i) Discharging time and air outlet temperature

The time-dependent variations of the experimental PCM temperature readings and computed calculations at thermocouple C5 located at the bottom of PCM panel and at x= 0.375 m and y= 0.03 m (Figure 3-7) were given in Figure 5-14 and Figure 5-15.

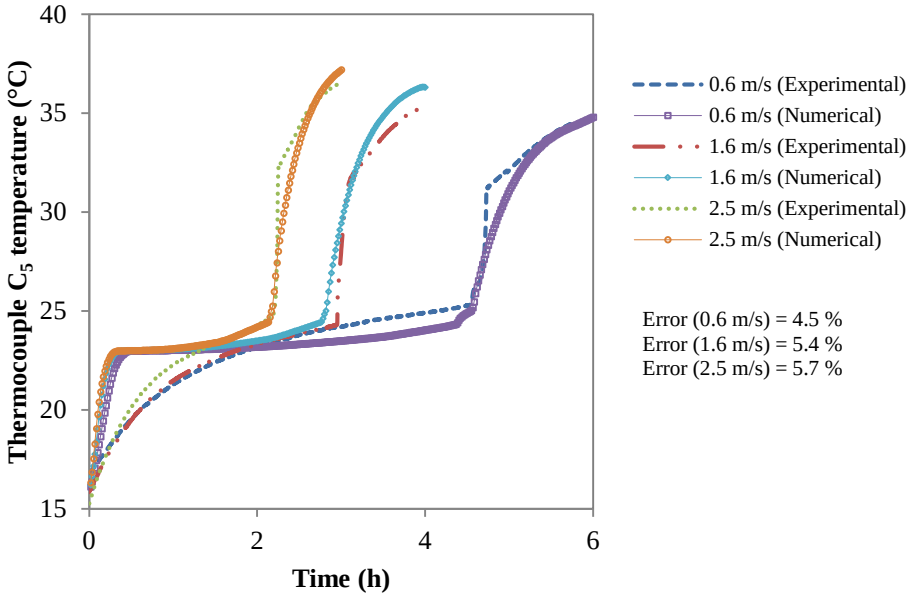

Figure 5-14 Discharging process (thermocouple C5, T= 38 °C) – enthalpy method

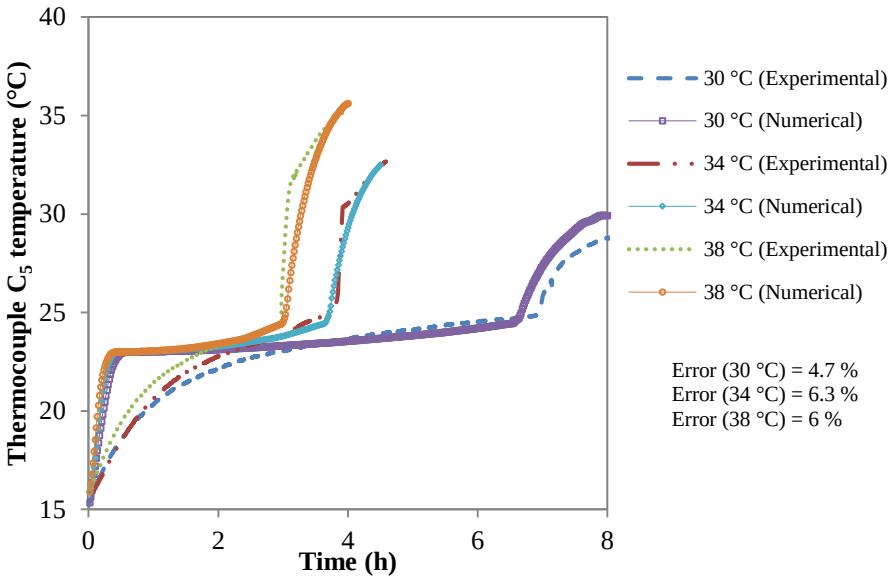

Figure 5-15 Discharging process (thermocouple C5, V = 1.6 m/s) – enthalpy method

Figure 5-14 and Figure 5-15 show the numerical and experimental temperatures at the thermocouple C5 for different air inlet temperatures and velocities. The three stages of the phase change of the PCM can be observed in all results, sensible heating and phase change followed again by sensible heating. The first part related to the sensible heating, presented the major differences between the experimental and the numerical results. The numerical results suggest a sensible heating that takes a very short period of time. The temperature increased from 16 °C to 23 °C during 0.4 h. This was followed by the phase change process represented by a quasi-horizontal curve (T≅constant) showing a drastic change in the shape of the curve while the process was moving from sensible heating to the phase change. This was due to the lever rule intrinsic in the enthalpy method (assuming that the enthalpy-temperature relationship was linear) (Cabeza, 2015). However in reality and represented by the experimental curve, the phase change was represented by a smooth increase of the temperature associated with the impurity of the PCM material (i.e.phase change temperature not constant). Therefore, the major differences are observed during the end of the sensible heating and at the start of the phase change process. Moving on, the numerical results present good agreement with the experimental results. Other possible sources of error for the differences between numerical and experimental results could be a neglect of the conduction resistance of the panel container, a neglect of the natural convection inside the PCM in the numerical model and the uncertainty in of the PCM measurement (experimental PCM temperature uncertainty varied from 0.57 % to 1.3 %). Figures 5-16 and 5-17 show the

comparison between the CFD and the experimental results for the air outlet temperature during the discharging process.

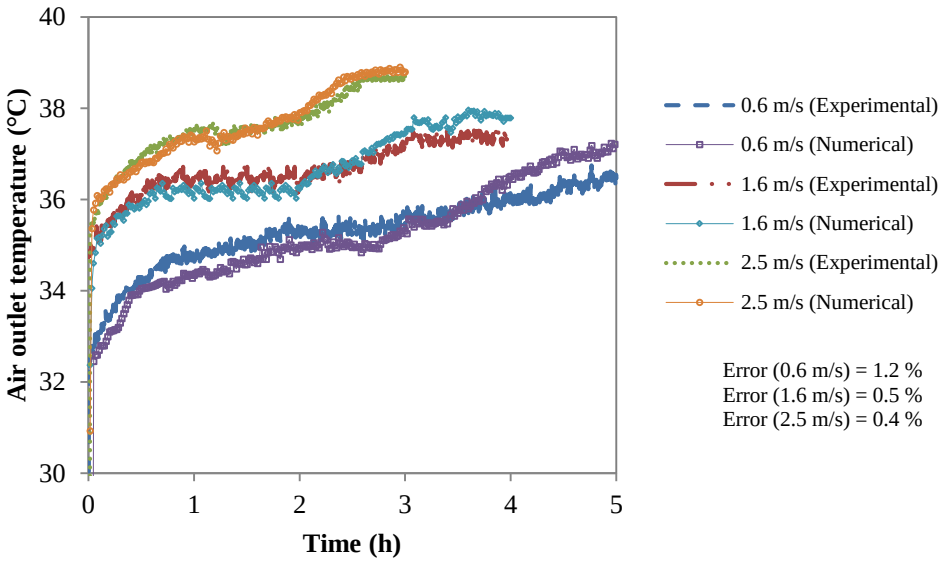

Figure 5-16 Discharging process (air outlet temperature, T= 38 °C) – enthalpy method

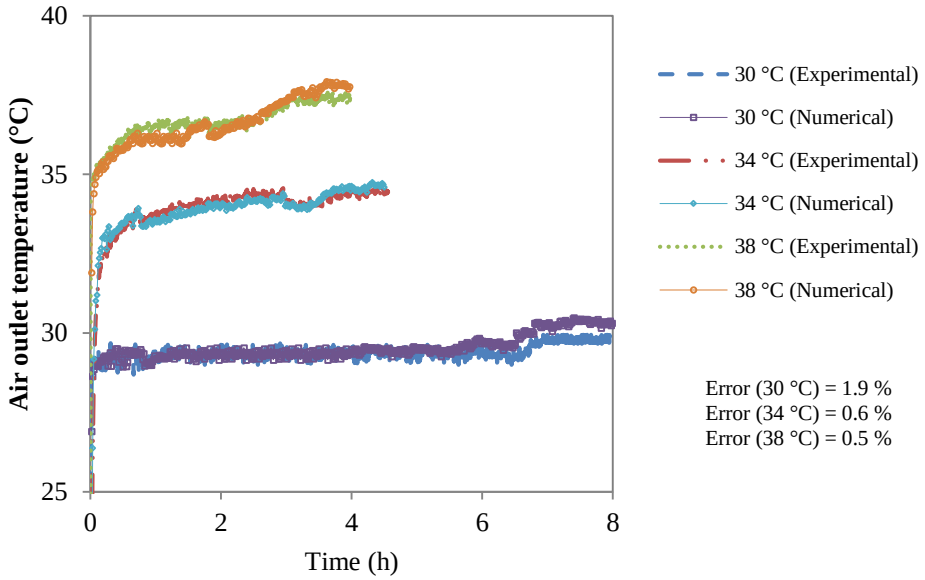

Figure 5-17 Discharging process (air outlet temperature, V= 1.6 m/s) – enthalpy method

Again, the air outlet temperature curve distinguishes three stages during the discharging cycle. Firstly the air outlet temperature increases at a faster rate associated with the sensible heating of the PCM, followed by a stabilised curve during the phase change of the PCM and

then again at a faster rate until the air outlet temperature meets the air inlet temperature related to the final discharging of the PCM panels. From the results shown in Figure 5-16 and 5-17, it can be observed that there is agreement between the numerical and experimental data with maximum difference of 0.4 °C for air inlet velocity of 0.6 m/s. For most cases, the present model calculates slightly higher values in the laterer stage. The deviations are likely to be associated with the location of the thermocouple (positioning the thermocouple's tip accurately was challenging), the internal and across the wall thermal resistances of the panel (neglected in the model) in addition to the experimental uncertainty (varying from 0.52 % to 1.6 %). Overall a good agreement has been achieved between the experimental and numerical results with a maximum error of 1.2 % and hence establishing confidence in the model for the discharging process

ii) Charging time and air outlet temperature

The time-dependent variations of the measured PCM temperature readings and computed calculations in the air duct at x= 0.375 m and y= 0.03 m are given in Figure 5-18 and Figure 5-19.

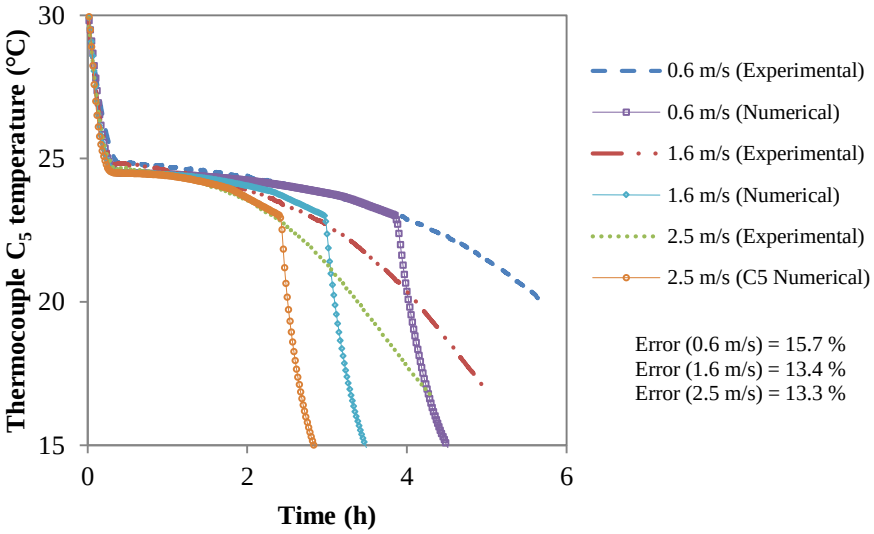

Figure 5-18 Charging process (thermocouple C5, T= 12 °C)– enthalpy method

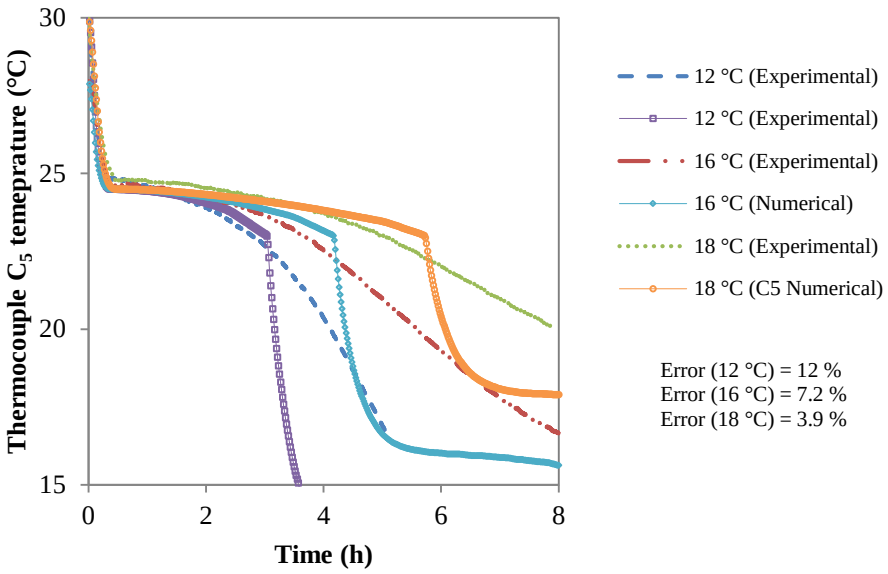

Figure 5-19 Charging process (thermocouple C5, V= 1.6 m/s) – enthalpy method

The temperature profiles presented in Figure 5-18 and Figure 5-19 show an overall consistency between the numerical and experimental results for the initial sensible cooling and phase change. However, in all cases the results deviated after the phase change was completed. Similar to what occurs in the discharging process, the lever rule assumed a quasi-horizontal line for the phase change due to the enthalpy (temperature linear relationship). Hence there was no smooth curve (temperature-time variation) linking the end of the phase change and the sensible heating as has happened in reality and was represented in the experimental results. The numerical and experimental air outlet temperatures for the inlet velocities and temperatures analysed in the experimental study are displayed in Figure 5-20 and Figure 5-21.

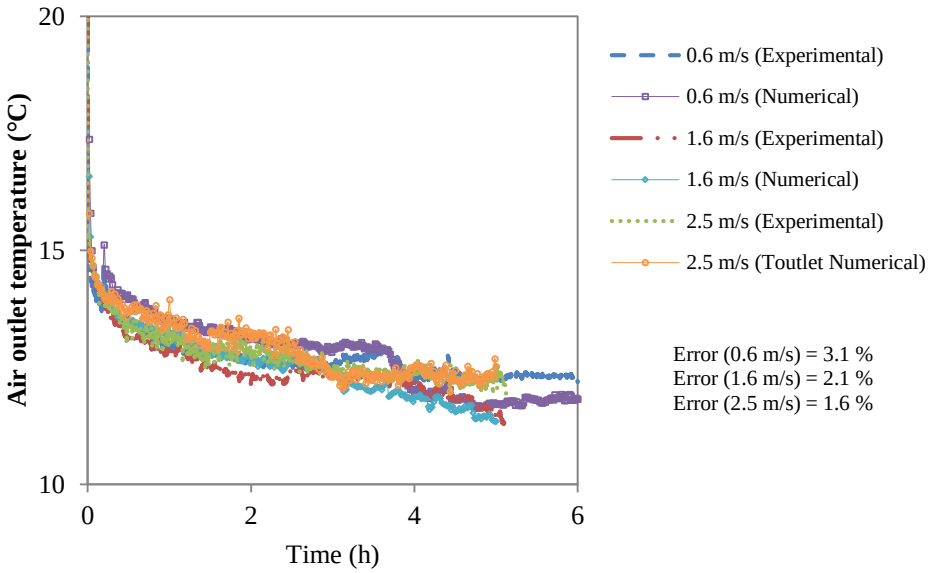

Figure 5-20 Charging process (air outlet temperature, T= 12 °C) – enthalpy method

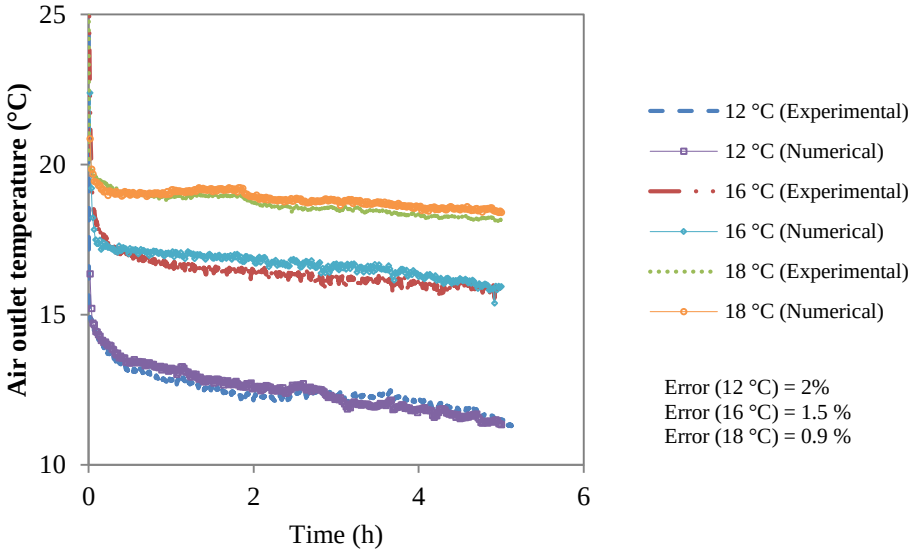

Figure 5-21 Charging process (air outlet temperature, V= 1.6 m/s) – enthalpy method

The air outlet temperatures displayed in Figure 5-20 and Figure 5-21 again show similarities with the experimental results, with a maximum temperature difference of 0.5 °C for air inlet velocity of 0.6 m/s.

Overall the enthalpy method provides good agreements between the numerical and experimental results. However, the lever rule presented limitations as also reported in Egolf and Manz (1994), Susman et al. (2011) and Kuznik and Virgone (2009). The Solidification & Melting model available in FLUENT applies the enthalpy formulation method and shares the lever rule paradigm, but does not provide the flexibility to vary the enthalpy temperature relationship or to provide the possibility of introducing temperature hysteresis (Susman et al., 2011). Hysteresis refers to the phenomenon whereby the PCM melts and freezes in different temperature ranges and with different enthalpies, i.e. different temperature–enthalpy curves for melting and freezing (Gowreensunker, 2013). Yet the Solidification and Melting model shows advantages such as providing the liquid fraction versus time inside the PCM panels which is difficult to obtain in any experiment. For instance Robak et al. (2011) validated the experimental data by comparing the melting fraction obtained numerically with photographic results of the phase change process over the time.

The experimental results were verified by applying the effective heat capacity method. This method is applied in FLUENT by coupling the Cp-T relationship obtained from the DSC analysis (Chapter 4).

5.9.4 Validation using the effective heat capacity method

The specific heat values for RT25 were obtained through the DSC analysis for two heating rates: 0.2 °C/min and 10 °C/min (Chapter 4). Preliminary results for a single case of the discharging process with an inlet temperature of 38 °C and an air velocity of 2.5 m/s were presented in Figure 5-22 for the PCM temperature and in Figure 5-23 for the air outlet temperature for the two heating rates.

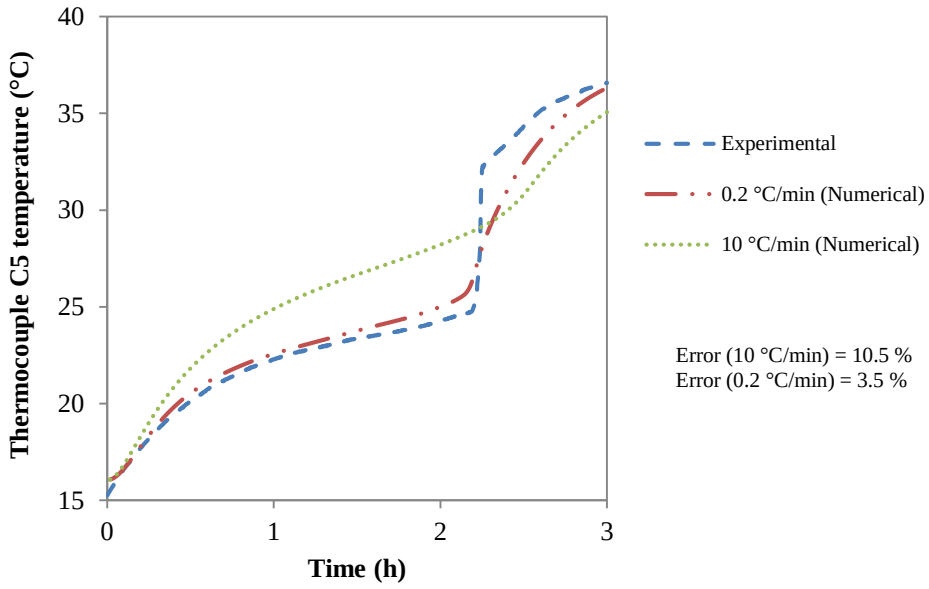

Figure 5-22 Discharging process with effective heat capacity method for DSC heating rates of 0.2 °C/min and 10 °C/min (T= 38 °C, V= 2.5 m/s)

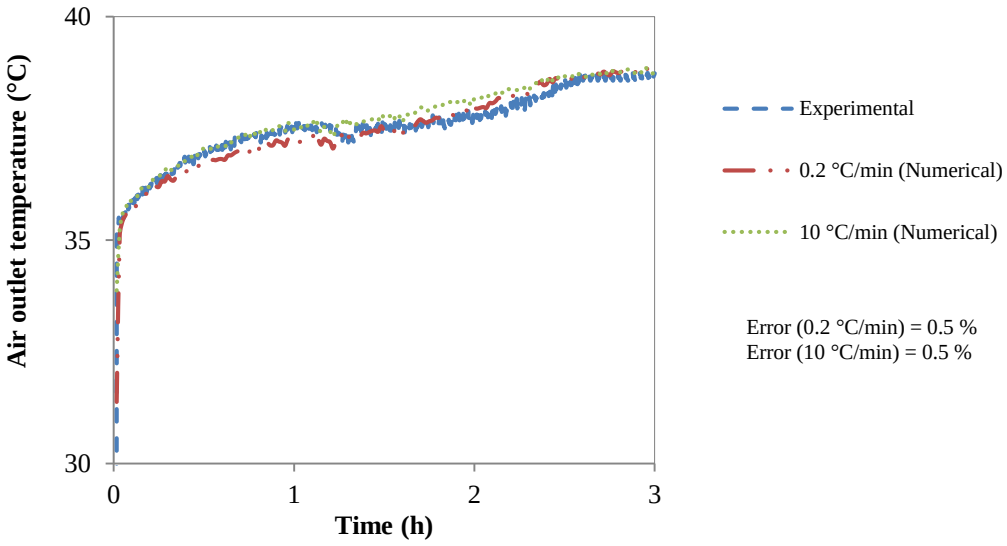

Figure 5-23 Discharging process with effective heat capacity method for DSC heating rates of 0.2 °C/min and 10 °C/min (T= 38 °C, V= 2.5 m/s)

Figure 5-24 and 5-25 plots the PCM and air outlet numerical and experimental temperatures. The numerical results for the PCM temperature with a heating rate of 10 °C/min shows a wider phase change temperatures range (18-31°C) deviating 2 °C to 4 °C from the experimental results. However, the numerical results with heating rate of 0.2 °C/min presents a smaller phase change range (22- 26 °C), closer to the experimental range and shows good

agreements over the whole process. The numerical results of the air outlet temperature for both rates have shown good agreements with the experimental results and showing that the air outlet temperature is not very sensitive to the PCM phase change temperature. Figures 5-24 and 5-25 present the experimental and numerical results of the charging process of the PCM temperature and the air outlet temperatures for an air inlet temperature of 12 °C and an inlet velocity of 2.5 m/s.

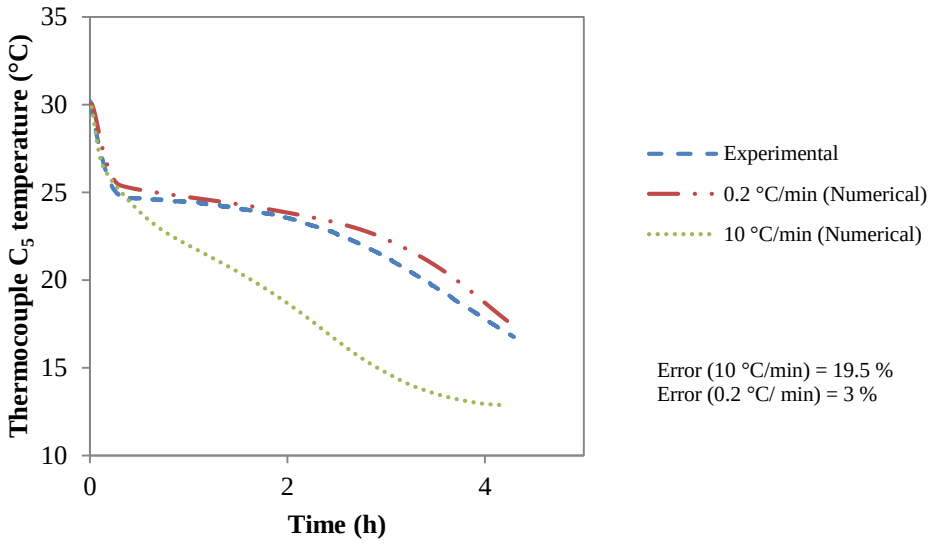

Figure 5-24 Charging process with effective heat capacity method for DSC heating rates of 0.2 °C/min and 10 °C/min (T= 12 °C, V= 2.5 m/s)

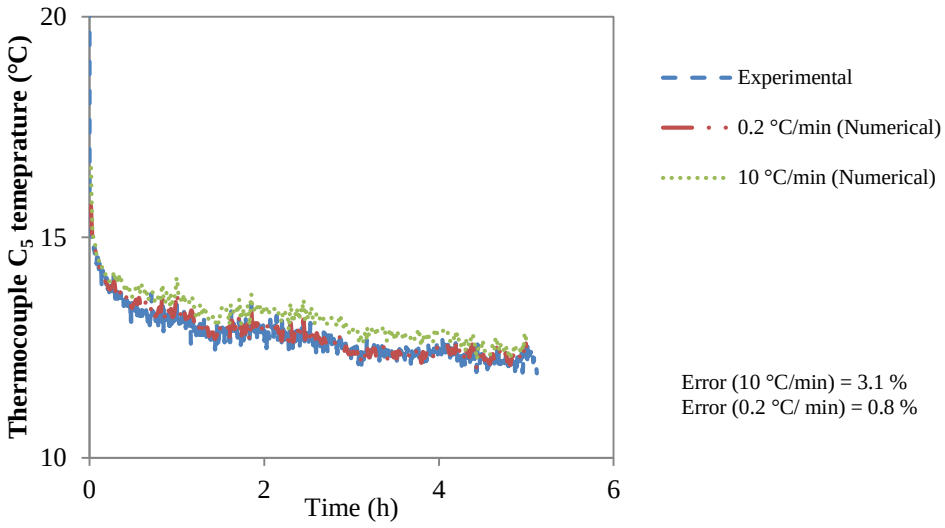

Figure 5-25 Charging process with effective heat capacity method for DSC heating rates of 0.2 °C/min and 10 °C/min (T= 12 °C, V= 2.5 m/s)

The numerical results obtained for the effective heat capacity method for a cooling rate of 0.2 °C/min shows an improved agreement with the experimental results showing an error of 0.8 % compared to a cooling rate of 10 °C/min presenting an error of 3.1 %. The phase change temperature range for a cooling rate of 10 °C/min corresponds to 26-15 °C, deviating from the experimental phase change range 23-25 °C. This was also obtained for the heating rate of 0.2 °C/min. Overall, these outcomes are expected as the C_p-T curves for smaller heating and cooling rates approximated the numerical results to the experimental results. A similar conclusion was stated by Mehling and Cabeza (2008). The deviation can be reduced experimentally by using smaller heating and cooling rates. From the above results, the effective capacity method was applied with the C_p-T relationship obtained for the heating rate of 0.2 °C/min.

i) Discharging time and air outlet temperature

The PCM temperatures for different air inlet temperatures and velocities were plotted in Figures 5-26 and 5-27.

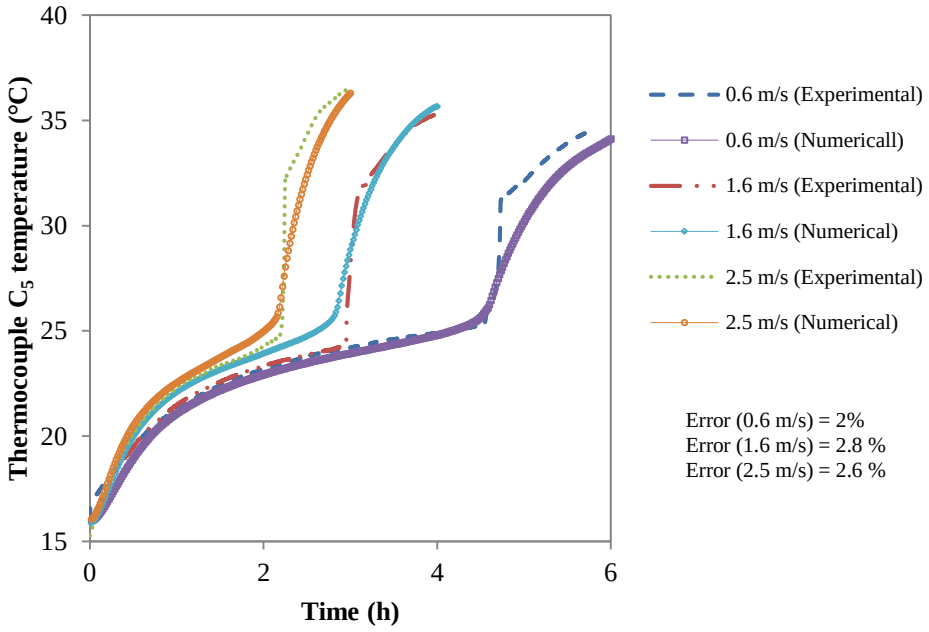

Figure 5-26 Discharging process (thermocouple C5, T= 38 °C) – effective heat capacity method

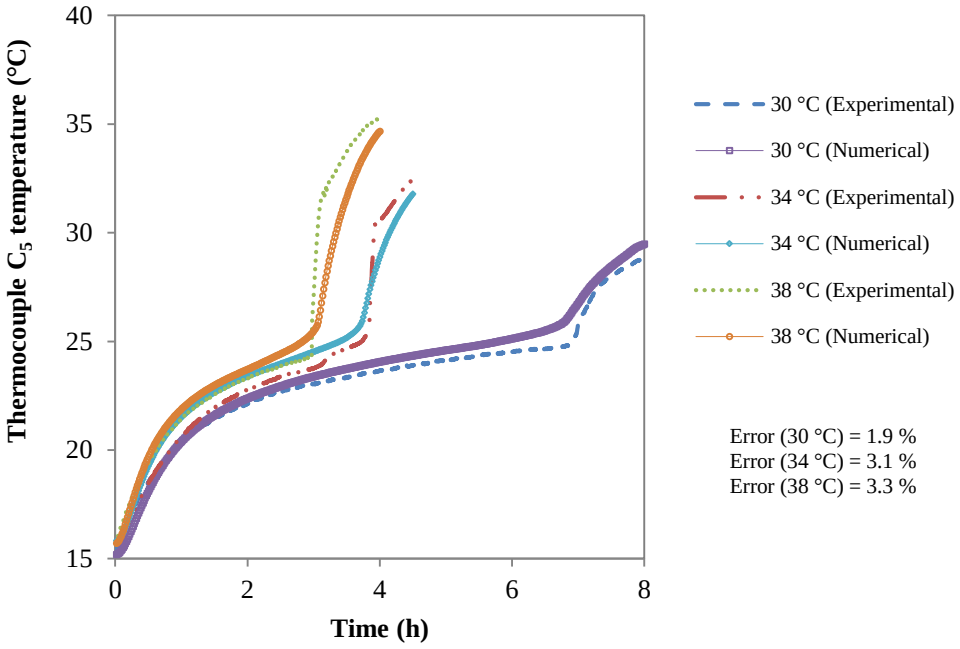

Figure 5-27 Discharging process (thermocouple C5, V= 1.6 m/s) – effective heat capacity method

Figures 5-26 and 5-27 show the comparison between the numerical and the experimental results during the discharging process for different conditions. The numerical results show similar trends to the experimental results over the entire process. Contrary to the enthalpy method for the effective heat capacity, the results show a smooth progression from the initial sensible heating to the phase change. This was because the c_p-T curve given into the model describes the phase change temperature range of the mixture accordingly. The maximum error observed for the PCM validation using the effective heat capacity is 3.3 %. The air outlet temperatures for different air inlet temperatures and velocities are plotted in Figure 5-28 and 5-29.

The air outlet temperature results for different velocities and temperatures are displayed in Figure 5-28 and Figure 5-29. In both cases, the numerical results are congruent with the experimental results. A maximum error of 1.9 % is observed for an air inlet temperature of 30 °C showing that the model is successful in calculating the air outlet temperature for the discharging process.

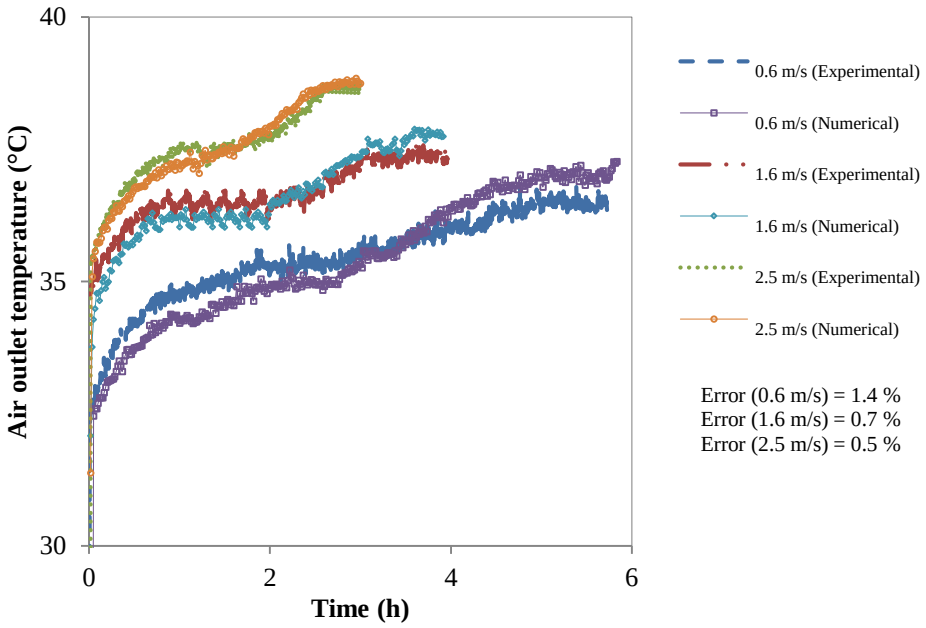

Figure 5-28 Discharging process (air outlet temperature, T= 38 °C) – effective heat capacity method

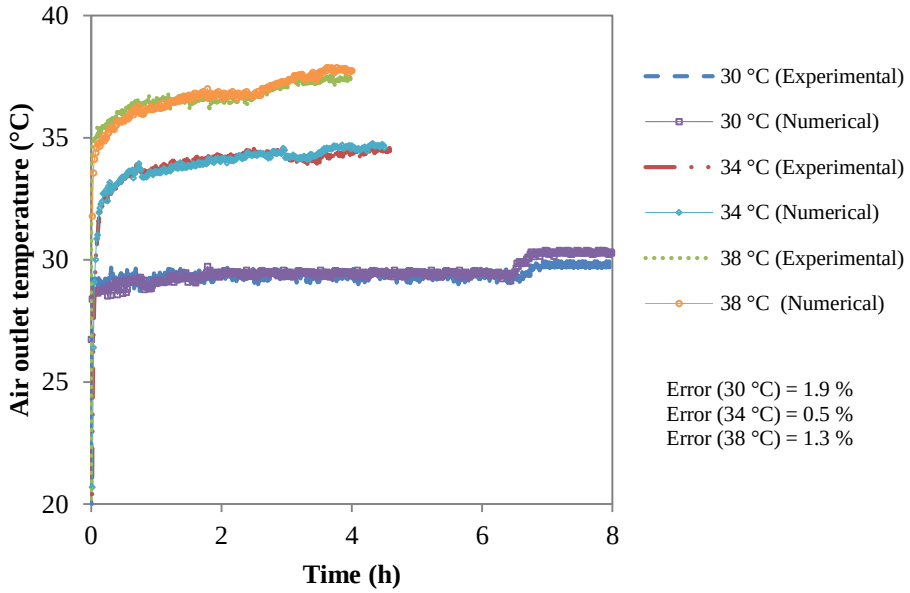

Figure 5-29 Discharging process (air outlet temperature, V= 1.6 m/s) – effective heat capacity method

ii) Charging time and air outlet temperature

The time-dependent variations of the measured PCM temperature readings and the numerical calculations at point C5, located at the bottom PCM panel and at x= 0.375 m and y= 0.03 m, are given in Figure 5-30 and 5-31.

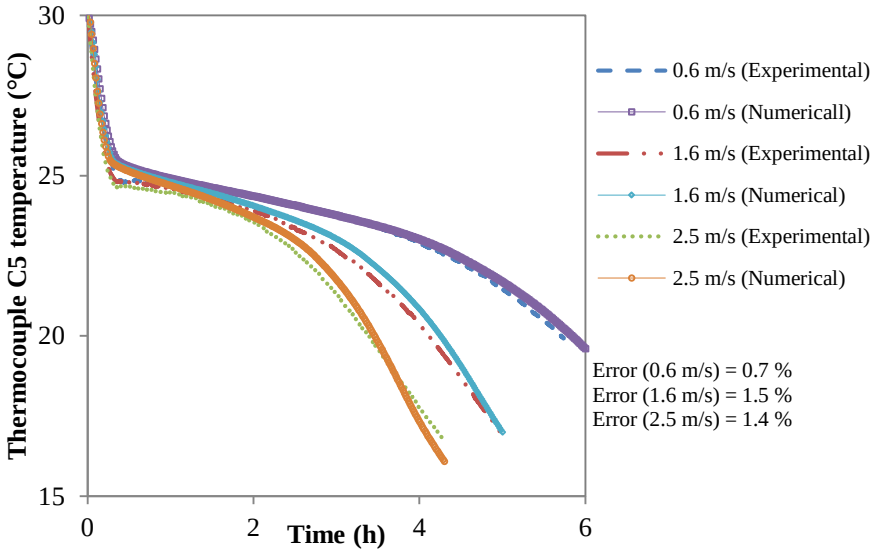

Figure 5-30 Charging process (thermocouple C5, T= 12 °C) – effective heat capacity method

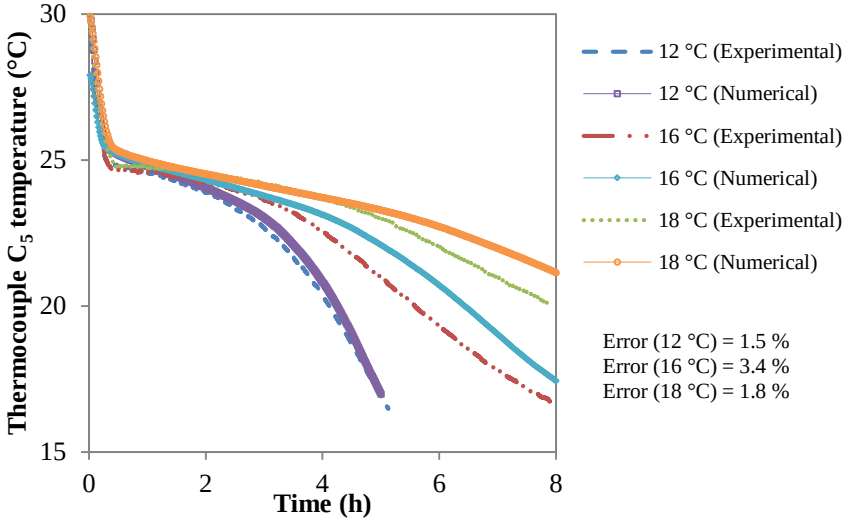

Figure 5-31 Charging process (thermocouple C5, V= 1.6 m/s) – effective heat capacity method

The numerical results present congruency with the experimental results, presenting a maximum error of 3.4 % for an air inlet temperature of 16 °C. Figures 5-32 and Figure 5-33 show the numerical and experimental temperature history comparison for the air outlet.

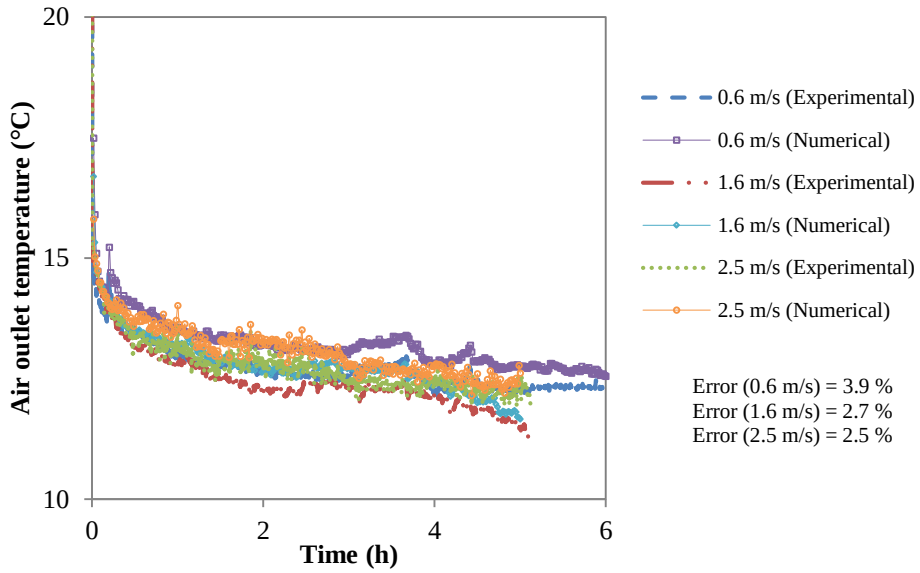

Figure 5-32 Charging process (air outlet temperature, T= 12 °C) – effective heat capacity method

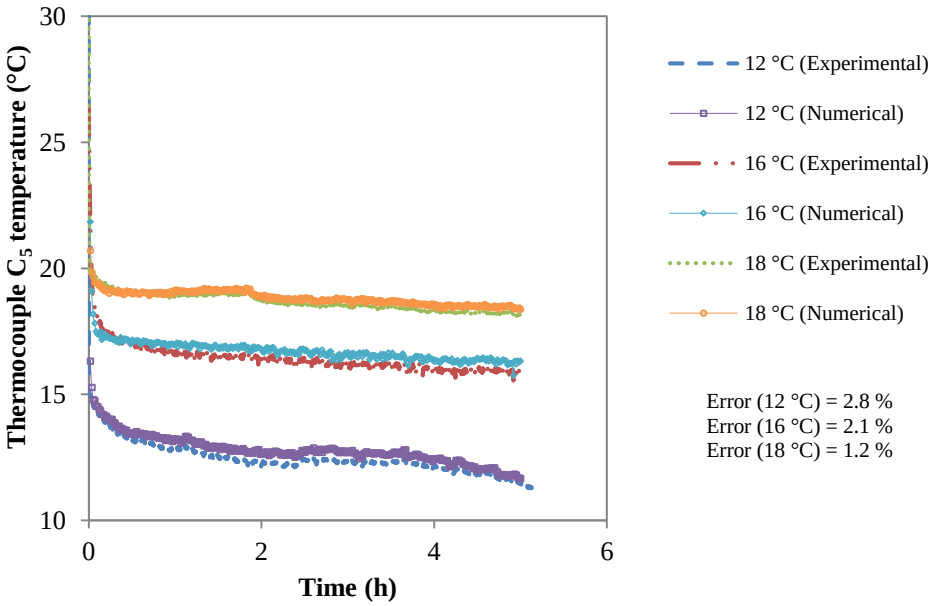

Figure 5-33 Charging process (air outlet temperature, V= 1.6 m/s)– effective heat capacity method

Figure 5-32 and Figure 5-33 present the transient air outlet temperature for the experimental and computational results. The results show that simulation and experiment agree quite well. The temperatures profiles have been estimated giving an overview of simulation results versus experimental results.

5.10 Conclusions

Successful experimental validation was achieved for the developed CFD numerical model, specifying the PCM and air outlet temperatures during the charging and discharging processes. It has been shown that the use of a suitable numerical model and the correct thermophysical properties enables good agreements to be achieved for the PCM charging and discharging time and air outlet temperatures. For the numerical models the effective heat capacity method gives the most promising results with percent error varying from 0.7 – 3.4 % for the PCM temperature and 0.5 – 3.9 % for the air outlet temperature. The enthalpy method shows "percent error" of 3.9 – 15.7 % for the PCM and 0.4 – 3.1 % for the air outlet temperatures. The lever rule intrinsic to the enthalpy method affects the sensible heating and cooling in the discharging and charging process respectively. The air outlet temperature however was not sensitive to this issue. For the effective heat capacity method, the validation of the CFD results by the experimental results infers that the heating rate of the DSC analysis should be carried out based on the experimental heating/cooling rates. This allows the correct phase change temperature range of the PCM to be obtained. It has been observed that for a heating rate of 10 °C/min there was a difference in the temperature range at which the phase change occurred, incurring a deviation between the numerical and experimental. Moreover, if the experimental phase change temperature range for the given application is available, the apparent heat capacity model based on this range will provide accurate results. Using a heating/cooling rate the 0.2 °C/min provided more accurate results and will be used further for the parametric and case study. From this study it was discovered that the developed CFD model can accurately calculates the behaviour of thermal storage units during the charging and discharging processes. Therefore, this CFD model based on the effective heat capacity method will be used in Chapter 6 for the investigation of multi-PCMs.

CHAPTER 6 – MODELLING OF AIR-MULTIPLE PCM UNIT FOR FREE COOLING AND VENTILATION

6.1 Introduction

This chapter intends to study the enhancement incurred by multiple PCMs for the free cooling and ventilation of buildings. The current studies on multiple PCMs assume a constant air inlet temperature that does not correspond to the real climatic conditions. Therefore, this research intends to use real climate data to numerically investigate an air -multiple PCMs unit for an office building located in Castelo Branco, Portugal. The air-multiple PCM unit stores night coldness to provide cooling during day time in order to achieve desirable comfort conditions in buildings. Three main criteria need to be satisfied (i) the air outlet temperature should meet the thermal comfort conditions in the building (ii) cooling time (i.e. discharging time) should be equal or more than cooling period demand during the day time and (iii) the charging of the PCMs should be completed during night-time (i.e. charging time). To fulfil the above mentioned criteria, RT25, RT20 and RT18 with melting temperatures of around 25, 20 and 18 °C respectively will be selected. In order to achieve the desired air temperature, cooling time and charging time of the PCMs, a parametric study will be developed. It will investigate the effect of multiple PCMs selection within the panels, followed by the effect of geometry e.g. height, length and the charging and discharging air mass flow rates. The analysis will be carried out through numerical simulation, by extending the validated CFD model that was developed and experimentally validated in Chapter 5. Furthermore, a case study comprising technical, economic and environmental analysis of air-multiple PCM unit for office building will also be carried out. Greenhouse gas mitigation potential and the potential savings of the air-multiple PCMs unit will be compared with conventional air-conditioning unit.

6.2 Principle of free cooling of buildings

The proposed unit intends to provide free cooling and ventilation that relies on low night ambient temperature through the charging and discharging processes as displayed in Figure 6-1 and Figure 6-2.

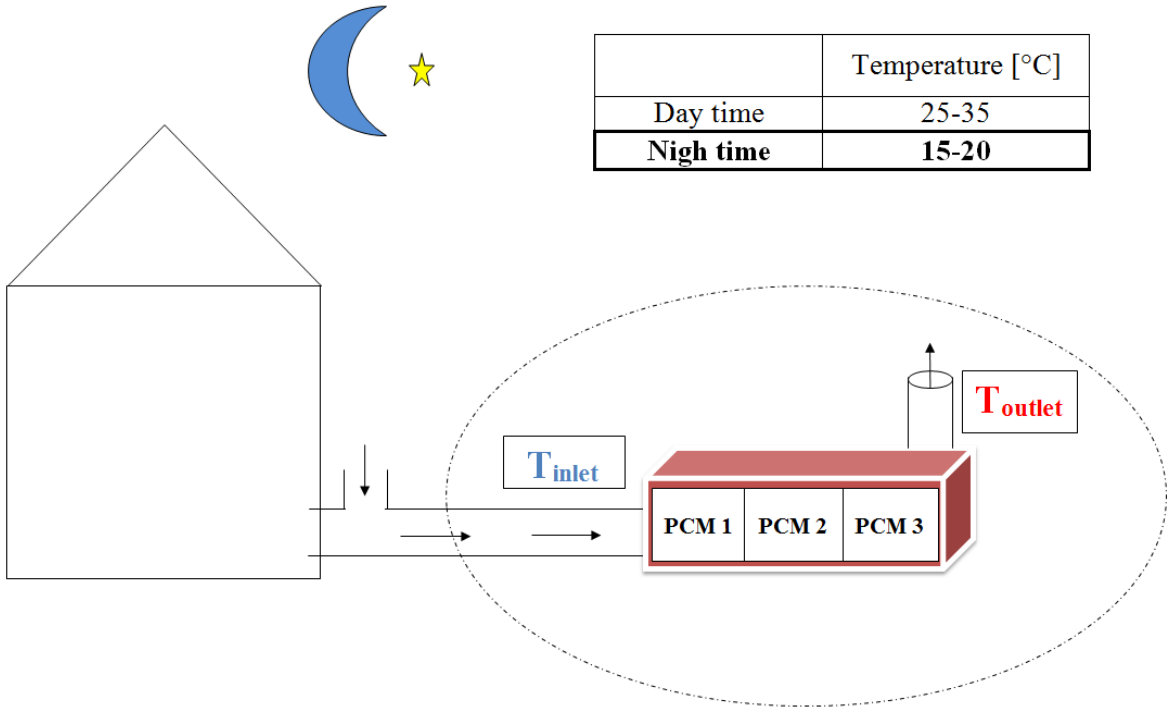

Figure 6-1 Charging of PCMs

Figure 6-1 demonstrates the charging of the PCMs panels through the night with air temperatures varying from 15 to 20 °C. Cold air during night-time flows along the PCM panels and coolness is exchanged between the PCM panels and the air. The process of heat transfer take place in two main phases (i) sensible cooling, represented by the sharp decrease of PCM temperature until it reaches its transition temperature and (ii) latent cooling after sensible cooling the PCM panels start to change their state from liquid to solid at an almost constant temperature that consequently raises the air temperature. This process continues until the PCMs panels are completely solidified, followed again by sensible cooling.

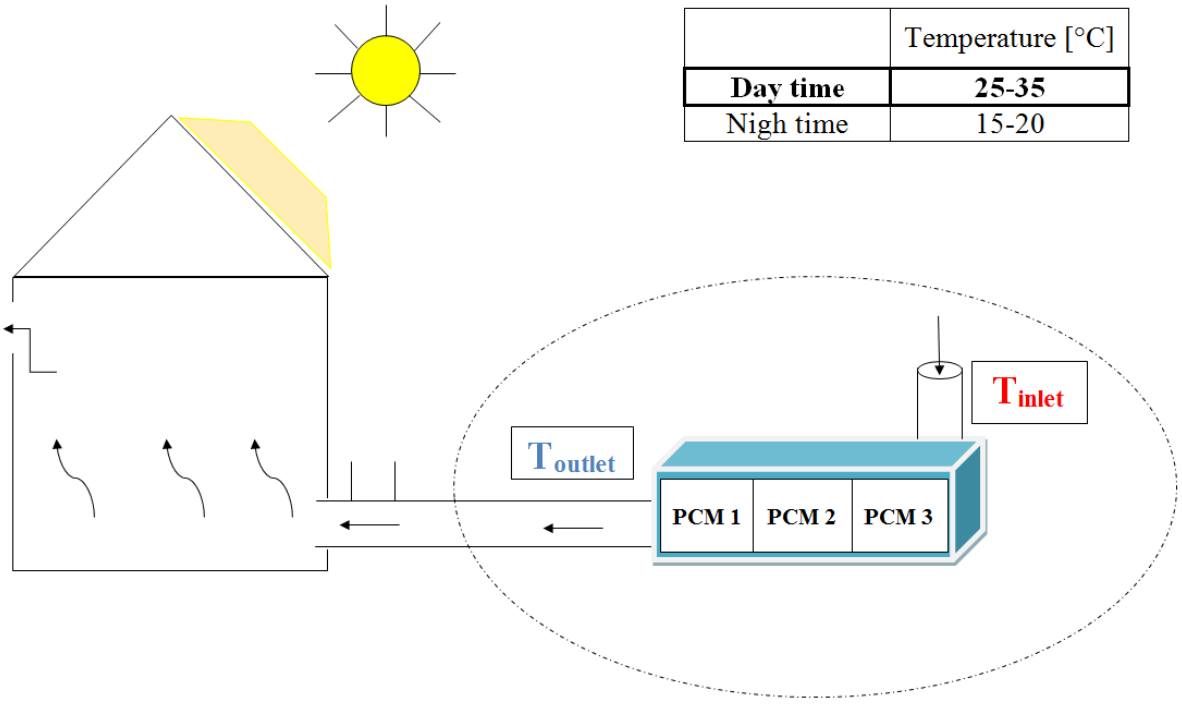

Figure 6-2 Discharging of PCM

Figure 6-2 shows the reversible process and the proposed schematics for free space cooling during daytime for a typical summer day. This process involves the passage of hot ambient air (25-35°C) through the cold PCM panels solidified during night-time. During this process, the heat is transferred from the air to the PCM panels and air receives the coldness stored in PCM unit, thus lowering its temperature. The PCM panels, which are in a solid state after the absorption of thermal energy, initiate a change of solid to liquid at almost constant temperature and consequently reduces the air temperature. The reduced air temperature is delivered into the building providing free cooling and ventilation respectively.

6.3 Identification of parameters for free cooling

In order to adequately design a unit for free cooling application, two parts have to be identified. Firstly the building typology is identified in order to establish the predominant occupancy throughout day. Secondly the daily temperature profiles, namely the diurnal temperature of the building location must be known. Depending on the building typology, as the occupancy period varies, the cooling demands also vary. Displaying the daily external temperature and taking into account the thermal comfort temperatures in buildings, allowed

the identification of overheating and requirements of cooling. Matching these variables allowed the identification of the main parameters of free cooling. These are the required cooling time (i.e. discharging time) and the maximum air outlet temperature to be delivered to the building. Finally, full charging of the PCM panels have to be guaranteed and the available charging time was identified based on the nocturne temperatures. The aforementioned procedure is displayed in Figure 6-3 below.

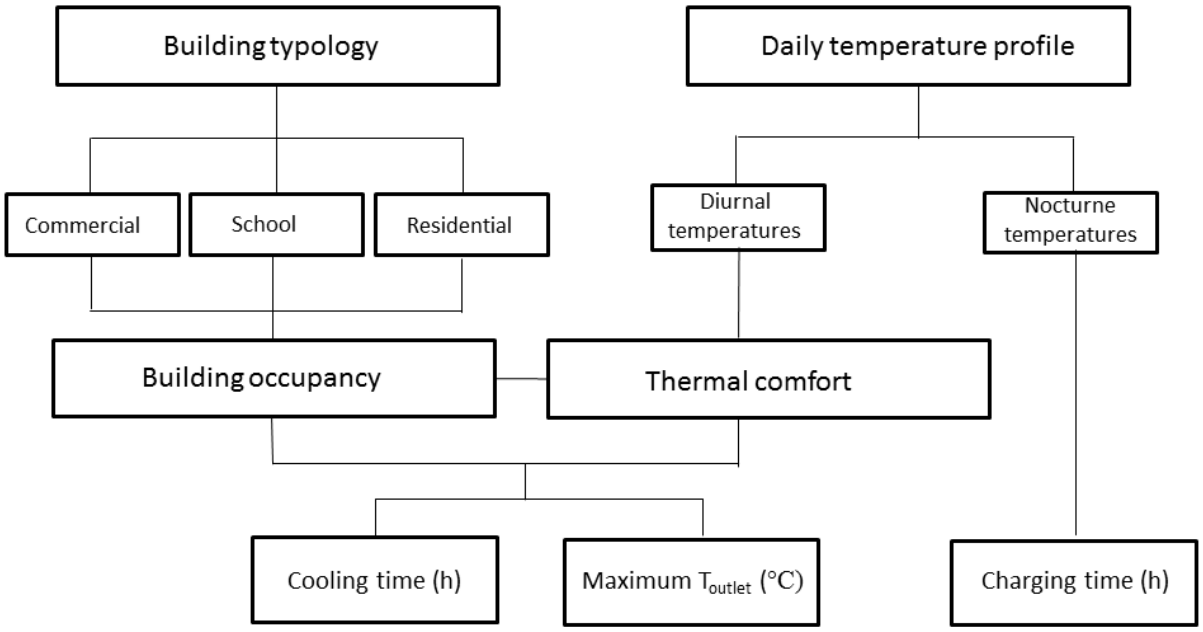

Figure 6-3 Procedure for PCM selection

6.3.1 Building occupancy

Offices, schools and residential buildings were chosen for the representation of different occupancies along the day and presented in Figure 6-4. These values were based on the current regulation on the thermal performance of buildings in Portugal for residential buildings (RCCTE, 2006) and for commercial buildings (RSECE, 2006).

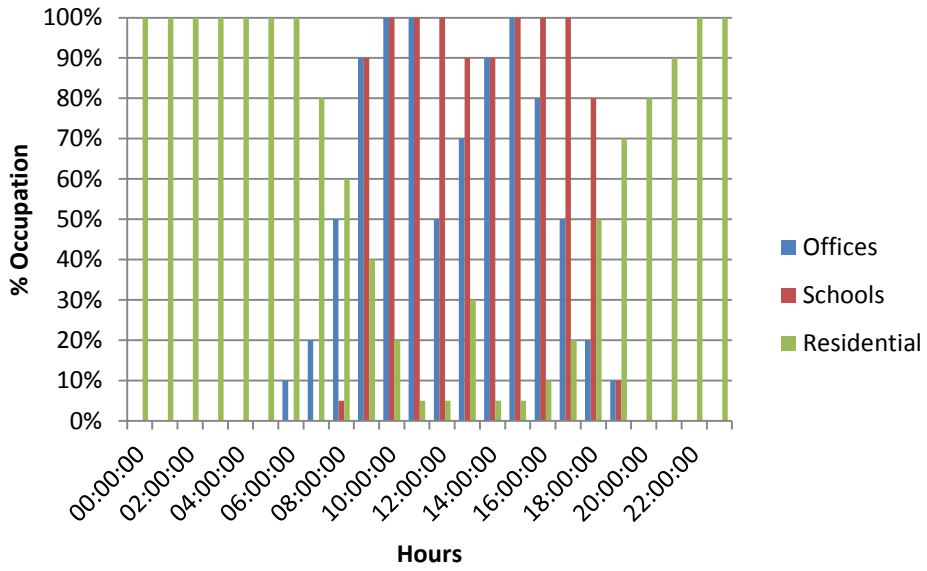

Figure 6-4 Hourly occupation profile in offices, schools and residential buildings (RCCTE, 2006 and RSECE, 2006)

It was observed that the predominant occupancy profile occurs between 9h to 18h for offices and schools and from 20h until 7h for residential buildings.

6.3.2 Daily temperature profile

SolTerm software was developed by the National Laboratory of Civil Engineering in Portugal (LNEC) and has been mostly used for performance analysis of solar systems (thermal and photovoltaic). It is recommended by current National Energy Certification (SCE) and approved by the Thermal Performance Characteristics of Buildings Regulation (RCCTE) and Energy Systems and Air Conditioning of Buildings Regulation (RSECE). SCE was established with similar objectives to the European Directive published on January 4, 2003 the Directive no. 2002/91/EC of 16 December 2002 concerning the performance of buildings. Among other requirements, it insists that the Member States establish and regularly update regulations to improve the thermal behavior of new and renovated buildings and to guarantee the conditions of Indoor Air Quality (IAQ). All measures must adhere to technical and economic requirements. SolTerm includes the weather conditions in Portugal, in addition to a fully climatic database involving 308 years of meteorological reference (Aguiar and Coelho,

2012). RCCTE (2006) sets the cooling season as the four summer months (June, July, August and September), when high external temperatures are more likely to require the cooling of the building's environment with small internal loads. Daily temperatures for the cooling season were exported from SolTerm. The selected days included the first and last day of the season and a few days in the middle of the season. These daily profiles were registered in the city of Castelo Branco in Portugal and displayed in Figure 6-5.

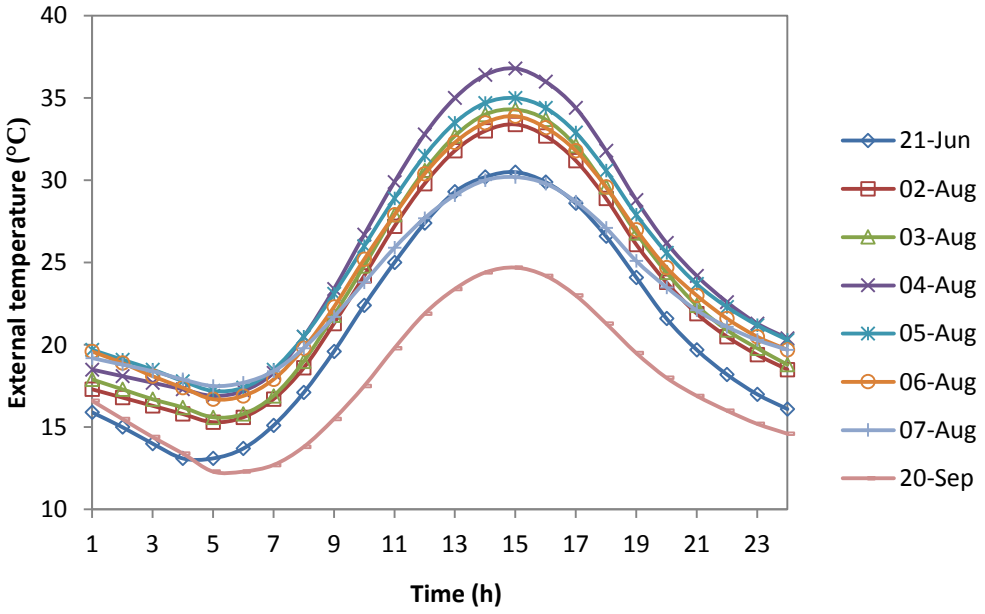

Figure 6-5 Typical temperature profiles for the summer in Castelo Branco, Portugal (Solterm, 2006)

During the cooling season, August represents the hottest month. The hottest day was registered on the 4th August with daytime temperature varying from 20-37 °C. Apart from 21th June, 4th August, 7th August and 20th September, the remaining days showed similar temperatures average of 16-20 °C and 20-35 °C during night-time and daytime, respectively. An average daily variation of 15 °C was observed during summer time in Castelo Branco, Portugal. In terms of thermal comfort temperatures in buildings, different reference values can be found given in the literature. In Portugal, RCCTE (2006) and RSECE (2006) established the comfort temperature range between 20 and 25 °C, independent of the external temperature and the occupant's perceptions. Furthermore adaptive models were developed taking into account the external temperature and occupancy perception as EN 15251 (CEN, 2007) and LNEC (Matias, 2010). These models specify the temperature range related to the

external temperature and also to the tolerance limit of the occupants in terms of thermal comfort. A possibility of thermal adaption through clothing, activity, posture etc. will make the occupants more tolerant. Considering the mild climate in Portugal, the comfort temperature range presented by the LNEC model (Matias, 2010) allowed the prediction that in most indoor spaces, the use of air conditioning can be substantially reduced. Both adaptive models are only valid for buildings without mechanical air conditioning apart from passive air conditioning systems with low flow rate such as fans, blinds, night ventilation or other passive cooling methods. They are also valid if method of controlling the temperature relies mainly on the opening and closing of windows and the occupant's activity is sedentary with metabolic rates ranging between 1.0 and 1.3 met.

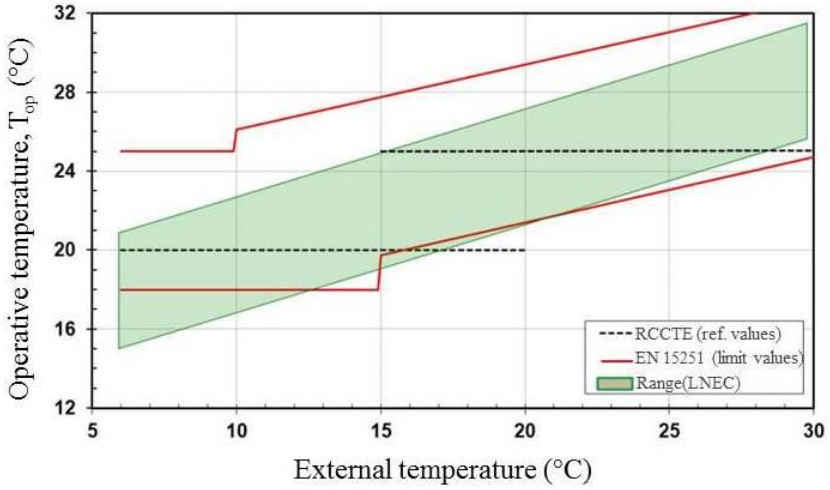

Figure 6-6 Thermal comfort temperature for RSECE (2006), EN 15251 (CEN, 2007) and LNEC (Matias, 2010)

It was observed from Figure 6-6 that both adaptive models enlarge the temperature range for the thermal comfort in buildings comparing with the non-adaptive method (RCCTE, 2006 and RSECE, 2006). The adaptive model by LNEC (Matias, 2010) presented comfort temperature varying from 15 to 31 °C. Matias (2010) also studied the thermal comfort temperatures for building that were air conditioned by means of mechanical systems. The comparison between these two scenarios is displayed in Figure 6-7.

Figure 6-7 Recommended values of comfort temperature on the average external temperature (adapted from Matias, 2010)

Figure 6-7 indicates that for non-air conditioned buildings the limit temperature values range for winter and summer time are 15 °C and 31 °C respectively. These figures changed in ± 3 °C when the space was conditioned as presented in Figure 6-7. It is evident that occupants have a greater tolerance of the higher external temperatures in non-air conditioned buildings rather than in air conditioned buildings. From the adaptive model presented by LNEC (Matias, 2010) and for conditioned buildings it is observed that the limit of comfort conditions is at 30 °C for an external temperature of 30 °C. In other words, it is assumed that overheating (i.e. discomfort conditions) takes place when external temperature is higher than 30 °C. Hence cooling is required when the external temperatures gets over that temperature.

6.3.3 Selected parameters to investigate the potential of free cooling

A typical day temperature profile during summer season was selected from Figure 6-5 and displayed in Figure 6-8. Overall, the daily temperature varies from 20-34 ° C during daytime and between 15-20°C during night-time.

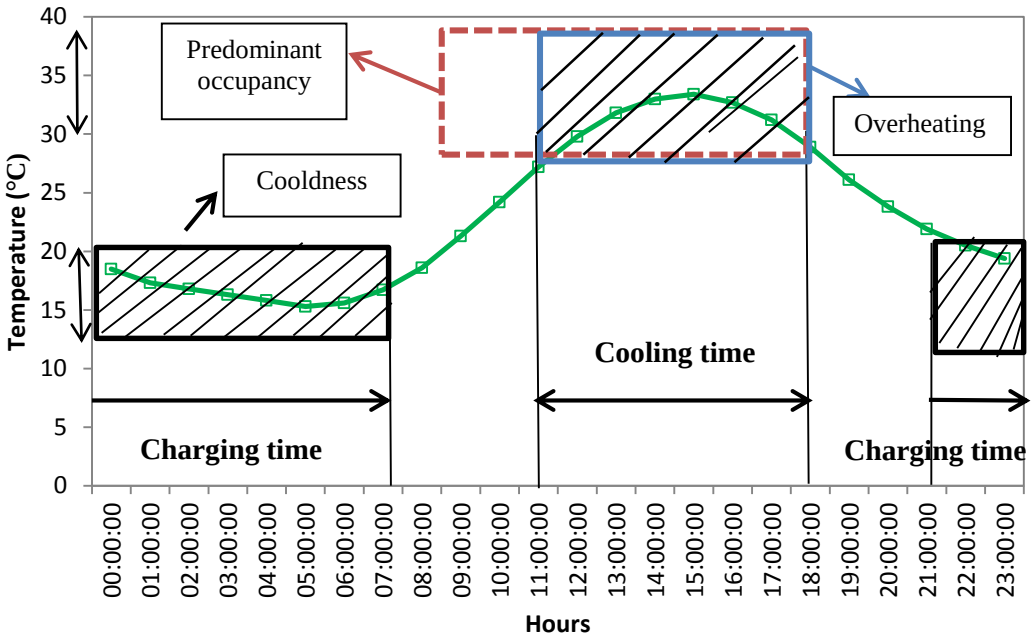

Figure 6-8 Typical daily temperatures during summer period

Following the procedure presented in Figure 6-3, the matching of the predominant occupancy period in an office building with overheating hours (based on the adaptive model, $T_{external} \geq$ 30°C) allowed the identification of the required cooling time: 11h-18h. It was observed that the cold temperature is available (when temperature drops below 20 °C) from 21h-7h (10 hours) setting up the criteria for the charging time of PCMs. To summarise, in order to guarantee free cooling in a typical office building, the air outlet should be delivered at $T_{outlet} \leq$ 30 °C from 11h-18h and the PCM have to be completely charged from 21h-7h.

6.3.4 Selected PCMs

From the experimental results in Chapter 3, for an air inlet temperature of 34 °C, the air outlet temperature dropped 1 °C, reaching 33 °C. For real applications this air outlet temperature is still too high in order to achieve the necessary thermal comfort conditions ($T_{outlet} \leq$ 30 °C). One way of further decreasing the air outlet temperature would be to choose a PCM with lower melting temperature. This however, that would decrease the discharging time (i.e cooling time) due to the higher temperature difference between the air inlet temperature and the PCM melting temperature. Besides when using a single PCM the temperature difference between the air inlet temperature and the PCM melting temperature would decrease in the air

flow direction. However, if multiple PCMs with different melting temperature were packed in the unit in decreasing order of their melting points, then nearly constant temperature difference can be maintained through the air flow direction during the discharging process (Mosaffa et al., 2013). The potential of multiple PCMs to improve the heat transfer between the air and the PCMs was discussed in section 2.3.6 of Chapter 2. To summarise, it maintains a higher driving temperature difference for the heat transfer process in the charging and discharging processes (Chiu and Martin, 2013). In maintaining a nearly constant heat flux from the PCM to the HTF (Mostaffa et al., 2013), a higher storage capacity and higher melt fraction can be achieved (Fang and Cheng, 2007). Therefore, choosing multiple PCMs with different melting temperatures matching with the thermal comfort of air conditioned buildings will reduce the air outlet temperature and also keep it more stabilized over the discharging process. For the multiple PCM unit additional to RT25 used in the experimental analysis other two PCMs with lower melting temperature were selected: RT20 and RT18. These two PCMs present melting temperatures of 20 °C and 18 °C. Mosaffa et al. (2013) reported that for building applications, PCMs with a phase change temperature of 18 -30 °C are preferred to meet the need for thermal comfort. The numerical analysis was undertaken by including these PCMs into the CFD model validated in Chapter 5. Following the CFD model further described in section 6.4, the air outlet temperature profile for single PCM (RT25) and multiple PCMs (RT18 + RT20 + RT25) with a height and length of 0.04 m and 1.5 m respectively were obtained and displayed in Figure 6- 9.

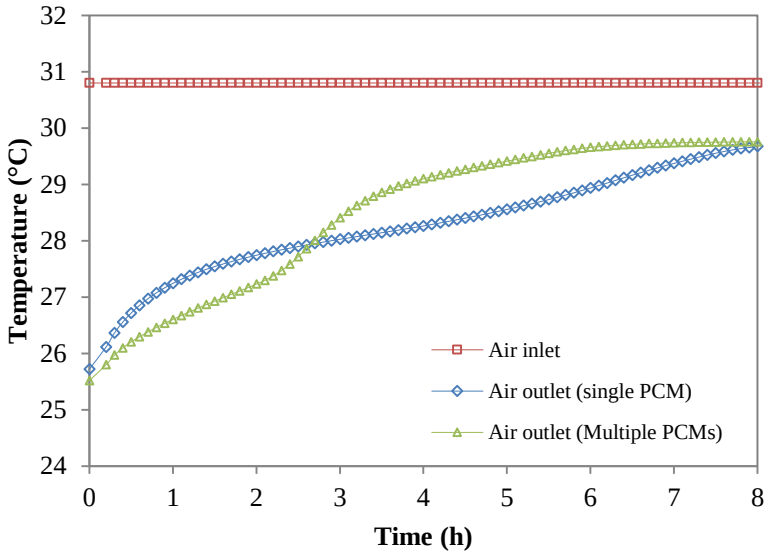

Figure 6-9 Transient air inlet and air outlet using single and multiple PCMs (T_{inlet}= 38 °C and m_{inlet}= 0.35 kg/s)

It was observed that for multiple PCMs, the air temperature remained lower and more uniform than for the single PCM in the first 3 hours. If the panel's dimensions are increased, the PCM mass is increased and therefore the phase change time is extended. Consequently the air circulating along the panels would keep exchanging heat with the PCMs and reduce its temperature. Therefore increasing the mass of multiple PCMs would allow a lower and uniform air outlet temperature for a longer period of time. Hence, multiple PCMs present themselves as beneficial for free cooling applications.

Experimental and numerical research carried out on air-multiple PCMs for free cooling applications are reported in the literature for a constant air inlet temperature based on the daily average temperature. However, this assumption does not reflect the actual daily temperature profile and may disrupt the charging and discharging time of the PCMs. For instance, for the current study, the air inlet temperature based on the average temperature from 11-18 h displayed at Figure 6-8 corresponds to 30.8 °C. Figure 6-10, 6-11 and 6-12 display the PCM temperature for the discharging process, applying a constant air temperature of 30.8 °C and the realistic temperature profile displayed in Figure 6-8 from 10h until 18h. The variable air inlet temperature was introduced in the model via a tabulated data file as described in section 6.4. The discharging temperature (T_m) is also identified for all PCMs.

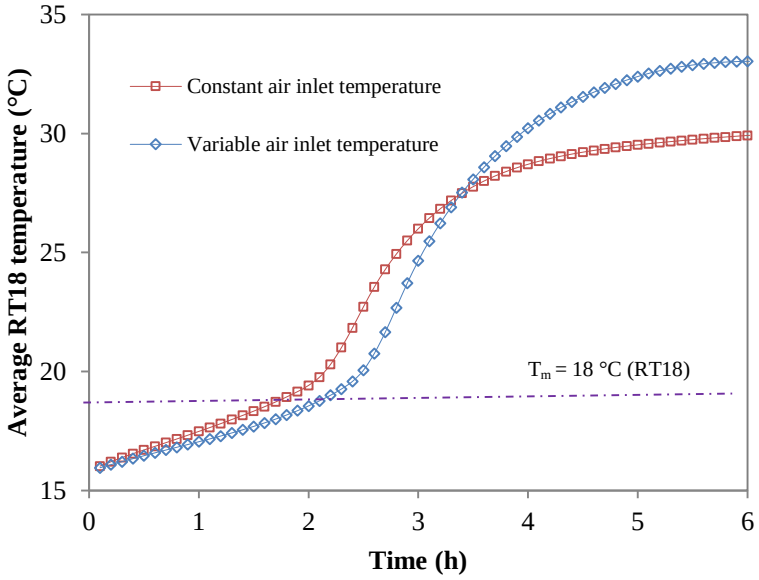

Figure 6-10 RT18 average temperature using constant air variable air inlet temperature for discharging process (m_{inlet}= 0.35 kg/s)

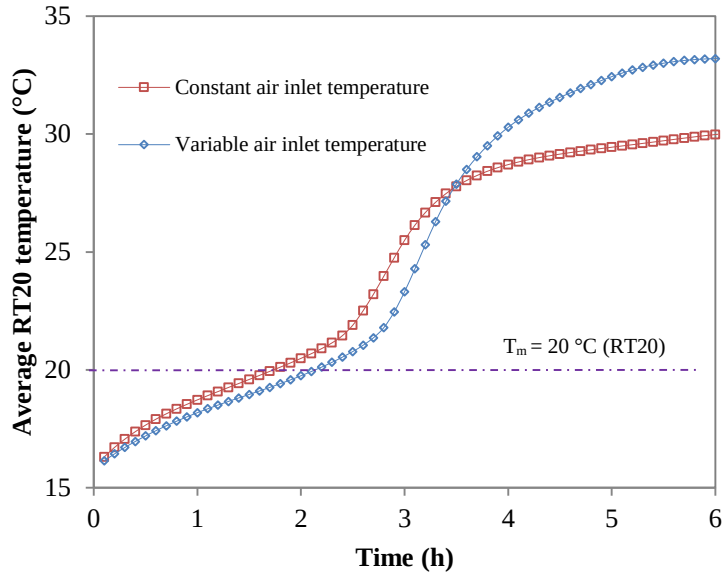

Figure 6-11 RT20 average temperature using constant air variable air inlet temperature discharging process (m_{inlet}= 0.35 kg/s)

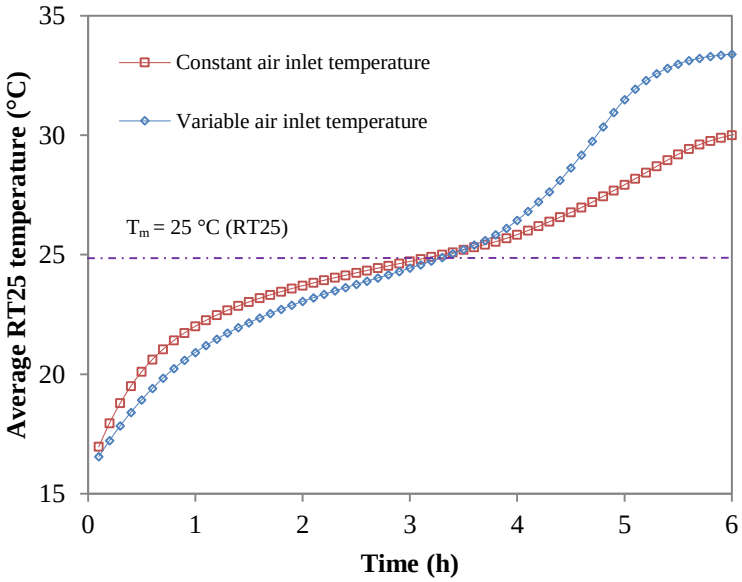

Figure 6-12 RT25 average temperature using constant air variable air inlet temperature discharging process (m_{inlet}= 0.35 kg/s)

Figures 6-10 to 6-12 display the PCMs temperature for a constant and variable air inlet temperature. Both cases present a full discharging of the three PCMs. For PCMs RT18 and RT 20 it is observed that the charging time is shorter for a constant air inlet temperature. The assumption of a constant air inlet temperature based on the daily average temperature

suggests a reduction of the melting time in 0.5 h and 0.3 h for RT 18 and RT 20 respectively. For RT25, the discharging time was similar for both scenarios. Temperature differences are observed however, namely during the first and last sensible heating stages. This also reflects the air outlet temperature difference displayed in Figure 6-9. Figures 6-13, 6-14 and 6-15 display the charging temperature of PCMs RT 18, RT20 and RT25 for a constant and variable air inlet temperature. The charging temperature (T_m) is also identified for all PCMs.

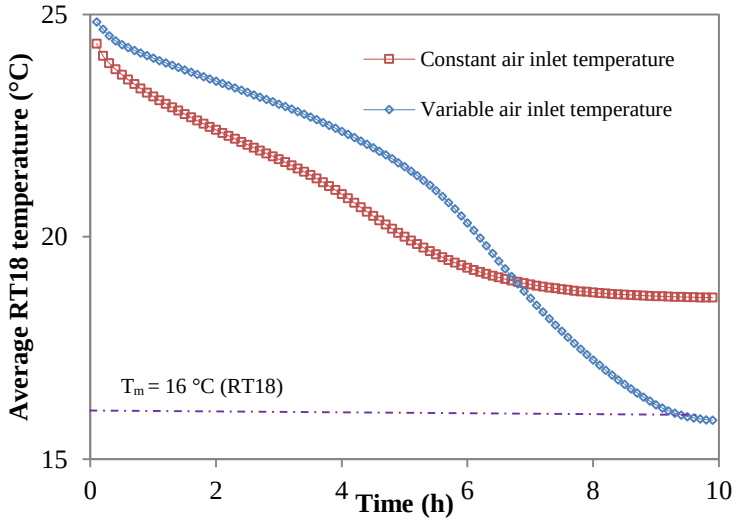

Figure 6-13 RT18 average temperature using constant air variable air inlet temperature charging process (m_{inlet}= 0.35 kg/s)

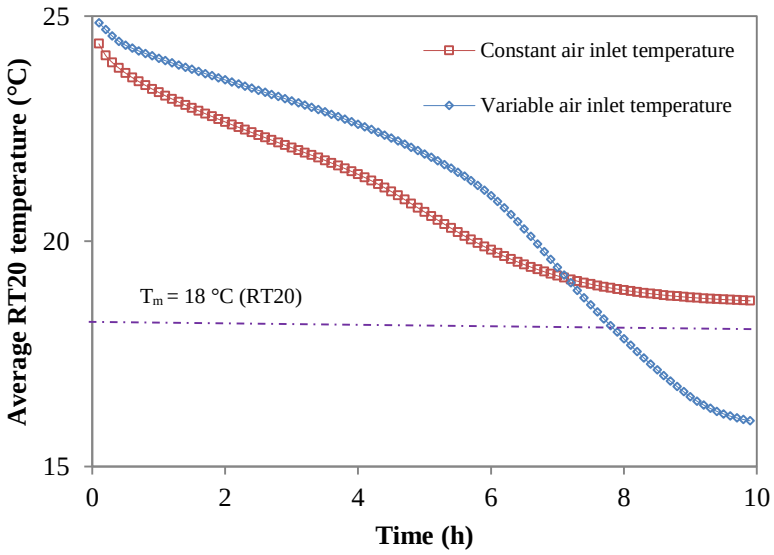

Figure 6-14 RT20 average temperature using constant air variable air inlet temperature charging process (m_{inlet}= 0.35 kg/s)

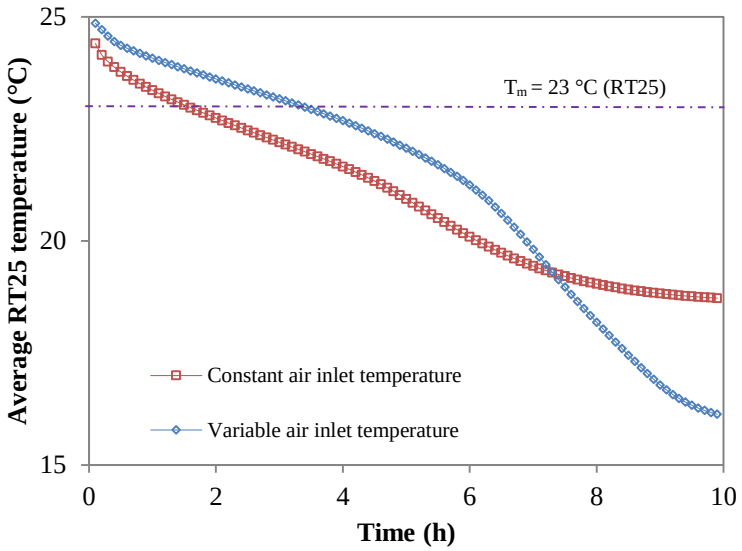

Figure 6-15 RT25 average temperature using constant air variable air inlet temperature charging process (m_{inlet}= 0.35 kg/s)

RT18, RT20 and RT25's temperature profiles for the charging process are displayed in Figure 6-13, 6-14 and 6-15. The complete charging process for both air inlet conditions is only observed for RT25 while for RT18 and RT20 the charging temperature is achieved only for the variable inlet temperature. These results suggest that adopting a constant air inlet temperature does not accordingly reflect the thermal behaviour of the PCMs for practical applications. Overall, the differences were more significant for the charging process namely the charging time strongly disrupted the performance of the PCM for free cooling applications. Hence, the current analysis is carried out for a variable air inlet temperature, reflecting the real climatic conditions.

6.4 Development of the CFD model

A transient simulation study was conducted to analyse the air outlet temperature for the air-PCM unit detailed in Table 6-1. The effective specific capacity method developed in Chapter 5 showed better agreements with the experimental results and hence is used in the analysis. The same geometry as the experimental air-PCM experimental unit is used, with variable length and height of the panels (Table 6-2).

Table 6-1 Specification of the air-PCM TES unit

Height of the PCM panels (H_{panel})	Table 6.2
Length of the PCM panels (L_{panel})	Table 6.2
Air channels height ($H_{channel}$)	0.02 m 0.04 m
Air duct thickness (wood layers)	0.01 m
PCM encapsulation thickness (steel plate)	0.003 m

A parametric study was carried out to determine the two main characteristics; (i) the best combination of multiple PCMs, (ii) the most suitable geometry and iii) the most suitable air mass flow rate. Firstly, a set of calculations are performed for an initial geometry (G.1) to analyse the effect of the PCM selection on the cooling time and attained air outlet temperature. Three PCMs denominated as PCM 1, 2 and 3 were allocated equally in the panels i.e. with the same mass fraction. The numerical layouts of PCMs 1, 2 and 3 within the PCM panel are displayed in Table 6-3. The best PCM selection with a longer cooling time and a lower air outlet temperature is adapted for different geometries where the length and height are varied (G.2- G.8). Table 6-4 summarises different numerical cases to get the best suitable option for the intended case study. The best value obtained for the height is also adopted in the study of the effect of the length.

Table 6-2 Geometries

Investigation	Geometry	Length (m)	H_{panels} (m)	$H_{airchannel}$ (m)	Description
Effect of the PCMs selection	G.1	1.5	0.02	0.02/0.04	Single panel Double panel Triple panel
Effect of the height	G.2	1.5	0.03		Double panel
	G.3		0.04		
	G.4		0.06		
	G.5		0.08		
Effect of the length	G.6	1.2	0.04		
	G.7	1.8			
	G.8	2.1			

Table 6-3 Numerical layouts

Description	Layout
Single panel	PCM 1
Double panel	PCM 2 or PCM 3 | PCM 1 or PCM 2
Triple panel	PCM 3 | PCM 2 | PCM 1

Table 6-4 Numerical cases

Geometry (Table 6.2)	PCMs			Nomenclature
G.1	RT25	-	-	PCM 1
	RT25	RT20	-	PCM 1+2
	RT25	RT18	-	PCM 1+3
	RT20	RT18	-	PCM 2+3
	RT25	RT20	RT18	PCM 1+2+3
G.2 G.3 G.4 G.5 G.6 G.7 G.8	RT25	RT20	-	PCM 1+2

6.4.1 Model assumptions and governing equations

The current model followed the assumptions presented in Chapter 5 that showed consistency with experimental data. The governing equations Eq. 5-9 to 5-11 are solved in FLUENT and air outlet temperature is determined.

6.4.2. Materials properties and turbulence model

The thermophysical properties of used PCMs (RT18, RT20 and RT25), steel as encapsulation material and air as HTF are given in Table 6-5. The thermophysical properties of the RT25, RT 20 and RT 18 presented in Table 6-5 were obtained from manufacturer data sheet (Rubitherm, 2014) and DSC analysis presented in Chapter 4.

Table 6-5 Thermophysical properties of selected materials

Material	Melting Temperature (°C)	Density (kg/m3)		Thermal Conductivity (W/m. °C)	Specific heat (J/kg. °C)
		Solid	Liquid		
RT 25 (PCM 1)	23-25	880	760	0.2	Figure 4-16 and 4-18
RT 20 (PCM 2)	18-20				
RT 18 (PCM 3)	16-18				
Steel	-	8030		16.27	502.48
Air	-	1.225		0.0242	1006.43

The air turbulence was specified by means of the k-ε model as it validated with the experimental results in Chapter 5.

6.4.3 Boundary and initial conditions

The current model used the same boundary conditions as the CFD model presented in Chapter 5, namely the air inlet, the air outlet, air duct walls, PCM panel walls, air and PCM domains which are listed in Table 5-3. The air inlet temperature was linked to the daily profile temperatures shown in Figure 6-8 and also through a tabulated data file. From the experimental results, it was observed that during the discharging process a lower velocity (0.6 m/s) reduces the air outlet temperature and extends the discharging time. These two parameters are crucial for free cooling application. Hence a velocity of 0.6 m/s equivalent to an air mass flow rate of 0.15 kg/s is adopted for the primary analysis. Furthermore this figure varies for the investigation of the mass flow rate on the charging and discharging time of the PCM panels under the daytime and night-time temperature profile (Figure 6-8). All PCMs in

the set are assumed to be at the initial temperatures of 16 ℃ and 25 ℃ for the charging and discharging processes respectively.

Table 6-6 Boundary conditions of the numerical simulation

Process		Boundary condition	
		Thermal	Flow
Discharging process	Air inlet	-	$P_{outlet} = 0$
	Air outlet	Transient table (Figure 6-8: 11h-18h)	Uniform mass flow inlet: 0.15 kg/s; 0.2 kg/s; 0.25 kg/s; 0.3 kg/s; 0.35 kg/s Direction: Normal to boundary
	Air duct and PCM panel walls	Equation 5-4	Stationary wall, no slip shear condition
Charging process	Air inlet	-	$P_{outlet} = 0$
	Air outlet	Transient table (Figure 6-8: 21h-7h)	Uniform mass flow inlet: 1.2 kg/s; 2 kg/s; 3 kg/s; 4 kg/s Direction: Outwards normal
	Air duct and PCM panel walls	Equation 5-4	Stationary wall, no slip shear condition

6.4.4 Mesh size independence study

The computational domain is represented by a 2-dimensional mesh. The mesh independence is studied using a coarse mesh (5503 elements), a medium mesh (22012 elements) and fine mesh (88048 elements respectively). The computational domains were divided into three

zones as presented in Figure 5-3 (Chapter 5): inlet, air-PCM heat transfer unit and outlet respectively. For all meshes, the hexagonal elements were used with a refined mesh in the near-wall zones where more complex fluid structures and heat transfer processes were foreseen to occur. The mesh refinement is performed by varying all mesh sizes at the same ratio through the adapt region tool available on FLUENT 15.0. The analysis was carried out for a steady state and the convergence criterion of $1x10^{-4}$ was used for the mass and momentum, $1x10^{-8}$ for the energy residuals and SIMPLE as the solver method. The mesh independence test was carried out to determine the optimal number of elements to use for the CFD simulations and it has been concluded that the medium mesh is sufficient to satisfy the spectral convergence. Medium mesh is used to perform the simulations to obtain the PCM and the air outlet temperatures presented in the next sections for various flow conditions.

6.5 Parametric study

A parametric study is carried out through investigating the effect of multiple PCM selection, followed by the height (H) and length (L) of the PCM panels on the air outlet temperature, cooling time (i.e. discharging time) and charging time. The best dimensions were further investigated in terms of mass flow rate. The most suitable case has been selected for the following requirements: air outlet temperature below 30 °C ($T_{outlet} \leq 30$ °C), cooling time (i.e discharging time) over 7 h ($t_{cooling} \geq 7$ h) and the charging of PCMs completed in 10 hours ($t_{charging} \leq 10$ h). The cooling time was defined as the period of the time when the air outlet temperature was lower that the air inlet temperature. In other words, it is the period of time that a temperature difference between inlet and outlet is observed.

For the discharging process, the most suitable arrangement of multiple PCM is expected by placing the PCMs in a decreasing order of their melting temperatures and vice versa for the charging process. The same approach was adapted in Chiu and Martin (2013), Wang et al. (2015) and Peiró et al. (2015). Ehen the air temperature gets closer to the PCM phase change temperature of the first PCM, this order will allow the other two PCMs to increase the temperature difference. The flow direction for discharging process was denominated as inflow and as reverse flow for the charging process.

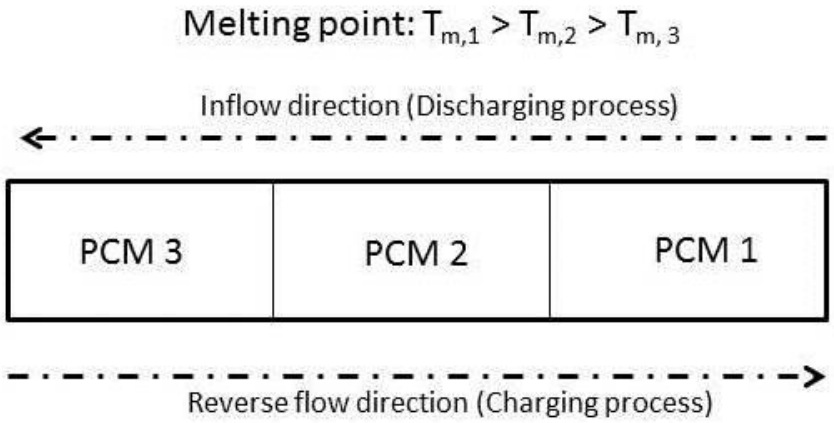

Figure 6-16 Suitable multiple PCM configuration for PCM 1, PCM 2 and PCM 3 considering their melting temperature (T_m)

Following the Figure 6-16 for the charging process with a constant air inlet temperature, the reverse flow should be adopted in order to solidify first the PCM with a lower melting point (PCM 3). This again will allow the air temperature to keep exchanging heat with the other two PCMs along the flow direction. In the current study, real air temperature data is used and it is observed from Figure 6-8 that the external temperature gradually reduces during the night with the lowest temperature observed in the early morning (4-6h). For this air temperature profile, it may be advantageous to adapt the inflow direction for the charging process, as the air temperature during the first hours is not low enough to solidify the PCM 3 (RT18). Hence, both flow directions are investigated for the charging process. This aspect is not investigated for the discharging process, as the air temperature during the day remains higher than the melting temperature of any of the selected PCMs. Figure 6-17 displays the temperature of PCM 3 (RT18) for the inflow and reversed air flow direction during the charging process.

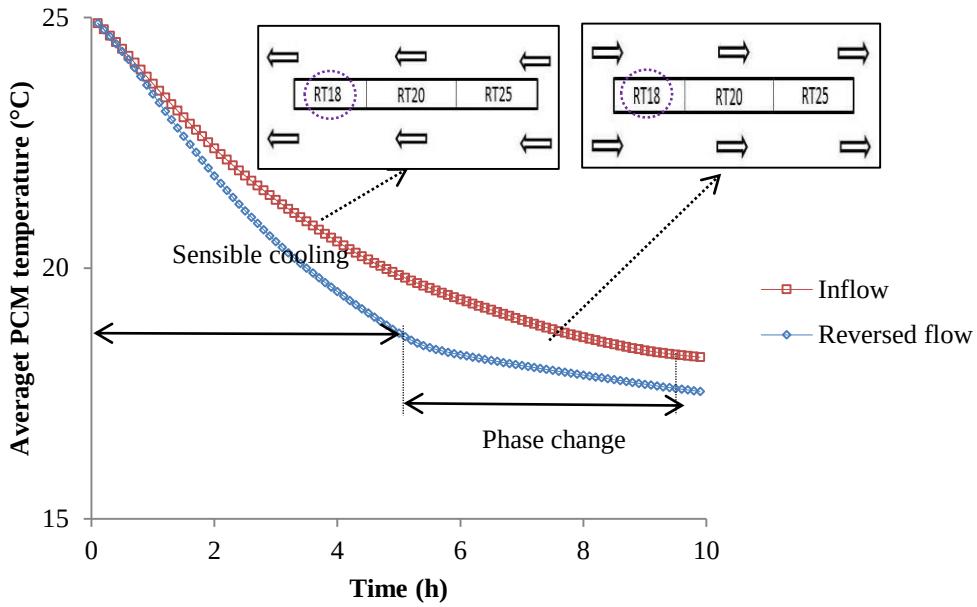

Figure 6-17 Average temperature profile of RT18 for inflow and reversed flow during the charging process (m= 1.2 kg/s and air inlet temperature Figure 6-8: 21h-7h)

Figure 6-17 shows that the section filled with RT18 achieved lower average temperatures for the reversed flow. RT18 starts the phase change at 18 °C until 16 °C (Table 6.5). For the reversed flow, the panel had experienced both sensible cooling (0-5h) and part of the phase change from 6 h onwards. Contrary to the normal flow, the panel had experienced only the sensible heating (T > 18 °C) during 10 h. This was due to the temperature difference between the air inlet temperature and the PCM section. For the reversed flow, the cold air inlet was firstly in contact with the RT 18, and a higher temperature difference allowed a faster cool down of the panel. For the normal flow direction the cold air inlet temperature firstly exchanged heat with RT25 then with RT 20 consequently increasing its temperature before it finally made contact with RT18. Therefore, the reversed flow direction was adopted in the current analysis for the charging analysis in the current study.

6.5.1 Effect of the PCM selection

The effect of the PCMs selection within the panels on both the air outlet temperature and cooling time was displayed in Figure 6-18. The PCM panels measured 0.02 m and 1.5 m in height and length respectively. As discussed in section 6.3.3, for free cooling applications, the air outlet temperature and cooling time play a significant role. An air outlet temperature

lower than 30 °C and a c≥oling time (i.e. discharging time) over 7 hours were desirable for an effective free cooling unit. For the first simulations, a velocity of 0.6 m/s is considered in the analysis, corresponding to a mass flow rate of 0.15 kg/s. The graphs for the discharging process are represented over 8 h to guarantee the required cooling time (t ≥7 h).

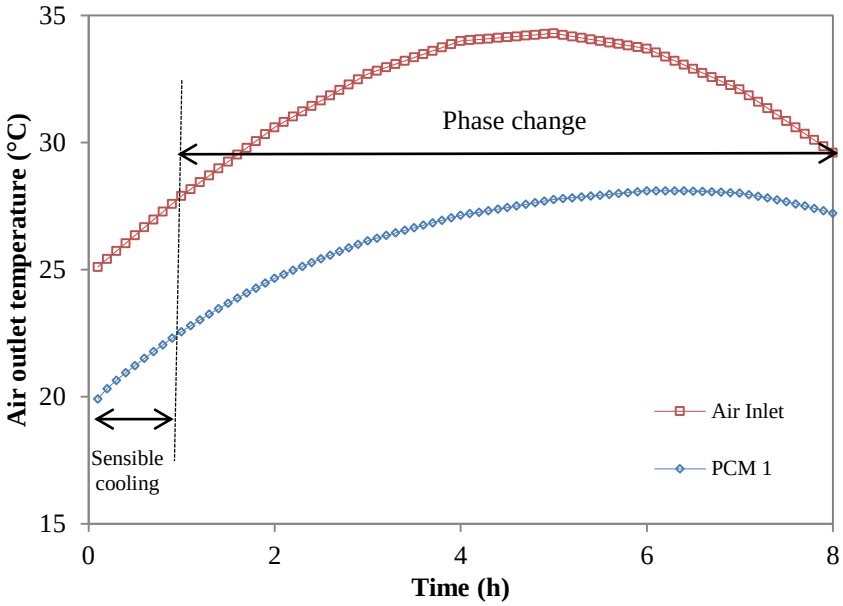

Figure 6-18a Effect of PCM selection on the air outlet temperature for discharging process (H= 0.02 m, L= 1.5 m, m = 0.15 kg/s and air inlet temperature Figure 6-8: 11h-18h)

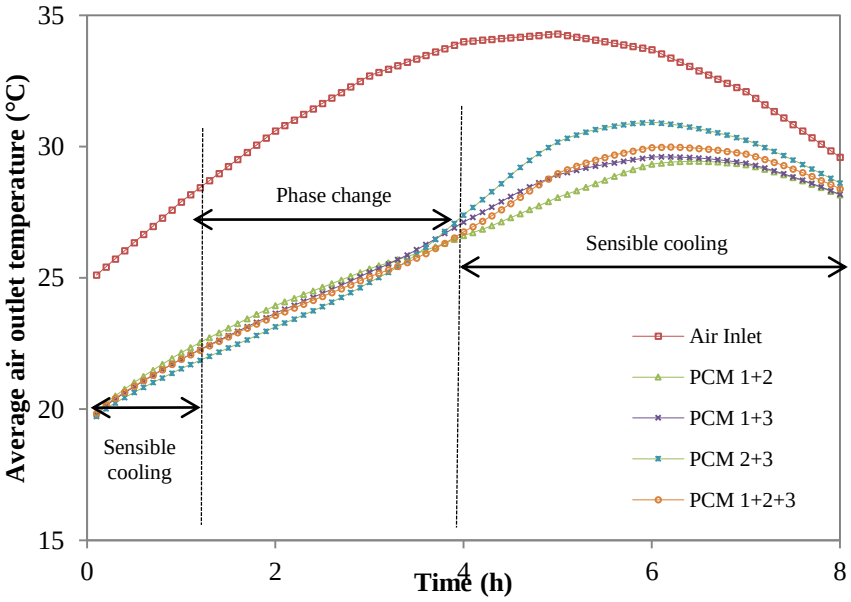

Figure 6-18b Effect of PCM selection on the air outlet temperature for the discharging process (H= 0.02 m, L= 1.5 m, m = 0.15 kg/s and air inlet temperature Figure 6-8: 11h -18h)

The discharging process included three stages. The first was characterised by sensible cooling exchanged between the air and the PCM, during which, the rate of energy added from the PCM to the air increased rapidly. This was followed by a stage during which the rate decreased slowly due to the phase change of the PCM panels. At the end of the phase change, sensible cooling followed and the air temperature increased rapidly. For the chosen dimensions and mass flow rate, the PCM 1+2, PCM 1+3, PCM 2+3 and PCM 1+2+3 presented the three stages of sensible cooling, phase change and sensible cooling. The first hour represented by sensible cooling is followed by the phase change until the 4^{th} hour and sensible cooling again takes place further on (Figure 6-18b). It has been observed that during the first two stages the air temperature remained below the 26 °C with a rapid increase for the last stage. On the contrary, in the case of PCM 1, only the first two stages were observed, allowing the air temperature to remain nearly constant over 7 hours (Figure 6-18a). In other words, for this case, the PCMs remained in the phase change stage and the air was kept at an almost constant temperature during the 7 h. However, multiple PCM cases showed lower air outlet temperatures during the first 4 hours, represented by the first two stages (i.e. until the end of the phase change) and this was due to the integration of PCMs with lower melting temperature. Therefore PCM 2+3 (including the two PCMs with a lower melting temperatures-RT20 and RT 18) presented the lowest air outlet temperature, this was followed by the case PCM 1+2+3 (RT25+RT20+RT18), case PCM 1+3 (RT25+RT18), and PCM 1+2 (RT25+RT20). Looking closely, the air outlet temperature over the required cooling time (i.e. 8 hours) and for the desirable conditions for free cooling ($T_{outlet} \leq 30°C$) have been achieved for PCM 1, PCM 1+2, PCM 1+3 and PCM 1+2+3. The design criterion for an effective free cooling system (Figure 6-3) also includes the full charging of the PCMs panel. The panels have to be completely charged during night-time to utilise their full cooling potential while during the day time discharging. Therefore, in addition to fulfilling criteria during the daytime, all cases needed to reach the full charging of the PCM panels during the night. For the multiple PCM cases, the charging temperature of each PCM was calculated separately, due to their varying melting temperatures (T_m). The average temperatures of each PCM were plotted for air inlet temperature (Figure 6-8: 21h-7h) and air mass flow rate of 1.2 kg/s and displayed in Figure 6-19 to 6-23. The melting temperatures (T_m) for each PCM taken from Table 6-5 are identified in the graphs.

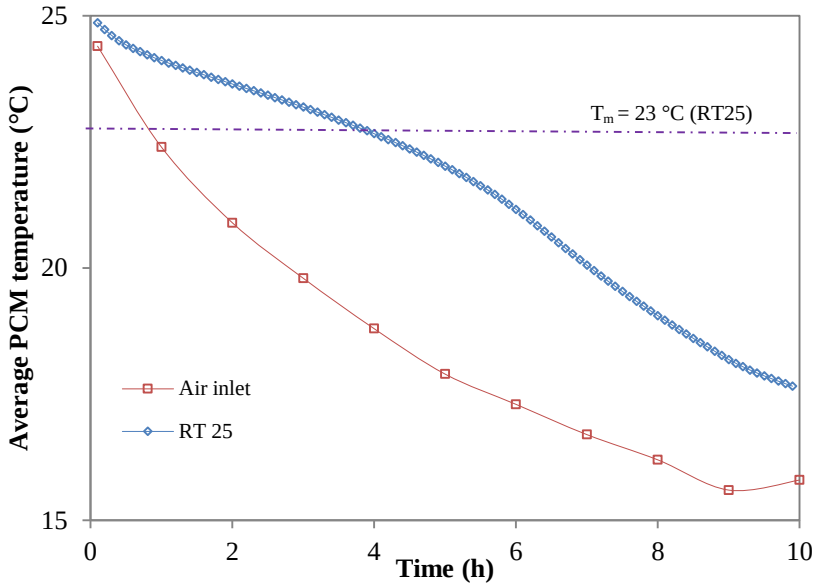

Figure 6-19 Average PCM temperature during the charging process for PCM 1 (H= 0.02 m, L= 1.5 m, m= 1.2 kg/s and air inlet temperature Figure 6-8: 21h-7h).

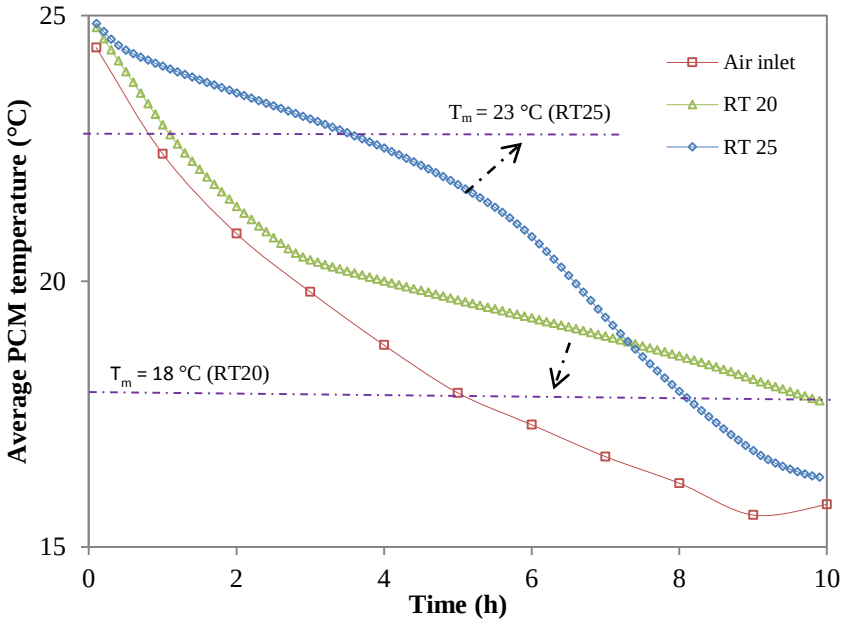

Figure 6-20 Average PCM temperature during the charging process for PCM 1+2 (H= 0.02 m, L= 1.5 m, m= 1.2 kg/s and air inlet temperature Figure 6-8: 21h-7h).

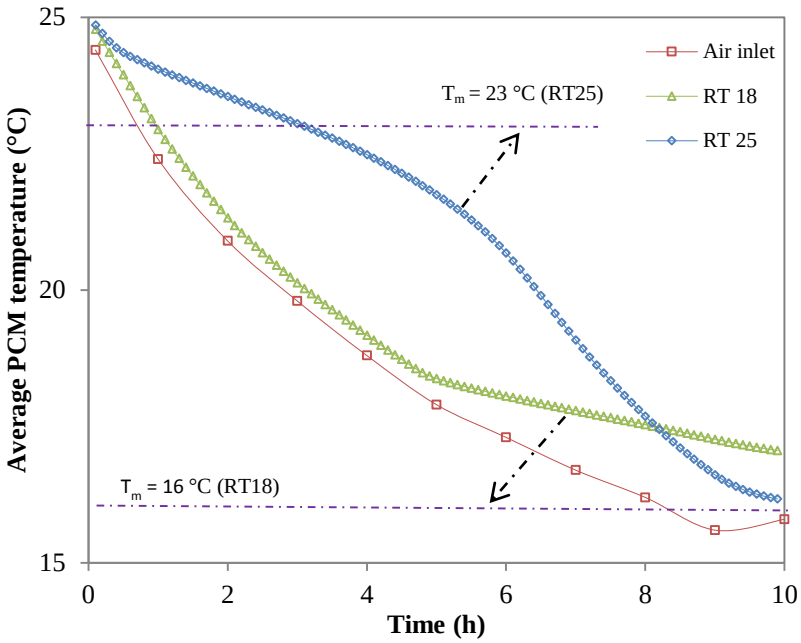

Figure 6-21 Average PCM temperature during the charging process for PCM 1+3 (H= 0.02 m, L= 1.5 m, m= 1.2 kg/s and air inlet temperature Figure 6-8: 21h-7h).

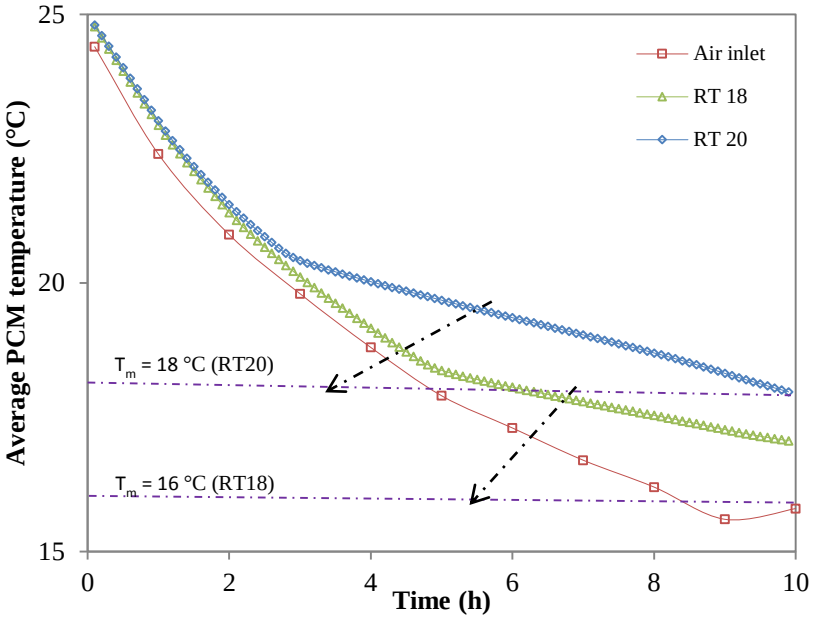

Figure 6-22 Average PCM temperature during the charging process for PCM 2+3 (H= 0.02 m, L= 1.5 m, m= 1.2 kg/s and air inlet temperature Figure 6-8: 21h-7h).

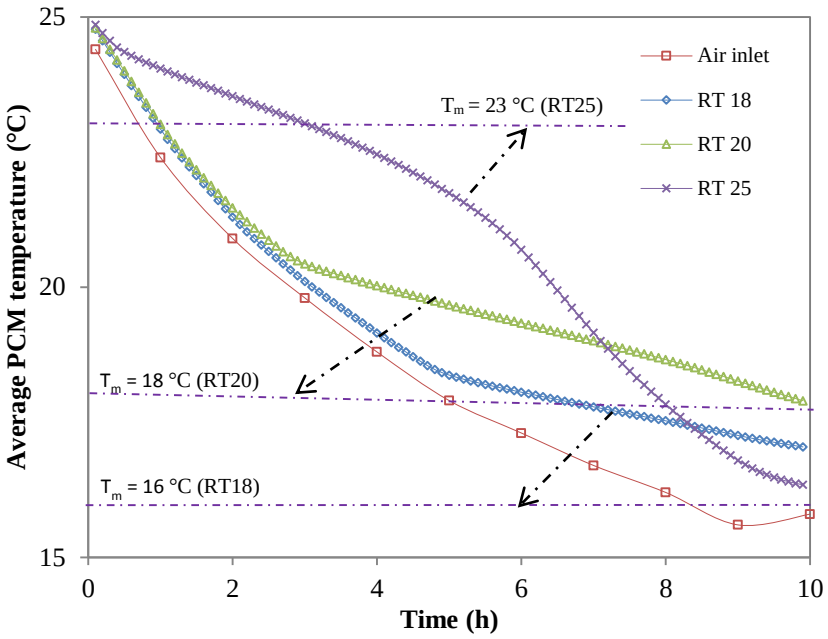

Figure 6-23 Average PCM temperature during the charging process for PCM 1+2+3 (H= 0.02 m, L= 1.5 m, m= 1.2 kg/s and air inlet temperature Figure 6-8: 21h-7h).

Table 6-5 presents the solidification temperature for RT 25, RT 20 and RT 18 at 23 °C, 18 °C and 16 °C respectively. In order to consider the panel completely solidified (i.e. fully charged) all PCMs had to reach these temperature values respectively. For instance RT 25 reached a temperature of 23 °C after 10 h for all cases (Figure 6-19, Figure 6-21, Figure 6-22 and Figure 6-23). RT 20 also reached 18 °C for all cases after the 10 h (Figure 6-20, Figure 6-22 and Figure 6-23). Contrary, RT 18 was not completely charged for all cases (Figure 6-21, Figure 6-22 and Figure 6-23). This was due to the night-time temperature, the air mass flow rate and the mass of the PCM panels. During the night-time, a inlet temperature below 16°C was observed only at 5h and 6h. As stated in Zalba et al. (2004, 2011) and Waqas and Kumar (2011) the charging process is strongly influenced by the air inlet temperature and flow rate. Hence, for the successful incorporation of this PCM, the full charging is achieved either by a lower air inlet temperature for a longer period of time, or with a higher air mass flow rate. Further investigation is carried out for RT18 of the PCM 1+ 2+ 3 case for lower air inlet temperatures (Figure 6-24b) and higher air mass flow rate (m) (Figure 6-25). The lower air temperatures considered in the analysis were obtained by evenly reducing the air temperatures displayed in Figure 6-8 from 22h to 6 h by 0.2 °C, 0.5 °C, 1 °C, 1.5°C and 2 °C.

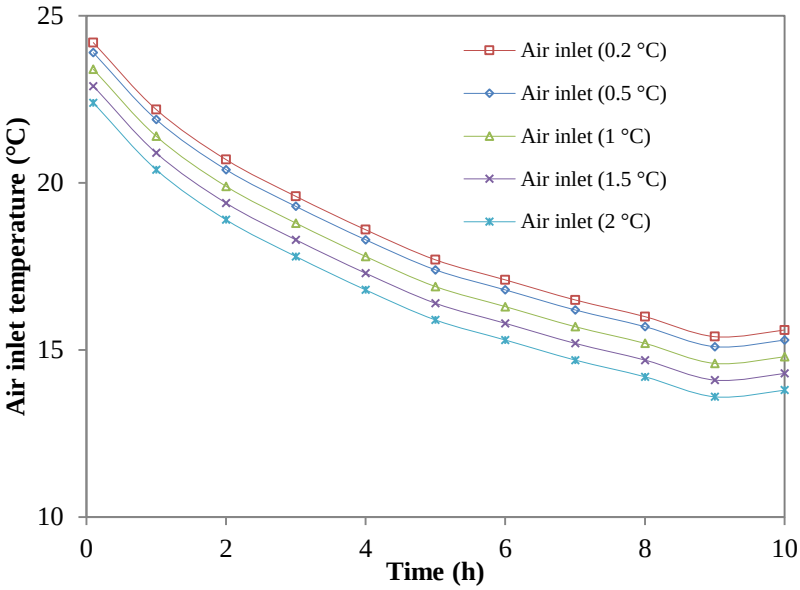

Figure 6-24a Air inlet temperature Figure 6-8: 22h – 6h evenly decreased by 0.2 °C, 0.5 °C, 1 °C, 1.5°C and 2 °C

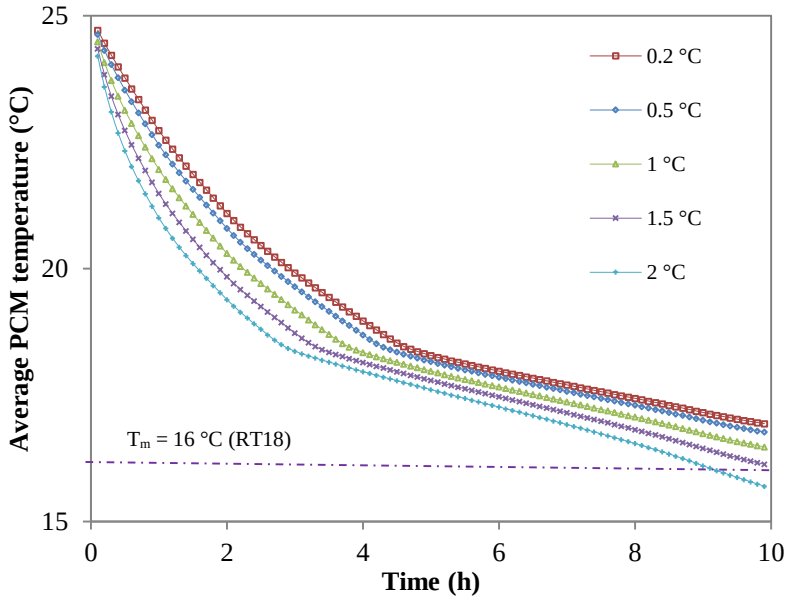

Figure 6-24b RT18 average temperature for PCM 1+2+3 (H= 0.02 m, L= 1.5 m, m= 1.2 kg/s and air inlet temperature Figure 6-8: 21h-7h evenly decreased by 0.2 °C, 0.5 °C, 1 °C, 1.5°C and 2 °C)

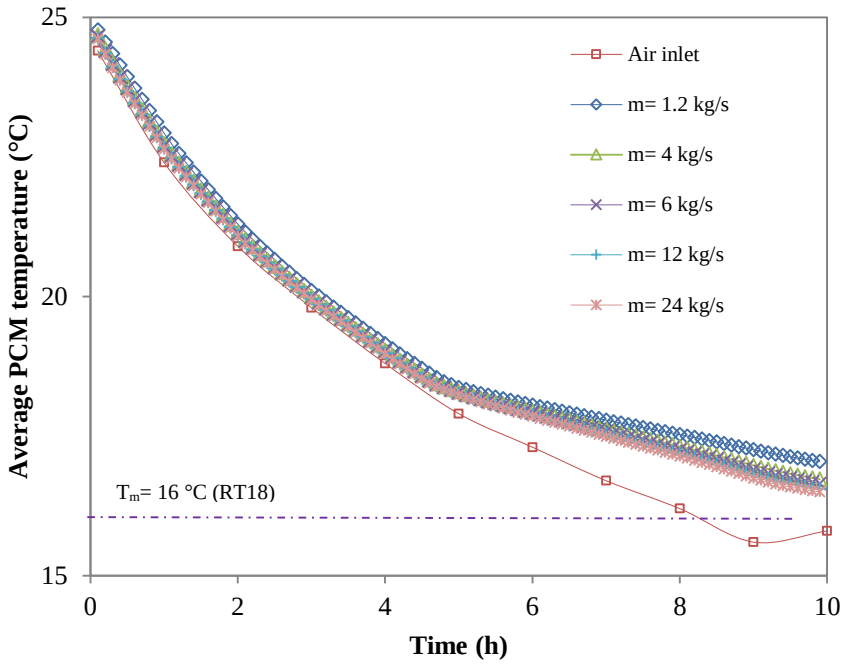

Figure 6-25 RT 18 average temperature for PCM 1 +2 +3 case (H= 0.02 m, L= 1.5 m, m= 1.2 kg/s, 4 kg/s, 6 kg/s, 12 kg/s and 24 kg/s and air inlet temperature Figure 6-8: 21h-7h)

Figure 6-25 shows that to further increase the air mass flow rate from 1.2 to 24 kg/s did not allow the material to reach its solidification temperature (16 °C). From these results, for the available night-time temperature, the further increasing of the air mass flow rate will also be insufficient to solidify the RT 18 of the other cases, as they include a higher mass fraction when compared to case PCM 1+2+3. However, reducing the air inlet temperature by 1.5 °C and 2 °C did decrease its solidification temperature to 16 °C and successfully solidified the PCM over the 10 h (Figure 6-24b). Therefore, RT 18 may be applied for applications where lower air inlet temperatures are available but not for the current study.

The mass of each PCM occupying the panel can be expressed as the mass fraction. Figure 6-19 to 6-23 also gives a perspective in terms of the effect of the mass fraction on the PCM temperature during the charging process for a constant height. The mass fraction of PCM within each panel can be quantified between 0 and 1, either none or completely filling the panel respectively. For instance the mass fraction of RT 25 within the panel varied from 1 (Figure 6-19), 0.5 (Figure 6-20 and 6-21) and 0.33 (Figure 6-23). It was observed that decreasing the mass fraction in terms of length did not significantly affect the temperature along the 10h. Similar results are also observed for RT 20 and RT 18 showing that the reduction of the mass fraction from 0.5 to 0.33 did not further decrease the temperature.

Hence, the cases including RT 18: PCM 1+3, PCM 2+3 and PCM 1+2+3 did not meet the free cooling requirements and were excluded from further investigation. PCM 1 and PCM 1+ 2 meet the free cooling requirements: air outlet temperature ($T_{outlet} \leq 30$ °C), cooling time ($\geq$ 7h) and complete charging of the panels during night-time ($\leq$ 10h). Furthermore, from Figure 6-18b the latest case has shown a lower average air inlet temperature for the first 4 hours and a higher air outlet temperature afterwards, due to the sensible heating when compared to case PCM 1. From these results, it was observed that the cases including PCMs with lower melting points allowed a decrease in the air outlet temperature. However, for the selected PCM dimensions (H= 0.02 m and L = 1.5 m) the air outlet temperature did not remain uniformly over the 8h due to the last stage (sensible cooling). Hence, increasing the mass of PCMs for case 1+2 will exclude the sensible cooling stage (i.e. extending the phase change stage) and therefore allow a lower and uniform air outlet temperature profile over the 8 hours. The increase of mass is achieved either by increasing the height or the length of the PCM panels. Therefore case PCM 1+2 is further investigated for different heights (H), length (L) and air mass flow rate for the charging and discharging processes during the available night-time and daytime temperatures.

6.5.2 Effect of the PCM panels height

The effect of the PCM panels height (0.02, 0.04 m, 0.06 m and 0.08m) on the air outlet temperature and cooling time has been investigated (Figure 6-26). A constant air mass flow rate of 0.15 kg/s was assumed for the discharging process. Halawa and Saman (2011) reported that the thicker the slabs the longer the melting time. Mosaffa et al. (2013) also concluded that for multiple PCMs, the larger thickness results in lower air outlet temperatures, as it will accommodate a larger quantity of PCMs to release the cold.

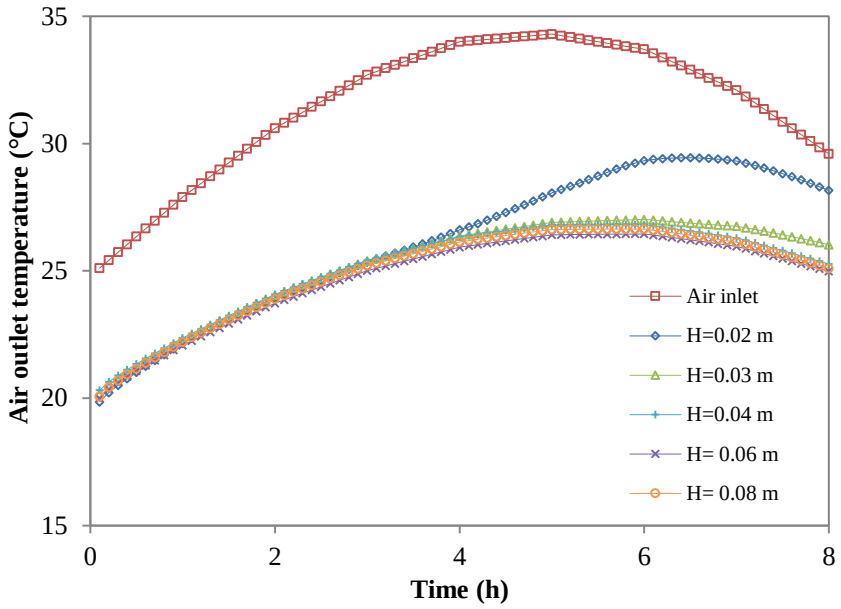

Figure 6-26 Effect of the height on the air outlet temperature for the discharging process (L= 1.8 m, m = 0.15 kg/s and air inlet temperature Figure 6-8: 11h-18h)

Figure 6-26 showed the air outlet temperature over 8 hours for different panel heights. It was observed that increasing the height of the panels from 0.02 m to 0.03 m presented the most significant variation. As previously discussed for 0.02 m the PCM did undergo the three stages and therefore after the phase change, due to the sensible heating, the temperature increased sharply after t= 4h. For a height of 0.03 m, the second sensible heating started almost at the end, slightly increasing the temperature in the last hour. The panels did remain at the phase change during the 8 hours for 0.04 m, 0.06 m and 0.08 m presenting similar results. As the mass of the PCM was increased the material did remain in the phase change stage until the end, translating a nearly constant air outlet temperature. Similar to Halawa and Saman (2011) and Mosaffa et al. (2013) it was observed that thicker slabs allowed longer cooling time and lower air outlet temperatures. Thinner panels contain less mass and were charged more quickly, resulting in a faster increase in the air outlet temperature near the end of the discharging period. Furthermore it was observed that for a constant mass flow rate, further increasing the panel heights to 0.06 m or 0.08 did not significantly reduce the air outlet temperature. The case under investigation included horizontal panels and the lower and the upper surfaces were exposed to the forced convection from the air coming from the right hand, as demonstrated in scenario 3 in Figure 3-9 (Chapter 3). The melting front was moving from the right to the left with the upstream nodes being the ones to exchange heat with the air at the maximum rate. Consequently the PCM inner nodes exchange heat between themselves

through conduction and at a lower rate due to the low thermal conductivity of these materials (0.2 W/m°. C). Moreover increasing the height did not increase the upstream nodes in contact with the air but rather increased the inner nodes and therefore it did not further affect the air outlet temperature. Again, the effect of the height also requires an investigation in terms of charging time. Figure 6-27 and Figure 6-28 display the average temperature of RT 20 and RT 25 respectively for height of 0.03 m, 0.04 m, 0.06 m and 0.08 m.

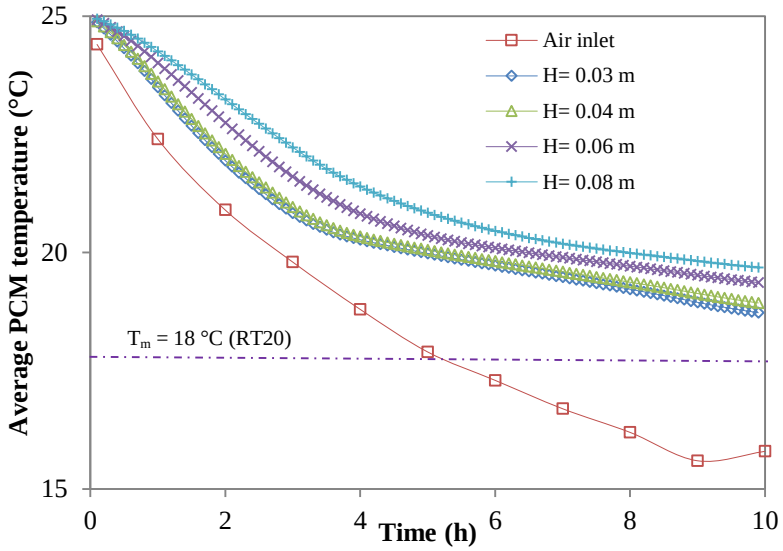

Figure 6-27 Effect of the height on the average temperature of RT 20 for PCM 1+ 2 during the charging process (L= 1.5 m, m = 1.2 kg/s and air inlet temperature Figure 6-8: 21h-7h)

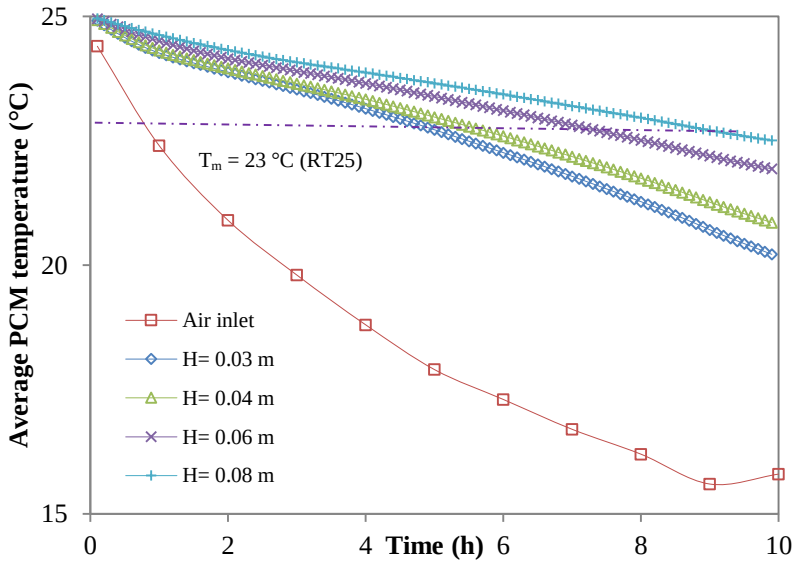

Figure 6-28 Effect of the height on the average temperature of RT 25 for PC 1+2 during the charging process (L= 1.5 m, m = 1.2 kg/s and air inlet temperature Figure 6-8: 21h-7h)

Figures 6-27 and 6-28 showed that for the mass flow rate of 1.2 kg/s, the height of 0.03 m and 0.04 m show the lowest temperatures for both PCMs. For all cases RT 20 did not reach the melting point of 18 ° C. That can be achieved however by increasing the air mass flow rate and is further discussed in 6.5.4. Balancing the air outlet temperature and the cooling time during the discharging process and the charging time, the best height was considered to be 0.04 m and further investigated in terms of length. Choosing 0.04 m rather than 0.06 m and 0.08 was also expected to benefit the charging process, requiring a lower mass flow rate to solidify the panels.

6.5.3 Effect of the length of PCM panels

The effect of the length on the air outlet temperature and cooling time was investigated for length of 1.2 m, 1.5 m, 1.8 m and 2.1 m and displayed in Figure 6-29. Again, Mosaffa et al. (2013) concluded that multiple PCM panels with larger slab lengths resulted in lower air outlet temperatures as it accommodated larger quantity of PCMs to release the cold.

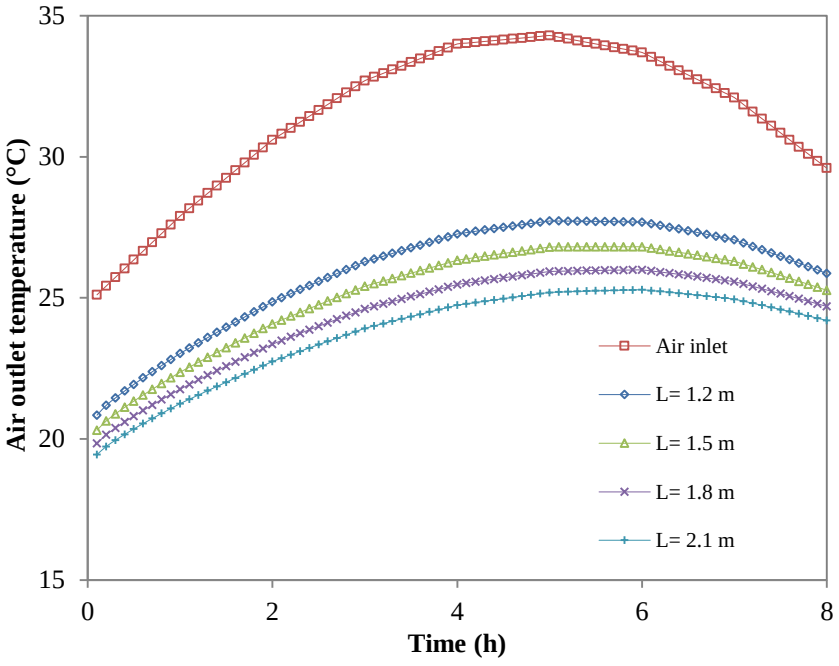

Figure 6-29 Effect of the length on the air outlet temperature for the discharging process (H= 0.04 m, m = 0.15 kg/s and air inlet temperature Figure 6-8: 11h-18h)

Figure 6-29 shows that for a smaller length, the air outlet temperature was increased. Again, this was directly related with the amount of PCM mass. Increasing the PCM mass increased the discharging time of the PCM panels and hence extended the phase change and consequently the period of the heat transfer and the temperature at an almost constant value. The increase of the selected lengths (1.2 m, 1.5 m, 1.8 m and 2.1 m) did further reduce the air outlet temperature, but not in a linear trend. In fact as the length was increased in 0.3 m increments, the temperature difference between each increment was reduced as displayed in Figure 6-30. For the first increment (1.2 m to 1.5 m) the temperature was reduced to 0.8 °C followed by 0.73 °C and 0.62 °C for the second and third increment respectively. Eventually, for a certain length the temperature difference becomes nearly zero. For the current application however further extending the length was not viable on a practical point of view.

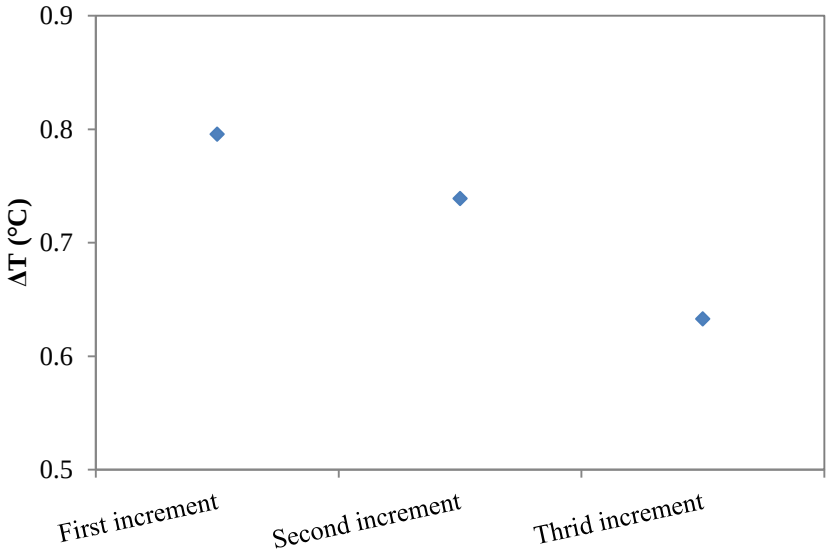

Figure 6-30 Air temperature difference for each length increment of 0.3 m.

The charging process for the selected lengths was investigated and displayed in Figure 6-31 and 6-32.

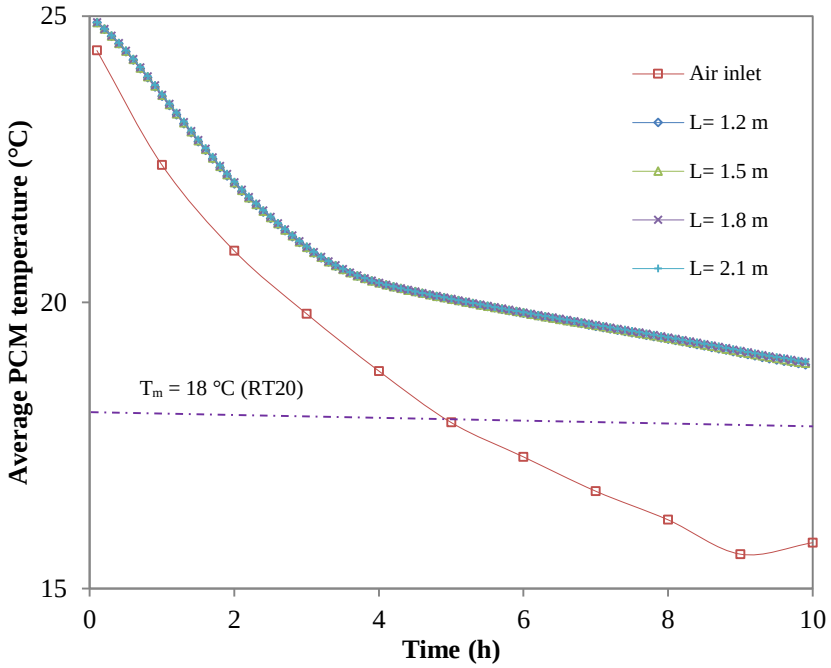

Figure 6-31 Effect of the length on the average temperature of RT 20 for PCM 1+ 2 during the charging process (H= 0.04 m, m = 1.2 kg/s and air inlet temperature Figure 6-8: 21h-7h)

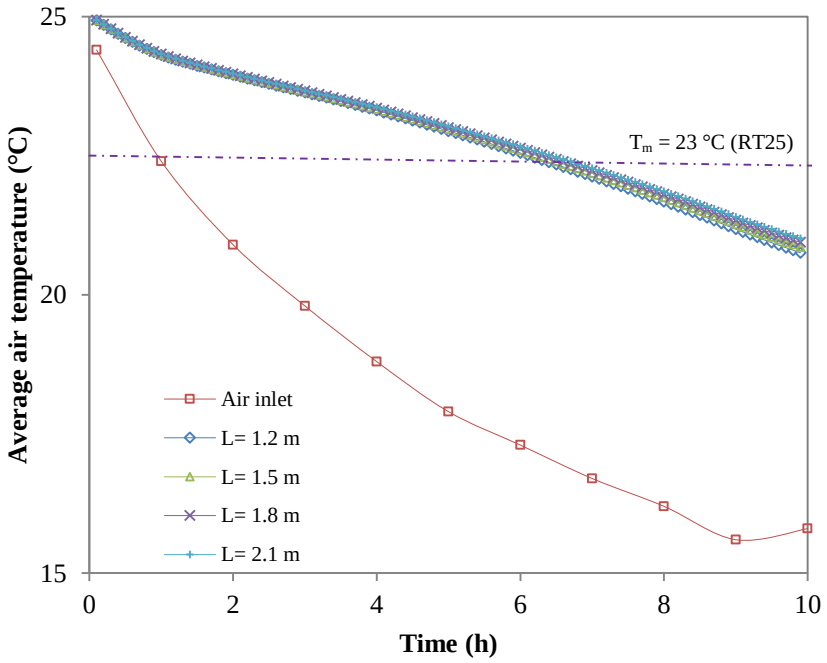

Figure 6-32 Effect of the length on the average temperature of RT 25 for PCM 1+ 2 during the charging process (H= 0.04 m, m = 1.2 kg/s and air inlet temperature Figure 6-8: 21h-7h)

During the charging process it was observed that the average temperature of RT 20 reached 19 °C after 10 h for all the lengths. Further increasing the mass flow rate is expected to lower the PCM temperature to its melting temperature (18 °C) and is presented in 6.5.4 The average temperature of RT 25 varied slightly (20.4 – 21 °C) for 1.2 m to 2.1 m respectively. Overall, it was observed that the length did not affect the charging temperatures of the PCMs. However, the cooling time and air outlet temperature were influenced for the selected lengths. Even though the air outlet temperature reached lower values for higher lengths, the chosen length has to fit into a practical scale for the current application. For instance, panels longer than 1.8 m will make the installation and maintenance complicated. Hence, for the current study the best PCM panel dimensions is considered as 0.04 m and 1.8 m height and length respectively.

6.5.4 Effect of the air mass flow rate

Theoretically and experimentally as observed in Chapter 3, lower air mass flow rates allow lower air outlet temperatures due to the longer time of contact between the hot air and the cold PCMs panels. However in practice, the cooling of buildings namely commercial buildings, require high flow rates linked to the requirements of fresh air supply. For instance, for an office building in Portugal, RSECE (2006) requires a fresh air supply of 35 m^3/h per occupant. Therefore the most suitable geometry of the panels (H= 0.04 m and L= 1.8 m) should be further investigated for higher air mass flow rates but guaranteeing the required air outlet temperature, $T_{outlet} \leq 30$ °C. In other words the air mass flow rate has been further increased until the air outlet reaches a maximum temperature of 30 °C.

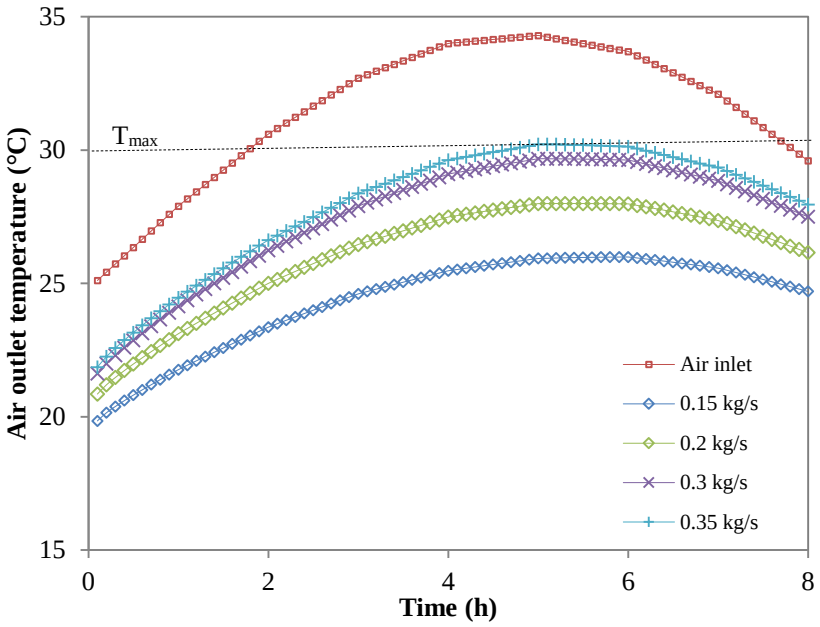

Figure 6-33 Effect of the air mass flow rate on the air outlet temperature for the discharging process (H= 0.04 m, L= 1.8m and air inlet temperature Figure 6-8: 11h-18h)

Figure 6-33 displays the air outlet temperatures for an air mass flow rate of 0.15 kg/s, 0.2 kg/s, 0.3 kg/s and 0.35 kg/s. It was observed that increasing the air mass flow rate did increase the air outlet temperature due to the shorter period of time that the hot air was in contact with the cold PCM panels. Increasing the flow rate from 0.15 kg/s to 0.2 kg/s increased the air outlet temperature from 26 °C to 28 °C at 5h. Hence, the maximum discharging air mass flow rate was observed to be 0.35 kg/s in order to keep the air outlet temperature below 30 °C over the 7 h.

The air mass flow rate is also investigated for the charging process. The analysis involved increasing the air mass flow rate until the melting temperature of 18 °C is reached for RT20. Figures 6-34 and 6-35 display the temperature of RT20 and RT25 for increasing air mass flow rates.

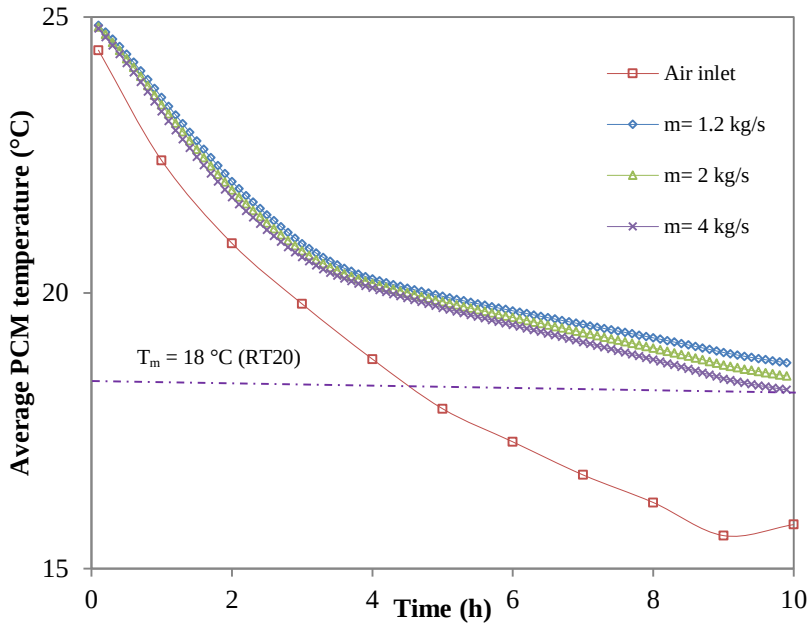

Figure 6-34 Effect of the air mass flow rate on the average temperature of RT 20 for PCM 1+ 2 during the charging process (H= 0.04 m, L= 1.8m and air inlet temperature Figure 6-8: 21h-7h)

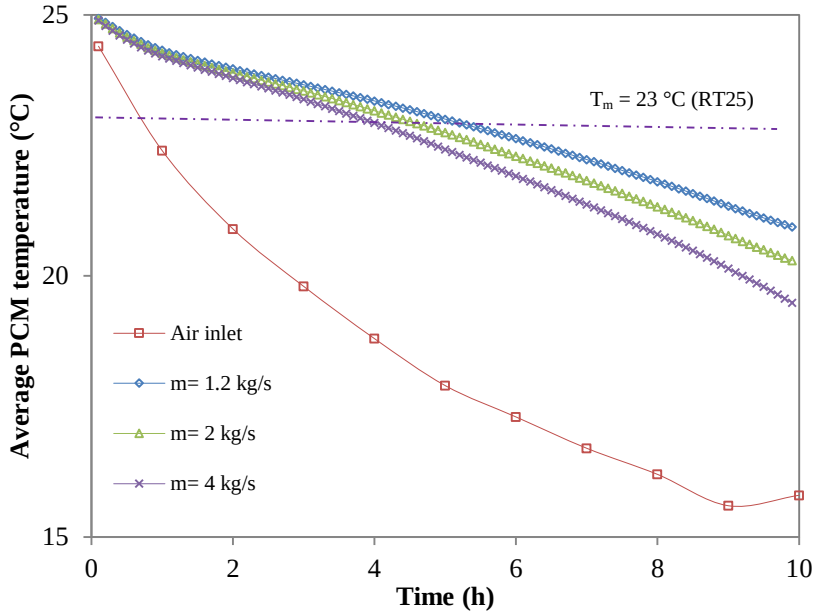

Figure 6-35 Effect of the air mass flow rate on the average temperature of RT 25 for PCM 1+ 2 during the charging process (H= 0.04 m, L= 1.8 m and air inlet temperature Figure 6-8: 21h-7h)

From Figures 6-34 and Figure 6-35 it is observed that RT 25 reached the solidification temperature of 23 °C for all flow rates. On the contrary, RT 20 reached 18 °C after the 10 h only for a mass flow rate of 4 kg/s. In order to guarantee that the entire panel was solidified after the 10 h, a flow rate of 4 kg/s has to be selected. A high power fan would be required to deliver a flow rate of 4 kg/s (11775 m^3/h) representing a high energy consumption. Also, varying the speed of the fan to fulfil such different charging and discharging air flow rates may be difficult to achieve using common variable speed devices. Hence an alternative solution must be found requiring lower mass flow rate for the full charging of the panels. From the previous results displayed in Figure 6-26, the second best height in terms of air outlet temperature and discharging time was a height of 0.03 m. However in terms of length it was found out that changing the length did not significantly affect the charging time (Figure 6-31 and Figure 6-32). Therefore, the investigation was further carried out for H= 0.03 m, keeping the length at 1.8 m.

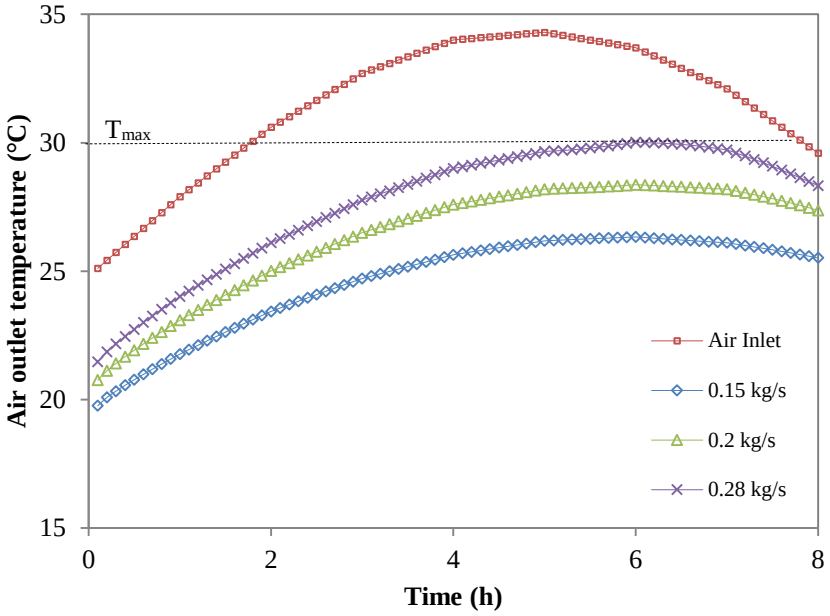

Figure 6-36 Effect of the air mass flow rate on the air outlet temperature for the discharging process (H= 0.03 m, L= 1.8 m air inlet temperature Figure 6-8: 11h-18h)

For the panels with 0.03 m and 1.8 m height and length respectively the air mass flow rate could be increased until 0.28 kg/s in order to keep the air outlet temperature below 30 °C.

The charging temperature for PCM 2 (RT20) for different air mass flow rates was analysed and displayed in Figure 6-37.

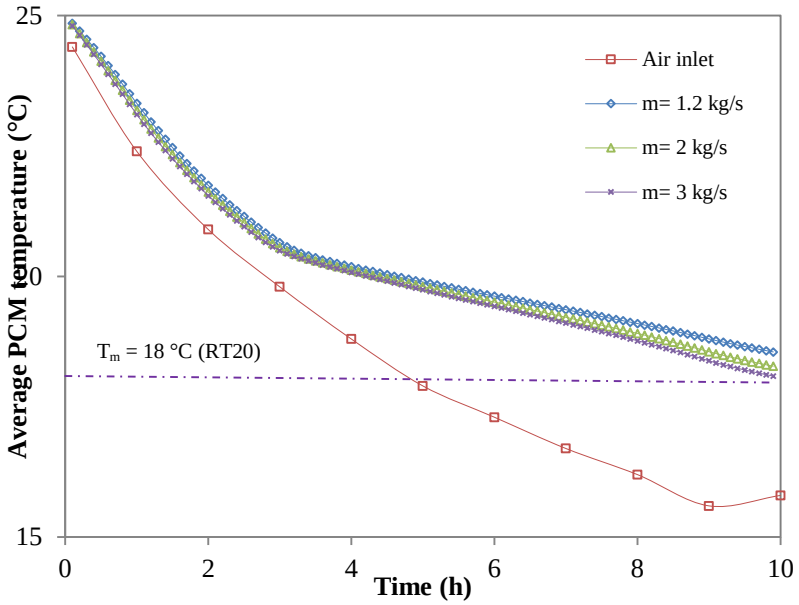

Figure 6-37 Effect of the air mass flow rate on the average temperature of RT 20 for PCM 1+ 2 during the charging process (H= 0.03 m, L= 1.8 m and air inlet temperature Figure 6-8: 21h-7h)

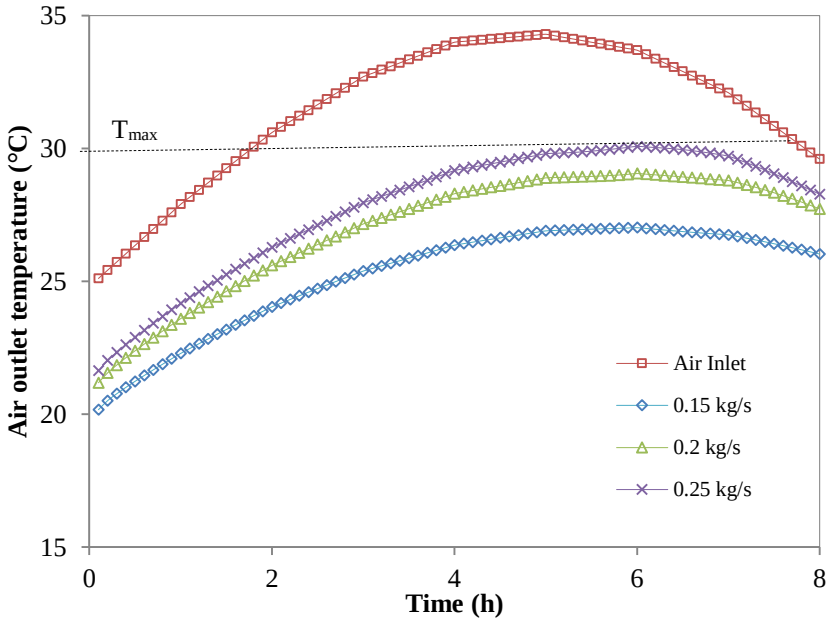

Figure 6-38 Effect of the air mass flow rate on the air outlet temperature for the discharging process (H= 0.03 m, L= 1.5 m, air inlet temperature Figure 6-8: 11h-18h)

From Figure 6-37 it was observed that a flow rate of 3 kg/ is required to completely charge the PCM panels. This figure remains high, requiring again a high power fan and inducing high energy consumption over the 10 h. Moreover a length of 1.5 m was investigated for the charging and discharging process and displayed in Figures 6-38 and 6-39.

Observing Figure 6-38, it was found that for the panels with 0.03 m and 1.5 m height and length respectively, the air mass flow rate could be increased until 0.25 kg/s in order to keep the air outlet temperature below 30 °C. Simultaneously, the charging temperature for PCM 1 (RT25) and PCM 2 (RT20) are analysed in Figures 6-39 and 6-40.

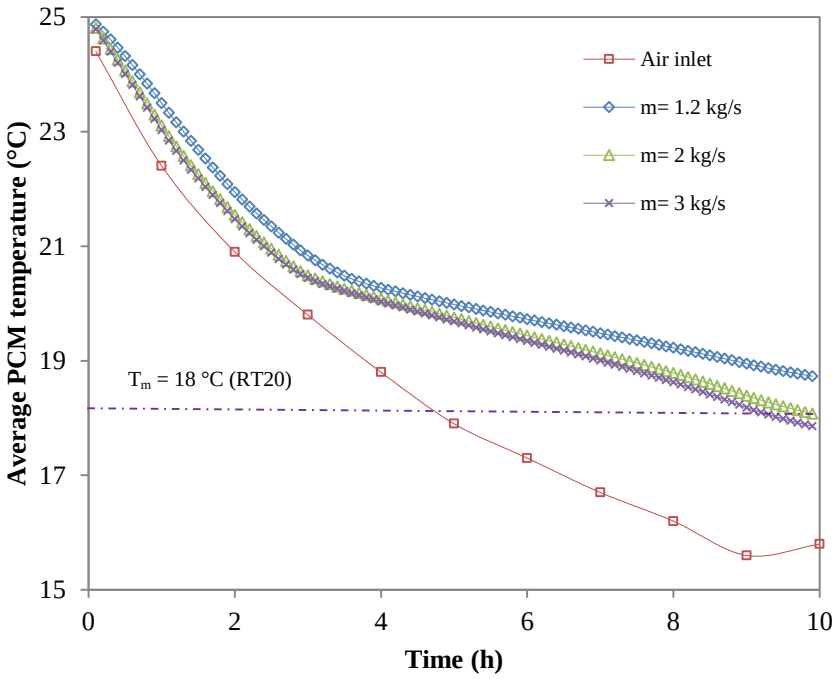

Figure 6-39 Effect of the air mass flow rate on the average temperature of RT 20 for PCM 1+ 2 during the charging process (H= 0.03 m, L= 1.5 m and air inlet temperature Figure 6-8: 21h- 7h)

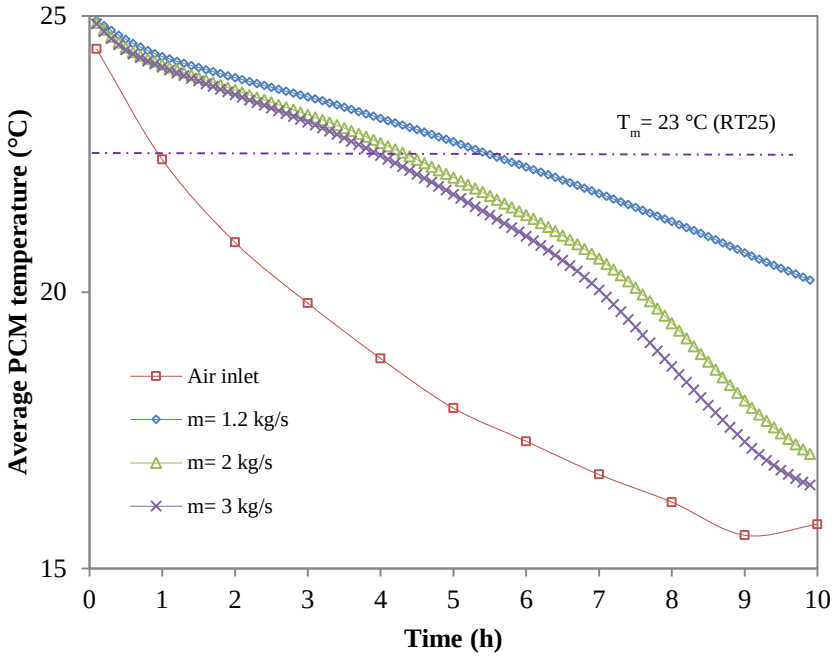

Figure 6-40 Effect of the air mass flow rate on the average temperature of RT 25 for PCM 1+ 2 during the charging process (H= 0.03 m, L= 1.5 m and air inlet temperature Figure 6.8: 21h- 7h)

From Figure 6-39 it was observed that for a panel length of 1.5 m, similar discharging air flow rate could be used as for a length of 1.8 m guaranteeing an air outlet temperature below 30 °C during the day time. However there were differences in terms of required air mass flow rate to fully charge the PCM 2 (RT 20) overnight. For a length of 1.5 m the PCM 2 was fully charged for a mass flow rate of 2 kg/s, while for a length of 1.8 m, a flow rate of 4 kg/s was required. Also, for a length of 1.5 m and mass flow rate of 2 kg/s, the panels were fully solidified after 9h reducing in one hour the process.

Overall, decreasing the height from 0.04 m to 0.03 m and the length from 1.8 m to 1.5 m required half of the air mass flow rate to completely solidify the panels during night-time and therefore significantly reduces the fan size and consequently the power. This is further investigated for the current application (section 6.6).

6.5.5 Delivered cooling load, Q_c

The cooling load is described and determined in the following Equation 3-2 (Chapter 3). The same calculation was performed for the best air-multiple PCM unit dimensions (H= 0.03 m and L= 1.5 m) and the mass flow rate (m= 0.25 kg/s). The hourly cooling load was displayed in Figure 6-41.

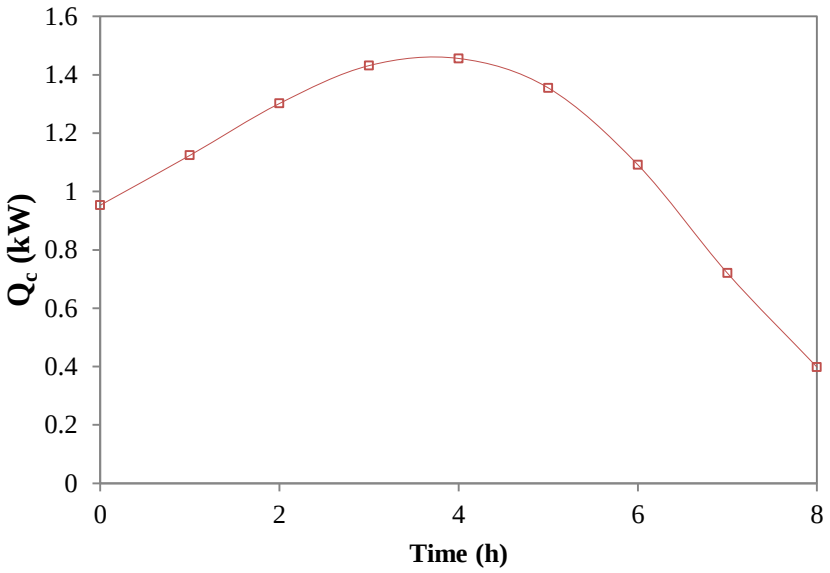

Figure 6-41 Cooling load for H= 0.03 m and L= 1.5 m and air mass flow rate of 0.25 kg/s

For the best geometric (H= 0.03 m and L= 1.5 m) and air mass flow rate of 0.25 kg/s (734.7 m^3/h) a cooling load is shown varying from 0.4 to 1.46 kW over the 8 h, with an average cooling load of 1.02 kW.

6.5.6 Effectiveness over the phase change, ε

Equation 6-1 was adapted from Equation 3-4 presented in Chapter 3. However, for the multiple PCMs unit the effectiveness was related with the average melting temperature of the two PCMs (Chiu and Martin, 2013)

$$\varepsilon_{discharging} = \frac{T_{in} - T_{out}}{T_{in} - T_{avg,PCM}} \quad (6\text{-}1)$$

Where T_{in} and T_{out} correspond to the air inlet and outlet temperatures and $T_{average}$, PCM the average temperature of the PCM was determined by (Fang and Chen, 2007)

$$T_{average,PCM} = \sum_i^n x_i \times T_{m,i} \quad (6\text{-}2)$$

Where x_i is the mass fraction and $T_{m,i}$ is the melting temperature of each PCM.

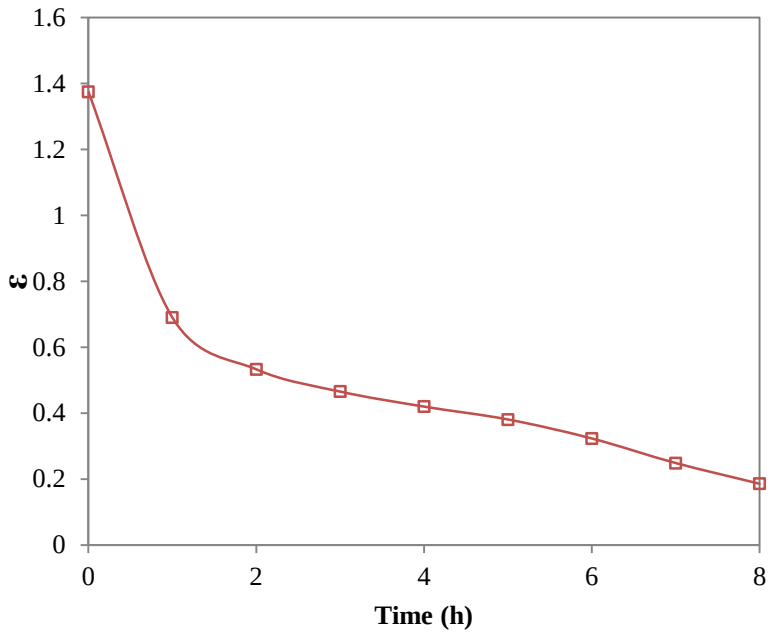

Figure 6-42 Effectiveness over the phase change process for H= 0.03 m, L= 1.5 m and air mass flow rate of 0.25 kg/s

The effectiveness of the proposed unit varied between 1.4 and 0.15 showing improvement when compared to the experimental unit when using multiple PCMs. A summary of the most suitable case achieved through the parametric study is presented in Table 6-7.

Table 6-7 Best case design

Panels height	0.03 m
Panels length	1.5 m
Panels width	1 m
Discharging air mass flow rate	0.25 kg/s 734.7 m^3/h
Charging air mass flow rate	2 kg/s 5877.6 m3/h
Delivered cooling load (Q_c)	8.19 kW
Average effectiveness (ε)	0.5

6.6 Case study

From the parametric study (section 6.5), the full discharge of the multiple PCM panels allowed the reduction of the external temperature below 30 °C, translated into a daily cooling load of 8.19 kW. The proposed unit intends to be driven by renewable energy (night coldness) with the only mechanical energy consumption coming from the fan. This will reduce the fossil-fuel energy and CO_2 emissions when compared to traditional Air Conditioning (AC) systems. The economic and environment benefits of running this system are investigated in this section. The case study corresponded to a 200 m^3 office building located in Castelo Branco, Portugal, accommodating 20 occupants. The required PCM, fan power and energy consumption are determined for the air-multiple PCM unit followed by the economical and environment analysis comparing the proposed unit with conventional AC system.

6.6.1 Required cooling and ventilation load

It is assumed that the air-multiple PCM unit is installed to provide free cooling and ventilation to an office room with 20 occupants in Castelo Branco in summer. The average temperature during summer is presented in Figure 6-8 taken from the SolTerm software, the database tool recommended by the current legislation in Portugal (RCCTE, 2006; RSECE, 2006). The cooling load is calculated only on the sensible cooling, providing comfortable temperature for the required fresh air supply. The fresh air supply is evaluated under the SCE approved by RCCTE (2006) and RSECE (2006) in Portugal. In the current study the cooling load to achieve the comfort temperature in buildings does not consider the 20 °C defined in RCCTE (2006) and RSECE (2006). It is instead based on the recent adaptive method presented and discussed in 6.3.2. From Figure 6-7, the recommended comfort temperatures vary from 16-30 °C for an external temperature between 5 °C and 32 °C. Therefore, for the recommended air supply for office buildings, 35 m^3/(h.occupant) (RSECE, 2006), taking into account 20 occupants and comfort temperatures delivered by the best case design of the air-multiple PCM unit, the required cooling load and ventilation. Q_C is presented in the Figure 6-43. It is observed that the required cooling and ventilation load is similar to the cooling load delivered by the air-multiple PCM investigated in the parametric study. Hence the economic and environmental analysis is based on the best case investigated in the parametric study and detailed in Table 6-7.

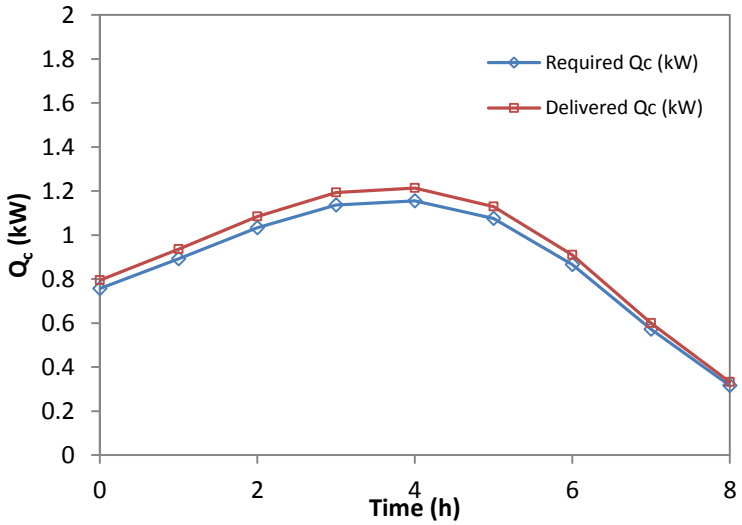

Figure 6-43 Required and delivered cooling load, Q_c

6.6.2 Economic and environmental analysis

The economic and environmental analysis was carried out by estimating the capital and running costs of the proposed unit and a conventional cooling unit followed by the payback time and related CO_2 emissions.

The proposed air-multiple PCM unit includes a paraffin wax PCM commercially available and comparatively inexpensive (£7/kg). Paraffins are compatible with most metallic containers materials and therefore the cost of the PCM encapsulation should not be a problem. As discussed in Chapter 2, the paraffin wax PCM suffers from negligible supercooling or phase segregation, which means paraffin wax has a long term stability. The manufacturer also guarantees RT20 and RT25 as a long life product. Long term reliability ensures that the PCM performs well after a large number of freezing and melting cycles. Hence, the unit will require little or no maintenance during a long period, resulting in a significant reduction in its cost. RT 20 and RT 25 PCMs are encapsulated into rectangular panels, each with a total volume of 0.045 m^3. The three panels, when filled with liquid PCM with a density of 760 kg/m^3 (Table 6-5), correspond to a total mass of 102.6 kg. Apart from the PCMs, the proposed unit includes the PCM encapsulation, fan and ductwork. The PCMs were encapsulated into rectangular containers made of steel and inserted into a rectangular ducting. The selected fan was based on the volumetric flow rate (m^3/h) and the total pressure drop (Pa) along the air duct. The air flow rate corresponded to 734.7 m^3/h and 5877.5 m^3/h for the discharging and charging process respectively. The total pressure drop was associated with the frictional pressure loss and was taken from the CFD model. It corresponded to 30 Pa and 484.38 Pa for the discharging and charging processes respectively. A fan was used to fulfil both flow rates and the pressure drop with power of 0.0359 kW and 0.853 kW for the discharging and charging processes respectively (Appendix D- Model MUB 042 500 EC). Moreover the COP of the proposed system was determined by:

$$COP = \frac{\int_{t=0}^{t=8h} Q_c\,(t)dT}{W_{fan}} \qquad (6\text{-}3)$$

where Q_c corresponded to the total cooling load and P_{fan1} and P_{fan2} to the power of the fan at the discharging and charging processes respectively. The COP of the proposed unit reached 1.03.

The total energy consumption of the proposed system was related only to the running of the fan at two air flow rates with different motor powers ($P_{fan,1}$ and $P_{fan,\ 2}$). The energy consumption corresponded to the summation of the energy consumption of the fan operating at a lower power (fan,1) and a higher power (fan,2) during the charging and discharging processes respectively.

$$W_{fan} = \left(P_{fan,1} \times t\right)_{charging} + \left(P_{fan,2} \times t\right)_{discharging} \quad (6\text{-}4)$$

The total consumption of the fan was based on 8 hours and 9 hours for the charging and discharging time respectively over 65 days (June- September) was 517.67 kWh/year.

A convectional cooling unit was proposed to provide the required cooling load of 1.2 kW. A four way blow ceiling cassette system (model PLA-ZRP) provided by Mitsubishi Electric was selected and a data sheet can be found in Appendix E. The COP of the proposed system was determined by:

$$COP_{AC} = \frac{Q_c}{W_{AC} + W_{fan}} \quad (6\text{-}5)$$

The motor power of the AC unit was set at 0.3617 kW and to run for 8 hours. The energy consumption of the unit was determined by:

$$W_{AC} = P_{AC} \times t \quad (6\text{-}6)$$

In addition, a centrifugal fan was selected to fulfil the fresh air requirements of 734.7 m^3/h (Appendix C-Model K250 EC). The energy consumption of the fan was determined by:

$$W_{fan} = P_{fan} \times t \quad (6\text{-}7)$$

Hence, the total energy consumption for the conventional air-conditioning unit and the fan was based on 8 hours a day over 65 days (June-September) and corresponded to 219.02 kWh. The equipment's capital and running costs were listed in Table 6-8.

Table 6-8 Equipments capital and running cost

	Multiple PCM unit		Traditional AC System
	Daytime	Night-time	
Capital cost	PCM (Web 6.1): £718.2 Steel encapsulation (Web 6.2): £313 Air duct (Web 6.3): £107 Fans (Web 6.4): £1100.5		Ceiling cassette system (Web 6.5): £2099 Fan (Web 6.4): £254.2
Maintain cost	£15 (once a year: cleanliness of air-filters)		£ 70 (once a year: cleanliness of the coils, air-filters, and the detection and remediation of leaks)
Cooling load	1.02 kW		1.02 kW
COP	1.03		2.12
Motor Power (fans/ air-conditioning)	0.0359 kW (daytime) 0.853 kW (night-time)		0.0595 kW/0.3617 kW
Annual running hours (3 months)	Daytime: 8 hours per day (520 h) Nigh-time: 9 hours per day (585 h)		8 hours per day (520 h)
Annual energy consumption (daytime)	18.67 kWh		219.02 kWh
Total annual energy consumption (daytime and night-time)	517.67 kWh		
Electricity price (Web 6.6)	Day tariff (8h-24h): £0.1890 /kWh Night tariff (24h-8h): £0.0978 /kWh		
Annual running cost (daytime)	£3.53		£41.4
Total annual running cost (daytime and night-time)	£52.3		£41.4

The total annual energy consumption corresponded to 517.67 kWh and 219.02 kWh for the air-multiple PCM unit and the air conditioner, respectively. The air-multi PCM unit presented higher energy consumption due to the running of the fan during night time. It can be observed from Table 6-8 that for the daytime the air-multiple PCM unit presented a much lower energy consumption (18.67 kWh) than the traditional AC (219.02 kWh). During the daytime the

proposed unit can save 200.35 kWh of electric energy during daytime per year comparing to the traditional air-conditioning unit. However, the unit does not operate effectively if the charging of the PCMs is not complete during nigh-time. The air-multiple PCM however, presents a slightly lower capital cost than the traditional air-conditioning system. Also, the maintenance cost is lower for the proposed unit as it involved only the cleaning of the air filters. The price of electricity in the Portugal for a bi-hourly package is £0.1890 and £0.0978 per kWh for daytime and night-time respectively (Web 6.6), translating to annual energy consumption of £52.3 and £41.4 for the air-multiple PCM and AC respectively. In order to make the unit competitive in terms of energy consumption and running cost, the charging process of the PCM has to be improved during night time. Enhancing the heat transfer between the air and PCM will decrease the air mass flow rate and consequently reduce the fan size and running costs.

The proposed unit presents environmental advantages such as the non-use of refrigerants such as chlorofluorocarbons (CFCs), hydrochlorofluorocarbons (HCFCs) and hydrofluorocarbons (HFCs) that are major contributors to ozone-layer breakdown and typically used as working fluids in AC. Also, CFCs, HGCFCs and HFCs require careful handling when AC are dismantled for recycling or tossed in landfills. US Environmental Protection Agency (EPA) as other environmental agencies are authorized to impose fines up to £16000 for failure to comply with the current regulation. Specialized companies are commonly in charge to handle the disposal of AC units. The use of AC can also promote personal health issues. AC without adequate maintenance can be a health hazard. Dirty components can allow allergens, pesticides and other particles to enter the space from the outside environment threatening the indoor air quality. The long exposure to those pollutants can result in health problems including allergies, asthma and eye, nose and throat irritation.

6.7 Conclusions

The PCM 2+3 represented the best PCM selection presenting the lowest air outlet temperature for the first 3 hours for an air flow rate of 0.15 kg/s and PCM panels with a height of 0.02 m and a length of 1.5 m. However PCM 3 (RT18) was not completely charged overnight. Increasing the air flow rate was not enough to overcome this issue. It was only by evenly reducing the night air temperatures in 1.5 and 2 °C that all PCMs would be fully charged. For the current climatic conditions, PCM 1+2 was found to be the most suitable PCM selection, fulfilling both the discharging and charging requirements. This case was further investigated for different heights and lengths of the PCM panels. A height of 0.03 m was considered the best dimension as further increasing the height did not significantly decrease the air outlet temperature during the discharging process. Also, at a height of 0.03 m, the panels were fully charged overnight. The best length was considered to be 1.5 m as it met the desirable air outlet temperature over the required cooling time and the PCM panels were fully charged during night-time with an acceptable air mass flow rate (2 kg/s) fulfilling a practical scale.

In summary, the best air mass flow rates were 0.25 kg/s and 2 kg/s for the discharging and charging processes respectively. The air- multiple PCM unit, including panels with 0.03 m height and 1.5 m length and an air flow rate of 0.25 kg/s presented an effectiveness over the phase change from 1.4 and 0.15. This is an improvement when compared to the experimental unit. It remained at a higher value (0.4) for a longer period of time (4h) meaning that the air-multiple PCMs unit provided a lower and uniform air outlet temperature for a longer period of time. The proposed unit presented an average cooling load of 1.02 kW.

The case study was related to the cooling of an office of 20 occupants, located in Castelo Branco, Portugal. The required cooling load was fitted with the cooling load delivered by the best case studied in the parametric study. It was found that the air-multiple PCM unit allowed a reduction in energy consumption during daytime of 200.35 kWh when compared to a traditional air-conditioning unit. However the proposed unit becomes economically uncompetitive when taking into account the energy consumption associated to the charging of the PCMs during night-time. Overall, the unit presents advantages such as the initial and maintenance cost and the prevention of personal health issues when compared to traditional ACs.

Chapter 7 – CONCLUSIONS AND RECOMMENDATIONS

7.1 Conclusions

The central aim of this research is to develop an effective air- multiple PCM unit to provide free cooling and ventilation for buildings. This aim is successfully achieved by carrying out the objectives presented in Chapter 1. The main findings from the research will be highlighted in this chapter.

7.1.1 Experimental results

The discharging time of the PCM panels is influenced by the air inlet velocity and air inlet temperature. The air inlet temperature had a major impact on the discharging time. Increasing the air temperature from 30 °C to 34 °C reduces the discharging time by half. Increasing air inlet velocity from 0.6 m/s to 1.6 m/s drastically reduces the discharging time. However, a further increase to 2.5 m/s did not significantly impact on discharging time.

The charging time is strongly influenced by the air inlet temperature, the charging time reduced proportionally with the decrease of the inlet temperature. On the other hand, further increasing the air inlet velocity to 2.5 m/s reduces the time by half an hour.

Overall, the air temperature difference achieves higher values for the discharging process than for the charging process. The air temperature difference for both processes is more significantly influenced by the air inlet velocity rather than the air inlet temperature. The air temperature difference reduces more effectively from 0.6 m/s to 1.6 m/s for both processes. Increasing the velocity to 2.5 m/s represented a temperature difference of only 0.7 °C and 0.3 °C for the discharging and charging processes respectively.

The cooling load associated to the discharging of the PCM panels is in average 70 W, 110 W and 130 W for temperature of 38 °C and air inlet velocity of 0.6 m/s, 1.6 m/s and 2.5 m/s respectively. The cooling load for a constant air inlet velocity of 1.6 m/s decreases for lower air inlet temperatures corresponding to 50 W and 70 W for 30°C, 34 °C and 38 °C respectively. The heating load related to the charging of the PCM panels achieves 30 W, 40

W and 50 W for a constant air inlet temperature of 38 °C and velocity of 0.6 m/s, 1.6 m/s and 2.5 m/s respectively..

Effectiveness over the phase change is higher for the discharging process that for the charging process. The highest values are reached for velocity of 0.6 m/s for both processes due to the longer contact between the air and the PCM panels.

7.1.2 DSC analysis

The DSC analysis allows the thermal characterisation of a sample of RT25, namely the phase change temperatures, specific heat and enthalpy.

For smaller heating rates, the melting temperature range narrows down, specific heat reached higher values and enthalpy remains the same.

The DSC testing performed with the experimental heating/cooling rates showed similar phase change temperature to those observed in the experiments and also listed by the manufacturer. The DSC testing using the heating/cooling suggested by ASTM D 4419 (1990) 10 °C/min, showed a wider phase change temperature of the sample and deviated from the experimental results and the manufacturer data.

7.1.3 Numerical results – experimental validation

Overall good agreements were achieved between the numerical and the experimental results for a CFD model including the enthalpy and the effective heat capacity methods.

The enthalpy method was applied through the Solidification and Melting model available in FLUENT. It assumes a constant enthalpy-temperature relationship (i.e. lever rule) presenting deviation between the experimental and numerical results mostly at the interface between the initial sensible heating and the beginning of the phase change (discharge process) and between the end of the phase change and the beginning of the sensible cooling (charging process).

Identifying the experimental heating/cooling rate, similar rate should be selected for the DSC analysis. This allows the determination of the realistic thermophysical properties of the PCMs and consequently improving the CFD model. The insertion of these properties, allows more accurate numerical results. The discrepancy between numerical and experimental results therefore was reduced for the effective heat capacity method as it described accordingly the thermophysical properties of the PCM through the specific heat- temperature relationship.

7.1.4 Numerical results – multiple PCMs unit

Multi-PCMs were reported in the literature as a heat transfer improvement for TES units. The selection of the PCMs should be undertaken according to their thermophysical, technical properties and economic viability. More specifically, for free cooling of buildings the PCMs melting temperature should meet the thermal comfort conditions and should achieve the full charging and discharging for the available air temperature. For the current study, the selection PCMs were: RT18, RT20 and RT25 with melting temperature of 18 °C, 20 °C and 25 °C respectively complying the thermal comfort conditions and based on the climate conditions in Portugal.

An air-PCM unit for the free cooling of building applications need to satisfy three parameters: air outlet temperature, cooling time (i.e. PCM discharging time) and PCM charging time. The air outlet temperature was based on the adaptive methods for comfort conditions in buildings, allowing higher air outlet comfort temperature and therefore less energy demand for cooling/heating applications. The required cooling time relies on the buildings typology and its daily occupancy profile. For this study, an office building was selected and the predominant occupancy was identified from 11h to 18h. Finally, the selected PCMs need to be fully charged during night-time for the full performance during daytime, corresponding to 22h until 6h.

The proposed air-multiple PCM unit allowed lower air outlet temperatures when compared to a single PCM unit, due to use of PCMs with lower melting temperatures. A PCM selection investigation was carried out by considering different PCMs arrangements within the panel for PCM panels with a height of 0.02 m and length of 1.5 m. The following PCM selection

achieved the required air outlet temperature (≤30°C): RT25; RT20+RT18; RT25+RT18; RT25+RT20+RT18.

The charging time was investigated for the above cases, where the air outlet temperature was successfully achieved. It was found that for the available air night temperatures it is not possible to completely solidify RT18, even for lower RT18 mass fractions. Increasing the mass flow rate has not overcome this issue. The complete charging of this PCM was observed to be only possible for air inlet temperatures reduced by 1.5 °C or more. Therefore, the cases including RT18 had to be excluded from further investigation. For the current climatic conditions, PCMs RT25+RT20 (PCM 1+2) was found to be the most suitable PCM selection fulfilling both the discharging and charging requirements.

The air outlet temperature and required cooling time (i.e. discharging time) were found to be directly related to the PCM mass. In this study, the investigation of the mass of case PCM 1+2 was achieved by investigating different heights and lengths of the PCMs panels. Further increasing the height from 0.04 m to 0.06m, 0.08 m did not reduce either the air outlet temperature or the cooling time. Increasing the length from 1.5 to 1.8 m and 2.1 m did reduce the air outlet temperature but as the length was increased by each increment, the air temperature difference between the inlet and outlet also reduced, therefore increasing the length was not found to be significant. The most suitable dimensions were considered as 0.04 m and 1.8 m for the height and length respectively.

For the best case, the air mass flow rate was increased until the air outlet temperature reached the limit of thermal comfort (≤30°C). It was found that the air mass flow rate of 0.25 kg/s and 2 kg/s for the discharging and charging processes respectively meet the air outlet temperature, cooling time and charging time requirements. It corresponded to effectiveness over the phase change from 1.4 to 0.15, showing improvements when compared to the experimental unit. The average cooling load corresponded to 1.02 kW.

A case study was investigated for free cooling and ventilation of an office including 20 occupants located in Castelo Branco, Portugal. The required cooling load matched with the cooling load provided by the best case studied in the parametric study. It was found that the air-multiple PCM unit allowed reducing the energy consumption during daytime in 200.35 kWh when compared with a traditional air-conditioning unit. However, the proposed unit

requires the full charging of the PCMs units during night time, increasing the energy consumption to 517.63 kWh and making it uncompetitive with a traditional AC. The unit does present several advantages such as the initial and maintenance cost and the improvement of personal health issues when compared to traditional ACs.

Overall, this research was a first trial for the development of an air-multiple PCM unit to provide free cooling and ventilation in buildings. The study included a small experimental unit to investigate the thermal performance of air-PCM unit and to validate a CFD model. The verified CFD model investigated the potential of multiple PCMs and allied with an extensive parametric study, allowed the development of a unit to provide free cooling and ventilation for an office building in Castelo Branco, Portugal. The economic and environmental analysis has shown that the proposed unit has potential through substantially reducing the energy consumption during the day time and presenting environmental benefits in the cooling of buildings. However, the energy consumption during night-time requires further investigation.

7.2 Recommendations

A comprehensive numerical and experimental study has been carried in this research to achieve a suitable air-multiple PCM unit for free cooling and ventilation purposes. However, still several questions need to be answered for further development of air-multiple PCM unit. The potential works require experimental and numerical research and further real life full scale field trial in a building. They are summarised as following:

7.2.1 Experimental work

One major drawback of LHS systems is the low thermal conductivity of most PCMs. Thus, thermal conductivity enhancement techniques are required in practical LHS application. In this research RT18 PCM fails to reach the solidification temperature of 16 °C due to the available temperature during night-time. The use of multi-PCMS has been investigated for the enhancement of the thermal performance of the unit. This technique enhanced the air outlet temperature when compared to single PCM. However, a high air mass flow rates it is

still required for the full charging of the selected PCMs over night-time. High air mass flow rate result in bigger fan size and consequently, significant energy consumption and running cost. The literature reveals that some metallic materials such as cooper and aluminium have much higher thermal conductivities than stainless steel. Hence, other heat transfer enhancements techniques need to be tested such as the use of aluminium or copper as the encapsulation material or the addition of fins within the PCM panels. Further development of containers in copper or aluminium may allow the use of the proposed system in practical application and may yield good results.

An air-single PCM unit has been investigated experimentally. However, a deeper understanding of the heat transfer enhancement of multiple PCMs could be achieved by including multiple PCMs in the experimental unit. The experimental testing of the full scale air- multiple PCMs unit investigated numerically in Chapter 6 would allow the validation of the CFD model and also enable a realistic thermal performance of the unit. Also, running the design life of the full scale unit requires long term examination in terms of chemical stability over a large number of charging and discharging cycles, and the absence of subcooling and corrosion of the encapsulation material. Hence, the next step in any further work would be to install and monitor the proposed unit throughout a year. This will enable a full evaluation of the thermal performance and economic analysis which will provide reliability for a commercial path.

7.2.2 Numerical work

The chosen multiple PCMs presented melting temperatures well below the air inlet conditions assuring their full melting process for all studied conditions. The numerical investigation should be extended by analysing the minimum temperature difference allowed between the air inlet temperature and the PCM melting temperature, guaranteeing their full melting and also the delivery of air outlet temperature below 30 °C over 8 hours. This will confirm if other PCMs with higher melting temperature such as RT27 and RT 29 may be selected for a multi-PCM unit.

The parametric study on the PCMs selection for the air-multiple PCM unit included equal mass fractions of the RT25 and RT20 within the panels. Further investigation of the effect of

the mass fraction on the PCMs may show further improvements in the thermal performance of the unit.

The numerical investigation analysed the potential of an air-multiple PCM unit under Portuguese climatic conditions. Furthermore, the unit can provide free cooling and ventilation for other countries. This can be accomplished by using different climatic data files from other countries.

7.2.3 Real life field trial

In order to understand performance on air-multiple PCM unit in situ climatic conditions, it is important to run real life trial for certain type of buildings. It will provide important experimental performance data to further develop the air-multiple PCM unit. The application for air-multiple PCM unit can further be done in various types of commercial, non-commercial buildings and data centres where cooling is required.

REFERENCES

A

Abhat, A. (1976). Experimental investigation and analysis of a honeycomb-packed phase change material device. In: AIAA 11th Thermophysics Conference; pp. 9 (Paper AIAA-76-437).

Abhat, A., Aboul-Enein, S., and Malatidis, N. (1981). Heat of fusion storage system for solar heating applications, C. Den Quden (Ed.). Thermal Storage of Solar Energy.

Abhat, A. (1983). Low temperature latent heat thermal energy storage: heat storage materials. Solar Energy 30: 313-332.

Aceves, A. M., Nakamura, H., Reistad, G. M., and Martines-Frias, J. (1998). Optimization of a Class of Latent Thermal Energy Storage Systems with Multiple Phase-Change Materials. Solar Energy Engineering 120: 14-19.

Adine, H. A., and Q*u*arnia, H.E. (2009). Numerical analysis of the thermal behaviour of a shell-and-tube heat storage unit using phase change materials. Applied Mathematical Modelling 33: 2132-2144.

Aguiar, R., and Coelho, R. E. (2012). Manual de Instalação e Utilização do software SolTerm – Versão 5. Laboratório Nacional de Energia e Geologia, I.P. Unidade de Análise Energética e Alterações Climáticas, Lisboa

Agyenim, F., and Hewitt, N. (2010). The development of a finned phase change material (PCM) storage system to take advantage of off-peak electricity tariff for improvement in cost of heat pump operation. Energy and Buildings 42: 1552-1560.

Agyenim, F., Hewitt, N., Eames, P., and Smyth, M. (2010). A review of materials, heat transfer and phase change problem formulation of latent heat thermal energy storage systems (LHTESS). Renewable and Sustainable Energy Reviews 14: 615-628.

Ahmad, M., Bontemps, A., Sallee, H., and Quenard, D. (2006). Thermal testing and numerical simulation of a prototype cell using light wallboards coupling vacuum isolation panels and phase change material. Energy and Building 38: 673-681.

Ahmad, M., Bontemps, A., Sallee, H., and Quenard, D. (2006). Experimental investigation and computer simulation of thermal behaviour of wallboards containing phase change material. Energy and Building 38: 357-366.

Alawadhi E., Alqallaf H. J (2011). Building roof with conical holes containing PCM to reduce the cooling load: Numerical study. Energy Conversion and Management 52: 2958-2964.

Aly, S. L., and El-Sharkawy, A. I. (1990). Effect of storage medium on thermal properties of packed beds. Heat Recovery Systems and CHP 10: 509-517.

Amin, N. A. M., Bruno, F., and Belusko, M. (2009). Optimisation of a phase change thermal storage system. In: World Academy of Science, Engineering and Technology 56: 765–769.

Ango, S. E., Bruneau, D., Sebastian, P., and Sommier, A. (2011). Caracterisation expérimentale des performances d'un échangeur à faisceau tubulaire air/MCP. Proceedings of SFT 2011 Congress, Perpignan, France, pp. 1005–1011.

Annunziata, E., Frey, M., Rizzi, F. (2013). Towards nearly zero-energy buildings: the state-of-art of national regulations in Europe. Energy 57, 125-133.

ANSYS FLUENT theory guide Nov 2010. Release 13.0.

Arasu, A. V., Sasmito, A. P., and Mujumdar A. S. (ca. 2012). Numerical performance study of the paraffin wax dispersed with alumina in a concentric pipe latent heat storage system .s.l.

Ardejani, F. D., Baafi, E., Panahi, K. S., Singh, R. N., and Shokri, B. J. (2011). Application of Computational Fluid Dynamics (CFD) for Simulation of Acid Mine Drainage Generation and Subsequent Pollutants Transportation through Groundwater Flow Systems and Rivers,

Computational Fluid Dynamics Technologies and Applications, Prof. Igor Minin (Ed.), ISBN: 978-953-307-169-5, InTech, DOI: 10.5772/16927.

Arkar, C., and Medved, S. (2005). Influence of accuracy of thermal property data of a phase change material on the result of a numerical model of a packed bed latent heat storage with spheres. Thermochimica 438: 192–201

Arkar, C., and Medved, S. (2007). Free cooling of a building using PCM heat storage integrated into the ventilation system. Solar Energy 81: 1078- 1087.

Arkar, C., Vidrih, B., and Medved, S. (2007). Efficiency of free cooling using latent heat storage integrated into the ventilation system of a low energy building. International Journal of Refrigeration 30: 134-143.

Arkar, C., and Medved, S. (2015). Optimization of latent heat storage in solar air heating system with vaccum tube air solar collector. Solar energy 111:10-20

ASHRAE (1993). Handbook of Fundamentals, American Society of Heating, Refrigerating and Air Conditioning Engineers, Inc., Atlanta.

ASHRAE (1995). ANSI-ASHRAE 55a-1995, Addendum to ANSI-ASHRAE Standard 55-1992, Thermal environmental conditions for human occupancy. Atlanta: American Society of Heating, Refrigerating and Air Conditioning Engineers, Inc

ASHRAE (2001). Handbook of Fundamentals, American Society of Heating, Refrigeration and Air Conditioning Engineers, Inc. Atlanta, GA

Assis, E., Katsman, L., Ziskind, G., Letan, R. (2007). Numerical and experimental study of melting in a spherical shell. International Journal of Heat and Mass Transfer 50: 1790- 1804.

ASTM D 4419 (1990). Standard test method for measurement of transition temperatures of petroleum waxes by differential scanning calorimetry (DSC), American Society for Testing and Materials.

ASTM E 1269 (1995). Standard test method for determining specific heat capacity by differential scanning calorimetry, American Society for Testing and Materials.

Athienitis, A., Liu, C., Hawes, D., Banu, D., and Feldman, D. (1997). Investigation of the thermal performance of a passive solar test-room with wall latent heat storage. Built Environment 32: 405-410.

B

Baetens, R., Jelle, B. P., and Hustavsen, A. (2010). Phase change materials for buildings applications: A state-of-art review. Energy and Buildings 42:1361-1368.

Bakker, A. (2009). Lecture 10 -Turbulence Models. Applied Computational Fluid Dynamics. Available at: [http://www.bakker.org/dartmouth06/engs150/].

Bansal, N. K., and Buddhi, D. (1982). An analytical study of a latent heat storage system in a cylinder. Energy Convers Manage 33: 235–42.

Barbour, J. P., and Hittle, D. C. (2005). Modeling Phase Change Materials with Conduction Transfer Functions for Passive Solar Applications. J Solar Energy Eng: 128: 58-68

Bardon, J. P., Vrignaud, E., and Delaunay, D. (1979). Etude experimentale de la fusion et de la solidification periodique d une plaque de paraffine, Rev. Gen. Therm., 212–213

Barreneche, C., Solé, A., Miró, L., Martorell, I., Fernández, A. I., and Cabeza, L. F. (2013). Study on differential scanning calorimetry analysis with two operation modes and organic and inorganic phase change material (PCM). Thermochimica Acta 553: 23–26

Bauer, C., and Wirtz, R.. (2000). Thermal characteristics of a compact, passive thermal energy storage device. Proceedings of the 2000 ASME IMECE, Orlando (Florida, USA).

Beausoleil-Morrison, I. (2000), The adaptive coupling of heat and air flow modelling within dynamic whole-building simulation, PhD Thesis, University of Strathclyde, Glasgow UK.

Beckaman, G., Gilli, P. V. (1984). Topics in Thermal Energy Storage. Springer-Verlag, New York

Bédécarrats, J. P., Strub, F., Falcon, B., and Dumas, J. P. (1995). Experimental and numerical analysis of the supercooling in a phase-change energy storage. In: Proceedings of the 19th international congress of refrigeration, Netherlands

Bédécarrats, J. P., Strus, F. P., Falcon, B., and Dumas, J. P. (1996). Phase-change thermal energy storage using spherical capsules: performance of a test plant. Int J refrigeration 19: 187-196.

Bédécarrats, J. P., Castaing-Lasvignottes, J., Strub, F., and Dumas, J. P. (2009). Study of a phase change energy storage using spherical capsules. Part I: Experimental results. Energy Convers Managent 50: 2527–36.

Bédécarrats, J. P., Castaing-Lasvignottes, J., Strub, F., and Dumas, J. P. (2009). Study of a phase change energy storage using spherical capsules. Part II: Numerical modelling. Energy Convers Manage 50: 2537–46.

Belusko, M., and Bruno, F. (2008). 140- Design methodology of PCM thermal storage system with parallel plates. In: EUROSUN, 1st Int. Conference Heating, Cooling and Buildings, EUROSUN, Lisbon, Portugal, October

Benmansour, A., Hamdan, M. A., and Bengeuddach, A. (2006). Experimental and numerical investigation of solid particles thermal energy storage unit. Appl Therm Eng 26: 513–8.

Bentilla, E., Sterrett, K., and Karre, L. (1966). Research and development study on thermal control by use of fusible materials. Northrop Space Laboratories Interim Report (NSL-65-16-1). NASA Marshall Space Flight Center; 179 pp.

Best Practice Programme Energy Consumption Guide 19, Energy use in offices, Carbon Trust, December 2000.

Bielsa, P. (2011). Almacenamiento termico de energia mediante cambio de fase. PhD Thesis. University of Zaragoza.

Buildings and Climate Change. A Summary for Decision-Makers, UNEP's Sustainable Buildings & Climate Initiative (SBCI), 2009, 987-92-807-3064-7

Biwole, P. H., Eclache, P., and Kuznik, F. (2013). Phase-change materials to improve solar panel's performance. Energy and Buildings 62: 59-37.

Bransier, J. (1979). Periodic latent heat storage, International Journal of Heat and Mass Transfer 22 (1979) 875–883.

Brent, A. D., Voller, V. R., and Reid, K. J. (1988). Enthalpy-porosity technique for modelling convection-diffusion phase change: application to the melting of a pure metal, Numerical Heat Transfer 13: 297-318.

Brousseau, P., and Lacroix, M. (1996). Study of the thermal performance of a multi-layer PCM storage unit. Energy Conversion and Management 37: 599-609

Bruno, F. (2004). Using phase change materials (PCMs) for space heating and cooling in buildings. AIRAH performance enhanced building environmentally sustainable design conference.

Bruno, F., and Saman, W. (2002). Testing of a PCM energy storage system for space heating. World Renewable Energy Congress VII, Germany.

Bugaje, I. M. (1997). Enhancing the thermal response of latent heat storage system. Energy Research 21: 759-766.

Butala, V., and Stritih, U. (2009). Experimental investigation of PCM cold storage. Energy and Buildings 41: 354-359.

C

Cabeza, L., Castell, A., Barreneche, C., Gracia, A., and Fernández, A. (2011). Materials used as a PCM in thermal energy storage in buildings: A review. Renewable and Sustainable Energy Reviews 15: 1675-1695.

Cabeza, L. (2015). Advances in Thermal Energy Storage Systems. Methods and Applications. Woodhead publishing series in energy.

Carlslaw, H. S., and Jaeger, J. C. (1959). Conduction of Heat in Solids. Oxford: Clarendon Press.

Carman, P. C. (1937). Fluid flow through granular beds, Trans. Inst. Chem. Eng. 15: 150–166.

Castell, A., Belusko, M., Bruno, F., and Cabeza, L. F. (2011). Maximisation of heat transfer in a coil in tank PCM cold storage system 88: 4120-4127

Castellón, C., Martorell, I., Cabeza, L. F., Fernández, A. I., and Manich, A. M. (2011). Compatibility of plastic with phase change materials (PCM). Int J of Energy Research 35: 765-771

Chaiyat, N. (2015). Energy and economic analysis of a building air-conditioner with a phase change material (PCM). Energy Conversion and Management 94: 150-158.

Charvát, P., Klimes, L., and Ostry, M. (2014). Numerical and experimental investigation of a PCM-based thermal storage unit for solar air systems. Energy and Buildings 68: 488-497

Chen C., Guo H., Liu Y., Yue H., and Wang C. (2008). A new kind of phase change material (PCM) for energy-storing wallboard. Energy and Buildings 40: 882-890

Cheralathan, M., Velraj, R., and Renganarayanan, S. (2007). Effect of porosity and the inlet heat transfer fluid temperature variation on the performance of cool thermal energy storage system. Heat Mass Transfer 43: 833–42.

Chiu, J. N. W., and Martin, V. (2012). Submerged finned heat exchanger latent heat storage design and its experimental verification. Applied Energy 93: 507-516

Chiu, J. N. W., and Martin, V. (2013). Multistage latent heat cold thermal energy storage design analysis. Applied Energy 2013; 112: 1438-1445

Chmielewski, M., and Gieras, M. (2013). Three-zone Wall Funtions for k-ε Turbulence Models. CMST 19: 107-114.

Choi, J. C., and Kim, S. D. (1992). Heat transfer characteristics of a latent heat storage system using MgCl2-6H2O. Energy 17:1153–64.

Chow, L., Zhong, J., and Beam, J. (1996). Thermal conductivity enhancement for phase change storage media. International Communications in Heat and Mass Transfer 23:91–100.

Climator (2015). Sweden. Available from <http://www.climator.com/en/home/>.

Costa, M., Oliva, A., Perez, S. C. D., and Alba, R. (1991). Numerical simulation of solid–liquid phase change phenomena. Comput Methods Appl Mech Eng 91: 1123–34.

Costa, M., Buddhi, D., and Oliva, A. (1998). Numerical simulation of a latent heat thermal energy storage system with enhanced heat conduction. Energy Conservation Management 39: 319-330.

Cristopia Energy Systems (2015). Available from < http://www.cristopia.com/>.

Cui, H., Yuan, X., and Hou, X. Thermal performance analysis for a heat receiver using multiple phase change materials. Applied Thermal Engineering 23 (2003): 2353-2361

D

David, D., Kuznik, F., and Roux, J. J. (2011). Numerical study of the influence of the convective heat transfer on the dynamical behaviour of a phase change material wall, Applied Thermal Engineering 31: 3117–3124.

Darzi, A. A., Moosania, S. M., Tan, F. L., and Farhadi, M. (2013). Numerical investigation of free cooling system using plate type PCM storage. International Communications in Heat and Mass Transfer 48: 155-163

De Jong, A., and Hoogendoorn, C. (1980). Improved of heat transport in paraffin for latent heat storage unit. Bul Electrotech Lab 44: 278-368

Diaconu, B.M., and Cruceru, M. (2010). Novel concept of composite phase change material wall system for year-round thermal energy savings. Energy and Building 42: 1759-1772.

Diaconu, B. M. (2011). Thermal energy savings in buildings with PCM-enhanced envelope: Influence of occupancy pattern and ventilation. Energy and Buildings 43: 101-107.

Diarce, G., Campos- Celador, Á., Martin, K., Urresti, A., García-Romer, A., and Sala, J. M. (2014). A comparative study of the CFD modeling of a ventilated active façade including phase change materials. Applied Energy 126: 307-317

Dincer, I., and Dost, S. (1996). A Perspective on Thermal Energy Storage Systems for Solar Energy Applications. International Journal of Energy Research 20: 547-557

Dolado, P. (2011). Almacenamiento térmico de energía mediante cambio de fase. Diseño y modelizacíon de quipos de almacenamiento para intercambio de calor con aire. Ph.D. Thesis, Departamento de Ingeniería Mecánica, University Zaragoza, Spain

Dolado, P., Lazaro, A., Marin, J.M., and Zalba, B. (2011). Characterization of melting a in a real PCM-air heat exchanger: Numerical model and experimental validation. Energy Convers Mgmt 52: 1890-1907

Dubovsky, V., Ziskind, G., and Letan, R. (2011). Analytical model of a PCM-air heat exchanger. Appl Thermal Eng 31: 3453- 3462.

Dumas, J. P., Bédécarrats, J. P., Strub, F., and Falcon, B. (1994). Modelization of a tank filled with spherical nodules containing a phase change material. In: Proceedings of the 10th international heat transfer conference, UK

Dutil, Y., Rousse, D. R., Salah, N. B., Lassue, S., and Zalewski, L. (2011). A review on phase-change materials: Mathematical modelling and simulation. Renewable and Sustainable Energy Reviews 15: 112-130.

E

Eftekhar, J., Haji-Sheikh, A., and Lou, D. (1984). Heat transfer enhancement in a paraffin wax thermal storage system. Journal of Solar Energy Engineering 106:299–306.

Eftekhar, J., Haji-Sheikh, A., and Lou, D. (1984). Heat transfer in paraffin wax thermal storage system. Proceedings of TNO Symposium on Thermal Storage of Solar Energy, Amsterdam, Holland: 99-110.

Egolf, P. W., and Manz, H. (1994). Theory and modeling of phase change materials with and without mushy regions. Journal of Heat and Mass Transfer 37: 2917-2924.

EIA (2006). International Energy Outlook 2006, U.S Department of Energy, June 2006.

EIA (2013). Annual Energy Outlook 2013-with Projections to 2040. DOE/EIA-0383, USA

El-Dessouky, H., and Al-Juwayhel, F. (1997). Effectiveness of a thermal energy storage system using phase-change materials. Energy Convers Manage 38: 601–17.

El-Sebaii, A., Al-Amir, S., Al-Marzouki, F. M., Faidah, A., Al-Ghamdi, A., and Al-Heniti, S. (2009). Fast thermal cycling of acetanilide and magnesium chloride hexahydrate for indoor solar cooking. Energy conversion and management 50: 3104-3111.

El-Sebaii, A. A., Al-Heniti, S., Al-Agel, F., Al-Ghamdi, A. A., and Al-Marzouki, F. (2011). One thousand thermal cycles of magnesium chloride hexahydrate as a promising PCM for indoor solar cooking. Energy Conversion and Management 52: 1771-1777.

EPS ltd (2015). Available from < http://www.epsltd.co.uk/>.

Esen, M. (1994). Numerical simulation of cylindrical energy storage tank containing phase change material on the solar assisted heat pump system and comparing with experimental results. Doctoral thesis, Department of Mechanical Engineering, Karadeniz Technical University, Trabzon, Turkey

Esen, M., and Ayhan, T. (1996). Development of a model compatible with solar assisted cylindrical energy storage tank and variation of stored energy with time for different phase change materials. Energy Convers Mgmt 37: 1775- 1785.

Ettouney, H., Alatiqi, M., Al-Sahali, M., and Al-Hajirie, K. (2006). Heat transfer enhancement in energy storage in spherical capsules filled with paraffin wax and metal beads. Energy Conversion and Management 47:211–28.

Eurostat (2012). Energy, transport and environment indicators, European Commission, European Union publication, Luxemburg. ISSN 1725-4566.

Evola, G., Marletta, L., and Sicurella, F. (2014). Simulation of a ventilated cavity to enhance the effectiveness of PCM wallboards for summer thermal comfort in buildings. Energy and Buildings 70: 480-489

F

Fan, L., and Khodadadi, J. (2011). Thermal conductivity enhancement of phase change materials for thermal energy storage: A review. Renewable and Sustainable Energy Reviews 15: 24-46.

Fang, M., and Chen, G. (2007). Effects of different multiple PCMs on the performance of a latent thermal energy storage system. Applied Thermal Engineering 27:994– 1000.

Farid, M. M., and Kanzawa, A. (1989). Thermal performance of a heat storage module using PCM's with different melting temperatures: Mathematical Modeling. Solar Energy Engineering 111: 152-158.

Farid, M., and Kanzawa, A. (1989). Thermal performance of a heat storage module using PCM's with different melting temperatures: Experimental. Solar Energy Engineering 112: 125-131.

Farid, M. M., and Husain, R. (1990). An electrical storage heater using the phase-change method of heat storage. Energy Conversion Management 30: 219-230.

Farid, M. M., and Khalaf, A. N. (1994). Performance of direct contact latent heat storage units with two hydrated salts. Solar Energy 52: 179-189.

Farid, M. M., Hamad, F. A., and Abu-Arabi, M. (1998). Phase change cool storage using dimethyl-sulfoxide. Energy Conversion Mgmt. 39: 819–826

Farid, M. M., Khudhair, A., Razack, S., and Al-Hallaj, S. (2004). A review on phase change energy storage: materials and applications. Energy Conversion and Management 45: 1597-1615.

Farrel, A., Norton, B., and Keneddy, D. (2006). Corrosive effects of salts hydrate phase change materials used with aluminium and copper. Journal of Materials Processing Technology 175: 198-205.

Feldman, D. and Shapiro, M. (1989). Fatty acids and their mixtures as phase-change materials for thermal energy storage. Solar Energy Mater 18: 201-216

Feldman, D., and Banu, D. (1996). DSC analysis for evaluation of an energy storing wallboard. Thermochim Acta 272: 243-251.

Fluent (2006). FLUENT 6.3 Documentation, Fluent Inc., Lebanon, US.

Fluent (2010). Theory Guide (Release 13.0, November 2010), Solidification and melting, Chapter 18: pp 569 -576

Fluent (2011). ANSYS FLUENT Release 13.0 User Manuallever rule

Fluent (2012). ANSYS FLUENT Release 14.5 User Manual

Fluent (2013). ANSYS FLUENT Release 15.0 User Manual

Fukai, J., Kanou, M., Kodama, Y., and Miyatake, O. (2000). Thermal conductivity enhancement of energy storage media using carbon fibres as thermal conductivity promoter. Energy Conversion Management 41: 1543-1556.

Fukai, J., Morozumi, Y., Hamada, Y., and Miyatake, O. (2000). Transient response of thermal energy storage unit using carbon fibers as thermal conductivity promoter. Proceedings of the 3rd European Thermal Science Conference, Pisa. Italy.

Fukai, Y., Hamada, J., Morozumi, Y., and Miyatake, O. (2002). Effect of carbon-fiber brushes on conductive heat transfer in phase change materials. International Journal Heat Mass Transfer 45: 4781-4792.

Fukai, J., Hamada, Y., Morozumi, Y., and Miyatake, O. (2003). Improvement of thermal characteristics of latent heat thermal storage units using carbon-fiber brushes: experiments and modeling. International Journal Heat Mass Transfer 46:4513-4525.

Fuzerland, R. (1980). A comparative study of numerical methods for moving boundary problems. Inst. Math. Appl. 26:411-429.

G

García-Romero, A., Delgado, A., Urresti, A., Martín, K., and Sala, J. M. (2009). Corrosion behaviour of several aluminium alloys in contact with a thermal storage phase change material based on Glauber's salt. Corrosion Science 51: 1263-1272.

Garg, H. P., Mullick, A. C., and Bhargava, A. K. (1985). Solar thermal energy storage. Dordrecht: D. Reidel Publishing Company

Gebremedhin, K. G., and Wu, B. X. (2003). Characterization of flow field in a ventilated space and simulation of heat exchange between cows and their environment, Journal of Thermal Biology, 28: 301–319.

Gerasimov, A. (2006). Modeling Turbulent Flows with FLUENT, Europe, ANSYS,lnc.

Ghoneim, A. A. (1989). Comparison of theoretical models of phase-change and sensible heat storage for air and water-based solar heating systems. Solar Energy 42: 209–20

Gibbs, M., and Hasnain, S. (1995). DSC study of technical grade phase change heat storage materials for solar heating applications, Proceedings of the 1995 ASME/JSME/JSEJ International Solar Energy. Conference. Part 2.

Gobbin, D, (1992) Role de la convection thermique dans les processus de fusion-solidification. Ecole d' ete, GUT-CET, Modélisation numérique en thermique, Institut d' etudes scientifiques de Cargèse.

Gong, Z., and Mujumdar, A. (1996). Cyclic heat transfer in a novel storage unit of multiple phase change materials. Applied Thermal Engineering 16: 807-815.

Gong, Z., and Mujumdar, A. S. (1997). Finite-element analysis of cyclic heat transfer in a shell and tube latent heat energy storage exchanger. Applied Thermal Engineering 17: 583–91.

Gong, Z., and Mujumdar, A. S. (1997). Thermodynamic optimization of the thermal process in energy storage using multiple phase change materials. Appl Thermal Eng 17: 1067- 1083.

Gowreesunker, B. L. (2013), Phase change thermal energy storage for the thermal control of large thermally lightweight indoor spaces, PhD Thesis, Brunel University, UK.

Gowreesunker, B. L., and Tassou, S. A. (2013). Effectiveness of CFD simulation for the performance prediction of phase change building boards in the thermal environment control of indoor spaces. Building and Environment 59: 612-625.

Guo, S., Li, H., Zhao, J., Li, X., and Yan, J. (2013). Numerical simulation study on optimizing charging process of the direct contact mobilized thermal energy storage. Applied Energy 112: 1416-1423.

Guobing, Z., Yinping, Z., Xin, W., and Kunping, L., and Wei, X. (2007). An assessment of mixed type PCM-gypsum and shape-stabilized PCM plates in a building for passive solar heating. Solar Energy 81: 1351–1360.

H

Hafner, B., and Schwarezer, K. (1999). Improvement of the heat transfer in a phase-change-material storage. Proceedings of the 4th workshop of IEA ECES IA annex 10, Bendikbeueren, Germany.

Halawa, E. (2005). Thermal performance analysis of a roof integrated solar heating system incorporating phase change thermal storage. Ph.D. Thesis, School AME, University of South Australia, Australia.

Halawa, E., Bruno, F., and Saman, W. (2005). Numerical analysis of a PCM thermal storage system with varying wall temperature. Energy Convers Mgmt 46: 2592- 2604.

Halawa, E., Saman, W., and Bruno, F. (2010). A phase change processor method for solving a one-dimensional phase change problem with convection boundary. Renewable Energy 35: 1688- 1695.

Halawa, E., and Saman, W. (2011). Thermal performance analysis of a phase change thermal storage unit for space heating. Renewable Energy 36: 259-264.

Hamada, Y., Ohtsu, W., and Fukai, J. (2003). Thermal response in thermal energy storage material around heat transfer tubes: effect of additives on heat transfer rates. Solar Energy 75: 317–28.

Hamdan, M. A., and Elwerr, F. A. (1996). Thermal energy storage using a phase change material. Solar Energy 56: 183-189.

Hasan, A. (1994). Phase change material energy storage system employing palmitic acid. Solar Energy 52: 143–54.

Hasnain, S. (1998). Review on Sustainable Thermal Energy Storage Technologies, Part I: Heat Storage Materials and Techniques. Energy Conversion 39: 1127-1138.

Hed, G., and Bellander, R. (2006). Mathematical modelling PCM air heat exchanger. Energy and Buildings 38: 82-89.

Henze, H., and Humphrey, J. (1981). Enhanced heat conduction in phase-change thermal energy storage devices. International Journal of Heat and Mass Transfer 24:459–74.

Hirata, T., and Nishida, K. (1989). An analysis of heat transfer using equivalent thermal conductivity of liquid phase during melting inside an isothermally heated horizontal cylinder. Heat Mass Transfer 32:1663–70.

Hogendoorn, C., and Bart, G. (1994). Performance and modelling of latent heat stores . Solar Energy 48: 53-58.

Hoover, M., Grodzka, P., and O'Neill, M. (1971). Space thermal control development. Lockheed Huntsville Research and Engineering Centre Final Report, LMSCHREC D225500; 81 pp.

Horbaniuc, B., Dumitrascua, G., and Popescub, A. (1999). Mathematical models for the study of solidification within a longitudinally finned heat pipe latent heat thermal storage system. Energy Conversion & Management 40: 1765–74.

Huang, M. J. (2011). The effect of using two PCMs on the thermal regulation performance of BIPV systems. Solar Energy Materials & Solar Cells 95: 957-963

I

Inglas PCM (2002). Available from < http://www.inglas.eu/>.

Instituto para la diversificación y Ahorro de la energía (IDAE). Eficiencia Energética y Energías Renovables (No. 8), Madrid, Octubre de 2006

International Energy Agency (IEA), Key World Energy Statistics, 2006.

Ismail, K., and Batista de Jesus, A. (1999). Modeling and solutions of the solidification problem of PCM around a cold cylinder, Numer. Heat Transfer, Part A 36: 95-114.

Ismail, K., and Abugderah, M. M. (2000). Performance of a thermal storage system of the vertical tube type. Energy Conversion & Management 41: 1165–90

Ismail, K., Alves, C., and Modesto, M. (2001). Numerical and experimental study on the solidification of PCM around a vertical axially finned isothermal cylinder. Applied Thermal Eng. 21: 53-77.

Ismail, K., and Henrıquez, J. R. (2002). Numerical and experimental study of spherical capsules packed bed latent heat storage system. Applied Thermal Engineering 22:1705–16.

Ismail, K., and Silva, M. G. E. (2003). Numerical solution of the phase change problem around a horizontal cylinder in the presence of natural convection in the melt region. Heat and Mass Transfer 46: 1791–9.

Iten, M., and Liu, S. (2014). A work procedure of utilising PCM as thermal storage systems based on air-TES systems. Energy Conversion and Management 77: 608-627.

J

Jeon, J., Seo, J., Jeong, S., and Kim, S. (2010). PCM application Methods for Residential Building Using Radiant Floor Heating Systems. Building Environment & Materials Lab, School of Architecture Soongsil University, Seoul 156-749, Republic of Korea.

Jian-you, L. (2008). Numerical and experimental investigation for heat transfer in triplex concentric tube with phase change material for thermal energy storage. Solar Energy 82: 977–85.

Jinyuan, T., Guan, H. Y., and Chaoqun, L. (2006). Computation Fluid Dynamics: A Practical Approach. USA: Butterworth-Heinemann, pp. 35– 37.

Jones B J, Sun D, Krishnan S, Garimella S V (2006). Experimental and numerical study of melting in a cylinder. Int J Heat Mass Transfer 49: 2724–38.

Jotshi, C. K., Goswami, D. Y., and Tomilnson, J. J. (1992). In: Proceedings of the 1992 ASES annual conference, USA

JRC (2012). Energy Efficiency Status Report, Electricity Consumption and Efficiency Trends in the EU-27.

K

Kamimto, M., Abe, Y., Sawata, S., Tani, T., and Ozawa, T. (1985). Latent heat storage unit using form-stable high density polyethylene for solar thermal applications. Proceedings for the International Symposium on Thermal Application of Solar Energy. Hakone (Kanagawa, Japan).

Kamimto, M., Abe, Y., Sawata, S., Tani, T., and Ozawa, T. (1986). Heat Transfer in latent heat thermal storage units using pentarythritol slurry, thermal energy storage. World Congress of Chemical Engineering, Tokyo, Japan.

Kaygusuz, K. (2003). Phase change energy storage for solar heating systems. Energy Source 25: 791-807.

Kenisarin, M., and Mahkamov, L. (2007). Solar energy storage using phase change materials. Renewable and Sustainable Energy Reviews 11: 1913-1965.

Khan, M., and Rohatgi, P. (1994). Numerical solution to a moving boundary problem in a composite medium. Numerical Heat Transfer 25: 209-221.

Khudair, A., Farid, M., Orkan, N., and Chen, J. (2003). Thermal performance and mechanical testing of gypsum wallboard with latent heat storage. Proceedings of the EM4 Indore workshop IEA ECES IA Annex 17: 21-24, Indore India

Khudhair, A., and Farid, M. (2004). A review on energy conservation in building applications with thermal storage by latent heat using phase change materials. Energy Convers Mgmt 45: 263-275.

Khudhair, A., and Farid, M. (2004). A review on energy conservation in building applications with thermal storage by latent heat using phase change materials. Energy Conversion and Management 45: 263-275.

Kousksou, T., Bédécarrats, J. P., Dumas, J. P., and Mimet, A. (2005). Dynamic modeling of the storage of an encapsulated ice tank. Appl Therm Eng 25:1534–48.

Kousksou, T., Bédécarrats, J. P., Strub, F., and Castaing-Lasvignottes, J. (2008). Numerical simulation of fluid flow and heat transfer in a phase change thermal energy storage. Int J Energy Technol Policy 6: 143–58.

Kürklü, A., Wheldon, A., and Hadley, P. (1996). Mathematical modelling of the thermal performance of a phase-change material (PCM) store: Cooling cycle. Appl Thermal Engineering 16: 613-623.

Kürklü, A. (1998). Energy storage applications in greenhouses by means of phase change materials (PCMs): a review. Renewable Energy 13: 89-103.

Kuznik, F., Virgone, J., and Noel, J. (2008). Optimization of a phase change material wallboard for building use. Applied Thermal Engineering 28: 1291-1298.

Kuznik, F., and Virgone, J. (2009). Experimental investigation of wallboard containing phase change material: Data for validation of numerical modeling. Energy and Buildings 41: 561-570.

Kuznik, F., Virgone, J., and Johanne, K. (2010). Development and validation of a new TRNSYS type for the simulation of external building walls containing PCM. Energy and Buildings 42: 1004-1009.

L

Lacroix, M., and Voller, V. (1990). Finite different solutions of solidification phase change problems: transformed versus fixed grids, Numer. Heat Transfer, Part B 17.

Lacroix, M. (1993). Numerical simulation of a shell and tube latent heat thermal energy storage unit. Solar Energy 50: 357–67.

Lacroix, M. (1993). Study of the heat transfer behaviour of a latent heat thermal storage with a finned tube. International Journal Heat Mass Transfer 36: 2083-2092

Lamberg, P., Jokisalo, J., and Sirén, K. (2000). The effects on indoor comfort when using phase change material with building concrete products. In: Proceedings of Healthy Buildings, Finland.

Lamberg, P. (2004). Approximate analytical model for two-phase solidification problem in a finned phase-change material storage 77: 131-152.

Lane, G. A. (1981). Adding strontium chloride or calcium hydroxide to calcium chloride hexahydrate heat storage material. Solar Energy 27: 73-75.

Laouadi, A., Lacroix, M. (1999). Thermal performance of a latent heat energy storage ventilated panel for electric load management. Int J Heat Mass 42: 275-286.

Lázaro, A., Doladom, P., Marin, J., and Zalba, B. (2009). PCM- air heat exchangers for free cooling applications in buildings. Experimental results of two real-scale prototypes. Energy Conversion and Management 50: 439-443.

Laustsen, J. (2008). Energy Efficiency Requirements in Building Codes, Energy Efficiency Policies for New Buildings (IEA Information paper).

Lecomte, D., and Mayer, D. (1985). Design method for sizing a latent heat store/heat exchanger in a thermal system. Applied Energy 21:55–78.

Lee, .K. O., Medina, M. A., Raith, E., and Sun, X. (2015). Assessing the integration of a thin phase change material (PCM) layer in a residential building wall for heat transfer reduction and management. Applied Energy 137: 669-706.

Liam, J. S., Bejan, A., and Kim, J. H. (1992). Thermodynamic Optimization of Phase-Change Energy Storga Using Two or More Materials. Energy resources technology 114: 84-90

Ling, Z., Chen, J., Fang, X., Zhang, Z., Xu, T., Gao, X., and Wang, S. (2014). Experimental and numerical investigation of the application of phase change materials in a simulative power batteries thermal management system. Applied Energy 121: 104-113

Liu, S., and Li, Y. (2015). Heating performance of a solar chimney combined PCM: A numerical case study. Energy and Buildings 99: 117-130.

Liu, B, and Majumdar, P. (2006). Numerical Simulation of Phase Change Heat Transfer in PCM-Encapsultaed Heat Sinks. In: The 18th IEEE Semi-Therm Symposium 2006.

Liu, Z., and Wang, Z. (2006). An experimental study on heat transfer characteristics of heat pipe heat exchanger with latent heat storage. Part I: Charging only and discharging only modes. Energy Convers Management 944-966

Liu, H., and Awbi, H. B. (2009). Performance of phase change materials boards under natural convection, Building and Environment 44: 1788–1793.

Lombard, L., Ortiz, J., and Pout Christine, P. (2008). A review on buildings energy consumption information. Energy and Buildings 40: 394-398.

Lombard, L., Ortiz, J., and Maestre, I. (2011). The map of energy flow in HVAC systems. Applied Energy 88: 5020-5031.

London, A. L., and Seban, R. A. (1943). Rate of Ice Formation. Transactions of ASME, 65, October, pp. 771-778.

H

Hasan, M., Mujumdar, A. S., and Weber, M. E. (1991). Cyclic melting and freezing, Chemical Engineering Science 46: 1573–1587.

M

Mankibi, M., Stathopoulos, N., Rezai, N., and Zoubir, A. (2015). Optimization of an air-PCM heat exchanger and elaboration of peak power reductions strategies. Energy and Buildings: In press

Matias, L. (2010). Desenvolvimento de um modelo adaptativo para definição das condições de conforto térmico em Portugal, Dissertação elaborada no Laboratório Nacional de Engenharia Civil para a obtenção do grau de Doutor em Engenharia Civil, Instituto Superior Técnico – Universidade Técnica de Lisboa.

Marín, J. M., Zalba, B., Cabeza, L. F., and Mehling, H. (2005). Improvement of a thermal energy storage using plates with paraffin-graphite composite. Heat Mass Transfer 48: 2561-2570.

Mehling, H., Hiebler, S., and Ziegler, F. (1999). Latent heat storage using a PCM- graphite composite material: advantages and potential applications. Proceedings of the 4th workshop of IEA ECES IA annex 10, Bendiktbeuern, Germany.

Mehling, H. (2000). Latent heat storage with a PCM-graphite composite material: experimental results from the first test store. Proceedings of the 6th workshop of IEA ECES IA annex 10, Stockholm, Sweden.

Mehling, H., Hiebler, S., and Ziegler, F. (2000). Latent heat storage using a PCM-graphite composite material. Proceedings of Terrastock 8th International Conference on Thermal Energy Storage 375-380, Stuttgart, Germany

Mehling, H., Heibler, S., and Cabeza, L. (2002). News on the application of PCMs for heating and cooling of buildings. IEA, ECES IA Annex 17, Advanced thermal energy storage trough phase change materials and chemical reactions – feasibility studies and demonstration projects. 3rd Workshop, 1-2 October 2002, Tokyo, Japan.

Mehling, H., and Cabeza, L. F. (2008). Heat and Cold Storage with PCM: An Up to Date Introduction Into Basics and Applications. Page 95, Springer.

Mehling, H., Hiebier, S., and Cabeza, L. (2002). News on the applications of PCMs for heating and cooling of buildings. Advanced thermal energy storage trough phase change materials and chemical reactions feasibility studies and demonstration project, third workshop, IEA, ECES IA Annex 17, 1-2 October, Tokyo, Japan.

Mehling, H., and Cabeza, L. F. (2008). Heat and Cold storage with PCM. An update introduction into basics and applications. Berlin: Springer.

Mettawee, E. S., and Assassa, G. M. R. (2007). Thermal Conductivity enhancement in a latent heat storage system. Solar Energy 81, 839–845.

Mitsubishi Chemical Corporation (2015). Available from <http://www.m-kagaku.co.jp/index_en.htm>.

Morcos, V. H. (1990). Investigation of a latent heat thermal energy storage system. Solar Wind Technol. 7: 197-202.

Moreno, P., Castelo, A., Solé, C., Zsembinszki, G., and Cabeza, L. F. (2014). PCM thermal energy storage tanks in heat pump system for space cooling. Energy and Buildings 82: 399-405.

Moreno, P., Solé, C., Castell, A., and Cabeza, L. (2014). The use of phase change materials in domestic heat pump and air-conditioning systems for short term storage: A review. Renewable and Sustainable Energy Reviews 39: 1-13.

Morrison, D., and Abdel-Khalik, S. (1978). Effect of phase chage energy storage on the performance of air based and liquid based solar heating systems. Solar Energy 20: 57-67

Mosaffa, A. H., Infante Ferreira, C. A., Talati, F., and Rosen, M. A. (2013). Thermal performance of a multiple PCM thermal storage unit for free cooling. Energy Conversion and Management 67: 1-7.

N

Nagano, K., Takeda S., Shimakura, K. (2004). Thermal characteristics of a direct heat exchange system between granules with phase change material and air. Applied Thermal Engineering 24: 2131-2144.

Nagano, K., Takeda, S., Mochida, T., Shimakura, K., Nakamura, T. (2006). Study of a floor supply air conditioning system using granular phase change material to augment building mass thermal storage – Heat response in small scale experiments. Energy and Buildings 38: 436-446.

Nakaso, K., Teshima, H., Yoshimura, A., Nogami, S., Hamada, Y., and Fukai, J. (2008). Extension of heat transfer area using carbon fibre cloths in latent heat thermal energy storage tanks. Chemical Engineering and Processing 47:879–85.

Neeper, D. A. (2000). Thermal dynamics of wallboard with latent heat storage. Solar Energy 68: 393-403.

Netzsch (2015). Thermal Analysis. Thermophysical Testing, Cure monitoring. Available from <http://www.ansys.com/staticassets/ANSYS/staticassets/partner/NETZSCH/netzash-brochure.pdf>.

Naumann, R., and Emons, H. H. (1989). Results of thermal analysis for investigation of salt hydrates as latent heat-storage materials. J Therm Anal 1989; 35: 1009–31.

O

Oró, E., Miróa, L., Barrenechea, C., Martorell, I., Farid, M. M., and Cabeza, L. F. (2013). Corrosion of metal and polymer containers for use in PCM cold storage. Applied Energy 109:449-453

Osterman, E., Butala, V., and Stritih, U. (2013). Room heat exchanger with PCM as a thermal accumulation for heating and cooling of buildings. 11th REHVA World Congress and the 8th International Conference on IAQVEC, Prague, Czech Republic.

Osterman, E., Hagel, K., Rathgeber, C., Butala, V., and Stritih, U. (2015). Parametrical analysis of latent heat and cold storage for heating and cooling of rooms. Applied Thermal Engineering 84: 138- 149.

P

Padmanabhan, P., and Murthy, M. (1986). Outward phase change in a cylindrical annulus with axial fins on the inner tube. International Journal Heat Mass Transfer 29: 1855-1868.

Pal, D., and Joshi, Y. (1998). Thermal management of an avionics module using solid-liquid phase-change materials. Journal of Thermophysics and Heat Transfer 12:256–62.

Pasupathy, A., and Velraj, R. (2008). Effect of double layer phase change material in building roof for year round thermal management. Energy and Buildings 40: 193-203.

Patankar, S. V. (1980). Numerical heat transfer and fluid flow. Washington, DC: Hemisphere Publishing Corporation.

Pérez-Lombard, L., Ortiz, J., and Pout, C. (2008). A review on buildings energy consumption information. Energy and Buildings 40: 394–398.

Pérez-Lombard, L., Ortiz, J., and Maestre I. R. (2011). The map of energy flow in HVAC systems. Applied Energy 88: 5020-5031.

Pedersen, C. O. (2007). Advanced zone simulation in EnergyPlus: Incorporation of variable properties and Phase Change Material (PCM) capability. Proceedings: Building Simulation, China.

Peiró, G., Gasia, J., Miró, L., and Cabeza, L. F. (2015). Experimental evaluation at pilot plant scale of multple PCms (cascade) vs. single PCM configuration for thermal energy storage. Renwable Energy 83: 729-736.

Pires, L. C. C. (2010). Desenvolvimento e estudo experimental de uma unidade para o arrefecimento passive de edif]icios. PhD thesis, Universidade da Beira Interior.

Poirier, D., Salcudean, M. (1988), On numerical methods used in mathematical modelling of phase change in liquid metals, ASME Journal of Heat Transfer 110: 562–70

Porisino, F. (1988). Salt hydrates used for latent heat storage: Corrosion of metals and reliability of thermal performance. Solar Energy 41: 193-197

Prakash, J., Garg, H. P., and Datta, G. A. (1985). Solar water heater with a built-in latent heat storage. Energy Convers Manage 25: 51–6.

Py, X., Olives, S., and Mauran, S. (2001). Paraffin porous graphite matrix composite as a high and constant power thermal energy storage material. International Journal Heat Mass Transfer 44: 2727-2737

R

Rady, M. (2009). Thermal performance of packed bed thermal energy storage units using multiple granular phase change composites. Applied Energy 86: 2704-2720.

Raj, V., and Velraj, R. (2010). Review on free cooling of buildings using phase change materials. Renewable and Sustainable Energy Reviews 14: 2819-2829.

Raj, V., and Velraj, R. (2011). Heat transfer and presure drop studies on a PCM-heat exchanger module for free cooling applications. International Journal of Thermal Sciences 50: 1573- 1582.

Ravikumar, M., and Srinivasan, P. (2008). Phase change material as thermal energy storage material for cooling of buildings. J Theo Appl Info Tech 4:503-511.

RCCTE (2006). Decreto de Lei nº 80/2006 - Regulamento das Características do Comportamento Térmico dos Edifícios.

Real, A., García, V., Domenech, L., Renau, J., Montés, N., and Sánchez, F. (2014). Improvement of a heat pump based HVAC system with PCM thermal storage for cold accumulation and heat dissipation. Energy and Buildings 83: 108-116

Regin, A. F., Solanki, S. C., and Saini, J. S. (2006). Latent heat thermal energy storage using cylindrical capsule: Numerical and experimental investigations. Renewable Energy 31: 2025-2041

Regin, A., Solanki, S., and Saini, J. (2008). Heat transfer characteristics of thermal energy storage system using PCM capsules: A Review. Renewable and Sustainable Energy Reviews 12: 2438-2458.

Reid, R. C., Prausnitz, J. M., and Poling, B. E. (1987). The properties of gases and liquids, 4th ed. New York:McGraw-Hill.

Robak, C., Bergman, T., and Faghri, A. (2011). Enhancement of latent heat energy storage using the embedded heat pipes. Int. Journal of Heat and Mass Transfer 54: 3476-3484

Rohidin, P., and Moshfegh, B. (2007). Numerical predictions of indoor climate in large industrial premises. A comparison between different k-ε models supported by field measurements, Building and Environment 42: 3872-3882

Rouault, F., Burneau, D., Sebastien, P., and Lopez, J. (2014). Experimental investigation and modelling of a low temperature PCM thermal energy exchange and storage system. Energy and Building 83: 96-107.

RSECE (2006). Decreto de Lei nº 79/2006 - Regulamento dos Sistemas Energéticos e de Climatização dos Edifícios.

Rubitherm Technologies GmbH (2015). Available from <http://www.rubitherm.de/>.

Rudd, A. (1993). Phase-change material wallboard for distributed thermal storage in buildings. ASHRAE Trans 99 part 2, paper no. 3724.

S

Sadasuke, I., and Naokatsu, M. (1991). Heat transfer enhancement by fins in latent heat thermal energy devices. Solar Eng, ASME: 223-228.

Saitoh, T., and Hirose, K. (1986). High-performance of phase change thermal energy storage using spherical capsules. Chemical Engineering Commun. 41: 39-58.

Salim, M., and Cheah, S. C. (2009). Wall y+ Strategy for Dealing with Wall-bounded Turbulent Flows. Porceedings of the International MultiConference of Engineers and Computer Sciences 2009 Vol II IMECS 2009, March 18-20, Hong Kong.

Saman, W., Bruno, F., and Halawa, E. (2005). Thermal performance of PCM thermal storage unit for a roof integrated solar heating system. Solar Energy 78: 341-349.

Sari, A., and Karaipekli, A. (2007). Thermal conductivity and latent heat thermal energy storage characteristics of paraffin/expanded graphite composite as phase change material. Applied Thermal Engineering 27:1271–1277.

Sari, A., Kaygusuz, K. (2002). Thermal and heat transfer characteristics in a latent heat storage system using lauric acid. Energy Conversion and Management 43: 2493–507.

Satzger, P., and Eska, B. (1997). Matrix-heat-exchanger for latent-heat cold storage. Proceedings on the 7th international conference on thermal energy storage.

Satzger, P., Eska, B., and Ziegler, F. (1998). Matrix-heat-exchanger for a latent-heat cold-storage. Proceedings of Megastock'98, Saporro (Japan).

Satzger, P., and Eska, B. (2000). Method/system for accumulating heat and cold in an accumulating composite material. European patent 0914399 B1.

Schranzhofer, H., Puschnig, P., Heinz, A., and Streicher, W. (2006). Validation of a TRNSYS simulation model for PCM energy storages and PCM wall construction elements. In: 10th International Conference on Thermal Energy Storage, USA.

Sreeniraj, R. V., Velraj, R., and Lakshmi, N. (2002). Thermal analysis of a finned-tube LHTS module for a solar dynamic power system. Heat and Mass Transfer 38: 409-417.

Seeniraj R V, and Narasimhan N L (2008). Performance enhancement of a solar dynamic LHTS module having both fins and multiple PCM. Solar Energy 82: 535-542.

Shabgard, H., Bergman, T. L., Sharifi, N., and Faghri, A. (2010). High temperature latent heat thermal energy storage using heat pipes. Int J Heat Mass Transfer 53: 2979- 2988.

Shamsundar, N., and Sparrow, E. M. (1975). Analysis of multidimensional conduction phase change via the enthalpy model. J Heat Transfer 97: 333–340

Shamsundar, N., and Srinivasan, R. (1978). Analysis of energy storage by phase change with an array of cylindrical tubes. In Kreith F, Boehm R, Mitchell J, Banerat R, editors. Proceedings of the ASME winter annual meeting 35-40, San Francisco, CA, USA.

Sharma, A., Sharma, S.D., and Buddhi, D. (2002). Accelerated thermal cycle test of acetamide, stearic acid and paraffin wax for solar thermal latent heat storage applications. Energy Conversion and Management 43: 1923-1930.

Sharma, A., Tyagi, V., Chen, C., and Buddhi, D. (2009). Review on thermal energy storage with phase change materials and applications. Renewable and Sustainable Energy Reviews 13: 318-345.

Shatikian, V. (2004). of a Phase-Change Material with internal fins. Ph.D. thesis. Ben-Gurion University of the Negev, Israel.

Shatikian, V., Ziskand, G., and Letan, R. (2005). Numerical investigation of a PCM-based heat sink with internal fins, International Journal of Heat and Mass Transfer 48: 3689–3706

Shmueli, H., Ziskind, G., and Letan, R. (2010). Melting in a vertical cylindrical tube: Numerical investigation and comparison with experiments. International Journal of Heat and Mass Transfer 53: 4082 – 4091.

Shukla, A., Buddhi, D., and Sawhney, R. L. (2008). Thermal cycling tests of few selected inorganic and organic phase change materials. Renewable Energy 33: 2606-2614.

Siegel, R. (1977). Solidification of low conductivity material conductivity particles. Int. Heat Mass Transfer 20: 1087-1089.

Silva, P. D. (2001). Modelação matemática e experimental de sistemas de acumulação térmica por calor latente, Ph.D Thesis, Universidade da Beira Interior, Portugal.

Silva, P. D., Gonçalves, L. C., and Pires. L. (2002). Transient behaviour of a latent-heat thermal-energy store: numerical and experimental studies. Appl Energy 73: 83-98.

Singh, H., Saini, R. P., and Saini, J. S. (2010). A review on packed bed solar energy storage systems. Renewable and Sustainability Energy Reviews 14:1059-1069.

Smith, R., and Koch, J. (1982). Numerical solution for freezing adjustment to a finned surface. In Heat Transfer (edited by Grigull, U., Hahne, E., Stephan, K., and Straub, J.). Proceedings of the seventh international heat transfer conference 69-74, München, Germany

Solomon, A. D. (1979). Melt time and heat flux for a simple PCM body. Solar Energy 22: 251–7.

Sparrow, E., Larsen, E., and Ramsey, J. (1981). Freezing on a finned tube for either conduction-controlled or natural-convection-controlled heat transfer. International Journal Heat Mass Transfer 24: 273-284.

Sreeniraj, R., Velraj, R., and Lakshmi, N. (2002). Thermal analysis of a finned-tube LHTS module for a solar dynamic power system. Heat Mass Transfer 38: 409-417.

Stetiu, C., and Feustel, H. (1996). Phase-Change Wallboards and Mechanical Night Ventilation in Commercial Buildings. Lawrence Berkeley National Laboratory, Berkeley, CA.

Stritih, U. (2004). An experimental study of enhanced heat transfer in rectangular PCM thermal storage. International Journal of Heat and Mass Transfer 47: 2841–2847

Susman, G., Dehouche, Z., Cheechern, T., and Craug, S. (2011). Tests of prototype PCM 'sails' for office cooling. Applied Thermal Engineering 31: 717-726.

T

Takeda, S., Nagano, K., Mochida, T., and Shimakura, K. (2004). Development of a ventilation system utilizing thermal energy storage for granules containing phase change materials. Solar Energy 77: 329-338.

Tan, F. L., Hosseinizadeh, S. F., Khodadadi, J. M., and Fan, L. (2009). Experimental and computational study of constrained melting of phase change materials (PCM) inside a spherical capsule. International Journal of Heat and Mass Transfer 52: 3464–3472

Tan, L., Kwok, Y, Date, A., and Akbarzadeh, A. (2012). Numerical study of natural convection effects in latent heat storage using aluminium fins and spiral fillers. International Journal of Mechanical and Aerospace Engineering 6: 238- 245

Tay, N. H. S., Belusko, M., and Bruno, F. (2012). Experimental investigation of tubes in a phase change thermal energy storage system. Applied Energy 90: 288-297

Tay, N. H. S., Bruno, F., and Belusko, M. (2012). Experimental validation of a CFD model for tubes in a phase change thermal energy storage system. International Journal of Heat and Mass Transfer 55: 574-585.

Tayeb, M. (1996). Use of some industrial wastes as energy storage media. Energy Conversion Management 37 (2): 127-133.

TEAP Energy Products (2015). Available from <http://www.teappcm.com/>.

Telkes, M. (1978). Remarks on thermal energy storage using sodium sulphate decahydrate and water. Solar Energy 20:107.

Tong, X., Khan, J., and Amin, M. (1996). Enhancement of heat transfer by inserting a metal matrix into a phase change material. Numerical Heat Transfer, Part A 30:125-141

TSI. Available from http://www.tsi.com/uploadedFiles/_Site_Root/Products/Literature/Manuals/flow_and_pressure.pdf.

Tu, J., Yeoh, G. H., and, Liu, C. (2008) 'Chapter 2 - CFD Solution Procedure—A Beginning'. in Computational Fluid Dynamics. by Tu, J., Yeoh, G. H., and Liu, C. Burlington: Butterworth-Heinemann, 29-64

Tu, J., Yeoh, G., and Liu, C. (2013) .Chapter 1 - Introduction in Computational Fluid Dynamics (Second Edition). ed. by Tu, J., Yeoh, G., and Liu, C. : Butterworth- Heinemann, 1-29

Turnpenny, J. R., Etheridge, D. W., and Reay, D. A. (2000). Novel ventilation cooling system for reducing air conditioning in buildings: Part I: testing and theoretical modelling. Appl Thermal Energy 20: 1019-1037

Turnpenny, J. R., Etheridge, D. W., and Reay, D. A. (2001). Novel ventilation system for reducing air conditioning in buildings. Part II: testing of prototype. Applied Thermal Engineering 21: 1203-1217.

Tyagi, V., and Buddhi, D. (2007). PCM thermal storage in buildings: A state of art. Renewable and Sustainable Energy Reviews 11: 1146-1166.

Tyagi, V. V., and Buddhi, D. (2008). Thermal cycle testing of calcium chloride hexahydrate as a possible PCM for latent heat storage. Solar Energy Materials Solar Cells 92: 891-899.

Tyagi, V., Kaushik, S., and Akiyama, T. (2011). Development of phase change materials based microencapsulation technology for buildings: A review. Renewable and Sustainable Energy Reviews 15: 1373-1391.

V

Vakilaltojjar, S. M. (2000). Phase change thermal storage system for space heating and cooling. Ph.D. Thesis, School AME, University of South Australia, Australia.

Vakilaltojjar, S., and Saman, W. (2001). Analysis and modelling of a phase change storage system for air conditioning applications. Applied Thermal Engineering 21: 249-263.

Velraj, R., Seeniraj, R., Hafner, B., Faber, C., and Schwarzer, K. (1997). Experimental analyisis and numerical modelling of inward solidification on a finned vertical tube for a latent heat storage unit. Solar Energy 60: 281-290.

Velraj, R., Seeniraj, R., Hafner, B., Faber, C., and Schwarzer, K. (1999). Heat transfer enhancement in a latent heat storage system, Solar Energy 65: 171-180.

Velraj, R., and Pasupathy, A. (2006). Phase Change Material Based Thermal Storage For Energy Conservation In Building Architecture. International Energy Journal 7:147-159

Visser, H. (1986). Energy storage in phase-change materials—development of a component model compatible with TRNSYS, Final report, Contract no. 2462-84-09 ED ISPNL, Delft University of Technology, Department of Applied Physics, Delft.

Voller, V. R., and Shadabi, L. (1984). Enthalpy methods for tracking a phase change boundary in two dimensions. International Communications in Heat and Mass Transfer 11: 239-249.

Voller, V. R. (1990). Fast implicit difference method for the analysis of phase change problems. Heat Transfer B 17: 155.

Vynnycky, M., and Kimura, S. (2007). An analytical and numerical study of coupled transient natural convection and solidification in a rectangular enclosure. Int J Heat Mass Transfer 50: 5204–14.

W

Wang, J., Ouyang, Y., and Chen, G. (2001). Experimental study on charging process of a cylindrical heat storage employing multiple- phase-change-materials. Int. J. Energy Res. 25: 439-447

Wang, P., Wang, X., Huang, Y., Li, C., Peng, Z. and Ding, Y. (2015). Thermal energy charging behaviour of a heat exchange device with a zigzag plate configuration containing multi-phase-change-materials (m-PCMs). Applied Energy 142: 328-336.

Waqas, A., and Kumar, S. (2011). Utilization of latent heat storage unit for comfort ventilation in buildings in hot and dry climates. Int J Green Energy 8: 1-24

Waqas, A., and Kumar, S. (2011). Thermal performance of Latent Heat Storage for Free Cooling of Buildings in a Dry and Hot Climate: An Experimental Study. Energy and Buildings 43: 2621-2630

Werner, R. (1987). Compatibility of organic latent storage materials and plastic container materials. Heat Recovery and CHP 7: 383-388.

Wood, R., Gladwell, S., Callahar, P., and Probert, S. (1981). Low temperature thermal energy storage system using packed beds of encapsulated phase-change materials. Proceedings of the International Conference on Energy Storage, Brighton, UK: 145-158.

X

Xiao W., Wang, X., and Zhang, Y. (2009). Analytical optimization of interior PCM for energy storage in lightweight passive solar room. Applied Energy 86: 2013-2018.

Xiao, M., Feng, B., and Gong, K. (2001). Thermal performance of a high conductive shape-stabilized thermal storage material. Solar Energy Mater. Solar Cells 69: 293-296

Xu X., Zhang, Y., Lin, K., Di H., and Yang., R. (2005). Modelling and simulation on the thermal performance of shape-stabilized phase change material floor used in passive solar buildings. Energy and Buildings 37: 1084-1091.

Y

Yamaha, M., and Misaki, S. (2006). The evaluation of peak shaving by a thermal storage system using phase-change materials in air distribution systems. HVAC&R Res Special Issue 12: 3c.

Yanbing, K., Yi, J., and Yinping, Z (2003). Modelling and experimental study on innovative passive cooling system –NVP system. Energy and Buildings 35:417-425.

Yang, H., and He, Y. (2010). Solving heat transfer problems with phase change via smoothed effective heat capacity and element-free Galerkin methods. International Communications in Heat and Mass Transfer 37: 385-392.

Ye, W., Zhu, D., and Wang, N. (2011). Numerical simulation on phase-change thermal storage/release in a plate-fin unit. Applied Thermal Engineering 31: 3871-3884

Ye, W., Zhu, D., and Wang, N. (2012). Fluid flow and heat transfer in a latent thermal energy unit with different phase change material (PCM) cavity volume fractions. Applied Thermal Engineering 42: 49 – 57

Z

ZAE Bayern (2015). Available from <http://www.zae-bayern.de/en/the-zae-bayern.html>.

Zalba, B., Marin, J., Cabeza, L., and Mehling, H. (2003). Review of thermal energy storage with phase change: materials, heat transfer analysis and applications. Applied Thermal Engineering 23: 251-283.

Zalba, B., Marin, J., Cabeza, L., AND Mehling, H. (2004). Free cooling of buildings with phase change materials. Int J of Refrigeration 27: 839-849.

Zhai, Z. J., Zhang, Z., Zhang, W., and Chen, Q. Y. (2007). Evaluation of various turbulence models in predicting airflow and turbulence in enclosed environments by CFD: Part 1 – summary of prevalent turbulence models. HVAC&R Res 13:853–70

Zhang, Y., and Faghri, A. (1996). Heat transfer enhancement in a latent heat thermal storage system by using internally finned tube. International Journal Heat Mass Transfer 39: 717-724.

Zhang, Y., Yan, Su., Zhu, Y., and Hu, X. (2001). A General model for analyzing the thermal performance of the heat charging and discharging process of latent heat thermal energy storage systems. Trans ASME J Sol Energy Eng 123: 232–6.

Zhao, C. Y., Lu, W., and Tian, Y. (2010). Heat transfer enhancement for thermal energy storage using metal foams embedded within phase change materials (PCMs). Solar Energy 84: 1402-1412

Zhong, Y., Guo, S., Shi, J., and Liu, L. (2010). Heat transfer enhancement of paraffin wax using graphite foam for thermal energy storage. Solar Energy & Solar Cells 94: 1011-1014.

Zhou, D., and Zhao, C. Y. (2011). Experimental investigations on heat transfer in phase change materials (PCMs) embedded in porous materials Appl. Therm. Eng. 31: 970 – 977.

Zhou, D., Zhao, C. Y., and Tian, Y. (2012). Review on thermal energy storage with phase change materials (PCMs) in building application. Appl Energy 92: 593-60.

Zhu, N., Pingfan, H., Lei, Y., Jiang, Z., and Lei, F. (2015). Numerical study on ground source heat pump integrated with phase change material cooling storage system in office building. Applied Thermal Engineering 87: 615- 623.

Zivkovic, B., and Fujii, I. (2001). An analysis of isothermal phase change material within rectangular and cylindrical containers. Solar Energy 70: 51–6.

Zukowsky, M. (2007). Mathematical modelling and numerical simulation of a short term thermal energy storage system using phase change material for heating applications. Energy Convers Mgmt 48: 155-165.

Websites

Web6.1 http://www.rubitherm.de/

Web6.2 http://www.themetalstore.co.uk/products/mild-steel-sheet

Web6.3 http://www.ductstore.co.uk/

Web6.4 http://www.systemair.com/

Web6.5 http://www.aircon247.com/

Web6.6 http://www.erse.pt/

Web6.7 http://www.energysavingtrust.org.uk/

Web6.8 http://www.pouparmelhor.com/noticias/precos-da-electricidade-2001-2013/

APPENDIX A – COMMERICAL PCMs (melting point between -10 °C and 32 °C)

PCM name	Type of product	Melting temperature [°C]	Melting enthalpy [J/kg]	Density [kg/m^3]	Price (£) / kg	Supply Companies
TH-10	n.a	-10	283,000	n.a	-	TEAP
STL-6/SN06	Salt solutions	-6	284,000	1.07	-	Mitsubishi Chemical, Cristopia
TH-4	n.a	-4	286,000	n.a	-	TEAP
STL-3/SN03	Salt Solutions	-3	328,000	1.01	-	Mitsubishi Chemical, Cristopia
TH 0	n.a	0	334,000	n.a	-	TEAP
A 4	n.a	4	227,000	0.766	-	EPS ltd
ClimSel C 7	n.a	7	130,000	n.a	7	Climator
E7	n.a	7	120,000	1.54	-	EPS ltd
A8	n.a	8	220,000	0.77	-	EPS ltd
RT [1] 6	Latent heat paraffin	8	174,000	0.86	6	Rubitherm GmbH
E10	n.a	10	140,000	1.52	-	EPS ltd
E13	n.a	13	140,000	1.78	-	EPS ltd
ClimSel C 15	n.a	15	130,000	n.a	7	Climator
E21	n.a	21	150,000	1.48	-	EPS ltd
RT 20	Paraffin	22	172,000	0.87	7	Rubitherm GmbH
A22	n.a	22	220,000	0.775	-	EPS ltd
ClimSel C 23	Salt hydrate	23	148,000	1.48	6	Climator
ClimSel C 24	Salthydrate	24	216,000	1.48	6	EPS ltd
TH 25	Salthydrate	25	159,000	n.a		TEAP
RT 25	Paraffin	26	232,000		7	Rubitherm GmbH
STL27	Salt hydrate	27	213,000	1.09	-	Mitsubishi Chemical
S27	Salt hydrate	27	207,000	1.47	-	Cristopia
A28	n.a	28	245,000	0.79	-	EPS ltd
PX [2] 27	Latent heat powder	28	112,000	0.64	8.6	Rubitherm GmbH
GR [3] 27	Latent heat granulate	28	72,000	0.75	6.2	Rubitherm GmbH
RT 27	Latent heat paraffin	28	179,000	0.87	6.2	Rubitherm GmbH
RT30	Paraffin	28	206,000	n.a	7.8	Rubitherm GmbH
TH29	Salt hydrate	29	188,000	n.a	-	TEAP
E30	n.a	30	201,000	1.3	-	EPS ltd
ClimSel C 32	Salt hydrate	32	212,000	1.45	6	Climator

[1]- shape stabilized PCM – paraffin as PCM in a polymer structure

[2]- silica powder as matrix material which contains 60% PCM and still flows as the pure powder

[3]- granulate – porous clay mineral and contains about 35% of PCM

APPENDIX B – AIR VELOCITY MEASUREMENTS

Table A.1 Main inlet velocity measurements

V= 0.6 m/s					
H (m) / W (m)	**0.025**	**0.075**	**0.0125**	**0.175**	**0.225**
0.0198	0.64	0.59	0.65	0.58	0.62
0.0594	0.62	0.6	0.67	0.61	0.59
0.099	0.58	0.61	0.58	0.55	0.61
0.1386	0.57	0.51	0.62	0.58	0.58
0.1782	0.69	0.58	0.68	0.67	0.61
V= 1.6 m/s					
H (m) / W (m)	**0.025**	**0.075**	**0.0125**	**0.175**	**0.225**
0.0198	1.59	1.42	1.68	1.48	1.51
0.0594	1.81	1.79	1.77	1.78	1.8
0.099	1.48	1.47	1.59	1.48	1.44
0.1386	1.51	1.45	1.39	1.43	1.51
0.1782	1.94	1.79	1.67	1.72	1.66
V= 2.5 m/s					
H (m) / W (m)	**0.025**	**0.075**	**0.0125**	**0.175**	**0.225**
0.0198	2.49	2.32	2.77	2.53	2.49
0.0594	2.48	2.91	2.76	2.79	2.47
0.099	2.48	2.45	2.35	2.46	2.39
0.1386	2.71	2.46	2.53	2.42	2.49
0.1782	2.10	2.08	288	2.8	2.6

Table A.2 Positions 1-6 velocity measurements

0.6 m/s							
Position	**L (m)**	**H (m)**	**W (m)**				
			0.025	**0.075**	**0.0125**	**0.175**	**0.225**
1	2	0.099	0.70	0.58	0.75	0.62	0.37
2	0.435	0.188	1.00	0.97	0.93	0.98	1.00
3	0.435	0.132	1.01	1.05	1.14	1.09	1.07
4	0.435	0.066	1.09	1.05	1.17	1.12	1.05
5	0.435	0.01	1.12	1.03	1.01	1.06	0.95
6	0	0.099	0.66	0.67	0.72	0.7	0.67
1.6 m/s							
Position	**L (m)**	**H (m)**	**W (m)**				
			0.025	**0.075**	**0.0125**	**0.175**	**0.225**
1	2	0.099	1.71	1.68	2.10	1.72	0.81
2	0.435	0.188	2.47	2.41	2.40	2.46	2.49
3	0.435	0.132	2.83	2.81	2.85	2.83	2.74
4	0.435	0.066	2.97	2.86	2.90	2.88	2.72
5	0.435	0.01	2.65	2.62	2.64	2.63	2.60
6	0	0.099	1.85	1.58	1.61	1.65	1.48
2.6 m/s							
Position	**L (m)**	**H (m)**	**W (m)**				
			0.025	**0.075**	**0.0125**	**0.175**	**0.225**
1	2	0.01	2.25	2.73	3.20	2.85	1.20
2	0.435	0.188	3.20	3.15	3.23	3.21	3.20
3	0.435	0.132	3.70	3.85	3.80	3.88	3.50
4	0.435	0.066	3.75	3.79	3.90	3.85	3.70
5	0.435	0.01	3.50	3.57	3.60	3.61	3.45
6	0	0.099	2.21	2.31	2.71	2.81	2.10

APPENDIX C – PCMs DATA SHEET

APPENDIX D – SELECTED FAN DATA SHEET

APPENDIX E – AIR CONDITIONING UNIT DATA SHEET

APPENDIX F – PUBLISHED PAPERS

Energy Conversion and Management 77 (2014) 608–627

Contents lists available at ScienceDirect

Energy Conversion and Management

journal homepage: www.elsevier.com/locate/enconman

Review

A work procedure of utilising PCMs as thermal storage systems based on air-TES systems

M. Iten, S. Liu *

Civil Engineering, Architecture and Building, Faculty of Engineering and Computing, Coventry University, Coventry CV1 2HF, United Kingdom

Available online at www.sciencedirect.com

ScienceDirect

Energy Procedia 70 (2015) 229 – 240

Energy Procedia

International Conference on Solar Heating and Cooling for Buildings and Industry, SHC 2014

Experimental study on the performance of RT 25 to be used as Ambient Energy Storage

Muriel Iten, Shuli Liu*

Civil Engineering, Architecture and Building, Faculty of Engineering and Computing, Coventry University, Coventry, CV1 2HF, United Kingdom